PISTON RING LUBRICATION ANALYSED BY A UNIFIED HYDRODYNAMIC THEORY OF THRUST BEARINGS

by

TOMOKI SHIMAUCHI

A thesis submitted for the degree of
DOCTOR OF PHILOSOPHY
of the University of London
and also for the
DIPLOMA OF MEMBERSHIP OF IMPERIAL COLLEGE

January 1980

Lubrication Laboratory, Department of Mechanical Engineering,
Imperial College of Science and Technology,
London SW7 2AZ

Without generality there is no reasoning, without concreteness there is no importance.

- Dr. Whitehead

ABSTRACT

The thesis is in three main parts.

1. A general solution of the one dimensional Reynolds' equation using a new non-dimensional grouping, which is free from dependent variables has been applied to tilting pad bearings under stationary conditions and fixed pad bearings under dynamic (squeeze) and reciprocating load. Starvation is also simply treated, both classical and elastohydrodynamic lubrication. This general solution allows the interpretation of several aspects of hydrodynamic lubrication of thrust bearings in a unified manner, which has never been considered possible.

2. Improvement of a test rig for piston ring lubrication and scuffing studied at the Laboratory. The device has been miniaturised and much electronic equipment incorporated.

3. The application of the theory to the experimental device is briefly studied.

ACKNOWLEDGEMENTS

My great thanks go to Professor A. Cameron for his continuous encouragement while supervising this work.

I am also indebted to my fellow members of the Lubrication Laboratory for their many useful discussions, especially to Dr. G. Stachowiak for his continuous interest and support for this thesis.

I am also indebted to Mr. R. Dobson, Mr. T. Wymark for their continued help in the development of the new test machine.

I would also like to express my thanks to Miss Jane Miles for her patience and understanding in typing the thesis.

I am especially grateful to Mr. R. Potter and Mr. P. Saunders of the drawing office for their valuable assistance from the design stage of the apparatus to the completion of this thesis.

My sincere thanks are also due to Komatsu Limited for enabling me to study at the Lubrication Laboratory, Imperial College. Especially Mr. K. Takase, Dr. E. Nakaniski and Mr. A. Nishida deserve my sincere thanks for their continuous encouragement from Japan.

Finally to my dear wife Toshiko, and daughter Eri without their sympathy and smile this thesis would not have been completed.

CONTENTS

TITLE PAGE			
ABSTRACT			ii
ACKNOWLEDGEMENTS			iii
CONTENTS			iv
LIST OF FIGURES			ix
NOMENCLATURE			xiii
CHAPTER ONE		INTRODUCTION AND LITERATURE SURVEY	1
1.1		General View and Background of the Thesis	1
1.2		Literature Survey	3
	1.2.1	Introduction	3
	1.2.2	Brief Survey on the Study of Piston Ring Lubrication	8
	1.2.3	Conclusion of Literature Survey	11
CHAPTER TWO		GENERAL SOLUTION OF ONE DIMENSIONAL REYNOLDS EQUATION	13
2.1		Introduction	13
2.2		General Solution of Reynolds equation for Infinitely Long Thrust Bearings	12
2.3		Comparison of the Non-dimensional parameters with Sommerfeld number	18
2.4		Comparison of Film Thickness for Different Surface Shape Bearings. (Steady State)	19
	2.4.1	Taper and Bearings	20
	2.4.2	Stepped Pads. Rayleigh Step.	22
	2.4.3	Partial Parabolic Bearing	23
	2.4.4	Comparison of Different Surface Shape Bearings	26
2.5		Discussion	27

CHAPTER THREE		MATHEMATICAL FORMULATION OF PARABOLIC FACE THRUST BEARINGS	36
3.1		Introduction	36
3.2		Theory of Hydrodynamic Lubrication of Parabolic Face Infinitely Long Thrust Bearings	36
	3.2.1	Load Carrying Capacity	36
	3.2.2	Centre of Pressure	42
3.3		Discussion	44
CHAPTER FOUR		TILTING PAD BEARING	50
4.1		Introduction	50
4.2		Flat Tilting Pad Bearing	51
4.3		Parabolic Tilting Pad Bearing with Sufficient Trailing Breadth	51
4.4		Parabolic Tilting Pad Bearing with Finite Trailing Breadth	58
4.5		Discussion	63
CHAPTER FIVE		STARVATION	74
5.1		Introduction	74
5.2		Starvation of Rigid Surface Isoviscous Lubrication	75
	5.2.1	Flat Inclined Pad Bearing Under Starved Conditions	76
	5.2.2	Parabolic Pad Bearing Under Starved Conditions	80
5.3		Starved Lubrication of EHL Line Contact	83
5.4		Discussion and Conclusion	92
CHAPTER SIX		DYNAMIC BEHAVIOUR OF PARABOLIC PAD BEARINGS	104
6.1		Introduction	104
6.2		Theoretical Formulation	104
6.3		Results of Calculation	109
6.4		Discussion	110

CHAPTER SEVEN		COMPARISON BETWEEN THREE DIFFERENCT BOUNDARY CONDITIONS	116
7.1		Introduction	116
7.2		Theory	117
7.3		Results and Discussion	119
7.4		Conclusions	124
CHAPTER EIGHT		HYDRODYNAMIC LUBRICATION OF PISTON RING	133
8.1		Introduction	133
8.2		Theory	134
	8.2.1	Crank Motion	134
	8.2.2	Load	136
	8.2.3	Solution Under Reynolds Condition	137
	8.2.4	Solution under full Sommerfeld Condition	138
	8.2.5	Solution at Dead Centre	140
8.3		Non-dimensional parameters for Piston Ring Lubrication	143
8.4		Results and Discussions	147
	8.4.1	Calculation Procedure	147
	8.4.2	Film Thickness Change During a Cycle	148
	8.4.3	General Presentation of Minimum Film Thickness in a Cycle	150
	8.4.4	Design Optimization	152
8.5		Conclusion	154
CHAPTER NINE		EXPERIMENTAL APPARATUS	162
9.1		Introduction	162
9.2		Apparatus	162
9.3		Instrumentation	165
	9.3.1	Friction Force	165
	9.3.2	Applied Load	167
	9.3.3	Electric Contact Resistance	167
	9.3.4	Stroke Length	168

9.4		Control	169
	9.4.1	Stroke Length Control	169
	9.4.2	Temperature Control	170
CHAPTER TEN		EXPERIMENTAL STUDY ON THREE REGIME OF LUBRICATION MODE UNDER RECIPROCATING MOTION	185
10.1		Introduction	185
10.2		Experimental Method	185
	10.2.1	Contact Resistance and General Procedure	185
	10.2.2	Reciprocating Frequency	186
	10.2.3	Stroke Amplitude	187
	10.2.4	Load	187
10.3		Test Specimen	187
	10.3.1	Sliding Test Specimens	187
	10.3.2	Lubricant	188
10.4		Results	189
10.5		Discussion	190
10.6		Conclusion	192
CHAPTER ELEVEN		GENERAL DISCUSSIONS, CONCLUSIONS AND SUGGESTIONS FOR FURTHER WORK	200
11.1		Introduction	200
11.2		The Meaning of Δh	201
11.3		Discussion on Piston Ring Lubrication	203
11.4		Conclusion	205
	11.4.1	Theory	205
	11.4.2	Experiment	206
11.5		Suggestions for Further Work	206
	11.5.1	Theory	206
	11.5.2	Experiment	207

REFERENCES 209

APPENDICES 216

Appendix 1 List of Program of Hydrodynamic Lubrication of Piston Ring 216

Appendix 2 List of Program of Curved Face Tilting Pad Bearings 224

Appendix 3 Assembly Drawing of the Apparatus

LIST OF FIGURES

CHAPTER TWO

Figure 2.1	Pressure in a Slider	30
Figure 2.2	Unwrapped Oil Film Thickness of a Journal Bearing	30
Figure 2.3	Taper Land Bearing	31
Figure 2.4	Rayleigh Step Bearing	31
Figure 2.5	Partial Parabolic Bearing	32
Figure 2.6	Performance of Taper Land Bearing	33
Figure 2.7	Performance of Rayleigh Step Bearing	34
Figure 2.8	Performance of Partial Parabolic Bearing	35

CHAPTER THREE

Figure 3.1(a)	Parabolic Face Thrust Bearing Under Reynolds Condition	46
Figure 3.1(b)	Parabolic Face Thrust Bearing Under Full Sommerfeld Condition	47
Figure 3.2	Performance of Parabolic Face Bearing	48
Figure 3.3	Centre of Pressure and Position of Pmax	49

CHAPTER FOUR

Figure 4.1	Performance of Flat Tilting Pad Bearing	65
Figure 4.2	Tilted Parabolic Thrust Bearing	66
Figure 4.3	Film Thickness of Parabolic Bearing Under Tilted Condition	67
Figure 4.4	Film Outlet Length of Parabolic Bearing for Tilted State	68
Figure 4.5	Tilting Parameter Bt Against Film Thickness H_o	69
Figure 4.6	Over Tilting Condition of Parabolic Tilting Pad Bearing	70
Figure 4.7	Tilting Parameter of the Parabolic Tilting Pad Bearing	71
Figure 4.8	Film Thickness of Parabolic Tilting Pad Bearing	72
Figure 4.9	H_{ob} against H_o for Parabolic Tilting Pad Bearing	73

CHAPTER FIVE

Figure 5.1	Starved Lubrication of Bearings	96
Figure 5.2	Starved Lubrication of Inclined Pad Bearing	97
Figure 5.3	Starved Lubrication of Parabolic Face Slider Bearing	98
Figure 5.4	Co-ordinate System of EHL Line Contact	99
Figure 5.5	Reduced Pressure Distribution Along the Inlet Axis	100
Figure 5.6	General Solution of EHL Film Thickness	101
Figure 5.7	EHL Film Thickness Against Inlet Film Distance	102
Figure 5.8	EHL Film Thickness Reduction Against Relative Inlet Distance	103
Figure 5.9	EHL Film Thickness Against Inlet Film Thickness	103

CHAPTER SIX

Figure 6.1	Parabolic Pad Bearing Under Squeeze Effects	113
Figure 6.2(a)	Load Carrying Capacity of a Parabolic Pad Bearing Under Squeeze	114
Figure 6.2(b)	Same as (a)	115

CHAPTER SEVEN

Figure 7.1(a)	Film Pressure Distribution Under Half Sommerfeld Condition	126
Figure 7.1(b)	Film Pressure Distribution Under Full Sommerfeld Condition	127
Figure 7.1(c)	Film Pressure Distribution Under Reynolds Condition	128
Figure 7.2(a)	Load Carrying Capacity of Parabolic Pad Bearing Under Different Boundary Condition (H_o = 1.0)	129
Figure 7.2(b)	Load Carrying Capacity of Parabolic Pad Bearing Under Different Boundary Condition (H_o = 2.5)	130
Figure 7.2(c)	Load Carrying Capacity of Parabolic Pad Bearing Under Different Boundary Condition (H_o = 0.2)	131
Figure 7.3	Effects of Outlet Geometry on the Solutions Under Modified Full Sommerfeld Condition	132

CHAPTER EIGHT

Figure 8.1	Crank Mechanism	155
Figure 8.2	Piston Ring Geometry and Pressure Distribution	156
Figure 8.3(a)	Film Thickness and Outlet Positions Over the Stroke	157
Figure 8.3(b)	Same as (a)	158
Figure 8.3(c)	Same as (a)	159
Figure 8.4	Minimum Film Thickness and its Position of Crank Angle Under Reciprocating Motion	160
Figure 8.5	Minimum Film Thickness Against Maximum Sliding Velocity Under Reciprocating Motion	161

CHAPTER NINE

Figure 9.1	Overall View of the Experimental Set Up	173
Figure 9.2	A View of the Apparatus	173
Figure 9.3	Schematic Diagram of the Apparatus	174
Figure 9.4	Dynamic Test Piece	175
Figure 9.5	Front Section of the Heater Box and Loading Schematic	176
Figure 9.6	Circuit Diagram of Charge Amplifier	177
Figure 9.7	Precise Rectifier and Smoothing Circuit	178
Figure 9.8	Analogue Divider Circuit	178
Figure 9.9	Circuit Diagram of Contact Resistance Measurement	179
Figure 9.10	Typical X-Y Display of Contact Resistance and Fr Friction Force	175
Figure 9.11	Stroke Measurement Slip	168
Figure 9.12	Direct Reading Method of Stroke Length	180
Figure 9.13(a)	Diagram of the Stroke Control Circuit (Wave Form Generator)	181
Figure 9.13(b)	Diagram of the Stroke Control Circuit (Control Signal Circuit)	181
Figure 9.13(c)	Diagram of the Stroke Control Circuit (Automatic Gain Control, A.G.C.)	182
Figure 9.14(a)	Circuit Diagram of the Temperature Controller (Control Signal Circuit)	183

Figure 9.14(b)	Circuit Diagram of the Temperature Controller (Power Switch Controller)	184

CHAPTER TEN

Figure 10.1	Three Regime of Lubrication	193
Figure 10.2	Test Specimens	194
Figure 10.3	Boundary Between Full and Partial Hydrodynamic Regime	195
Figure 10.4	Boundary Between Partial Hydrodynamic and Boundary Lubrication Regime	196
Figure 10.5	Talisurf Traces of the Test Specimen	197
Figure 10.6	Non-dimensionalised Experimental Results (1)	198
Figure 10.7	Non-dimensionalised Experimental Results (2)	199

CHAPTER ELEVEN

Figure 11.1	Flow Balance in a Narrow Passage	202

NOMENCLATURE

General rule of notation.

Dimensional quantities are in general small letters.

Nondimensional quantities are in general capital letters.

Suffix

0	minimum film thickness, reduced pressure (EHL)
1	inlet side of the bearing
2	outlet side of the bearing
R	Reynolds condition
S	Starved condition
t	tilted condition
g	gas pressure (piston ring lubrication)
i	film inlet (EHL)
f	flooded condition (EHL)
mini	minimum film thickness during a cycle. (Piston ring lubrication).
max	maximum pressure

b	breadth of a bearing. Contact breadth of Hertzian contact.
Br	Offset of parabola
Cr	Crank ratio
$E_{1,2}$	Youngs modulus
h	film thickness
$\bar{h}$	film thickness at which $\frac{dp}{dx} = 0$
h_e	film thickness deposited on the outgoing surface
h_i	film thickness deposited on the incoming surface
Δh	difference betweeen inlet and minimum film thickness (inlet wedge height). Vertical deformation length of Hertzian contact
H_o	non-dimensional minimum film thickness = $\frac{h_o}{\Delta h}$

H_{ob}	$= \frac{h_o}{b}\sqrt{\frac{w}{\eta U}}$
ℓ	connecting rod length
n	revolution speed
p	pressure
P	non-dimensional pressure $= \frac{pb}{\eta U}\left(\frac{\Delta h}{b}\right)^2$
q	film flow quantity
r	crank radius
R_1, R_2	radius of curvature (EHL)
t	time
u	sliding velocity
U	non-dimensional sliding velocity $= \frac{\eta u}{w}\left(\frac{b}{\Delta h}\right)^2$
U_α	non-dimensional sliding velocity (EHL) $= \frac{\eta_o u \alpha}{b}\left(\frac{b}{\Delta h}\right)^2$
v	squeeze velocity
V	non-dimensional squeeze velocity $= \frac{v/\Delta h}{u/b}$
w	load per unit length
W	non-dimensional load $= \frac{w}{\eta u}\left(\frac{\Delta h}{b}\right)^2$
x	co-ordinate in the direction of sliding
X	non-dimensional co-ordinate $= \frac{x}{b}$
$\bar{x}$	co-ordinate position at which $\frac{dp}{dx} = 0$
x_e	position of centre of load
X_e	non-dimensional position of centre of load $= \frac{x_e}{b}$
α	viscosity pressure coefficient (EHL)
η	viscosity
θ	crank angle
λ	surface shape parameter of thrust bearings
$a_{1,2}$	poisson ratio

CHAPTER ONE

INTRODUCTION AND LITERATURE SURVEY

1.1 General View and Background of the Thesis

The substance of the thesis is about the behaviour of the piston ring in general. It covers curved tilting pad bearings, starved lubrication, dynamically (squeeze) loaded thrust bearings and piston ring lubrication. All of them are analysed in a unified manner, using consistent non-dimensional groups. Such an approach in solving the EHL problems is new and unknown in the literature and it may throw some light on EHL in general.

To fullfil assumed aims extensive work has been put into both the theoretical analysis and the experimental work. It mus be admitted that the new approach in solving the EHL problems requried intensive theoretical studies, therefore the major emphasis in this thesis is put rather on the theory than the experiment.

The beginning of this work started with the improvement of the experimental apparatus which has been developed in the Lubrication Laboratory at Imperial College (6). The rig has been successfully applied to the study of boundary lubrication under high repetition rate and slow sliding velocity. Nevertheless the apparatus has several drawbacks as following:

1. Stroke length cannot be measured and cannot be controlled.
2. Operating range is limited because of its structural vibration.
3. Accessibility of the test pieces in the apparatus is not so good as to allow convenient replacement of test pieces.
4. The power of the driving vibrator of the test specimens was more than enough for a normal test condition and too bulky.

How these drawbacks are remedied in the newly developed apparatus is described in Chapter Nine.

The concept of the apparatus including the original one is as follows:

1. Normal lubricated machine components rub each other repeatedly whether reciprocal or one directional. Thus it is desirable to reproduce the large number of repeated rubing cycles in the experimental rig.
2. It is desirable to control the total temperature of the rubbing surface including flash temperature if ever possible. But the theoretical flash temperature is proportional to the friction coefficient which varies depending on the rubbing condition. Thus it is considered to be better to avoid this flash temperature effect rather than including this uncontrollable effect.
3. In piston ring lubrication, normally most critical conditions occur at near top dead centre where sliding velocity is small and contact pressure is high.

As a natural consequence of this, "high repetition rate but slow sliding speed" reciprocating apparatus was developed (6) (7). Thus the project of this thesis was a continuation of the predecessor and much electronic instrumentation was incorporated.

At the final stage of the development of the new apparatus it was considered to be necessary to examine the theoretical hydrodynamic condition of the apparatus in order to find out the theoretical boundary between hydrodynamic lubrication and boundary lubrication.

A simple computer program which simulates reciprocating hydrodynamic lubrication was developed. In the theoretical formulation of the Reynolds equation new non-dimensional groups were introduced. When the numerical results were summarised by these non-dimensional groups it was found, to the author's surprise, that only two non-dimensional

parameters completely decide the hydrodynamic behaviour of thrust bearings under reciprocating mode, constant viscosity and load. It was found that this theoretical fact has not been published and also that the new non-dimensional groups introduced have not been used clearly in the published theory of thrust bearings. Thus it was decided to pursue the possible applicable range of the new non-dimensional groups. The final conclusion is that by this non-dimensional grouping it becomes possible to interpret several aspects of the hydrodynamic lubrication of thrust bearings in a unified manner. These will be discussed from Chapter Two to Chapter Eight.

In Chapter Nine and Ten the theoretical results of reciprocating hydrodynamic lubrication will be compared with the experimental results of the newly developed apparatus.

1.2 Literature Survey

1.2.1 Introduction

The purpose of lubrication is to separate two surfaces sliding past each other with a film of some material which can be so easily sheared that the shear force so produced is as small as possible, thus the possible damage of the surfaces is zero, or practically negligible and the energy loss caused by shear force and relative movement is minimum.

It is necessary to arrange wherever possible, that there is a lubricant film of sufficient thickness to ensure that no direct contact occurs between the opposing surfaces, thus eliminating wear; the lubricant viscosity and dimensions of the bearing surfaces can be so chosen to enable this to happen. This type of lubrication which occurs in most journal bearings and thrust bearings, is known as full fluid or hydro-

dynamic lubrication. The lubricant in practically every case is mineral oil because it can be so formulated with low production cost that it satisfies almost every requirement of practical purposes. In some cases emulsions, water, air, synthetic lubricant or even liquid sodium is employed where unusual requirements of operating conditions are imposed.

Historically it is of interest that it was only with the advent of accurately made metallic machine parts during the Industrial Revolution, and the increase of rotational speeds beyond those of the windmill and cart axle, that fully hydrodynamic lubrication became the normal type of lubrication and was consequently studied.

Dry or greasy lubrication, such as would be found in slow moving surfaces lubricated by natural fats or oils, received a lot of attention from quite early days. A number of very distinguished workers conducted experiments in friction. Among them Amontons and Coulomb both found that the frictional force required to move a body is proportional to the applied load, and has a constant coefficient; that is:

$$F = \mu N$$

where μ is called the friction coefficient.

Although the formula is simple this is not a fundamental law. The more careful attention is placed on the experiment to measure μ, the more erratic behaviour is observed. This is because μ is affected by the smoothness or hardness of the surfaces, dirt, oxide or other foreign matter. At the present time, in fact, it is impossible even to estimate the coefficient of the friction between two substances from their physical properties, though excellent work has been carried out (1) (2) (3). Thus the fundamental law of friction still is not clearly

understood in spite of the enormous engineering value of an accurate analysis. Almost every study on this being carried out now is a "trial and error" type for practical purposes and categorised as "boundary lubrication".

In comparison to boundary lubrication, hydrodynamic lubrication is more clearly understood as normally, only the viscosity of the lubricant is the physical property of importance. Fundamental theory of hydrodynamic lubrication was completed by Reynolds who analysed the experimental results of high pressure generation of a railway bearing conducted by B. Tower. He showed that the converging, wedge-shaped film was necessary to generate an oil film pressure. Although the procedure was laborious he obtained the solution of infinitely long journal bearing under the correct boundary conditions which were subsequently known as "Reynolds condition". This famous paper is the foundation on which all subsequent lubrication theory is based. About twenty years later another famous paper on journal bearings appeared by Sommerfeld. He gave the analytical solution of infinitely long journal bearing lubrication in a surprisingly simple formula using an ingeneous integration of the equation. The reason of its simplicity is that he applied the boundary condition which neglected the effect of cavitation of the oil under negative pressure which subsequently became known as "Sommerfeld condition". In his theoretical formulae he used a non-dimensional quantity which is now called Sommerfeld number and showed that the Sommerfeld number is solely a function of the eccentricity ratio of the bearing which is also non-dimensional. That is

$$\Delta = f(\varepsilon)$$

where

$$\Delta = \frac{W/L}{U\eta}\frac{C^2}{R^2} \quad : \quad \text{Sommerfeld number}$$

W = total load

L = axial length

U = surface speed

η = viscosity

C = radial clearance

R = bearing radius

ε = eccentricity ratio

As the Sommerfeld number is decided by design geometries and operating condition and the eccentricity ratio the parameter can be used as a similarity quantity for every infinitely long journal bearing. Thus this expression is used for almost all analytical and experimental studies on journal bearings.

For finite length bearings the aspect ratio L/R must be included. and for other additionally complex cases, i.e. dynamically loaded condition or turbulent lubrication, another non-dimensional quantity must be included. But essentially the fact that Sommerfeld number is a decisive parameter which represents the bearing condition is the same.

The scientific analysis of thrust bearings started some years later than that of journal bearings. It was not until Michell published his celebrated work in 1905 that the theoretical analysis of them really began. From then the performances of thrust bearings have been analysed by the non-dimensional terms $\frac{\eta U}{W/L}$ and $\frac{h_1}{h_o}$, where h_o is the (minimum) outlet film thickness and h_1 the (maximum) inlet film thickness, the others are the same as journal bearings. The term $\frac{\eta u}{W/L}$

is usually multiplied by the square of a (bearing breadth/film thickness) ratio but there is no accepted convention. In some cases h_1/h_o is replaced by $(h_1 - h_o)/h_o$, or for sector-shaped pads, thrust factor T, be

$$T = \frac{\eta N}{p} \left(\frac{L}{b}\right)^2 , \quad b = h_1 - h_o$$

is used.

When discs or parabolas are analysed

$$W^* = \frac{W h_o}{U\eta LR}$$

is used.

Thus it is somewhat of a puzzle why there is no accepted convention of non-dimensional forms for thrust bearings in contrast to those of journal bearings. The parameter $\frac{W/L}{\eta U} \frac{h_o^2}{B^2}$ is most frequently used because it looks similar to Sommerfeld number. But the meanings of them are completely different in the sense that Sommerfeld number can be defined solely by independent quantities but the parameter $\frac{W/L}{\eta U} \frac{h_o^2}{B^2}$ can not, as it contains the dependent quantity h_o.

As all lubrication theory of thrust bearings must be based on the same basic Reynolds equation, there cannot be much difference in the non-dimensional expressions of thrust bearings..

This question has never been taken up before seriously and is the main reason for this theoretical part.

Between the two lubrication modes, hydrodynamic lubrication and boundary lubrication, there exists another lubrication mode. This is called elastohydrodynamic lubrication (EHL) and extensively

studied by Dowson (26) et al theoretically. The theory itself is near completion except the theory of EHL traction. In this mode of lubrication hydrodynamic pressure generated affects the viscosity of lubricant or changes the shape of hydrodynamic fluid passage elastically. Thus the hydrodynamic equation must be modified. This interference of elasticity and viscosity with hydrodynamic condition makes the analysis extremely complex. Analytical treatment is only possible under certain approximate assumptions. Fortunately certain simplifying assumptions can be applied for most cases of practical importance, i.e. gears or roller bearings. This will be briefly discussed in the thesis in relation to starvation.

1.2.2 Brief Survey on the Study of Piston Ring Lubrication

Few analyses of piston ring lubrication are recorded between the invention of the piston ring in 1854 by Ramsbottom and the work of Castleman in 1937 (8). The latter recognized the occurence of oil films many times thicker than boundary oil layers. Since then piston ring lubrication has been studied experimentally and theoretically by several authors.

Eilon and Saunders (9) carried out the theoretical analysis with parabolic approximation of the ring face profile and took into account only the wedge action of the film. Lloyd (10) included the squeeze action of the film into his theoretical analysis, however, there was a problem of boundary condition that the negative pressure of the film was taken into account. Furuhama (11) in his series of papers avoided the problem of boundary condition by approximating the ring face profile by two parabolics connected by straight lines at its middle. Thus, he could put an outlet boundary pressure at the point where the film started to diverge. More recently Ting (12)

treated the problem more simply by specifying the outlet boundary pressure at the minimum film thickness point. Allen et al (13) in their comprehensive computer program which takes into account the thermal and elastical distortion of a piston, piston axis tilt etc. applied the so called full Sommerfeld condition and discarded the negactive pressure for the calculation of load carrying capacity of the film. Wakuri et al (14) in his theoretical and experimental study idealised the piston ring lubrication by approximating the ring profile with a symmetric parabola. In their theoretical analysis they applied the Reynolds condition on the film outlet boundary condition. They concluded that the theoretical solution under Reynolds condition agreed with the experimental results.

The theoretical treatments of the hydrodynamic lubrication especially boundary conditions have been briefly reviewed above. It has been shown that there is no accepted convention of the film outlet boundary condition. Whatever the boundary condition in theoretical analysis, it must be imperative to examine how approximate the theoretical model is to the physical situation. However no published study on this is found. In Chapter Seven this will be discussed in detail.

Whether theoretical or experimental, the results must be presented numerically or graphically. The most accepted convention is to present the results in actual physical quantities. Thus there is no accepted convention of non-dimensional groups. Baker et al (15) analysed the oil transport by piston rings and showed non-dimensional functions which represent the comparability of two cycle engine piston rings irrespective of engine cylinder scale. But the physical mechanism of their non-dimensional functions was not shown.

The study on piston ring lubrication must be related to practical problems, otherwise it is of no importance. Main practical problems of piston ring lubrication are piston ring scuffing and oil consumptions. Excellent field survey was conducted by Neal (16). He surveyed a large number of field experience and treated the scuffing problem as a scale model related to other engine performances, oil consumption and wear rate.

Despite its practical importance the mechanism of scuffing is not clearly understood. Several mechanisms have been proposed, but none has been persuasive enough to be accepted as a universal design criteria of scuffing. This present state of ignorance of the scuffing was excellently reviewed by Dyson (17). Thus the state of ignorance reflects all the studies carried out on piston ring scuffing. This is most symbolically reflected in the "definition" of scuffing by the Institution of Mechanical Engineers (18). That is

"Gross damage characterised by the formation of local welds between sliding surfaces".

This is not a definition but an observation of scuffing.

One of the most comprehensive experimental studies on piston ring scuffing was carried out by Willen et al (19) (20). They correlated the results of scuffing tests between experimental rig and actual engine by a correlating factor $PV^{7/16}$. Considering the complexity of the phenomenon the correlation was good. This suggests a possible line of investigation on scuffing by the use of flash temperature concept as $PV^{7/16}$ should somehow be related to the flash temperature of the sliding contacts.

Flash temperature concept (21) was proposed by Blok in 1937 (22) and extensively reviewed in 1969 (23). This concept is the only practical design criteria which has been mainly applied on scuffing of gears lubricated by plain mineral oil. Although this has been applied on the study of scuffing of concentrated contacts, this has not been applied on the study of piston ring scuffing.

Oil consumption is also a problem of practical importance as well as scuffing. Scuffing has been studied more than this problem, as too much consumption is not a destructive problem in an actual engine. Oil consumption is sometimes related to piston ring scuffing, as the effort to reduce the oil consumption frequently raises the problem of piston ring scuffing (16). Oil consumption of piston rings was studied by Wakuri (24) and Dykes (25) experimentally and theoretically. They gave a qualitative discussion on the mechanism of oil consumption of engines.

It was found in the brief literature survey on piston ring lubrication that there existed a big gap between theory and experiment or practice. One main purpose of this thesis is to try to narrow this gap by introducing a new non-dimensional grouping which greatly simplifies the theoretical analysis of piston ring hydrodynamic lubrication.

1.2.3 Conclusion of the Literature Survey

Conclusions of the literature survey which lead to this thesis are as follows.

1. No satisfactory non-dimensional expressions which are free from dependent variables were found in the analysis of thrust bearings

under steady conditions.

2. No one has managed to express the numerical results of hydrodynamic lubrication of piston ring in a general form.
3. Although there are three different boundary conditions in the theoretical analysis of hydrodynamic lubrication of piston rings, no published study was found which compared their differences quantatively.

CHAPTER TWO

GENERAL SOLUTION OF ONE DIMENSIONAL REYNOLDS EQUATIONS

2.1 Introduction

Although "general" solution of one dimensional Reynolds equation can be found in standard text books of lubrication it is not general in the sense that the general solution given is usually presented using two non-dimensional parameters both of which include a dependent variable h_o; minimum film thickness. Thus, in order to find h_o under certain operating conditions iterative procedure is needed.

Analytical procedures for different surface shape bearings are also different depending on the function which expresses the surface shape. Thus there is no general analysis of the hydrodynamic lubrication of different surface shapes and the analysis is, in fact, case by case analysis for different surface shapes (4) (5) (27).

The reason for this has been found that the conventional non-dimensional groups do not correctly represent the physical condition expressed by the Reynolds equation. Thus new non-dimensional groups will be introduced in this chapter and "general" solution of hydrodynamic lubrication of infinitely long thrust bearings will be presented. The results will be applied on several fixed surface shape thrust bearings in the following section.

2.2 General Solution of Reynolds Equation for Infinitely Long Thrust Bearings

Hydrodynamic pressure equation of film lubrication for a pad separated by a variable film thickness h against position x and time t from a plane surface moving with velocity u is given by Reynolds as

$$\frac{\partial}{\partial x}\left(h^3\frac{\partial p}{\partial x}\right) + \frac{\partial}{\partial y}\left(h^3\frac{\partial p}{\partial y}\right) = 6\eta u\frac{\partial h}{\partial x} + 12\eta\frac{\partial h}{\partial t} \qquad (2.1)$$

when assumptions as following are given

1. Flow is isoviscous and one dimensional
2. Squeeze term $\frac{\partial h}{\partial t}$ is constant against x, i.e., no tilting motion, thus writing $\frac{\partial h}{\partial t} = v$

The equation (2-1) reduces to

$$\frac{d}{dx}\left(h^3\frac{dp}{dx}\right) = 6\eta u\frac{dh}{dx} + 12\eta v \qquad (2.2)$$

When the surface shape h is given as a function of x, the integration of the equation is

$$\frac{dp}{dx} = 6\eta u\frac{h(x) - h(\bar{x})}{h(x)^3} + 12\eta v\frac{x - \bar{x}}{h(x)^3} \qquad (2.3)$$

Where $\bar{x}$ is an integral constant which must be defined by boundary conditions as

$$\frac{dp}{dx} = 0 \text{ at } x = \bar{x}$$

$$\text{or at } h = \bar{h} = h(\bar{x})$$

Referring to Figure 2.1, supposing the bearing surface shape is given as a function of co-ordinate x as hp(x), the equation (2.3) becomes

$$\frac{dp}{dx} = 6\eta u \frac{hp(x) - hp(\bar{x})}{\{h_o + hp(x)\}^3} + 12\eta V \frac{x - \bar{x}}{\{h_o + hp(x)\}^3} \qquad (2.4)$$

The equation (2.4) can be non-dimensional as follows

$X = \frac{x}{b}$, $\bar{X} = \frac{\bar{x}}{b}$ b is defined in page 30.

$$Hp(X) = \frac{hp(x)}{\Delta h} = \frac{hp(bX)}{\Delta h}$$

$$H_o = \frac{h_o}{\Delta h}$$

Then the equation becomes

$$\frac{dp}{dx} = 6\frac{\eta u}{\Delta h^2} \frac{Hp(X) - Hp(\bar{X})}{\{H_o + Hp(X)\}^3} + 12\frac{\eta v}{\Delta h^2} \frac{b}{\Delta h} \frac{X - \bar{X}}{\{H_o + Hp(X)\}^3} \qquad (2.5)$$

When $u \neq 0$ squeeze velocity can be non-dimensionalised by u,

$$V = \frac{v}{u}\frac{b}{\Delta h} = \frac{v}{\Delta h} / \frac{u}{b} \qquad (2.6)$$

Now the complete non-dimensionalisation is possible

$$\frac{dP}{dX} = 6 \frac{Hp(X) - Hp(\bar{X})}{\{H_o + Hp(X)\}^3} + 12V \frac{X - \bar{X}}{\{H_o + Hp(X)\}^3} \qquad (2.7)$$

where

$$P = \frac{pb}{\eta u} \left(\frac{\Delta h}{b}\right)^2$$

Integration of the equation gives non-dimensional pressure distribution.

$$P = 6 \int_{0}^{X} \frac{Hp(X) - Hp(\bar{X})}{\{H_o + Hp(X)\}^3} dX + 12V \int_{0}^{X} \frac{X - \bar{X}}{\{H_o + Hp(X)\}^3} dX \qquad (2.8)$$

Integral constant $\bar{X}$ is given as

$P = 0$ at $X = 0$ (full Sommerfeld condition)

or, $P = 0$ at $\frac{dP}{dX} = 0$ at $X = \bar{X}$ (Reynolds condition)

Whichever the boundary condition, $\bar{X}$ is given as a function of H_o and V only for a given bearing surface shape Hp(X), as the left hand side of the equation is zero.

Integration of the equation (2.8) gives the load carrying capacity w of the bearing.

As

$$p = P \frac{\eta u}{b} \left(\frac{b}{\Delta h}\right)^2$$

$$w = \frac{\eta u}{b} \left(\frac{b}{\Delta h}\right)^2 \int_{X_{out}}^{1} P dx = \eta u \left(\frac{b}{\Delta h}\right)^2 \int_{X_{out}}^{1} P dX$$

where

$$X_{out} = \frac{x_{out}}{b}$$

and $X_{out} = 0$ (full Sommerfeld condition)

$X_{out} = \bar{X}$ (Reynolds condition)

Writing $W = \frac{w}{\eta u}\left(\frac{\Delta h}{b}\right)^2$, the non-dimensional load carrying capacity is given as follows

$$W = 6\int_{X_{out}}^{1}\int_{0}^{X}\frac{Hp(X) - Hp(\overline{X})}{\{H_o + Hp(X)\}^3}\,dX\,dX$$

$$+ 12V\int_{X_{out}}^{1}\int_{0}^{X}\frac{X - \overline{X}}{\{H_o + Hp(X)\}^3}\,dX\,dX \qquad (2.9)$$

As $\overline{X}$ and X_{out} is given by the boundary condition as a function of H_o and V only the right hand side of the equation is also a function of H_o and V only for a given bearing surface shape Hp(X). The conclusion of this analysis is:

For a given bearing surface shape the non-dimensional load carrying capacity of the bearing W is a function of non-dimensional film thickness H_o and squeeze velocity V only. The function which relates these parameters is decided by the non-dimensional surface shape function Hp(X).

Thus,

$$W = f_w(H_o, V) \qquad (2.10)$$

When the condition is steady, i.e. V = 0

$$W = f_w(H_o) \qquad (2.11)$$

As W is defined by overall bearing geometries Δh and b, and

operating conditions w, η, u, which are all independent variables, unified comparison of film thickness for different bearing shapes becomes possible. This does not cause any inconvenience that the non-dimensional parameter includes the unknown value h_o, pointed out before.

Mention must be given on the method of non-dimensionalisation of co-ordinates. In the foregoing analysis no limitation was imposed on the reference dimensions Δh and b. Thus b, for example, should not necessarily be total bearing breadth. Any convenient dimension which represents the horizontal dimension of the bearing can be used as a reference dimension. This is also the case for Δh.

2.3 Comparison of the Non-dimensional Parameter with Sommerfeld Number

From the theory of the infinitely long journal bearing, the Sommerfeld number Δ is only a function of eccentricity ratio (4).

$$\Delta = f(\varepsilon) \tag{2.12}$$

Explanation of the parameters were already given in Chapter One.

If the journal bearing film thickness is unwrapped as shown in Figure 2.2, the journal bearing can be analysed as a thrust bearing. Referring to Figure 2.2, the notations of equation (2.11) can be changed as follows

$$H_o = \frac{h_o}{\Delta h} = \frac{(1 - \varepsilon)c}{\varepsilon c} = \frac{1 - \varepsilon}{\varepsilon}$$

$$W = \frac{w}{\eta u} \left(\frac{\Delta h}{b}\right)^2 = \frac{\varepsilon}{2\pi} \frac{w}{\eta u} \left(\frac{C}{R}\right)^2$$

Then the equation (2.11) becomes

$$\frac{\varepsilon}{2\pi} \frac{w}{\eta u} \left(\frac{C}{R}\right)^2 = f_w \left(\frac{1 - \varepsilon}{\varepsilon}\right)$$

Rearranging

$$\frac{w}{\eta u} \left(\frac{C}{R}\right)^2 = 2\pi \frac{1}{\varepsilon} f_w \left(\frac{1 - \varepsilon}{\varepsilon}\right) \qquad (2.13)$$

The left hand side of the equation is the Sommerfeld number and the right hand side is a function of ε only. Thus the equation (2.11) has the same meaning as equation (2.12). The effects of curvature of the journal bearing should only modify the shape of the function.

Thus the parameter W has the same physical meaning as the Sommerfeld number. The reciprocal of W can be used in a similar manner as Sommerfeld reciprocal (4).

2.4 Comparison of Film Thickness for Different Surface Shape Bearings. (Steady State).

As shown by the equation (2.11) the non-dimensional film thickness $H_o = \frac{h_o}{\Delta h}$ is a function of non-dimensional load $W = \frac{w}{\eta u}\left(\frac{\Delta h}{b}\right)^2$ only. But Δh is usually a design variable in the sense that Δh should be optimized to give a maximum film thickness for a given overall bearing geometry b. Thus it is convenient to normalise the film thickness by b. This can easily be achieved as follows

$$H_{ob} = \frac{h_o}{b} \sqrt{\frac{w}{\eta u}} = H_o W^{\frac{1}{2}} \qquad (2.14)$$

Thus the film thickness can be compared for different bearing surface shapes in terms of H_o or H_{ob} for a given operating condition W. In the following section the reciprocal of W is preferred, that is

$$\left.\begin{aligned} U &= \frac{nu}{w}\left(\frac{b}{\Delta h}\right)^2 \\ \text{and}\quad H_{ob} &= H_o\, U^{-\frac{1}{2}} \end{aligned}\right\} \qquad (2.15)$$

U is called non-dimensional sliding velocity as it is proportional to actual sliding velocity.

2.4.1 Taper Land Bearing

Referring to Figure 2.3, same procedure as given in reference (4) gives the equation as follows

$$\frac{W}{6} = \lambda^2\left\{\ell n\left(1 + \frac{1}{H_o}\right) - \frac{2H_o + 3}{2(H_o + 1)^2} - \bar{X}\,\frac{1}{2H_o(H_o + 1)^2}\right\} + (1 - \lambda^2)\,\frac{\bar{X}}{2H_o^3}$$

where

$$\bar{X} = \frac{\lambda H_o^2}{\lambda H_o(2H_o + 1) + 2(\lambda - 1)(H_o + 1)^2} \qquad (2.16)$$

When $\lambda = 1$ the formulae for inclined pad bearing can be obtained.

The equation (4.9) is calculated and results are shown in figure 2.5.

In the figure the relationship between non-dimensional film thickness H_o and non-dimensional sliding velocity U for different value of λ are plotted. The scale of H_{ob} is also included in the figure as an inclined scale, because the relationship between these

parameters, $H_o = H_{ob} \cdot U^{\frac{1}{2}}$ is expressed as straight lines with gradient $\frac{1}{2}$ in the log-log scale. The lines for the values of λ of 0.6, 0.7 and 0.9 are so close that they are not shown in the figure. They lie between the lines of λ = 0.5 and 1.0.

Upper table is the numerical value of each parameter which gives the maximum H_{ob} for several values of λ. It is also shown that the maximum load carrying capacity occurs when $H_o \approx 0.8$, and $\lambda = 0.8$, at which point $H_{ob} = 0.4385$. When these values are converted to commonly used parameters the same values will be obtained as given in reference (4).

The optimum design value of Δh can be obtained from the values of H_o and H_{ob} given in the table as following

$$\frac{\Delta h}{b} = \frac{H_{ob}}{H_o} \sqrt{\frac{\eta u}{w}} \qquad (2.17)$$

Thus the optimum design value Δh is a function of non-dimensional operating condition $\frac{\eta u}{w}$ and the reciprocal of this is often called as a duty parameter.

The advantage of these non-dimensional over conventional expressions are clear. U is only a function of operating condition and bearing design geometry and does not contain unknown values. Thus U directly gives film thickness H_o or H_{ob} and vice versa. This direct estimation of film thickness can never be achieved by conventional non-dimensional expressions, because both ordinates contain unknown film thickness h_o.

From the figure a few commonly known facts about thrust bearing theory can be directly observed.

. The lines for the values of $\lambda = 0.5 \sim 1.0$ are very close together,

which means the performance of thrust bearings is not significantly affected by the shape of the surface.

The values of H_{ob} do not change so much around the value of $H_o = 1.0$, which means that as long as the ratio of inlet and outlet film thickness is chosen near 2.0 the performance of the thrust bearing is not far from the optimum condition.

2.4.2 Stepped Pads. Rayleigh Step

Lord Rayleigh (28) investigated analytically the optimum surface shape of bearing to carry the maximum possible load for a given bearing breadth. Using the calculus of variations, he obtained a step-shaped film, known subsequently as the Rayleigh Step, which is shown in Figure 2.4. The equation of the load carrying capacity of this can be obtained from the reference (4) by changing the notations as follows.

$$U = W^{-1} = \frac{(1 - \lambda)(H_o + 1)^3 + \lambda H_o^3}{3\lambda(1 - \lambda)} \qquad (2.18)$$

The equation is calculated and plotted in Figure 2.7. The explanation of the figure is exactly the same as that of the taper land bearing.

Maximum load carrying capacity is when $\lambda = 0.7183(0.7212)$, $H_o = 1.1546(1.1494)$, $H_{ob} = 0.4542(0.45416)$, $U = 6.4628$. The values in the bracket are calculated from figures given by the reference (4). Although H_{ob} agrees in four significant figures there is slight difference in other two values. The values given in the table are the results of numerical calculation step of 10^{-6} for the value of H_o and 10^{-4} for the value of λ.

The advantage of this non-dimensional expression is obvious again. Although the infinitely long Rayleigh Step bearing considered here gives the maximum attainable film thickness value $H_{ob} = 0.4542$, which is 11.3% bigger than that of inclined pad, and 3.6% bigger than that of optimized taper land bearing, at slow speed (or under high load) the reduction of film thickness is drastic for the Rayleigh Step. This is the so called stalled condition of the Rayleigh Step bearing at which minimum film thickness is zero. This stalled condition does not occur in other convergent surface shape bearings.

The formula of load carrying capacity of the stalled Rayleigh Step bearing can simply be obtained from the equation (2.18) as an asymptotic solution.

At stall $H_o = 0$ then the equation gives

$$U_s = W_s^{-1} = \frac{1}{3\lambda}$$

or $$W_s = 3\lambda \qquad (2.19)$$

Thus the advantage and disadvantage of Rayleigh Step bearing against taper land bearing becomes clear.

2.4.3 Partial Parabolic Bearing

In order to complete the comparison, a bearing which has a surface shape of parabola connected to a straight line as shown in Figure 2.5 is analysed.

As no published formula was found for this, the equation must be found from the Reynolds equation. From equation (2.8) under steady state condition

$$P = 6 \int_{0}^{X} \frac{H_p(X) - H_p(\bar{X})}{\{H_o + H_p(X)\}^3} \, dX \tag{2.20}$$

When the co-ordinates as shown in the figure are used the surface function of the parabola $H_p(X) = X^2$, where $X = \frac{x}{\lambda b}$. Then the equation for the parabolic part is

$$\frac{(P - P_o)(\lambda b)}{\eta u} \left(\frac{\Delta h}{\lambda b}\right)^2 = \frac{(P - P_o)b}{\eta u} \left(\frac{\Delta h}{b}\right)^2 \frac{1}{\lambda}$$

$$= 6 \int_{0}^{X} \left\{\frac{1}{(H_p + X^2)^2} - \frac{H_o + \bar{X}^2}{(H_o + X^2)^3}\right\} dX$$

$$= 6 \{\alpha(X,0) - (H_o + \bar{X}^2)\gamma(X,0)\} \tag{2.21}$$

where $\alpha(X,0)$ and $\gamma(X,0)$ are the integral functions of each term and are shown in Chapter Three.

Then for the straight part using λb as a reference breadth.

$$\frac{Pb}{\eta u} \left(\frac{\Delta h}{b}\right)^2 \frac{1}{\lambda} = 6 \int_{-X^2}^{X} \frac{H_o - \bar{H}}{H_o^3} \, dX = 6 \frac{-\bar{X}^2}{H_o^3} (X + X_2) \tag{2.22}$$

where $X_2 = (1 - \lambda)/\lambda$

Integral constant $\bar{X}$ can be obtained by equating the pressure po at X = 0. From equation (4.21) applying the boundary condition that p = 0 at the inlet (X = 1)

$$-\frac{po}{\eta u} \left(\frac{\Delta h}{b}\right)^2 \frac{1}{\lambda} = 6 \{\alpha(1,0) - (H_o + \bar{X}^2)\gamma(1,0) \tag{2.23}$$

For the straight part Po can be directly obtained by putting X = 0. Thus equating

$$-\frac{1}{\lambda}\ \frac{P_{o_b}}{\eta u}\ (\frac{\Delta h}{b})^2 \quad \frac{1-\lambda}{\lambda}\ \frac{\overline{X}^2}{H_o^3} = 6\ \{\alpha(1,0) - (H_o + \overline{X}^2)\gamma(1,0)\} \tag{2.24}$$

This is solved as

$$\overline{X}^2 = \frac{\lambda H_o^3\ \{\alpha(1,0) - H_o\gamma(1,0)\}}{(1-\lambda) + \lambda H_o^3\gamma(1,0)} \tag{2.25}$$

Then the load carrying capacity can be obtained by integrating the pressure for both parts. As P_o is given by the equation (2.24). For the parabolic part

$$w_p = \frac{\eta u}{b}\ (\frac{b}{\Delta h})^2 \lambda \int_o^{\lambda b} 6\{\alpha(X,0 - (H_o + \overline{X}^2)\gamma(X,0)\}\ dx + \int_o^{\lambda b} P_o dx$$

Then non-dimensional load capacity is

$$W_p = \frac{w_p}{\eta u}\ (\frac{\Delta h}{b})^2 = 6\lambda^2\ \{\alpha_i(1,0) - (H_o + \overline{X}^2)\gamma_i(1,0)\} - 6\lambda(1-\lambda)\ \frac{\overline{X}^2}{H_o^3} \tag{2.26}$$

Where α_i and γ_i as integral function of α and γ are given in Chapter Three.

For the straight part, considering linear pressure distribution,

$$w_s = \frac{P_o(1 - \lambda)b}{2} = -(1 - \lambda)^2 . 3\eta u . (\frac{b}{\Delta h})^2 \frac{\bar{X}^2}{H_o^3}$$

Then non-dimensionally

$$W_s = \frac{w_s}{\eta u} (\frac{\Delta h}{b})^2 = -3(3 - \lambda)^2 \frac{\bar{X}^2}{H_o^3} \qquad (2.27)$$

The negative sign is caused by the co-ordinate being so chosen that u is negative, so W_p is also negative. Thus the total load carrying capacity of the bearing is the sum of the two parts

$$W = 6\lambda^2 \{\alpha_i(1,0) - (H_o + \bar{X}^2)\gamma_i(1,0)\} - 6\lambda(1 - \lambda) \frac{\bar{X}^2}{H_o^3} - 3(1 - \lambda)^2 \frac{\bar{X}^2}{H_o^3} \qquad (2.28)$$

As $\bar{X}^2$ is given by the equation (2.25), the equation (2.28) gives the non-dimensional load carrying capacity of the partial parabolic bearing. Calculated results of the equation are plotted in Figure 2.8. The similar trend as with the taper land bearing can be observed. When $\lambda = 1$ the curve is the solution of a symmetric parabola under half Sommerfeld condition, or simply the solution of a half parabola.

2.4.4 Comparison of Different Surface Shape Bearings

Three different surface shape bearings were analysed. The optimum values of parameters of them which give the maximum H_{ob} are summarised in Table 2.1.

It is shown that the differences of the maximum H_{ob} for different bearings are small, less than 10%. And the values of H_o for three bearings are near one.

This was the conclusion of Lord Rayleigh that there is little to choose between various forms of bearings, given the value of inlet and outlet film thickness ratio is near two. The other conclusion was than concave surface shape gives the maximum load carrying capacity for a given bearing breadth. This is shown in the table that the values of H_{ob} is the largest for the Rayleigh step and smallest for the partial parabola.

When the performances of these three optimized bearings are shown in the same graph almost the same performances will be obtained, except stalled condition of Rayleigh step. Thus the Rayleigh step bearing should be avoided for the application which requires a wide range of operating condition, in spite of its maximum attainable film thickness.

2.5 Discussion

Using the non-dimensional expressions proposed, three different surface shape bearings were analysed and the performance was compared in a same scale quantitatively. This quantative comparison in the same scale has never been carried out before. This is because there has never been an accepted convention of the non-dimensional expression. The normalisation of the film thickness among the published papers has been done using the different methods, i.e. inlet outlet film thickness ratio, reciprocal of H_o radius of curvature of the surface etc. Thus the unified comparison of the performance of different surface shape thrust bearings was practically impossible. Thus all the standard lubrication text books stop at the point where it gives the qualitative description that there is little difference between different surface shapes for a given inlet and outlet film thickness ratio.

Advantages of the non-dimensional expression shown in this text over the conventional expression can be emphasised from another point of view.

One of the conventional expressions is to use inlet and outlet film thickness ratio, $1 + \frac{\Delta h}{h_o}$ in the notation of this text, against "load factor", $H_{ob} = \frac{w}{\eta u} \frac{h_o^2}{b^2}$. As already shown the value of H_{ob} has it maximum at around the value of $\frac{h_o}{\Delta h} = 1$. Thus the curve decreases for both directions. This gives a rather misleading impression as if there exists a theoretical inherent disadvantage of instability for the fixed geometry thrust bearings (4). As the film thickness gets smaller, $1 + \frac{\Delta h}{h_o}$ increases, the "load carrying capacity" $\frac{w}{\eta u} \frac{h_o^2}{b^2}$ decreases thus the bearing is "unstable".

This is not true because "load factor" $\frac{w}{\eta u} \frac{h_o^2}{b^2}$ includes the film thickness h_o squared thus for the bearing to be unstable, the "load factor" must decrease more than square of the film thickness. This condition never occurs and the truth can be found by the presented graphs. When the abscissa is converted to "true" load factor $W = U^{-1} = \frac{w}{\eta u} (\frac{b}{\Delta h})^2$, this is achieved by symmetrically reversing the curves about the value of U = 1.0. Then the results are monotonic increases of load w, as all the other quantities are constant, against decrease of film thickness h_o for all shape analysed bearings. Thus the considered bearings are always stable.

All the advantages of the presented non-dimensional expressions comes from the "correct" interpretation of the Reynolds equation as shown in the section of general solution of Reynolds equation. This can easily be expanded to include the effects of reciprocating motion or squeeze effects as shown before. It can also be expanded to include the effect of inlet oil starvation, which will be discussed later, or to include the tilting effects of thrust bearings, which will also be

discussed in the next Chapter.

Before finalising this discussion mention must be given to the curves of small values of λ which are included for the taper land and partial parabolic bearings. The reason is to point out the facts that the reduction of the value of H_{ob} is not significant for a small value of λ. Even when the inlet convergent zone is one percent of the total bearing breadth, the maximum attainable film thickness H_{ob} is about 10% of optimum condition. This indicates the possible important role of corner chamfer or corner round off of a tilting pad bearings, as it has no positive convergent zone for its starting condition.

It might be possible to reduce wear of tilting pad bearings by fully utilising this theoretical fact,particularly when its operation is intermittent.

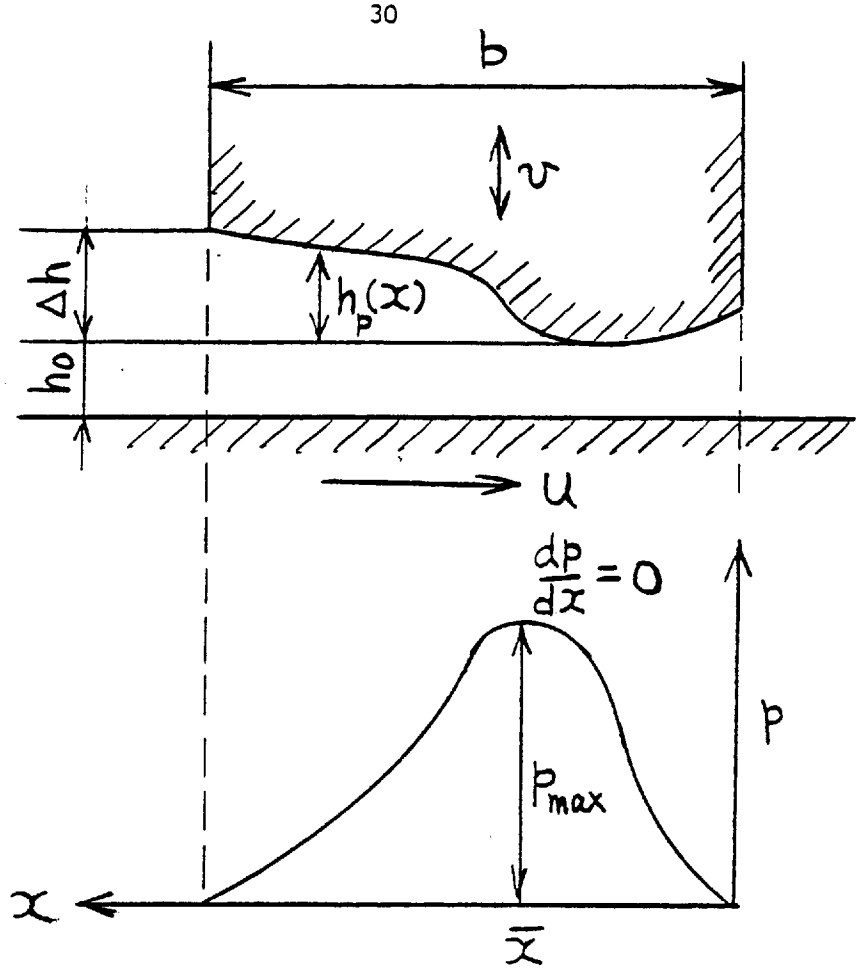


Figure 2.1 Pressure in a Slider

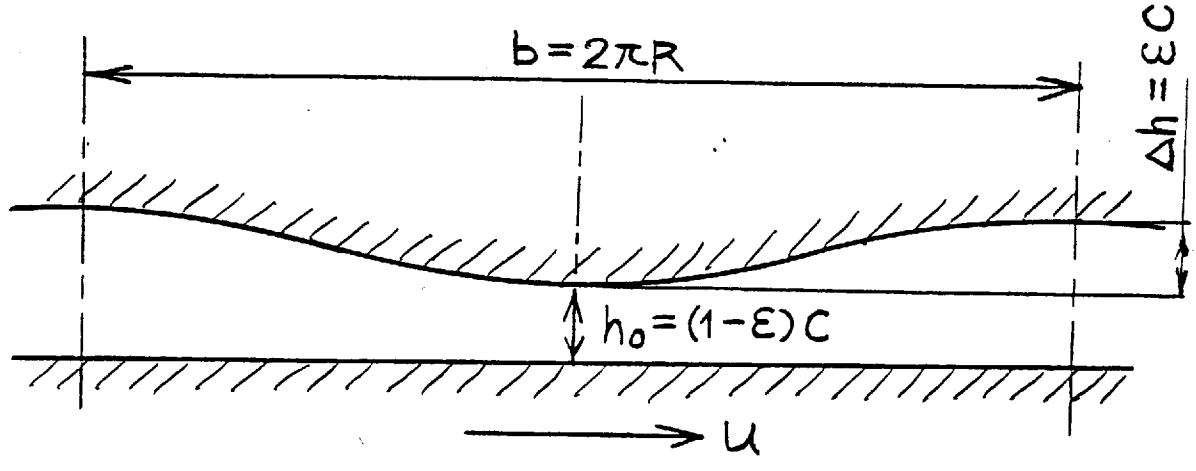


Figure 2.2 Unwrapped Oil Film Thickness of a Journal Bearing

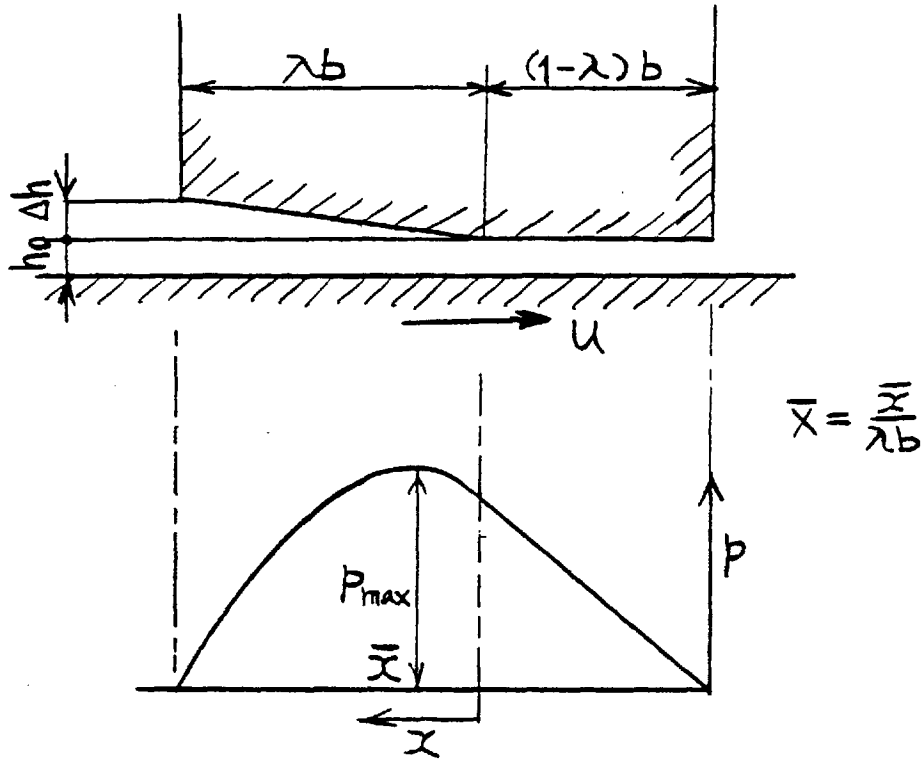


Figure 2.3 Taper Land Bearing

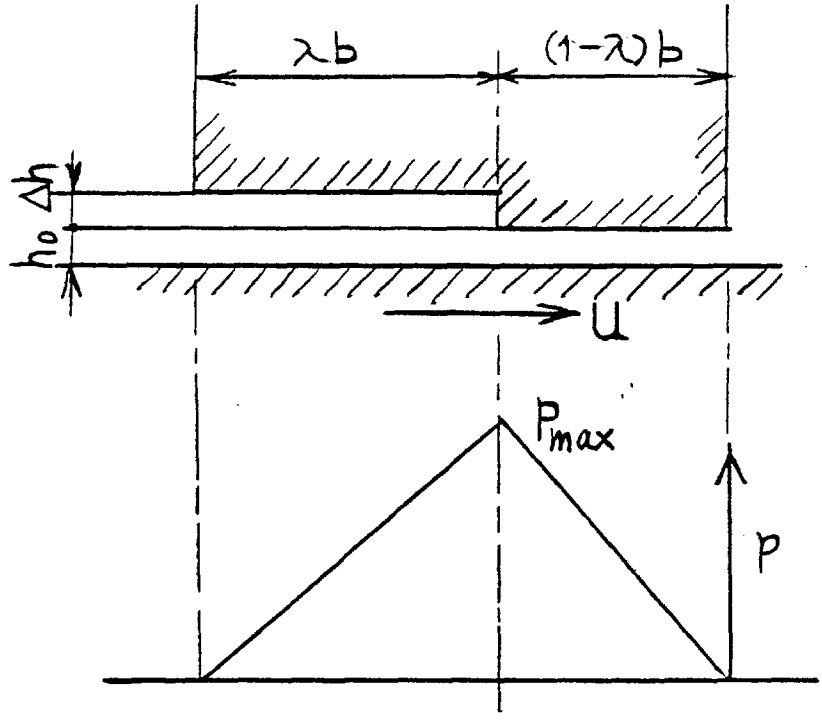


Figure 2.4 Rayleigh Step Bearing

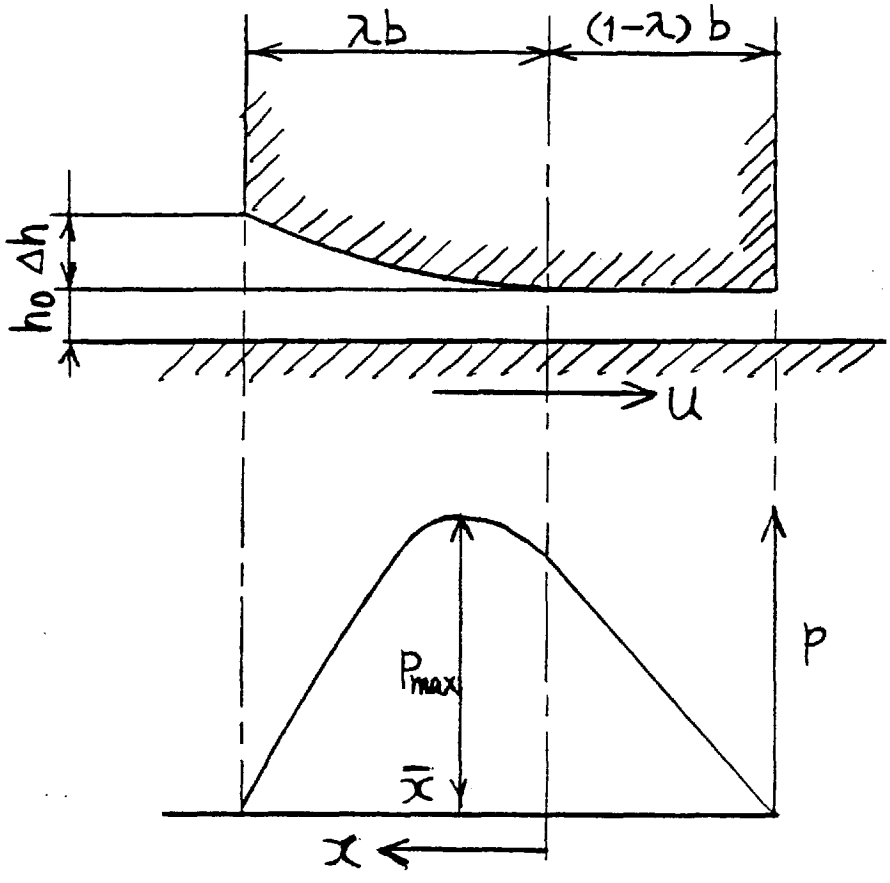


Figure 2.5 Partial Parabolic Bearing

	λ	Hob	Ho	U
RAYLEIGH STEP	0.7183	0.4542	1.1546	6.463
TAPER LAND	0.8025	0.4385	0.8060	3.378
PARTIAL PARABOLA	0.9473	0.4223	0.6984	2.735

Table 2.1 Comparison of Optimized Designs

λ	1.0	0.9	0.8025	0.8	0.7	0.5	0.1
H_{ob}	0.4003	0.4310	0.4385	0.4385	0.4323	0.3923	0.1908
H_o	0.8412	0.7855	0.8052	0.8060	0.8378	0.8987	0.9850
U	4.416	3.321	3.371	3.3780	3.756	5.249	26.66

Numerical Values for Maximum H_{ob}

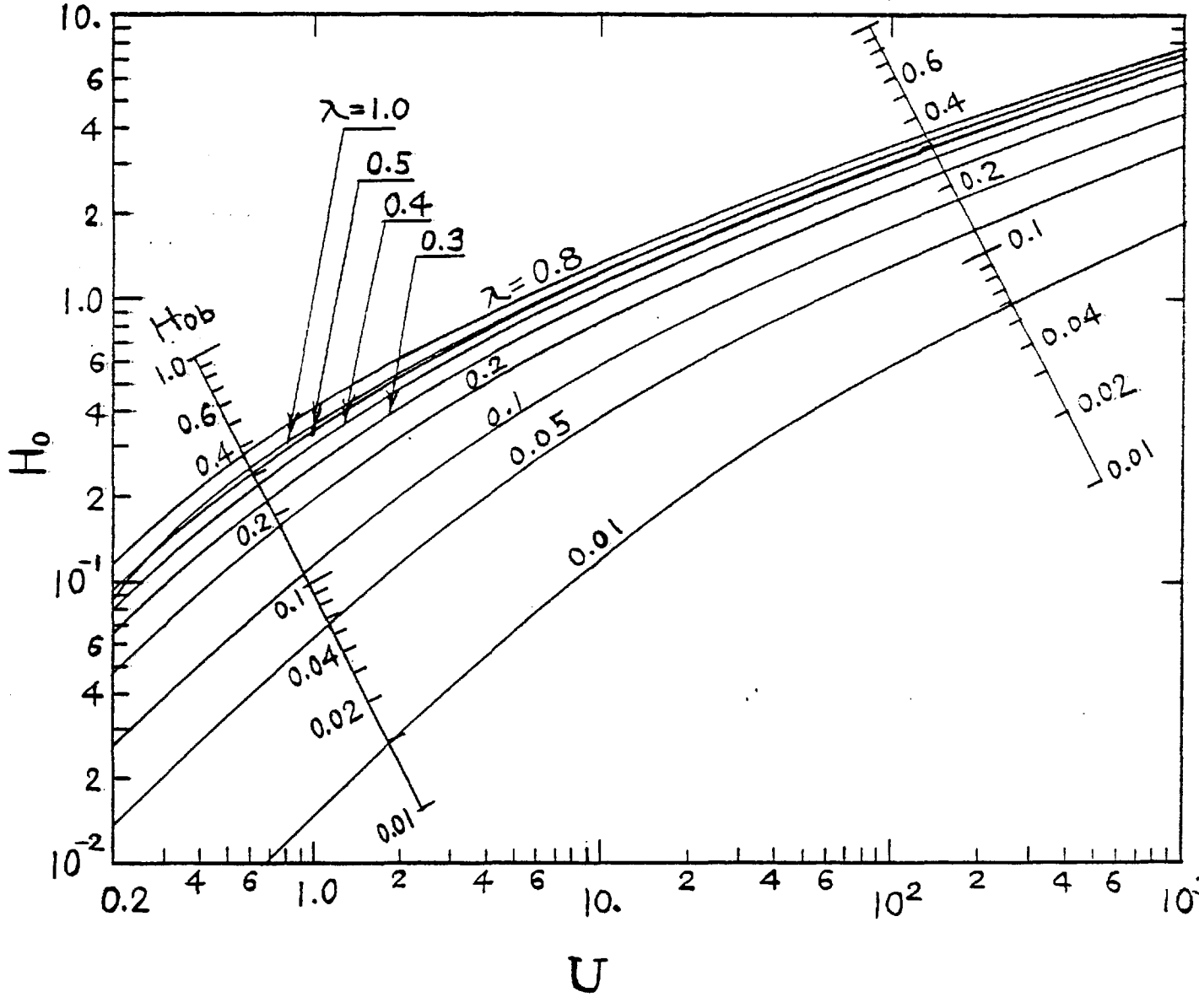


Figure 2.6 Performance of Taper Land Bearing

λ^*

λ	0.9	0.8	0.7183	0.7	0.6	0.5	0.1
H_{ob}	0.4073	0.4472	0.4542	0.4539	0.4436	0.4215	0.2075
H_0	0.7522	1.0000	1.1546	1.1857	1.3405	1.4757	1.9087
U	3.412	5.0000	6.463	6.825	9.129	12.258	84.604

Numerical Values for Maximum H_{ob}

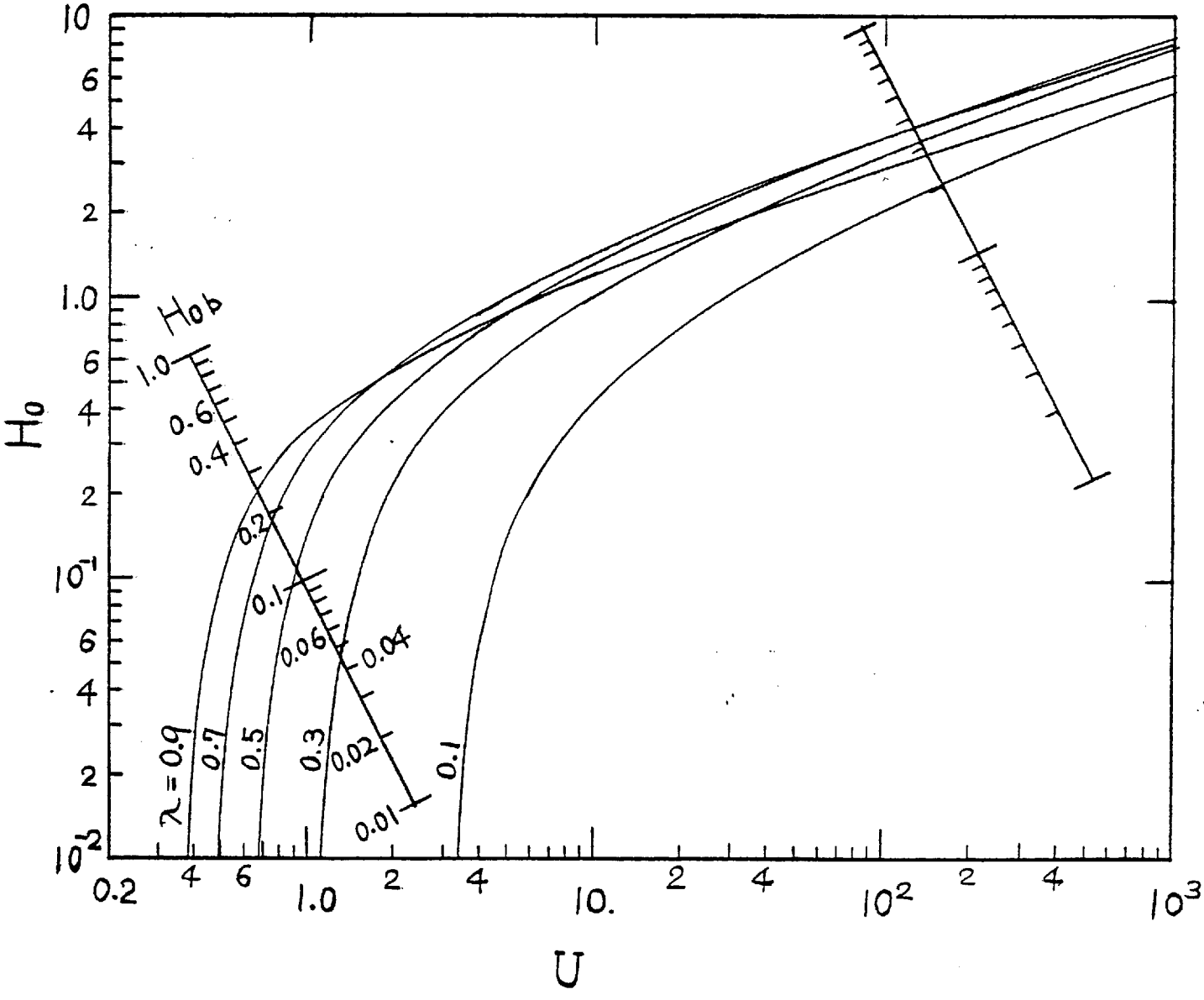


Figure 2.7 Performance of Rayleigh Step Bearing

λ	1.0	0.9473	0.9	0.8	0.7	0.5	0.1
H_{ob}	0.4211	0.4223	0.4214	0.4141	0.4006	0.3566	0.1712
H_o	0.7102	0.6984	0.6926	0.6889	0.6908	0.6987	0.7076
U	2.8448	2.7352	2.7020	2.7677	2.9735	3.8386	17.074

Numerical Values for Maximum H_{ob}

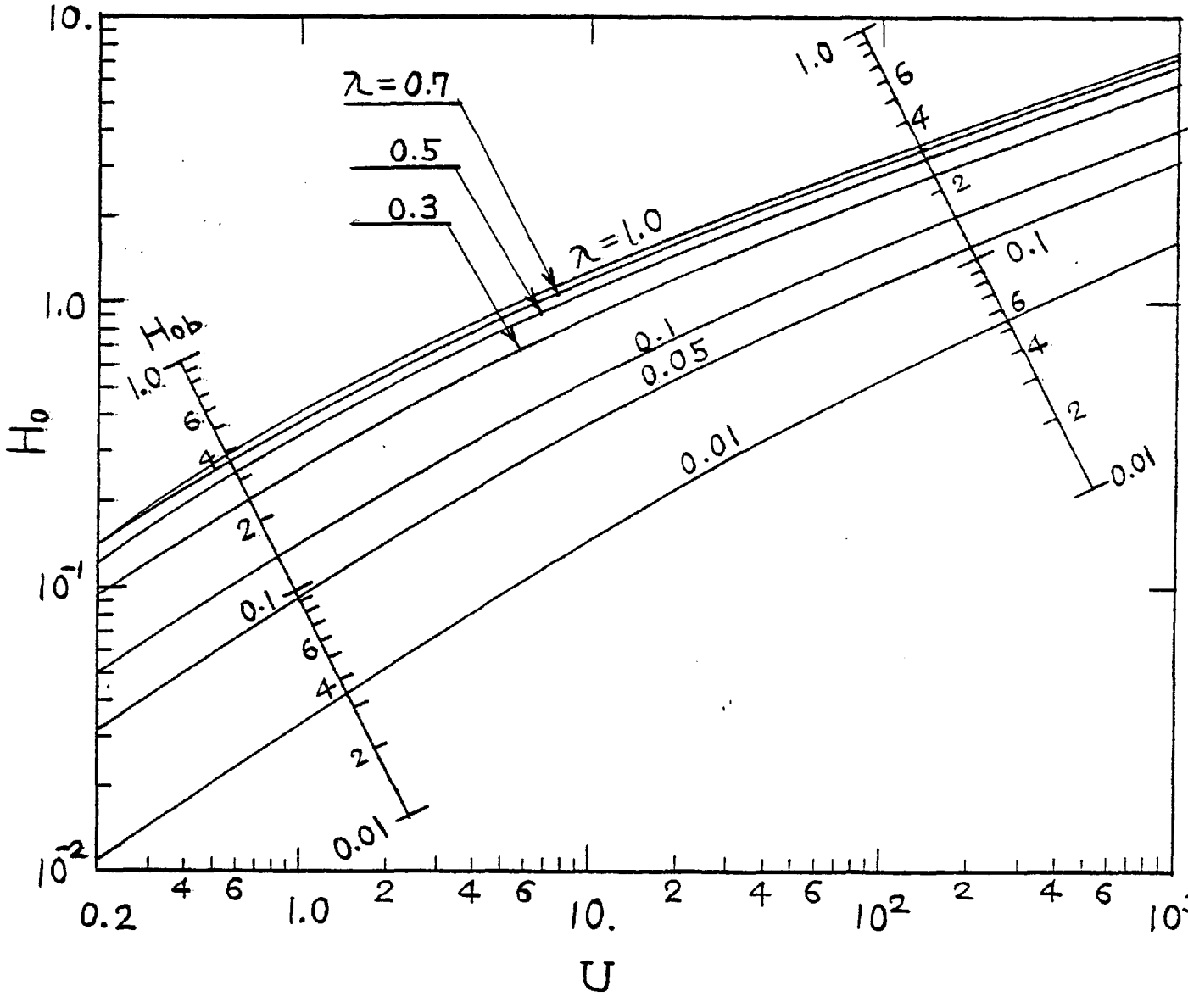


Figure 2.8 Performance of Partial Parabolic Bearing

CHAPTER THREE

MATHEMATICAL FORMULATION OF PARABOLIC FACE THRUST BEARINGS

3.1 Introduction

The reasons why this section is not included in the foregoing Chapter are twofold. One is to formulate necessary non-dimensional functions of parabolic face bearings, as this surface shape will be analysed for tilting pad bearings and starved conditions in the following Chapters. The other is that it is not reasonable to compare the performance of this bearing with other bearings discussed before. As the bearing has a divergent zone, there exists a part of bearing surface which has no contribution of load carrying capacity under the Reynolds condition. Thus the parameter H_{ob} cannot be defined in a way similar to the bearings considered before. The reference width of the parabolic face thrust bearing is taken as a width of convergent zone. Thus the maximum H_{ob} of this bearing under Reynolds condition is greater than any other bearing discussed before, as it has an excess breadth of divergent zone.

In this Chapter mathematical formulation of parabolic surface bearings under steady state condition ($V = 0$) will be presented and a few numerical results will be shown.

3.2 Theory of Hydrodynamic Lubrication of Parabolic Face Infinitely Long Thrust Bearings

3.2.1 Load Carrying Capacity

Referring to Figure (3.1)(a)(b) surface profile function $hp(x)$ of the parabola is

$$hp(x) = \Delta h_1 (\frac{x}{b_1})^2$$

This is non-dimensionally

$$Hp(X) = X^2 \tag{3.1}$$

where $X = \frac{x}{b_1}$ and $Hp = \frac{hp}{\Delta h_1}$

As the condition is steady, (V = 0) from the equation (2.8)

$$P = 6 \int_{X_{out}}^{X} \frac{X^2 - \bar{X}^2}{\{H_o + X^2\}^3} \, dX$$

$$= 6 \int_{X_{out}}^{X} \{\frac{1}{H_o + X^2)^2} - \frac{H_o + \bar{X}^2}{(H_0 + X^2)^3}\} \, dX \tag{3.2}$$

Where integration lower limit is chosen at the film outlet X_{out}.

$X_{out} = \bar{X}$, for Reynolds condition

or $X_{out} = \frac{b_2}{b_1} = -B_r$, for full Sommerfeld condition

B_r : offset of parabola

The equation (3.2) is integrated to give

$$P = 6\{\alpha(X, X_{out}) - (H_o + \bar{X}^2)\gamma(X, X_{out})\} \tag{3.3}$$

Where α and γ are integral functions of each term of the equation (3.2) as follows

$$\alpha(X,X_{out}) = \int_{X_{out}}^{X} \frac{1}{(H_o + X^2)^2}\, dX$$

$$= \frac{1}{H_o^{1.5}} \int_{X'_{out}}^{X'} \frac{1}{(1 + X'^2)^2}\, dX'$$

$$= \frac{1}{H_o^{1.5}} \{\alpha'(X') - \alpha'(X'_{out})\}$$

where

$$\alpha'(X') = \frac{X'}{2(1 + X'^2)} + \frac{1}{2}\tan^{-1} X'$$

$$X' = \frac{X}{\sqrt{H_o}}, \quad X'_{out} = \frac{X_{out}}{\sqrt{H_o}}$$

X' is a converted integration variable.

$$\gamma(X,X_{out}) = \int_{X_{out}}^{X} \frac{1}{(H_o + X^2)^3}\, dX$$

$$= \frac{1}{H_o^{2.5}} \int_{X'_{out}}^{X'} \frac{1}{(1 + X'^2)^3}\, dX$$

$$= \frac{1}{H_o^{2.5}} \{\gamma'(X') - \gamma'(X'_{out})\}$$

where

$$\gamma'(X') = \frac{X'}{4(1 + X'^2)^2} + \frac{3X'}{8(1 + X'^2)} + \frac{3}{8}\tan^{-1} X'$$

The integral constant $\bar{X}$ is obtained by applying the inlet boundary condition on the equation (3.3), P = 0 at X = 1. Thus

$$\alpha(1,X_{out}) - (H_o + \bar{X}^2)\gamma(1,X_{out}) = 0 \tag{3.4}$$

For full Sommerfeld condition

$$\bar{X}^2 = \frac{\alpha(1, -B_r) - H_o\gamma(1, -B_r)}{\gamma(1, -B_r)} \tag{3.5}$$

For Reynolds condition the equation (3.4) is

$$\alpha(1,\bar{X}_R) - (H_o + \bar{X}_R^2)\gamma(1,\bar{X}_R) = 0 \tag{3.6}$$

This equation cannot be solved analytically, but can be solved numerically by the Newton method (29).

Once the integral constant $\bar{X}$ is obtained analytically or numerically, the equation (3.3) can be integrated to give load carrying capacity w.

$$w = \int_{x_{out}}^{b_1} p\, dx = \int_{x_{out}}^{b_1} P \frac{\eta u}{b_1} \left(\frac{b_1}{\Delta h_1}\right)^2 dx$$

Writing non-dimensional load carrying capacity

$$W = \frac{w}{\eta u}\left(\frac{\Delta h_1}{b_1}\right)^2$$

$$W = 6\int_{X_{out}}^{1} \{\alpha(X,X_{out}) - (H_o + \overline{X^2})\gamma(X,X_{out})\}dX$$

$$= 6\{\alpha_i(1,X_{out}) - (H_o + \overline{X^2})\gamma_i(1,X_{out})\} \qquad (3.7)$$

Where α_i and γ_i are integration functions of α and γ and as follows.

$$\alpha_i(1,X_{out}) = \int_{X_{out}}^{1} \alpha(X,X_{out})\, dX$$

$$= \frac{1}{H_o}\int_{X'_{out}}^{X'_1} \{\alpha'(X') - \alpha'(X'_{out})\}\, dX'$$

$$= \frac{1}{H_o}\{\alpha'_i(X'_1) - \alpha'_i(X'_{out}) - (X'_1 - X'_{out})\alpha'(X'_{out})\}$$

Where $\alpha'_i(X') = \int \alpha'(X')dX' = \frac{1}{2}\tan^{-1}X'$

and $X'_1 = \frac{1}{\sqrt{H_o}}$

$$\gamma_i(1,X_{out}) = \int_{X_{out}}^{1} \gamma(X,X_{out})dX$$

$$= \frac{1}{H_o^2}\int_{X'_{out}}^{X'_1} \{\gamma'(X') - \gamma'(X'_{out})\}dX'$$

$$= \frac{1}{H_o^2}\{\gamma'_i(X'_1) - \gamma'_i(X'_{out}) - (X'_1 - X'_{out})\gamma'(X'_{out})\}$$

Where $\gamma'_i(X') = -\frac{1}{8(1 + X'^2)} + \frac{3}{8}X'\tan^{-1}X'$

Although the actual formulae are complex, equation (3.7) gives the non-dimensional load carrying capacity of the parabolic face thrust bearing under both boundary conditions. The difference between both boundary boundary conditions occurs for the calculation of $\overline{X}$ of equations (3.5) or (3.6) and integration lower limit for load carrying capacity $X_{out} = -B_r$ or $X_{out} = \overline{X}$. The criteria of applicability of both boundary conditions is that; when the Reynolds outlet position $\overline{X}_R$ calculated by the equation (3.6) is within the bearing breadth, Reynolds condition is applied, otherwise full Sommerfeld condition is applied. That is,

When $\overline{X}_R < -B_r$ Reynolds condition

$\overline{X}_R < -B_r$ full Sommerfeld condition

The above procedure can be summarised as a function as

$$W = f_w(H_o, B_r) \tag{3.8}$$

This is the general expression of load carrying capacity of infinitely long parabolic face bearing with finite trailing breadth.

Equation (3.8) is calculated and the results are plotted as a solid line U which is a reciprocal of W under Reynolds condition for all the range. In the figure Reynolds outlet position $\overline{X}_R$ is also plotted. As shown the maximum value of $\overline{X}_R$ is 0.5, if $B_r > 0.5$ always Reynolds condition is realised. For this case equation (3.8) is more simplified as

$$W = f_w(H_o) \tag{3.9}$$

for $B_r > 0.5$

In the figure maximum film pressure is included which is calculated by the equation (3.3) putting $X = -\bar{X}_R$.

The chain line next to the solid line of U is for the case of a half parabola which is the same as Figure 2.8, $\lambda = 1.0$ ($B_r = 0$ in the load function of equation (3.8)). This is added for comparison.

The table above shows the numerical values for maximum H_{ob} which is referred only to the breadth of convergent zone.

3.2.2 Centre of Pressure

The centre of pressure is the position through which the load acts. It is given by taking moments about the origin. Let the distance of the centre of pressure from the origin be x_e as shown in Figure 3.1(a),(b). The total moment by the film pressure is given

$$x_e w = \int_{x_{out}}^{b_1} px\, dx$$

Converting the equation to a non-dimensional form

$$X_e W = \int_{X_{out}}^{1} PX\, dX \qquad (3.10)$$

Where the definitions of X_e as used elsewhere in this thesis remain unaltered. As non-dimensional pressure P is given by the equation (3.3),

$$\frac{X_e W}{6} = \int_{X_{out}}^{1} \{\alpha(X,X_{out}) - (H_o + \bar{X}^2)\gamma(X,X_{out})\}X \; dX$$

$$= \int_{X_{out}}^{1} \{X\alpha(X,X_{out}) - (H_o + \bar{X}^2)X\gamma(X,X_{out})\}\, dX$$

Changing the integration variable X to X', and using the functions defined before

$$\frac{X_e W}{6} = \frac{1}{H_o^{0.5}} \int_{X'_{out}}^{X'_1} X'\alpha'(X')dX' - \frac{1 + \bar{X}'^2}{H_o^{0.5}} \int_{X'_{out}}^{X'_1} X'\gamma'(X')dX'$$

$$- \frac{1}{H_o^{0.5}} \{\alpha'(X'_{out}) - (1 + \bar{X}'^2)\gamma'(X'_{out})\} \int_{X'_{out}}^{X'_1} X'dX'$$

Where $X' = \frac{1X}{\sqrt{H_o}}$, $\bar{X}' = \frac{1\bar{X}}{\sqrt{H_o}}$, $X'_1 = \frac{1}{\sqrt{H_o}}$, $X'_{out} = \frac{X_{out}}{\sqrt{H_o}}$

Gives:

$$\frac{X_e W}{6} = \frac{1}{H_o^{0.5}} \{\alpha_m(X'_1, X'_{out}) - (1 + \bar{X}'^2)\gamma_m(X'_1, X'_{out})\}$$

$$\frac{1}{2H_o^{0.5}} \{\alpha'(X'_{out}) - (1 + \bar{X}'^2)\gamma'(X'_{out})\}(X'^2_1 - X'^2_{out}) \qquad (3.11)$$

The functions α_m and γ_m are given as follows

$$\alpha_m(X'_1, X'_{out}) = \alpha'_m(X'_1) - \alpha'_m(X'_{out})$$

where

$$\alpha'_m(X') = \frac{1}{4}(X' - \tan^{-1}X' + X'^2 \tan^{-1}X')$$

$$\gamma_m(X'_1, X'_{out}) = \gamma'_m(X'_1) - \gamma'_m(X'_{out})$$

where

$$\gamma'_m(X') = \frac{1}{16}(3X' - \frac{2X'}{1 + H'^2} - \tan^{-1}X' + 3X'^2 \tan^{-1}X')$$

As all the quantities other than X_e are given by the foregoing formulae the centre of pressure can be calculated by the equation (3.11). Again the above procedure can be summarized as a function as following

$$X_e = f_e(H_o, B_r) \qquad \text{for} \qquad B_r < 0.5 \tag{3.12}$$

$$X_e = f_e(H_o) \qquad \text{for} \qquad B_r \geq 0.5 \tag{3.13}$$

Numerical results of the equations are plotted in Figure 3.3. The solid lines are the solution under Reynolds condition and the broken lines are the solution under half Sommerfled condition or simply the solution for $B_r = 0$. In the figure the position of maximum film pressure is also included for comparison. The difference of the centres of pressure for both cases ($B_r > 0.5$ and $B_r = 0$) is not big. This is because most of the film pressure is generated within the convergent zone of the bearing.

3.3 Discussion

The results of figure (3.2) are compared with available published numerical results (4). In the figures assymptotic relationships for the case of $H_o \to 0$ based on the numerical values when $H_o = 10^{-6}$ are shown. Among them the relationship between U and H_o is of particular interest as it should agree with the Martin formula of parabolic cylinder lubrication (30)(31). When the formula shown in Figure 3.2 is expressed dimensionally,

$$h_o = 1.222 \frac{\eta u}{w} \qquad \frac{b_1^2}{\Delta h_1} = 2.444 \frac{\eta u R}{w}$$

where $R = \dfrac{b_1^2}{2\Delta h_1}$: radius of curvature

This is the Martin formula as it is the formula for rolling cylinders. This relationship is shown in Figure 3.2 as a broken line. The difference between the solid line and broken line is caused by the inlet position being finite for the solid line, which is specified by Δh_1 and b_1, but infinite for the broken line. Thus it suggests that this non-dimensional expression shown by the solid line automatically includes the effects of inlet lubricant starvation of parabolic cylinder lubrication and will be discussed later in detail.

By the figure it is shown that the Martin formula can be applied with negligible error up to the film thickness H_o about 0.02. This means that an inlet film thickness more than 50 times minimum film thickness has negligible contribution for hydrodynamic pressure generation. Even when $H_o = 0.1$ the error is about 20%. This also means that the parabolic approximation of circular cylinder is quite accurate for small H_o, as the error of this approximation occurs near the inlet of the bearing.

For the bearings of $0 < B_r < 0.5$ the curve of U is the same as the solid line of Figure 3.2 for small H_o, and lies between the solid line and the chain line for large H_o. But the variation is small.

Assymptotic relationships of X_e and H_o shown in Figure 3.3 agree within four significant figures with the solution of circular disc lubrication given by the reference (4).

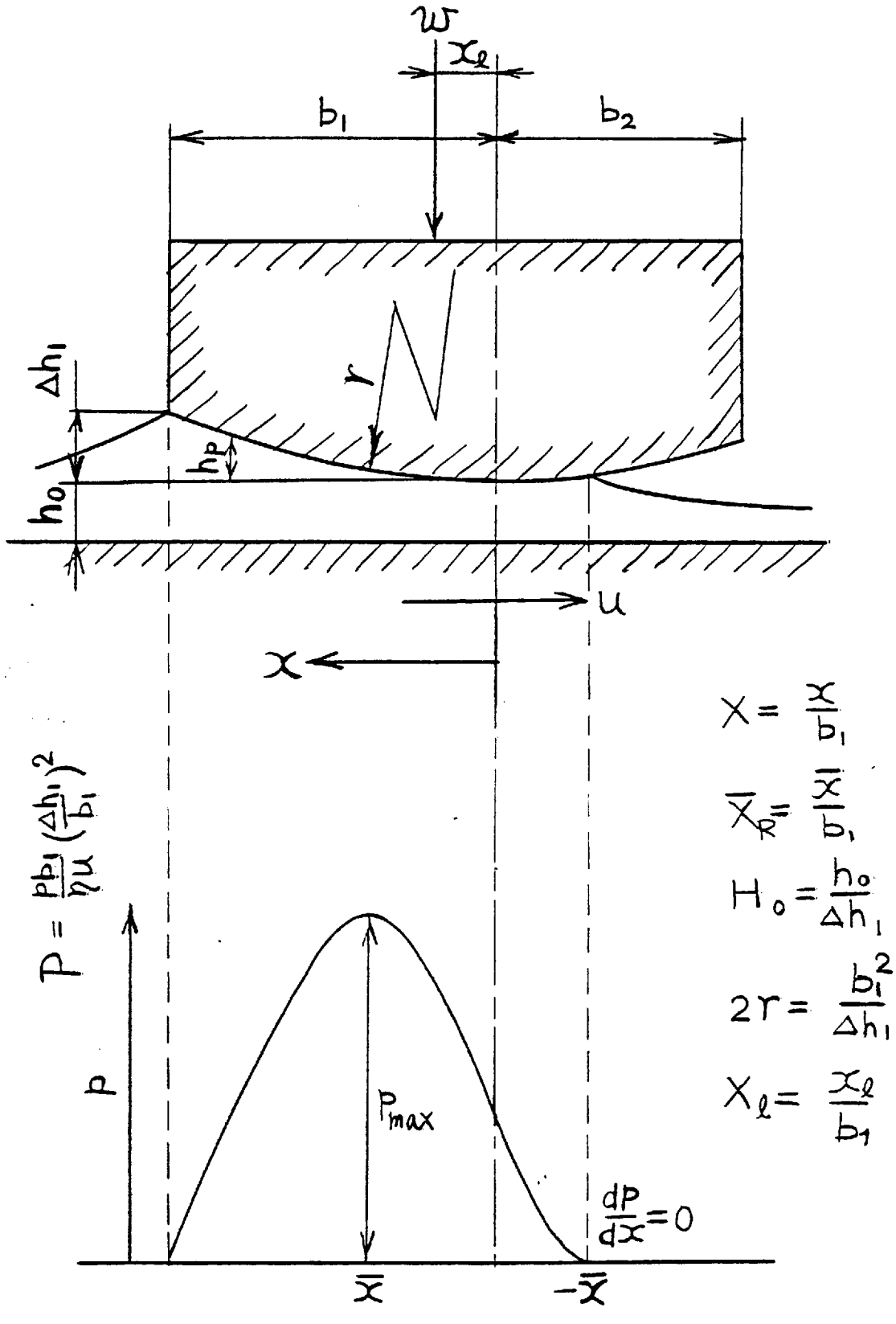


Figure 3.1(a) Parabolic Face Thrust Bearing Under Reynolds Condition

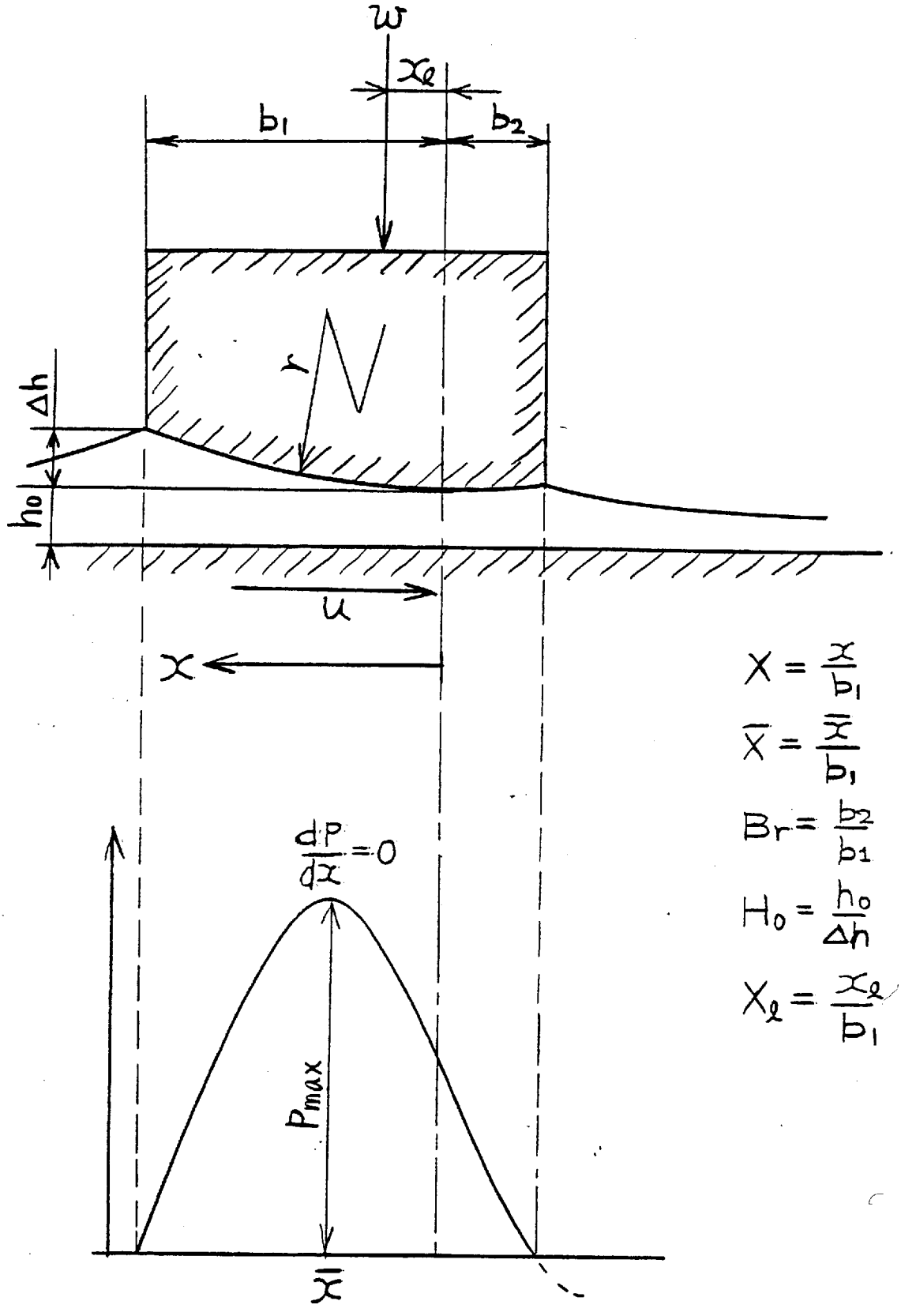


Figure 3.1(b) Parabolic Face Thrust Bearing Under Full Sommerfeld Condition

H_{ob}	0.5049
H_o	0.8308
U	2.7074

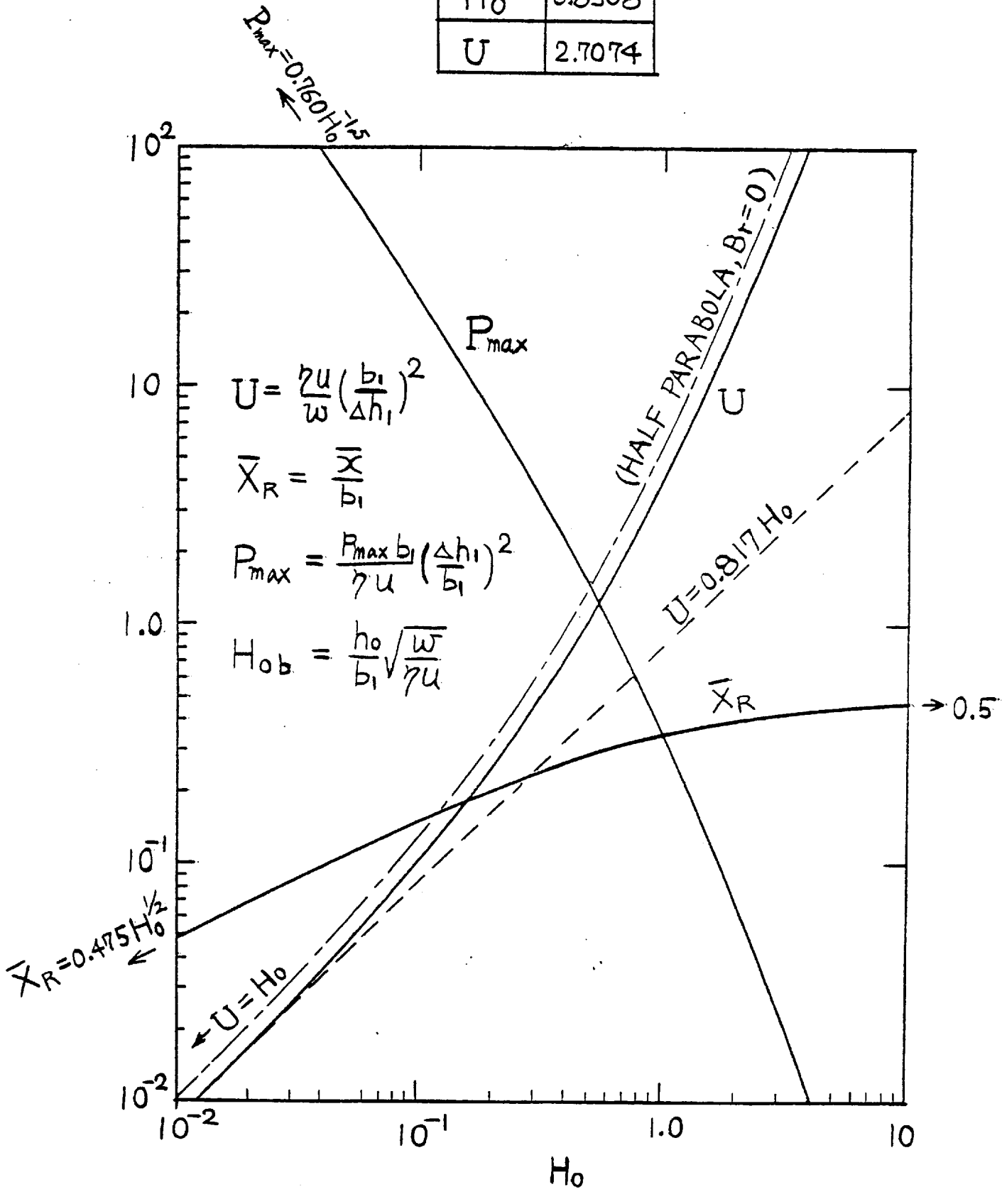


Figure 3.2 Performance of Parabolic Face Bearing

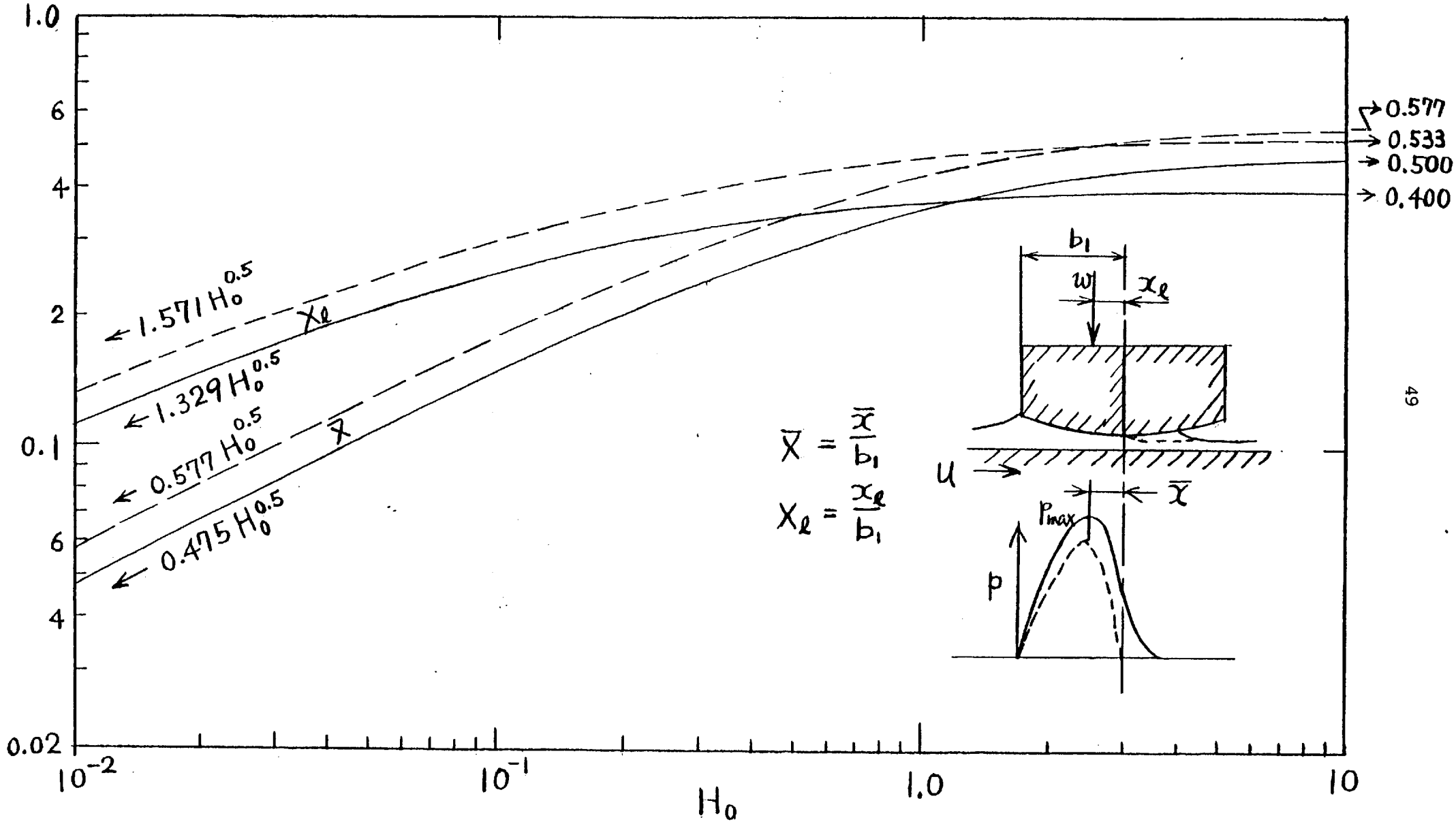


Figure 3.3 Centre of Pressure and Position of P_{max}

CHAPTER FOUR

TILTING PAD BEARING

4.1 Introduction

It was shown that for a given surface shape the non-dimensional load carrying capacity and non-dimensional centre of load are only the functions of non-dimensional film thickness H_o.

For the flat inclined pad bearing it was recognised that the centre of pressure is a function of inlet and outlet film thickness only, i.e., $1 + \frac{1}{H_o}$ in the notation of this text. Then it was deduced that the pivot position of flat tilting pad bearing defines the inlet and outlet film thickness ratio. But the theory could not be expanded to include curved shape tilting pad bearings.

Although an excellent publication by Raimondi (32) is available, the method to obtain the performance curve of curved tilting pad bearings is not analytical and the results are not comprehensive enough to give a whole picture of the effects of curvature of tilting pad bearings.

In this Chapter, although it is one dimensional, the effects of curvature of tilting pad bearing will be analysed analytically and comprehensive results will be presented.

The fact, that for flat pad bearings the non-dimensional centre of pressure is a function of H_o, thus $1 + \frac{1}{H_o}$, only comes from the fact that the non-dimensional surface profile function Hp(X) is the same whatever the tilting angle of the flat tilting pad bearing, as long as the Reynolds equation can be applied.

Thus the theory for the fixed surface thrust bearings can easily be expanded to include the tilting effects if the tilting of the bearing does not change the non-dimensional surface profile function

Hp(X). This is the case for flat surface and parabolic surface and they are analysed in the following section.

4.2 Flat Tilting Pad Bearing

The formula of non-dimensional centre of pressure as a function of $1 + \frac{1}{H_o}$ is available in the reference (4).

Referring to Figure 4.1,

$$X_L - 1 = \frac{2(3 + K)(1 + K)\,\ell n\,(1 + K) - K(6 + 5K)}{2K\{(2 + K)\ell n(1 + K) - 2K\}} \qquad (4.1)$$

where

$$K = 1 + \frac{1}{H_o}$$

The equation (4.1) is calculated and the results are plotted in Figure 4.1. In the figure H_{ob} based on the data shown in Figure 2.6 is also included. The numerical values for maximum H_{ob} are shown in the figure.

Thus once the pivot position is given, this gives H_o and H_{ob} from the figure. The optimum pivot position for the maximum H_{ob} is $X_e = 0.4225$, which gives $H_{ob} = 0.4003$. Thus the film thickness h_o is

$$h_o = 0.4003\ b\sqrt{\frac{nu}{w}}$$

Due consideration of the corner chamfer or corner round off is helpful to reduce the wear on starting up the bearings as discussed above.

4.3 Parabolic Tilting Pad Bearing with Sufficient Trailing Breadth

The exact meaning of the title of this section is "the analysis of infinitely long tilting pad bearing of parabolic section with

sufficient trailing breadth to ensure Reynolds condition for the entire operating range of the bearing". The bearing is named simply "parabolic tilting pad bearing" against "flat tilting pad bearing".

It has always been somewhat of a puzzle to know why centrally pivoted thrust "flat" pad bearings work so well (4). Theoretically this pivot position gives $H_o \to \infty$ and the corresponding value of $H_{ob} = 0$ thus no film generation. But as already shown the value of H_{ob} is very sensitive for the small value of λ for partial parabola or taper land bearings. Thus slight corner chamfer or corner round off by positive machining or by running-in wear, whatever the cause, makes a significant increase of the capability of film generation of the bearings without any tilting effects. For example, if 10% of total bearing breadth has a convergent zone, the maximum value of H_{ob} is 0.1908 (Figure 2.6) for a tapered inlet convergence. This is about 50% of that of the optimized tilting flat bearing. The hydrodynamic pressure so generated is mainly at the inlet zone of the bearing, thus the tilting moment is generated and the bearing tilts, and more load carrying capacity is generated and equilibrium is reached.

It has become more and more obvious that when pads are loaded they deflect and the equations for flat pads are only a very rough approximation to the truth. The flat surface distorts to roughly a circle or parabola. If the distorted surface is a parabola the theoretical analysis already formulated in the foregoing chapter can easily be expanded to include the tilting effects. This is because tilting of the parabolic face bearing does not change the non-dimensional surface profile function $Hp(X) = X^2$, as long as the radius of the curvature does not change. Thus the same equations for load carrying capacity as shown already can be used if the reference dimensions Δh_1 and b_1 under tilted condition are used in non-dimensional parameters.

Referring to Figure 4.2, the non-dimensional equation for load carrying capacity was given by the equation (3.9) for Reynolds condition. That is

$$W_t = f_w(H_{ot}) \tag{4.2}$$

The suffix t is added to mean that the reference dimensions Δh_1 and b_1 should be replaced by that for tilted condition Δh_t and b_{1t}.

The function f_w can be shown by a graph of W_t versus H_{ot}, as shown in figure 3.2, or can be expressed as a program using the procedure formulated in Chapter Three.

W_t and H_{ot} in the equation (4.2) can be expressed by the reference dimensions before tilt.

$$W_t = \frac{w}{\eta u}\left(\frac{\Delta h_t}{b_{1t}}\right)^2 = \frac{w}{\eta u}\left(\frac{\Delta h_1}{b_1}\right)^2 \cdot \left(\frac{\Delta h_t}{\Delta h_1}\right)^2 \cdot \left(\frac{b_1}{b_{1t}}\right)^2$$

$$H_{ot} = \frac{h_o}{\Delta h_t} = \frac{h_o}{\Delta h_1} \quad \frac{\Delta h_1}{\Delta h_t}$$

Thus the tilting can be expressed either by $\frac{\Delta h_t}{\Delta h_1}$ or $\frac{b_t}{b_1}$ as these two are related as following.

$$H_t = B_t^2$$

where

$$H_t = \frac{\Delta h_t}{\Delta h_1}$$

$$B_t = \frac{b_{1t}}{b_1}$$

Both parameters are useful because H_t means the lift of the bearing

inlet and B_t means the increase of the bearing convergent breadth under tilt. Both parameters are equal to 1.0 for no tilting condition.

Using these parameters of tilt the equation (4.2) can be expressed by the parameters before tilt as following.

$$W = \frac{1}{H_t} f_w \left(\frac{H_o}{H_t}\right)$$
$$\text{or} \quad W = \frac{1}{B_t^2} f_w \left(\frac{H_o}{B_t^2}\right) \qquad (4.3)$$

As the function f_w is already given by Figure 3.2 ($U = W^{-1}$), the load carrying capcity W under tilted conditions can be obtained by considering the non-dimensional parameters. In a log-log scale this procedure is to shift the curve to the direction of 45°. This is shown in Figure 4.3. The figure can be used to estimate the film thickness of parabolic face piston ring under tilted condition.

The applicable range of Figure 4.3 is whether the Reynolds film outlet exceeds the actual bearing breadth or not, and is shown in Figure 4.4. The procedure to make Figure 4.4 is similar to that of load carrying capacity. Since the Reynolds outlet position is a funcition of H_o only,

$$\bar{X}_R = f_R(H_o) \qquad (4.4)$$

f_R is expressed in Figure 3.2 or can be a computer subprogram. Under tilted condition

$$\bar{X}_{Rt} = f_R(H_{ot})$$

where

$$\bar{X}_{Rt} = \frac{\bar{x}_{Rt}}{b_{1t}}$$

The equation can be modified similarly as before.

$$\frac{\bar{x}_{Rt}}{b_{1t}} = \frac{b_1 + \bar{x}_R - b_{1t}}{b_{1t}} = \frac{b_1}{b_{1t}} + \frac{\bar{x}_R}{b_1}\frac{b_1}{b_{1t}} - 1$$

$$= \frac{1}{B_t} - 1 + \frac{\bar{X}_R}{B_t}$$

Thus

$$\bar{X}_R = B_t - 1 + B_t f_R \left(\frac{H_o}{B_{t^2}}\right) \qquad (4.5)$$

The equation (4.5) is plotted for different values of B_t in Figure 4.4. The assymptotic of $H_o \to \infty$ and $H_o \to 0$ is given as following

$$\bar{X}_R = B_t \qquad \text{for } H_o \to 0$$

$$\bar{X}_R = \frac{3}{2}B_t - 1 \qquad \text{for } H_o \to \infty$$

In Figure 4.3 both positive ($B_t > 1.0$) and negative ($B_t < 1.0$) tilting effects are shown. For the case of $H_o \to 0$ all the lines approach assymptotically to the Martin formula shown as a broken line in the figure. This is because as long as the inlet film thickness is greater than 50 times the minimum film thickness, there is negligible film pressure generation near the inlet as explained before.

The above discussion is for the case of externally (or forceably) tilted parabolic thrust bearings. For the case of parabolic tilting pad bearing it must so adjust itself that the centre of pressure coincides with the loading position.

The formulae of centre of pressure is given by the equation (3.13) as a function of film thickness only and shown in Figure 3.3. The same

discussion as before can be applied and

$$X_{et} = f_e(H_{ot}) \tag{4.6}$$

where

$$X_{et} = \frac{x_{et}}{b_{1t}} \text{ as shown in Figure 4.2.}$$

The natural way to chose the reference dimension of the parabolic tilting pad bearing b_1 is to use the distance between bearing inlet and loading position. This is because when the bearing is not moving (stationary) theoretically the curved face should touch on the lower surface right under the position of loading. This condition can be used as a condition of "no tilt". When the bearing starts to move it tilts from that condition depending on the hydrodynamic pressure. Thus the loading position of parabolic tilting pad bearing is at the centre of parabola of the upper figure of 4.2. The self adjusting parabolic tilting pad bearing must adjust itself so that the x_e of the lower figure of Figure 4.2 must be zero.

Thus $x_{et} = b_{1t} - b_1$, then the equation (4.6) becomes,

$$1 - \frac{1}{B_t} = f_e\left(\frac{H_o}{B_t^2}\right)$$

or

$$B_t = \frac{1}{1 - f_e\left(\frac{H_o}{B_t^2}\right)} \tag{4.7}$$

Thus the parabolic tilting pad bearing adjusts the tilting quantity B_t to satisfy the equation (4.7) depending on the film thickness H_o.

The function (4.7) is solved numerically by function iteration method (29) to give the relationship between H_o and B_t. The program used is listed in Appendix II. The results are shown in Figure 4.5.

The tilting parameter B_t varies from 1.0 (no tilt) for $H_o \to 0$ to $\frac{5}{3}$ for $H_o \to \infty$.

Thus as the relationship between H_o and B_t are obtained, the load carrying capacity W and Reynolds outlet position $\bar{X}_R$ can be obtained by the equation (4.3) and (4.5). They are plotted as broken lines in Figure 4.3 and Figure 4.4. The maximum value of $\bar{X}_R$ is 1.5, so if the offset of parabola with reference to loading position, B_r is greater than 1.5, the parabolic tilting pad bearing always operate under the Reynolds condition.

As explained before design optimization can be obtained by maximizing the value of H_{ob}. Under the Reynolds condition the reference total bearing breadth cannot be defined, as a fixed value, as the film outlet varies. But if the distance between inlet and loading position is used as a reference bearing breadth it can be defined as $H_{ob} = \frac{h_o}{b_1}\sqrt{\frac{w}{\eta u}}$. The points of maximum value of this are shown in Figure 4.3, 4.4 and 4.5 as dots. Numerical values at this point are $H_{ob} = 0.800$, $H_o = 2.503$, $U = 9.85$, $B_t = 1.590$ and $\bar{X}_R = 1.157$. As the film outlet position is given as $\bar{X}_R = 1.157$ the total bearing breadth up to this position can be used as a reference for H_{ob}. This gives

$$H_{ob} = 0.800/(1 + 1.157) = 0.371$$

Compared with the value of the optimized flat tilting pad bearing (0.4003) the value is more than 90%. This condition can be realised under the front loading rather than centre loading of the bearing. For the case of centre loaded parabolic tilting pad bearing the solution must be obtained under the full Sommerfeld condition and the optimum value of H_{ob} must be greater than 0.371. This is discussed

in the next section.

4.4 Parabolic Tilting Pad Bearing with Finite Trailing Breadth

As was discussed in the foregoing section if the trailing breadth of the bearing defined by B_r is less than 1.5 the Reynolds condition must be replaced by full Sommerfeld condition during its operating condition. This is the case for the centre loaded parabolic tilting pad bearing ($B_r = 1.0$).

The procedure of the analysis is the same as before but the effects of finite trailing breadth are taken into account. Already in Chapter Three the functions of the load carrying capacity and the position of centre of pressure is given for the parabolic bearing with finite divergent zone by the equation (3.8) and (3.12). Thus the equations can be used if the reference geometries of the bearing under tilted condition are used.

Thus,

$$W_t = f_w(H_{ot}, B_{rt})$$

$$X_{et} = f_e(H_{ot}, B_{rt})$$

Where referring to Figure 4.2

$$W_t = \frac{w}{\eta u}\left(\frac{\Delta h_t}{b_{1t}}\right)^2$$

$$H_{ot} = \frac{h_o}{\Delta h_t}$$

$$B_{rt} = \frac{b_{2t}}{b_{1t}}$$

$$B_{rt} = \frac{b_{2t}}{b_{1t}}$$

$$X_{et} = \frac{x_e}{b_{1t}}$$

The method of conversion of each parameter was already shown except B_{rt}.

$$B_{rt} = \frac{b_{2t}}{b_{1t}} = \frac{b_1}{b_{1t}} \frac{b_1 + b_2 - b_{1t}}{b_1} = \frac{1 + B_r}{B_t} - 1$$

Thus the same discussion as before produces,

$$W = \frac{1}{B_t^2} f_w \left(\frac{H_o}{B_t^2}, \frac{1 + B_r}{B_t} - 1\right) \tag{4.8}$$

$$B_t = \frac{1}{1 - f_e \left(\frac{H_o}{B_t^2}, \frac{1 + B_r}{B_t} - 1\right)} \tag{4.9}$$

These equations are the same as the equations (4.3) and (4.7) except the term of the bearing offset ratio (or the position of loading). The equations (3.8) and (3.9) can be applied when $B_t \leq 1 + B_r$. But if $B_t > 1 + B_r$ the theoretical minimum film thickness defined at the centre of parabola and acutal minimum film thickness becomes different as shown in Figure 4.6. For this case the non-dimensional surface profile function $H_p(X)$ of parabolic bearing does not change if the theoretical dimensions of the bearing under tilted condition b_{1t} and Δh_t are used for non-dimensional parameters. And also the functions f_w and f_e do not change if the film thickness is non-dimensionalised by the theoretical inlet wedge height Δh_t. The difference is that the lower limit of integration becomes positive

(upstream of the centre of parabola). Thus the slight modification of the procedure can accommodate this "over tilted" condition of the bearing. Thus the theoretical minimum film thickness h_{ot} is expressed by actual film thickness h_o as follows

$$h_o - h_{ot} = \Delta h_1 \left(\frac{b_{1t} - b_1 - b_2}{b_1}\right)^2$$

Non-dimensionalising

$$H_{ot} = H_o - (B_t - 1 - B_r)^2$$

where

$$H_{ot} = \frac{h_{ot}}{\Delta h_1} \quad \text{and} \quad H_o = \frac{h_o}{\Delta h_1}$$

Thus the equation (3.8) and (3.9) becomes,

When $B_t > B_r + 1$

$$W = \frac{1}{B_t^2} f_w \left(\frac{H_{ot}}{B_t^2}, \frac{1 + B_r}{B_t} - 1\right) \tag{4.10}$$

$$B_t = \frac{1}{1 - f_e \left(\frac{H_{ot}}{B_t^2}, \frac{1 + B_r}{B_t} - 1\right)} \tag{4.11}$$

where $H_{ot} = H_o - (B_t - 1 - B_r)^2$

The term which expresses the offset of parabola $\frac{1 + B_r}{B_t} - 1$ is negative under this condition and full Sommerfeld condition is applied.

The equations (4.10) and (4.11) can be used as long as $H_{ot} > 0$.

But when $H_{ot} \leq 0$ and the theoretical centre of parabola is under the lower sliding surface, the equations cannot be used because the integral functions formulated in Chapter Three are different. So different integral functions must be formulated under this condition. But this was not tried as it was considered that the procedure up to the equation (4.11) gave almost all the necessary performance curves of the parabolic tilting pad bearing.

The actual procedure of calculation is as follows. The function f_e and f_w are subprograms which contain the formulations of Chapter Three. First, H_o is assumed for a certain bearing geometry B_r. Then the equation (4.9) is solved by function iteration method (29) until both sides of the equation agree within 10^{-6}. In the course of the iteration B_t is compared with $B_r + 1$ and if the former is greater than the latter, the equation (4.11) is applied. And if H_{ot} becomes negative the calculation stops. When B_t is obtained the equations (4.8) or (4.10) gives the load carrying capacity depending on the value of B_t.

The actual program is listed in Appendix II.

The results are plotted in Figure 4.7, 4.8 and 4.9. In Figure 4.7 the tilting parameter B_t against film thickness H_o for different bearing supporting position B_r is plotted. When $B_r = 1.0$ it is for centre loading condition. The curve of $B_r > 1.5$ is the same as that of Figure 4.5 as discussed before. It is clearly shown that, for the bearing with small trailing breadth ($B_r < 1.5$), the tilting parameter deviates from that of $B_r \geq 1.5$ at certain film thickness and rapidly increases. The curves of small B_r terminate in the figure, as H_{ot} becomes negative at that point as explained before. The dots at the middle of the curves indicate the condition at which the centre of

parabola coincides with the trailing edge of the bearing ($B_t = 1 + B_r$). For a small film thickness all the curves are the same as the excess breadth of the bearing under the Reynolds condition have no effect on hydrodynamic pressure generation.

Figure 4.8 is non-dimensional film thickness H_o and sliding velocity $U(= W^{-1})$. It is also shown that for small H_o (or small U) there is no difference for all values of B_r shown, but that for large H_o (or large U) there are differences between different values of B_r. The reason of termination of some of the curves is the same as for Figure 4.7. Figure 4.8 can be used to estimate the film thickness of parabolic tilting pad bearing directly but it is not convenient to optimize the bearing design or operating condition. The film thickness h_o which is included in H_{ob} shown in the figure is normalised not by the total bearing breadth but by the leading breadth. Thus Figure 4.9 is produced by the same data as Figure 4.8.

In Figure 4.9 the ordinate is $\frac{h_o}{b_1 + b_2}\sqrt{\frac{w}{\eta u}}$, and the abscissa is H_o. As the parameter is normalised by the total bearing breadth, the curves for different values of B_r are separated and gives clear guidance of optimization of the bearing condition.

The optimum condition which gives the maximum film thickness for a given total bearing breadth is realised at about the point where $B_r = 0.8$, $H_o = 2.0$ and $H_{ob} = 0.421$. This value of H_{ob} is about 5% more than that of the optimized flat tilting pad bearing. Thus 5% more film thickness can be generated by the parabolic tilting pad bearing than by the optimized flat tilting pad bearing at its optimum.

For centre loaded pad bearing ($B_r = 1.0$) the optimum value of H_{ob} is almost the same as optimized flat tilting pad bearing. Thus it is clear that the centre loaded "flat" tilted pad bearing can support equivalent load as the optimum pivoted flat tilting pad bearing if

the condition allows the flat surface to distort to give certain convex curvature.

Actual value of curvature to realise the optimum condition can be calculated as follows. For the case of the centre load condition ($B_r = 1.0$) by the figure

$$H_o = \frac{h_o}{\Delta h_1} = 2.6$$

$$H_{ob} = \frac{h_o}{b_1 + b_2} \sqrt{\frac{w}{\eta u}} = 0.40$$

thus

$$\frac{\Delta h_1}{b_1 + b_2} = \frac{H_{ob}}{H_o} \sqrt{\frac{\eta u}{w}} = 0.154 \sqrt{\frac{\eta u}{w}}$$

Thus the optimum value of curvature is a function of operating condition $\frac{\eta u}{w}$ the reciprocal of which is often called as duty parameter. Assuming the typical values u = 10m/s, w = 10^5N/m, η = 0.01Pas, then,

$$\frac{\Delta h_1}{b_1 + b_2} = 1.54 \times 10^{-4} \approx 10^{-4}$$

Thus for the typical total bearing breadth 100mm

$$\Delta h_1 \approx 0.01\text{mm}$$

This small distortion must easily occur in actual conditions thermally or elastically.

4.5 Discussion

Generally of the non-dimensional expression of general solution

of the one dimensional Reynolds equation was demonstrated. No extra mathematical equation was necessary to analyse the curved tilting pad bearing other than the non-dimensional expressions formulated in Chapter Three. Just a simple manipulation of non-dimensional parameters in the equation of Chapter Three enabled the comprehensive analysis of parabolic tilting pad bearings. Although the analysis is only for the case of infinitely long bearings, this comprehensive analysis has never been achieved before, because conventional non-dimensional grouping does not allow the theory to expand to include the tilting effects easily.

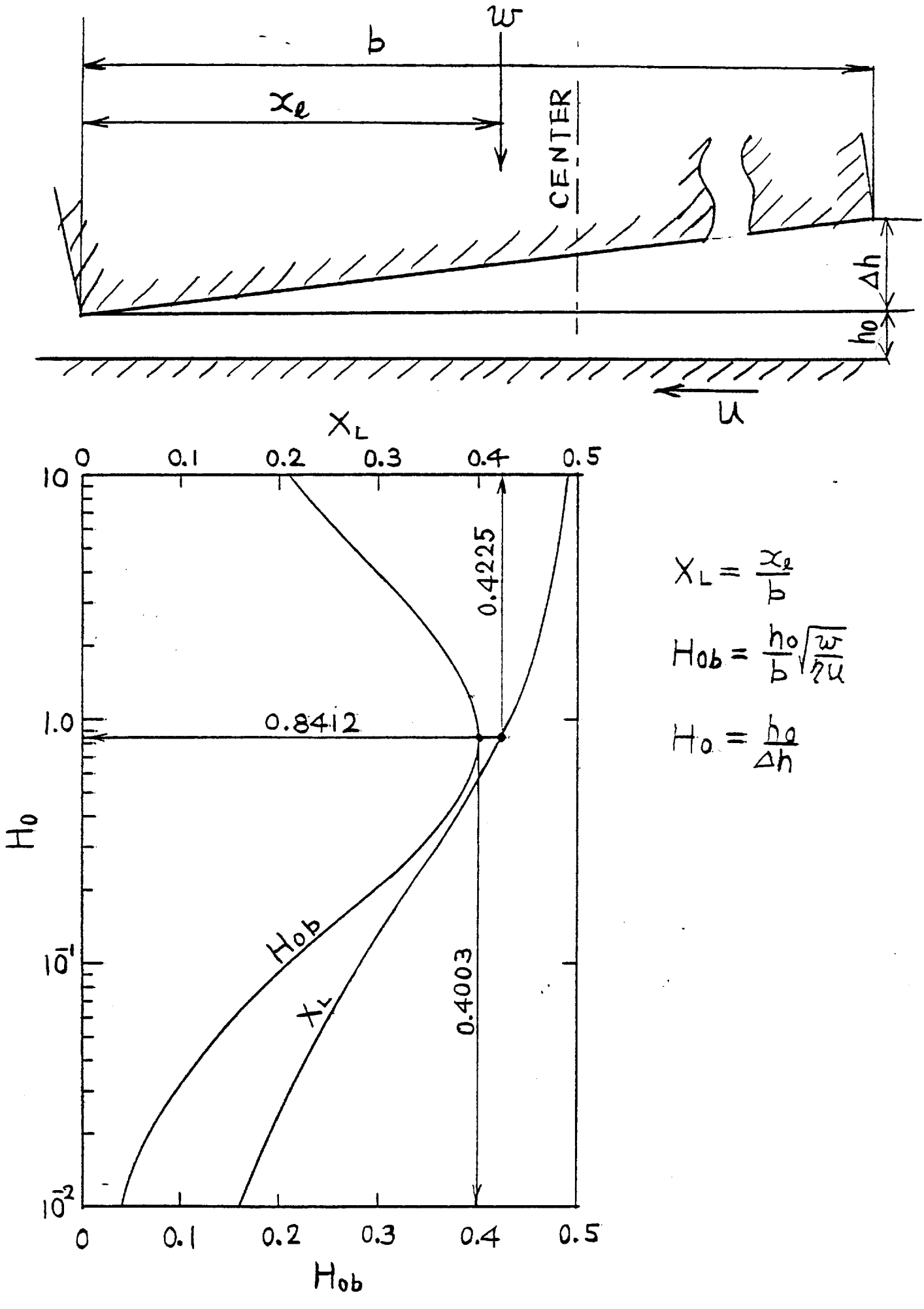


Figure 4.1 Performance of Flat Tilting Pad Bearing

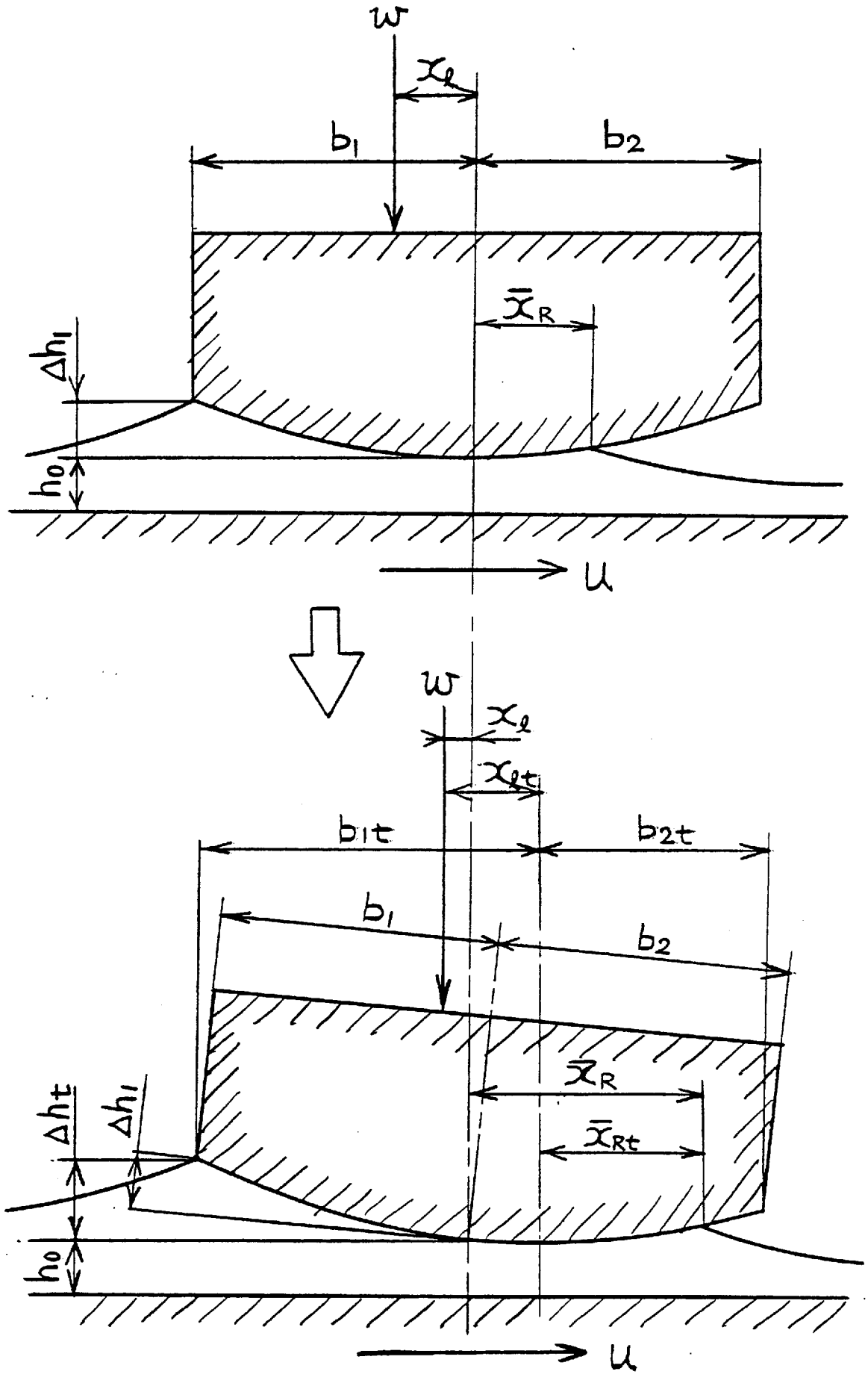


Figure 4.2 Tilted Parabolic Thrust Bearing

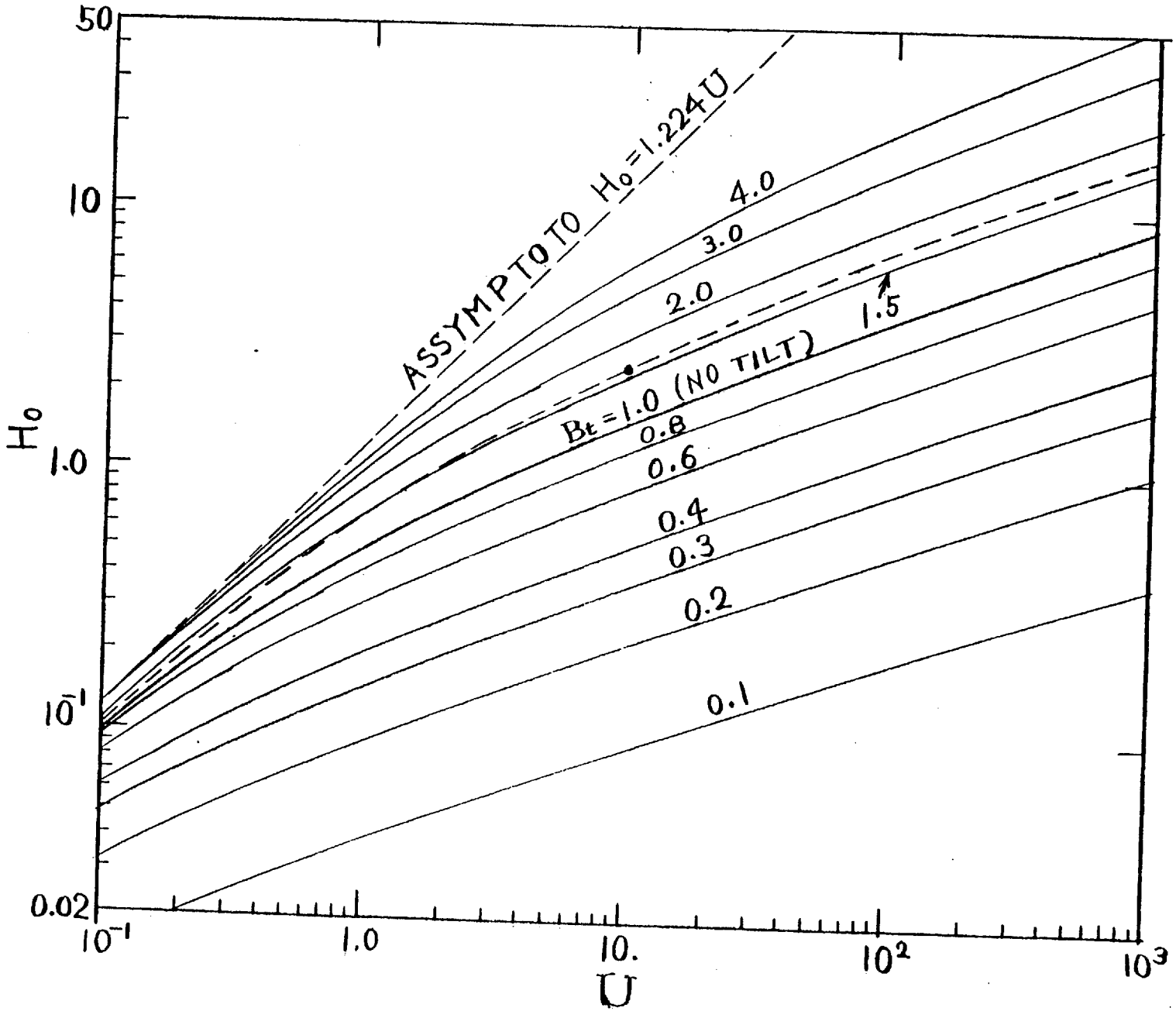


Figure 4.3 Film Thickness of Parabolic Bearing under Tilted Condition

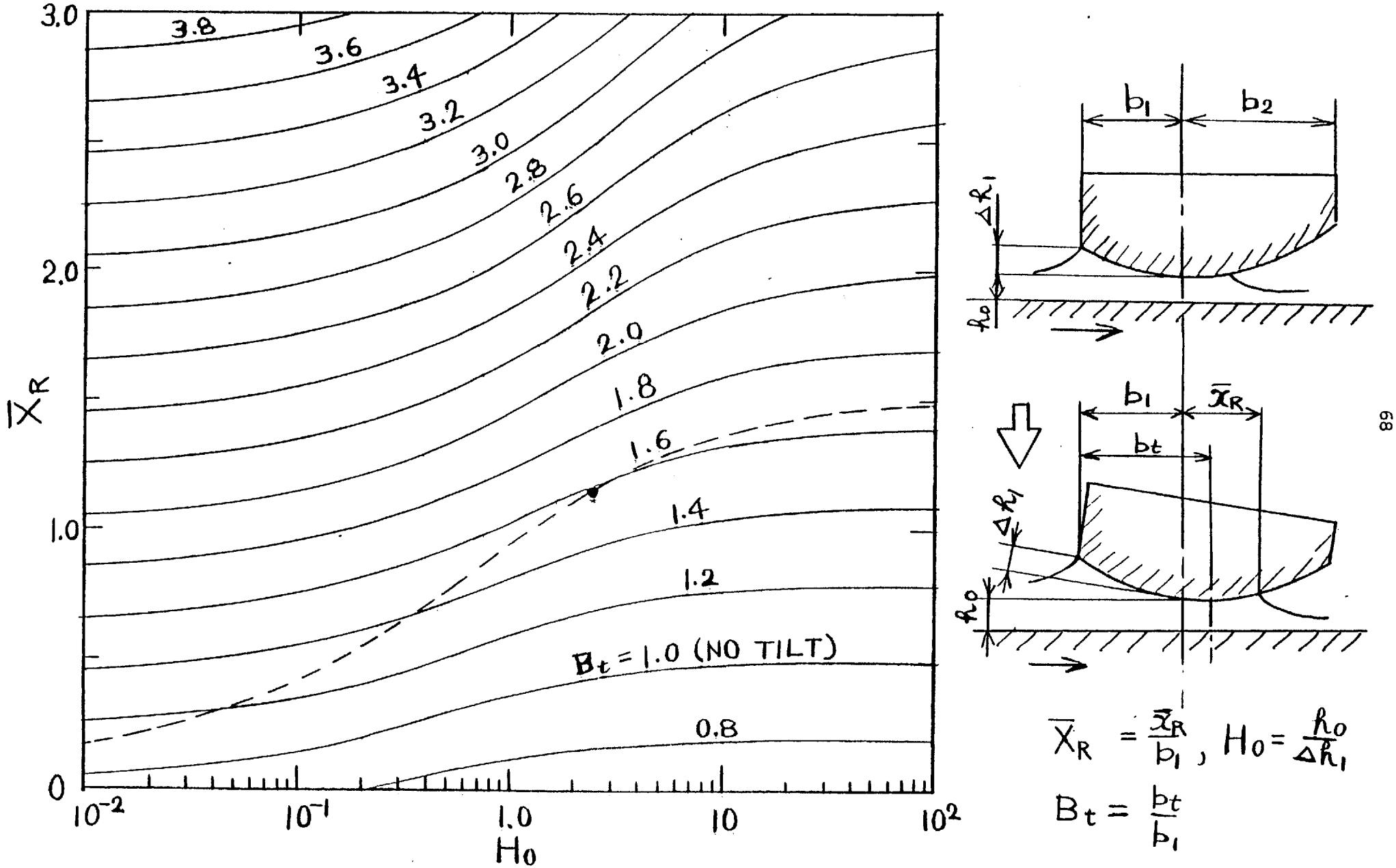


Figure 4.4 Film Outlet Length of Parabolic Bearing

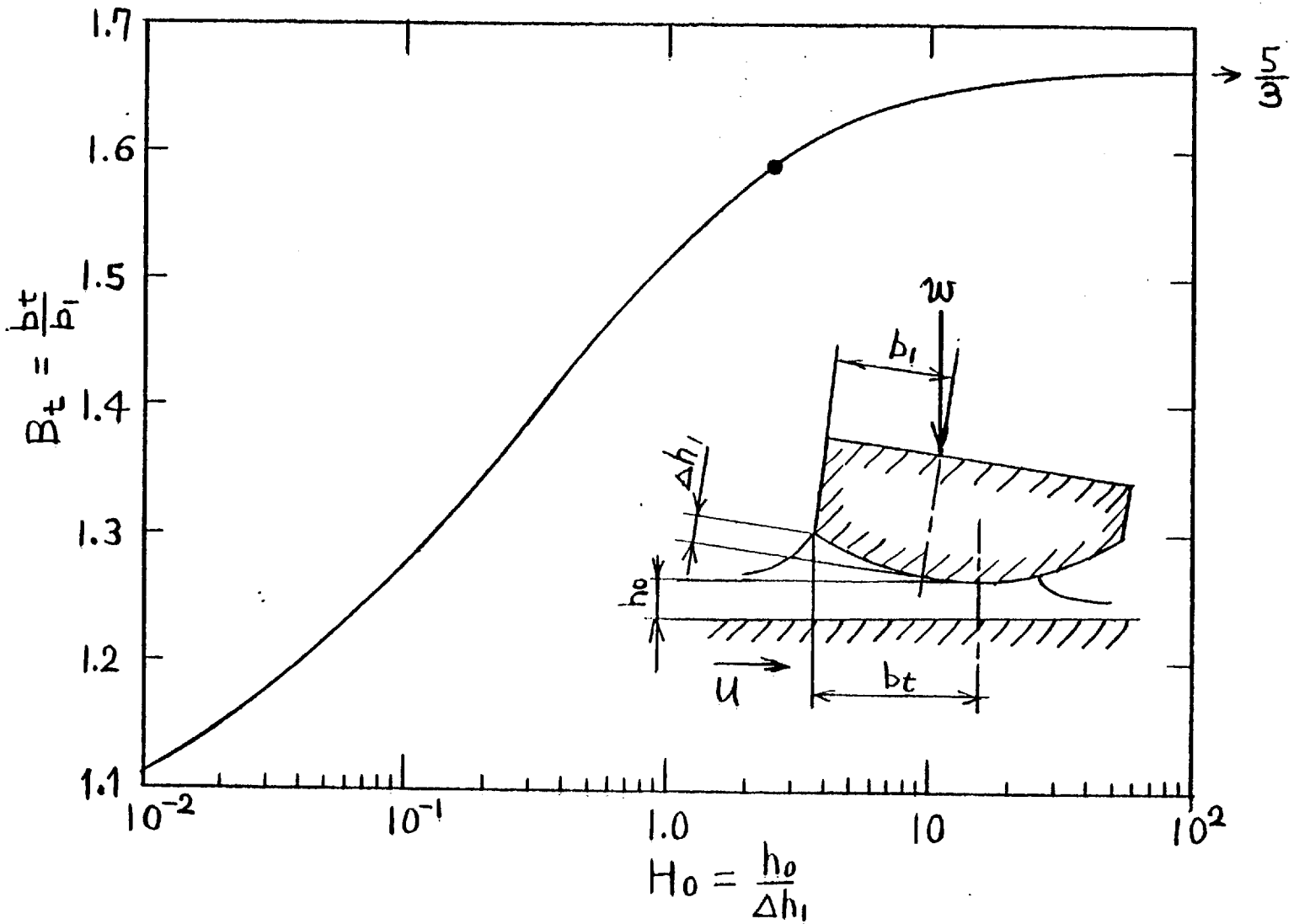


Figure 4.5 Tilting Parameter B_t Against Film Thickness H_o

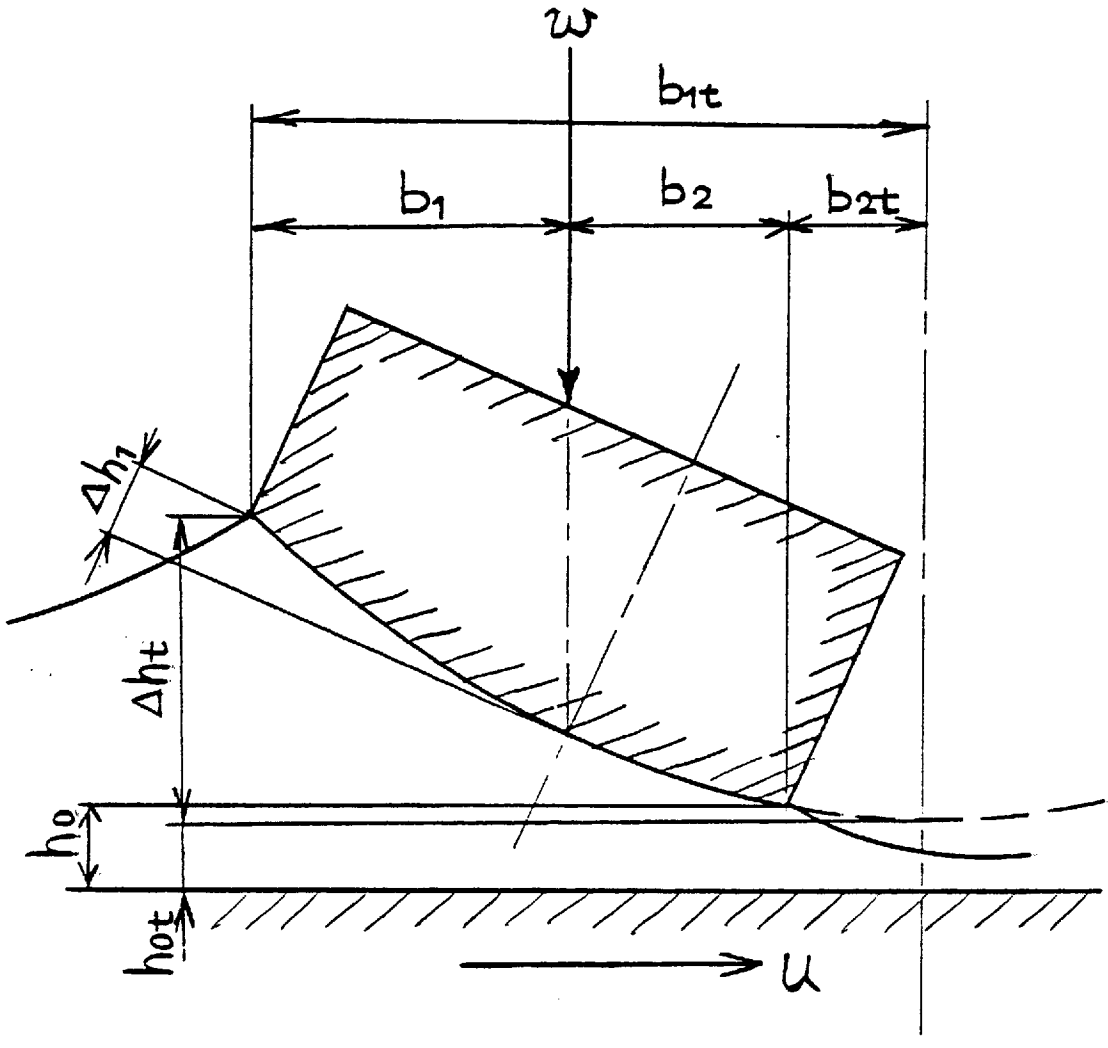


Figure 4.6 Over Tilted Condition of Parabolic Tilting Pad Bearing (exaggerated)

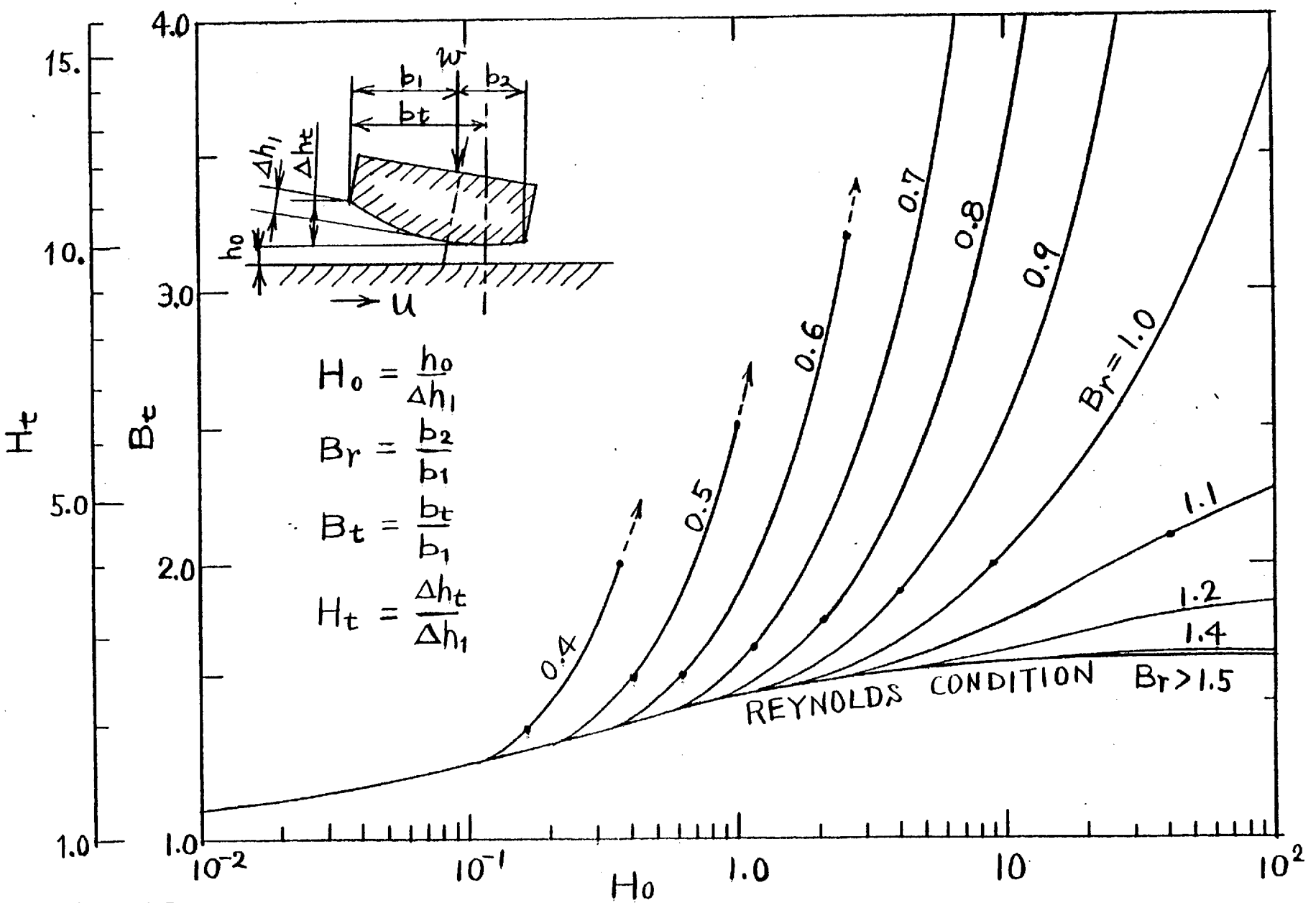
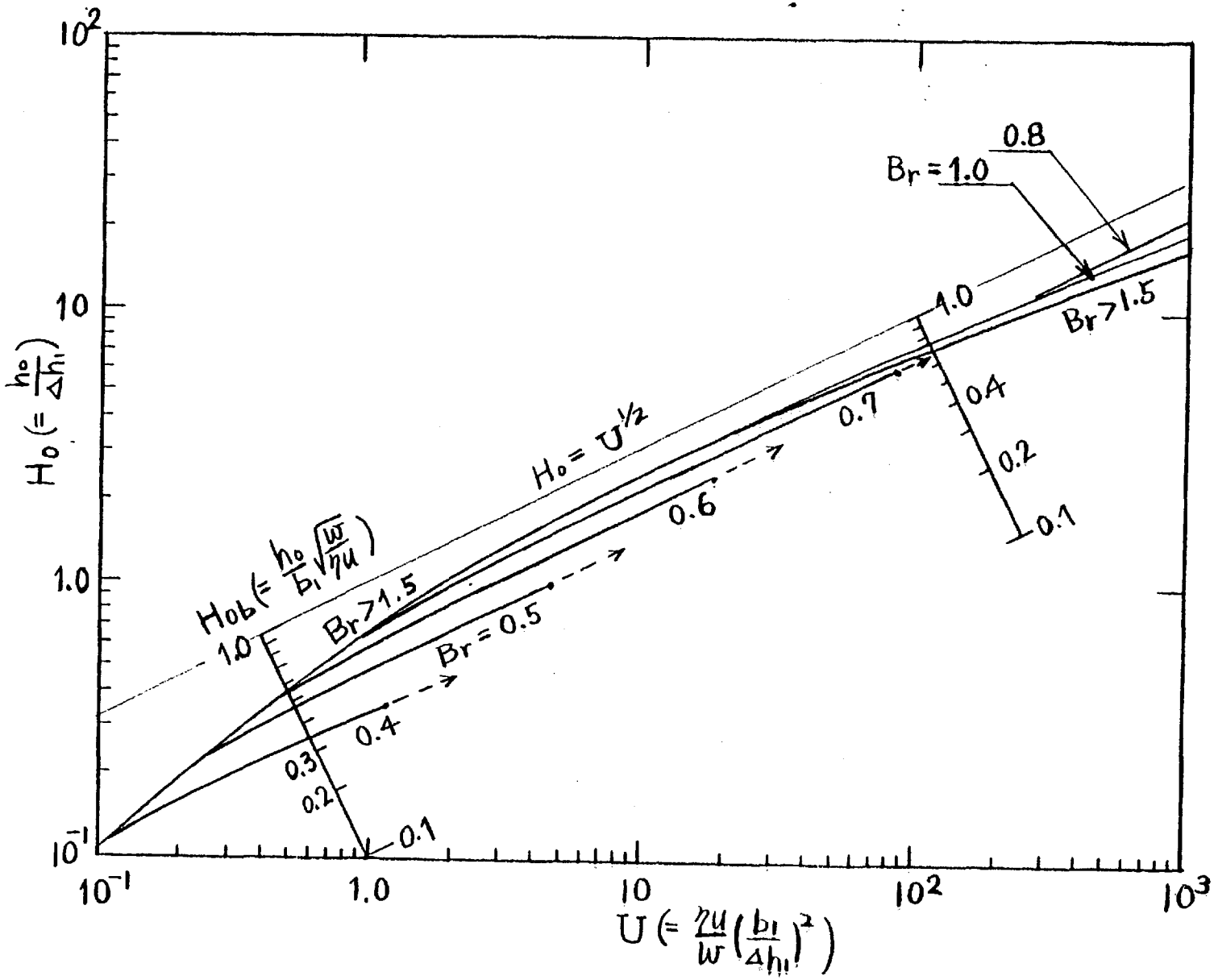
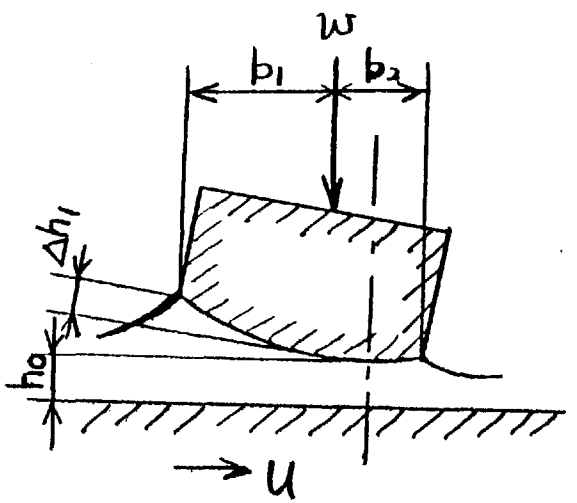


Figure 4.7 Tilting Parameter of the Parabolic Tilting Pad Bearing





$$B_r = \frac{b_2}{b_1}$$

$$H_0 = \frac{h_0}{\Delta h_1}$$

$$U = \frac{\eta u}{w}\left(\frac{b_1}{\Delta h_1}\right)^2$$

$$H_{0b} = H_0 U^{-1/2}$$

Figure 4.8 Film Thickness of Parabolic Tilting Pad Bearing

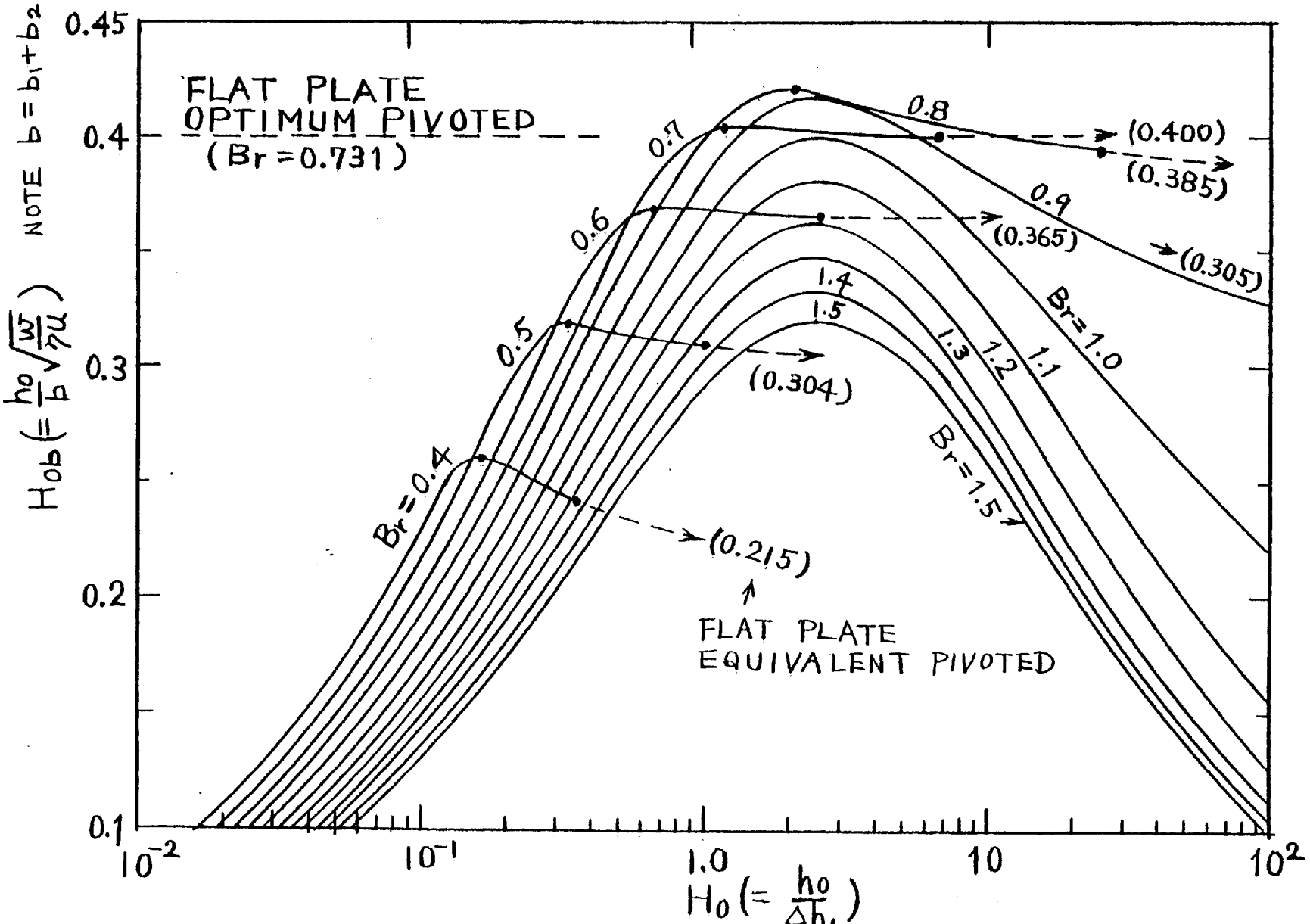


Figure 4.9 H_{ob} against H_o for Parabolic Tilting Pad Bearing

CHAPTER FIVE

STARVATION

5.1 Introduction

In recent years a growing interest was shown in relation to the operation of hydrodynamic films under starved conditions, in both rigid surface lubrication and EHL contacts. This is because it was experimentally found that it is not unusual for rolling bearings (33)(34)(35) and for piston rings (36)(37)(38)(39) to operate under starved conditions. In certain conditions it is even desirable to operate the rolling bearing under mildly starved conditions especially for high speed bearings as the excess lubricant contributes only for heat generation by viscous friction loss (40)(42).

Starvation is an important feature in an actual piston ring lubrication as they are normally used as a ring pack and it is certain that the second or subsequent rings must operate under the limited lubricant supply left over the liner surface by the first ring. This was realised as a discrepancy between the measured and theoretical film thickness. This was studied by Hamilton et al (38)(39) experimentally and theoretically. In their analysis they studied only the simplest case, i.e., one double tapered and one single tapered ring. They compared the theory and experiment over the central portion of the ring stroke and the agreement was good. They concluded that starvation is an essential feature of the lubrication of piston rings in a ring pack.

Mention must be made of their theory since they used the same non-dimensional forms as given in this text. They used the non-dimensional form as following,

$$\frac{WS^2}{6U\eta} = f(\frac{H_1}{h_2})$$

$\frac{WS^2}{U\eta}$ is exactly the same as W used in this text, and $\frac{H_1}{h_2}$ in their notation is the reciprocal of non-dimensional minimum film thickness H_o. But as they call the term s, which is the same as $\frac{\Delta h}{b}$ in this text, the slope of the ring face, they confined their discussion "to a ring with a triangular profile of apex height H_1". Thus they left unanswered the question of whether the non-dimensional form is general or not.

Theoretical study of EHL line contacts including classical condition under starved lubrication was extensively carried out by Wolveridge et al (41). In their analysis they introduced many non-dimensional parameters which are difficult to interpret physically. So although a graph and a table are presented for the estimation of film thickness under starved condition, the procedure is rather a simple mathematical manipulation of the non-dimensional quantity and gives scant impression of the physical situation.

In this Chapter the non-dimensional expression of Chapter Three will be expanded to include the analysis of lubricant starvation. EHL lubrication under starved condition is additionally analysed using non-dimensional groups which have clear meanings of physical condition.

5.2 Starvation of Rigid Surface Isoviscous Lubrication

It was shown that the non-dimensional expressions formulated in Chapter Three can easily be expanded to included the tilting effects if the effects do not change the non-dimensional surface profile function Hp(X) under the tilted condition.

This is also the case for the starved condition. Referring to

Figure 5.1 starvation can be defined by reducing the film inlet dimensions from those of the geometrical bearing inlet Δh_1, b_1 to the starved film inlet geometry Δh_s, b_s. Thus if the non-dimensional surface profile function Hp(X) is unaltered by this change of film inlet geometry, exactly the same argument as Chapter Four can be applied. Fortunately for the flat pad and the parabolic pad bearings, this is so. For the case of the taper load bearing or partial parabolic bearing this is not so as the starved geometry b_s changes the value of λ shown in Chapter Two.

5.2.1 Flat Inclined Pad Bearing Under Starved Condition

The same non-dimensional expressions can be applied for the starved condition if the reference geometry of starved condition is used in the expression.

$$W_s = f_w (H_{os})$$

where

$$W_s = \frac{w}{\eta u}\left(\frac{\Delta h_s}{b_s}\right)$$

$$H_{os} = \frac{h_o}{\Delta h_s}$$

The parameters can be converted into the forms which are expressed by actual bearing geometry.

$$W_s = \frac{w}{\eta u}\left(\frac{\Delta h_s}{b_s}\right)^2 = \frac{w}{\eta u}\left(\frac{\Delta h_1}{b_1}\right)^2 \left(\frac{\Delta h_1}{b_1}\right)^2 \left(\frac{\Delta h_s}{\Delta h_1}\right)^2 \left(\frac{b_1}{b_s}\right) = W\frac{H_s^2}{B_s^2}$$

$$H_{os} = \frac{h_o}{\Delta h_s} = \frac{h_o}{\Delta h_1}\cdot\frac{\Delta h_1}{\Delta h_s} = \frac{H_o}{H_s}$$

where

$$B_s = \frac{b_s}{b_1} \quad , \quad H_s = \frac{h_s}{\Delta h_1}$$

Either parameters B_s or H_s can be used as a starvation parameter. For the inclined flat pad bearing the relationship between these parameters is

$$H_s = B_s$$

Thus the non-dimensional expression for starved conditions becomes extremely simple.

$$W = f_w\left(\frac{H_o}{B_s}\right) \quad \text{or} \quad f_w\left(\frac{H_o}{H_s}\right) \tag{5.1}$$

Thus the minimum film thickness under starved conditions can be obtained by a simple manipulation of the parameter H_o. Function f_w is shown graphically in Figure 2.6 ($\lambda = 1.0$). The equation (5.1) can be expressed in a log-log scale just by shifting the curve in the scale of H_o by the amount of B_s, or just multiplying the film thickness given by Figure 2.6 by the starvation parameter $B_s (= H_s \leq 1.0)$.

The procedure shown above might be used if the starved condition can be defined by $B_s (= H_s)$. In practice starvation must also be defined by the inlet oil flow, because starvation is normally caused by insufficient lubricant film thickness deposited on the incoming sliding surface.

Now the oil flow of the inclined pad bearing under fully-flooded condition can be obtained as following. From a standard text book (4) of lubrication, film thickness $\bar{h}$ where $\frac{dp}{dx} = 0$ is given as

$$\bar{H} = 2\,\frac{H_o(H_o + 1)}{2H_o + 1}$$

where

$$\bar{H} = \frac{\bar{h}}{\Delta h}$$

(see the notation index)

For a steady state condition this defines the non-dimensional flow quantity of the bearing and half of it is the non-dimensional film thickness deposited on the outgoing sliding surface H_e. Thus for fully flooded conditions,

$$H_e = f_f(H_o) \tag{5.2}$$

where

$$H_e = \frac{h_e}{\Delta h}$$

$$f_f(H_o) = \frac{H_o(H_o + 1)}{2H_o + 1}$$

h_e : film thickness deposited on the outgoing surface under full flooded condition.

For the starved condition the same argument as before gives,

$$H_{es} = B_s\, f_f\left(\frac{H_{os}}{B_s}\right) \tag{5.3}$$

where

$$H_{es} = \frac{h_{es}}{\Delta h_1}$$

h_{es} : film thickness deposited on the outgoing surface under starved condition

Equations (5.1) and (5.3) are plotted in Figure 5.2. In the figure H_e and H_{es} are shown as H_e. For a steady state starved condition incoming flow and outgoing flow must be equal in order to satisfy the flow continuity condition. Thus

$$H_i = H_e$$

where

$$H_i = \frac{h_i}{\Delta h}$$

h_i : incoming oil flow expressed by the film thickness on the incoming surface

If the incoming oil flow is greater than the outgoing flow, the excess lubricant fills the bearing surface and changes the value of B_s, and the condition is not steady. If the bearing surface is already filled with lubricant ($B_s = 1.0$) the condition is full flooded and the excess lubricant is simply accumulated at the inlet side of the bearing as excess lubricant.

From the figure one can directly estimate the necessary incoming film thickness to make the bearing full flooded under certain operating conditions specified by $U(= W^{-1})$. And it is clearly shown that once starvation occurs the film thickness is almost entirely dependent on the incoming film thickness and is not dependent on any other variables. This is because the increase of U (increase of u η or decrease of w) under limited lubricant supply is off-set by decrease of film pressure generation area (B_s). The assymptoto is, that the bearing film thickness is twice as much as the incoming film thickness. This is shown in the Figure 5.2 as a decrease of B_s under starved condition, and each line for different values of H_e assymptoti-

cally approachs to $H_o = 2H_e$.

5.2.2 Parabolic Pad Bearing under Starved Condition

It was mentioned in Chapter Three that the difference between the Martin formula and the curve for the parabolic bearing in Figure 3.2 means the starved condition of the parabolic cylinder lubrication if starved film geometries are used.

But it is possible to express the starvation based on the fixed geometries of the parabolic pad bearing $\Delta h_1, b_1$, especially for the analysis of piston ring lubrication.

For the load carrying capacity of the parabolic pad bearing the equation (3.9) was given for full flooded and under Reynolds conditions. The equation can be used for starved condition replacing the reference geometries.

Referring to Figure 5.1(c)

$$W_s = f_w(H_{os})$$

where

$$W = \frac{w}{\eta u}\left(\frac{\Delta h_s}{b_s}\right)^2 = \frac{w}{\eta u}\left(\frac{\Delta h_1}{b_1}\right)^2 \cdot \left(\frac{\Delta h_s}{\Delta h_1}\right)^2 \cdot \left(\frac{b_1}{b_s}\right)^2$$

$$H_{os} = \frac{h_o}{h_s} = \frac{h_o}{h_1} \cdot \frac{h_1}{h_s}$$

Using the relationship of parabola $\frac{\Delta h_s}{\Delta h_1} = \left(\frac{b_s}{b_1}\right)^2$. Similar procedure as before gives

$$W = \frac{1}{B_s^2} \cdot f_w\left(\frac{H_o}{B_s^2}\right) \tag{5.4}$$

where

$$B_s = \frac{b_s}{b_1} \quad : \text{ starvation parameter}$$

$$(H_s = \frac{\Delta h_s}{\Delta h_1} = B_s^2)$$

The equation (5.4) is exactly the same as the equation (4.3) for parabolic tilting pad bearing. The parameter B_t is replaced by B_s. As $B_s \leq 1.0$ the effects of starvation on load carrying capacity is the same as negative tilting effect ($B_t \leq 1.0$).

As for the oil flow Reynolds outlet, $\bar{X}_R$ is already obtained in Chapter Three Figure 3.2 and it can be converted to film thickness $\bar{H}$.

$$H = \bar{X}_R^2 + H_o$$

Again half of it is the outgoing film thickness deposited on the surface. As $\bar{X}_R$ is a function of H_o only

$$H_e = f_f(H_o) = \frac{1}{2}(\bar{X}_R^2 + H_o)$$

where

$$H_e = \frac{h_e}{\Delta h_1}$$

For starved condition

$$H_{es} = f_f(H_{os})$$

Converting the parameters

$$H_{es} = B_s^2 f_f \left(\frac{H_o}{B_s^2}\right) \qquad (5.5)$$

where

$$H_{es} = \frac{h_{es}}{\Delta h_1}$$

Thus the equation (5.4) and (5.5) are plotted in Figure 5.3 in the same manner as Figure 5.2.

Figure 5.3 can be interpreted in almost the same way as Figure 5.2 for flat inclined pad bearing. But the effects of the incoming film thickness on the minimum film thickness under starved condition is more pronounced than that of flat inclined pad bearing. To explain this, consider:

As shown in Figure 3.2 $\overline{X}_R$ has assymptotic solutions as following:

$$\overline{X}_R = 0.475\, H_o^{\frac{1}{2}} \qquad \text{for} \qquad H_o \to 0$$

$$\overline{X}_R = 0.5 \qquad \text{for} \qquad H_o \to \infty$$

When these are converted to outgoing film thickness,

$$H_e = 0.613\, H_o \qquad \text{for} \qquad H_o \to 0$$

$$H_e = 0.5\, H_o \qquad \text{for} \qquad H_o \to \infty$$

For starved condition, by the equation (5.5), H_{es} is the same as H_e. Thus the exist flow film thickness is 50% to 61.3% of minimum film thickness for all over the operating range. Maximum change is only 20% and this is the reason that the curves for various values of H_e in the figure gives almost constant H_o against U.

For the flat inclined pad bearing the equation (5.2) gives teh assymptotic solution as following:

$$H_e = H_o \qquad \text{for} \qquad H_o \to 0$$

$$H_e = \frac{H_o}{2} \qquad \text{for} \qquad H_o \to \infty$$

For the starved conditon equation (5.3) gives H_{es} is equal to H_e for both assymptotic cases. Thus the change of H_o under starved condition is a little more than that of the parabolic pad bearing.

5.3 Starved Lubrication of EHL Line Contact

In this section EHL line contact under starved condition as well as fully flooded condition will be analysed. The theory itself is same as that found in any published textbooks (4) which is based on the Grubin assumptions. But the results will be presented using non-dimensional groups which have more clear relationship to physical conditions than any other published expression. The crux of the analysis is the importance of hydrodynamic film dimensions, Δh and b, which, as already shown in the foregoing chapters, greatly simplified the classical hydrodynamic lubrication of thrust bearings.

The theory of this section is based on the so called Grubin assumptions as following.

1. The shape of the hydrodynamic film passage of EHL line contact is decided by Hertzian condition only. Thus, the hydrodynamic dimensions are functions of elastic loading condition only.
2. Hertzian contact pressure is so large that the "reduced" pressure in all the Hertzian contact area is constant, which is $1/\alpha$; where α is the pressure viscosity coefficient of the lubricant.

The validity of these assumptions was examined by Dowson et al (43) by comparing the results of this assumption with the numerical results

based on rigorous formulation which satisfies the hydrodynamic and elastic equations simultaneously. The discrepancy is never more than about 20 per cent (43). Thus the Grubin assumptions are frequently used for the analysis of EHL starved condition (35)(40)(41).

Based on the Grubin assumptions hydrodynamic film shape is given solely by the Hertzian equation as following (4). Referring to Figure 5.4,

$$h = \frac{bP_{max}}{E} \{ \frac{x}{b} \sqrt{\frac{x^2}{b^2} - 1} - \ell n \, (\frac{x}{b} + \sqrt{\frac{x^2}{b^2} - 1}) \}$$

where

P_{max} : maximum Hertzian contact pressure

b : half Hertzian contact breadth

x : co-ordinate from the cnetre of the contact

$$\frac{1}{E} = \frac{1 - a_1^2}{E_1} + \frac{1 - a_2^2}{E_2}$$

E_1, E_2 : Young's modulus

a_1, a_2 : Poison ratio

As the inside of the curly bracket of the equation is non-dimensional, non-dimensionalization of the equation can be completed simply by the term $\frac{bP_{max}}{E}$ which has a dimension of length. But it is more clear to express the term by actual length of the contact.

From the Hertzian theory

$$\frac{P_{max} b}{E} = \frac{b^2}{2R} = \Delta h$$

if the deformation is small compared with the radius of the surface

$\frac{b^2}{2R}$ is actually the vertical depression of the surface from the undeformed condition which is shown in Figure 5.4 as Δh.

Thus the equation can be non-dimensionalized by the actual length Δh.

$$H(X) = X\sqrt{X^2 - 1} - \ell n\ (X + \sqrt{X^2 - 1}) \tag{5.6}$$

where

$$X = \frac{x}{b}\ ,\ H = \frac{h}{\Delta h}$$

Now the non-dimensional surface shape is given, hydrodynamic equation can be introduced. As the procedure of the equation can be found elsewhere (4) the mathematical formulation will be presented with brief explanation.

The Reynolds equation is

$$\frac{dp}{dx} = 6\eta u\ \frac{h - \bar{h}}{h^3}$$

where $u = u_1 + u_2$

η is given by an exponential function of the pressure,

$$\eta = \eta_o\ e^{\alpha p}$$

where α : pressure viscosity coefficient.

Then the Reynolds equation becomes

$$\frac{dp}{dx}\ e^{-\alpha p} = 6\eta_o u\ \frac{h - \bar{h}}{h^3}$$

The left hand side of the equation can be modified as

$$\frac{dp}{dx}\ e^{-\alpha p} = \frac{d}{dx}\ (\frac{1 - e^{-\alpha p}}{\alpha}) = \frac{dp_o}{dx}$$

where

$$p_o = \frac{1 - e^{-\alpha p}}{\alpha} \quad : \text{ reduced pressure.}$$

Replacing the pressure by reduced pressure, the equation reduces to the original form,

$$\frac{dp_o}{dx} = 6\eta_o u \frac{h - \bar{h}}{h^3}$$

Applying the assumption (2) $\bar{h} = h_o$, then non-dimensional form of the equation is

$$\frac{dP_o}{dX} = 6 \frac{H(X)}{\{H_o + H(X)\}^3}$$

where

$$P_o = \frac{P_o b}{\eta_o u} \left(\frac{\Delta h}{b}\right)^2$$

$$H_o = \frac{h_o}{\Delta h}$$

$$X = \frac{x}{b}$$

H(X) is given by the equation (5.6)

Integration of the equation gives the non-dimensional reduced pressure distribution,

$$P_o = 6 \int_{X_i}^{X} \frac{H(X)}{\{H_o + H(X)\}^3} \, dX$$

Analytical integration is not possible, but a simple trapesoidal

method gives the numerical values of integral as a function of X, X_i and H_o. This the equation can be expressed as,

$$P_o = 6\, f(X, X_i, H_o) \tag{5.7}$$

The equation expresses the reduced pressure built up along the inlet axis X. The start of pressure built up is expressed by integration lower limit X_i where p = 0. When $X_i = \infty$ the function is for full flooded condition and when X_i is finite it is for starved condition.

The equation (5.7) was calculated by the trapesoidal rule and integration steps ΔX were taken arbitrarily as following

$$\Delta X = 5 \times 10^{-5} \quad \text{for} \quad X < 0.01$$
$$\Delta X = 5 \times 10^{-4} \quad \text{for} \quad 0.01 \leq X < 0.1$$
$$\Delta X = 2 \times 10^{-3} \quad \text{for} \quad 0.1 \leq X < 1.0$$
$$\Delta X = 1 \times 10^{-2} \quad \text{for} \quad 1.0 \leq X < 2.0$$
$$\Delta X = 2 \times 10^{-2} \quad \text{for} \quad 2.0 \leq X < 5.0$$
$$\Delta X = 5 \times 10^{-2} \quad \text{for} \quad 5.0 \leq X \leq 50$$

Numerical integration terminates when X = 50, where the increase of integration is less than 10^{-7} per 1.0 of X. Thus the theoretical infinite is 50 numerically.

The results are shown in Figure 5.5. The abscissa is X - 1.0 which is a non-dimenisonal distance from the edge of the Hertzian contact. The ordinate is non-dimensional reduced pressure $P_o/6$. It is shown that for a large value of X the reduced pressure decreases inversely proportional to the square of the distance (X - 1.0) indicating that a film inlet zone, which is several times longer than the Hertzian

contact breadth, has negligible contribution to the pressure generation.

The value of $\frac{P_o}{6}$ when X = 1.0 (X - 1.0 → 0 in the figure) is the so called Grubin integral and the numerical values are compared with those of published data (4). This is shown in the table above Figure 5.5. As the methods of non-dimensionalization are different the values of reference (4) is converted to agree with this thesis. The difference is small, less than 1%. Considering the approximations involved in the assumptions it is not worthwhile to examine the reason of this difference.

The figure shows the reduced pressure built up from the infinitely distant (numerically 50) film inlet position. If the inlet position X_i is finite (starved condition) the difference between the values of $P_o/6$ at X and $X = X_i$ is the pressure built up under starved condition.

The assumption (2) gives that the reduced pressure p_o at the edge of the Hertzian contact X = 1.0 is $1/\alpha$. Thus

$$P_{o\alpha} = 6\, f(1, X_i, H_o) = G(X_i, H_o) \qquad (5.8)$$

where

$$P_{o\alpha} = \frac{b}{\eta_o u \alpha} \left(\frac{\Delta h}{b}\right)^2$$

As $P_{o\alpha}$ is solely decided by the loading $(b, \Delta h)$ and operating condition (η_o, u, α), the equation gives the relationship between the film thickness H_o and operating condition $P_{o\alpha}$ under the film inlet position X_i. This is calculated based on Figure 5.5 and shown Figure 5.6. $P_{o\alpha}$ is converted to its reciprocal in the figure and shown as a non-dimensional surface velocity U_α. By this conversion the dependence of the EHL film thickness on the surface velocity is more clearly observed.

As shown in the figure for a range considered the equation of EHL film thickness under full flooded condition can be expressed by,

$$H_o = 0.935\, U_\alpha^{8/11} \tag{5.9}$$

This can be converted to a conventional form using Hertzian contact equations as following,

$$\frac{b}{\Delta h} = \frac{E}{P_{max}} = (\pi \frac{ER}{w})^{\frac{1}{2}}$$

$$b = 2R\frac{P_{max}}{E} = 2R(\frac{1}{\pi}\frac{w}{ER})^{\frac{1}{2}}$$

$$\Delta h = \frac{b^2}{2R} = 2R(\frac{1}{\pi}\frac{w}{ER})$$

Putting these Hertzian equations into the equation (5.9),

$$\frac{h_o}{R} \cdot \frac{\pi}{2}\frac{ER}{w} = 0.935\ \{\frac{\eta_o u\alpha}{R} \cdot \frac{1}{2}\ (\frac{ER}{w})^{3/2}\}^{8/11}$$

Rearranging and collecting constants,

$$\frac{h_o}{R} = 1.2534\ (\frac{\eta_o u\alpha}{R})^{8/11}\ (\frac{ER}{w})^{1/11} \tag{5.10}$$

When the surface velocity u is taken as average surface velocity u/2 and the definition of reduced Young's modulus is changed to 2E in order to agree with the notation of Dowson (43), the constant of the equation becomes,

$$1.2534 \times 2^{8/11} \times (\frac{1}{2})^{1/11} = 1.948 \simeq 1.95$$

Thus the formula agrees with that given by the reference (43).

In Figure 5.6 the effects of starvation on the EHL film thickness is clearly shown. As the starvation becomes severe (X_i reduces), EHL

film thickness reduces and the reduction ratio varies depending on the operating condition U_α. As the figure shows the EHl film thickness for both the fully flooded and starved conditions, it is general and no other artificial starvation parameter is necessary. All the parameters in the figure represent the physical condition. This generality of the expression can never be realised by any conventional method. This is because, as shown in the derivation of the equation, the conventional EHL formulae (5.10) are the results of combining the hydrodynamic equation with the Hertzian equations which, in the Grubin assumptions, are independent of each other. Thus the conventional formula conceals the importance of the hydrodynamic parameters in an EHL contact. In contrast to this, equation (5.9) is simple, as it expresses the hydrodynamic condition independently on the Hertzian condition. The Hertzian condition is included in the non-dimensional parameters as Δh and b. In the design practice of concentrated contacts, it is essential to calculate Hertzian conditions to estimate the fatigue life of the surfaces, independently on the consideration of EHL conditions. Thus there is no advantage to combine the equations to give EHL film thickness directly.

Based on Figure 5.6, several other methods are possible to express the effects of starvation. Figure 5.7 is simply made by replacing the co-ordinate of the parameters and shows the EHL film thickness variation against film inlet distance. It is shown that for a large value of X_i the EHL film thickness reduction under starved condition is negligible. Thus the boundary between starved and full flooded condition can be defined as a condition at which the EHL film thickness reduction ratio from full flooded condition is a certain set value. This value is arbitrarily taken as 0.03 and the boundary is shown in the figure as a broken line. In the figure EHL film thickness ratio

between starved and full flooded condition is also shown. It can be observed that the trends of EHL film thickness from the boundary of starvation are similar for all the curves shown. Thus it is possible to summarise the starvation effects on EHL film thickness with reference to the "start of starvation". This start of starvation is a boundary between the two conditions and approximate relationship is given as

$$X_{if} - 1 = 2.6\, H_{of}^{0.56} \tag{5.11}$$

where

X_{if} : minimum film inlet distance for flooded condition

H_{of} : film thickness under flooded condition

This equation can be converted to the form which agrees with that of Hamrock (44).

From Hertzian condition,

$$\frac{h_o}{\Delta h} = 2 \left\{ \left(\frac{R}{b}\right)^2 \cdot \left(\frac{h_o}{R}\right) \right\}$$

Thus

$$X_{if} = 1 + 3.83 \left\{ \left(\frac{R}{b}\right)^2 \cdot \left(\frac{h_o}{R}\right) \right\}^{0.56} \tag{5.12}$$

Hamrock gave

$$X_{if} = 1 + 3.06 \left\{ \left(\frac{R}{b}\right)^2 \left(\frac{h_o}{R}\right) \right\}^{0.58} \tag{5.13}$$

Considering the difference between rigorous numerical calculation and the semi-analytical results based on the approximation, the agreement is fairly good. Hamrock's formula is a result of statistical analysis based on about ten calculated data. So it is not definite.

Based on the equation (5.11) which gives the boundary between full flooded and starved condition, all the curves in Figure 5.7 are summarised by the relative starvation inlet distance $(X_i - 1)/(X_{if} - 1)$ and are shown in Figure 5.8 as a solid line. Maximum variation between the curves summarised is about 0.02 in the vertical scale of the figure. Results of Hamrock (44) are also included in the figure as a broken line. Although there is a difference in the starting point of the starved condition shown in equations (5.12) and (5.13), the tendencies of film thickness reduction for both results are nearly the same.

The film inlet distance X_i can be converted to inlet film thickness as following,

$$H_i = H_o + H(X_i)$$

where

$H_i = \frac{h_i}{\Delta h}$: inlet film thickness

$H(X_i)$: equation (5.6)

Thus the starvation can be expressed by inlet film thickness H_i and shown in Figure 5.9. It is shown that the reduction of EHL film thickness becomes significant when the inlet film thickness becomes less than about 10 times of EHL film thickness, which agrees with experimental results (45).

5.4. Discussion and Conclusion

The generality of the non-dimensional expression was again demonstrated in the analysis of classical hydroydnamic lubrication under starved conditions. Simple modification of the equations for

full flooded conditions allowed the comprehensive analysis of the effects of starvation on the minimum film thickness shown in Figure 5.2 and Figure 5.3. The figures give the whole picture of hydrodynamic lubrication for classical cases for both full flooded and starved conditions. The figures include information of load carrying capacity (U^{-1} = W) sliding velocity (U) film flow (H_e) and film pressure zone (B_s) which are all related to the minimum film thickness (H_o).

In the analysis of starvation the term of film flow (H_e) was often neglected and the starvation was expressed only by the term of film pressure zone (B_s). This is a serious omission, as the film flow is the most decisive parameter under starved condition as shown in Figure 5.2 and Figure 5.3. Constantinescu (46) studied the classical starvation phenomena in terms of fluid flow. Although his analysis takes into account the effects of surface tension of the film meniscus, the graphs shown in the paper have no information of the load carrying capacity under starved condition.

In the analysis of EHL starvation of this chapter the term of film flow was not discussed. This is because, for EHL lubrication, once starvation occurs EHL film thickness is "completely" a function of incoming film thickness. Under the Grubin assumptions outgoing film thickness is the same as the EHL flat film thickness. If incoming film thickness is greater than the outgoing film thickness, the excess lubricant is accumulated in the inlet zone of the EHL contact and increases the pressure build up zone. If this increase of pressure build up zone can generate more hydrodynamic pressure than before, the EHL film thickness increases, if it can not, the condition is full flooded. For the opposite case the opposite occurs, i.e. the lubricant at the inlet zone is carried away to the exit and the EHL film thickness reduces. Thus, under steady state starved

condition, the EHL film thickness is always the same as the averaged incoming film thickness expressed by the equation as following.

$$h_o = \frac{u_1 h_{i1} + u_2 h_{i2}}{2}$$

where

h_o : EHL flat film thickness

h_{i1}, h_{i2} : incoming film thickness

u_1, u_2 : surface velocity

One of the conventional experimental methods to study the starvation of EHL contacts is to measure the length of film inlet zone. This is actually measuring the results of physical adjustment to satisfy the flow continuity condition.

Thus although many graphs are presented on the analysis of starvation, the conclusion is simple.

Once starvation occurs the film thickness of the contact (classical or EHL) is entirely defined by the incoming film thickness.

In the expression of EHL film thickness a simple formula (5.9) was presented. Advantage of that expression over a conventional expression (5.10) can be emphasised from another point of view other than its simplicity. It is a common engineering practice to machine the surface of gears or rollers slightly crowned in order to avoid the undesirable edge loading. This crowning makes the contact elliptic rather than rectangular. Thus the conventional formula (5.10) can not be applied directly, or an ellipticity parameter must be introduced (44). This ellipticity parameter normally makes the formula more

difficult to understand the physical reality because it must be expressed by a certain artificial function. But the formula (5.9) automatically accommodates the elliptic contact as long as the crowning is small, and this is usually the case. If the crowning is small the surface deformation function H(X) given by the equation (5.6) is not far from the actual situation. Thus once the elliptic contact deformation dimensions Δh and b are calculated, the equation (5.9) or Figure 5.6 can be applied directly to given an EHL flat film thickness. Normally Hertzian contact condition must be calculated independently for other design considerations, i.e., surface fatigue or contact rigidity. This feature can never be realised by conventional expressions because it is a result of artificial combination of two independent equations under Grubin assumptions.

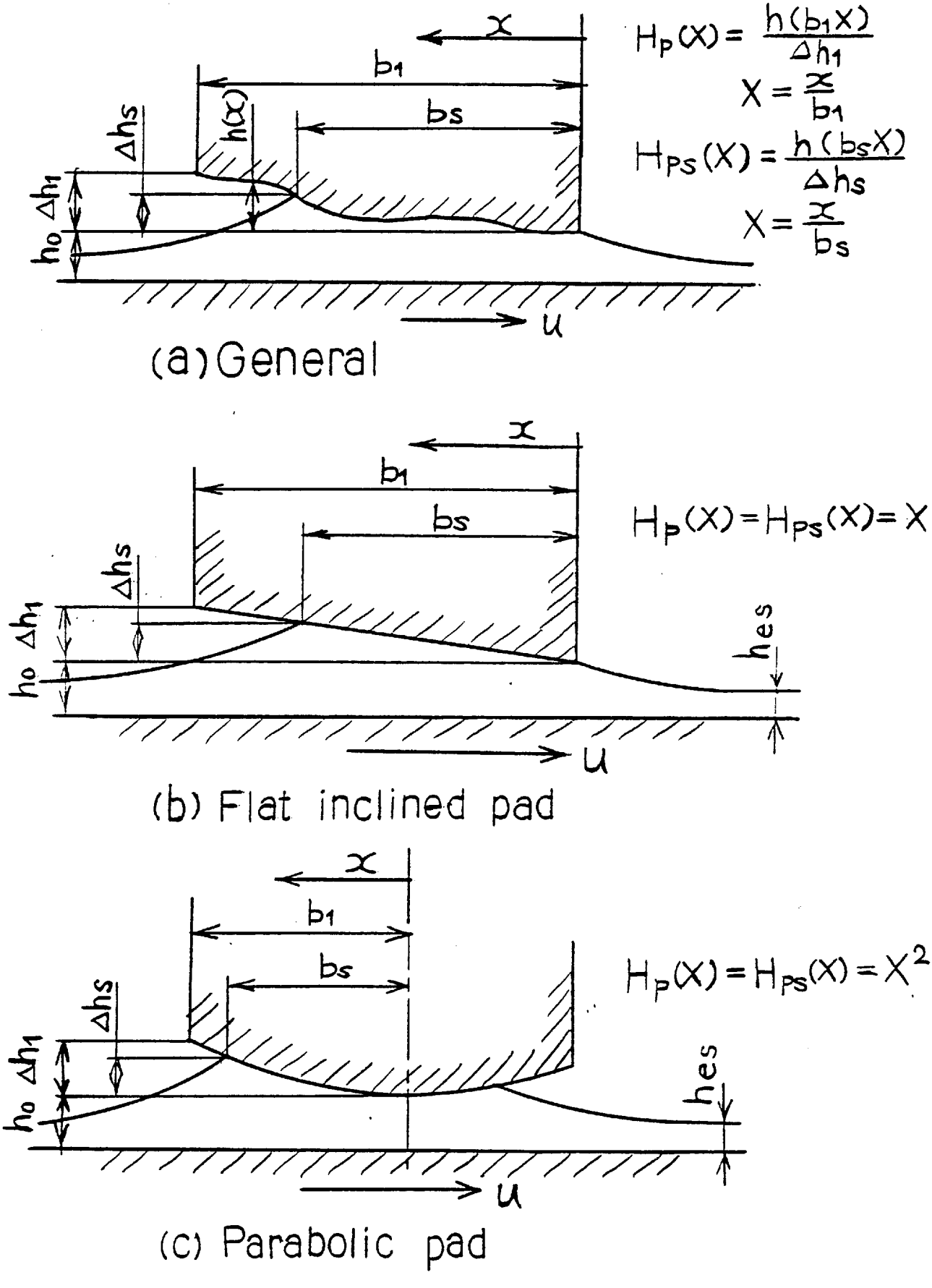


Figure 5.1 Starved Lubrication of Bearings

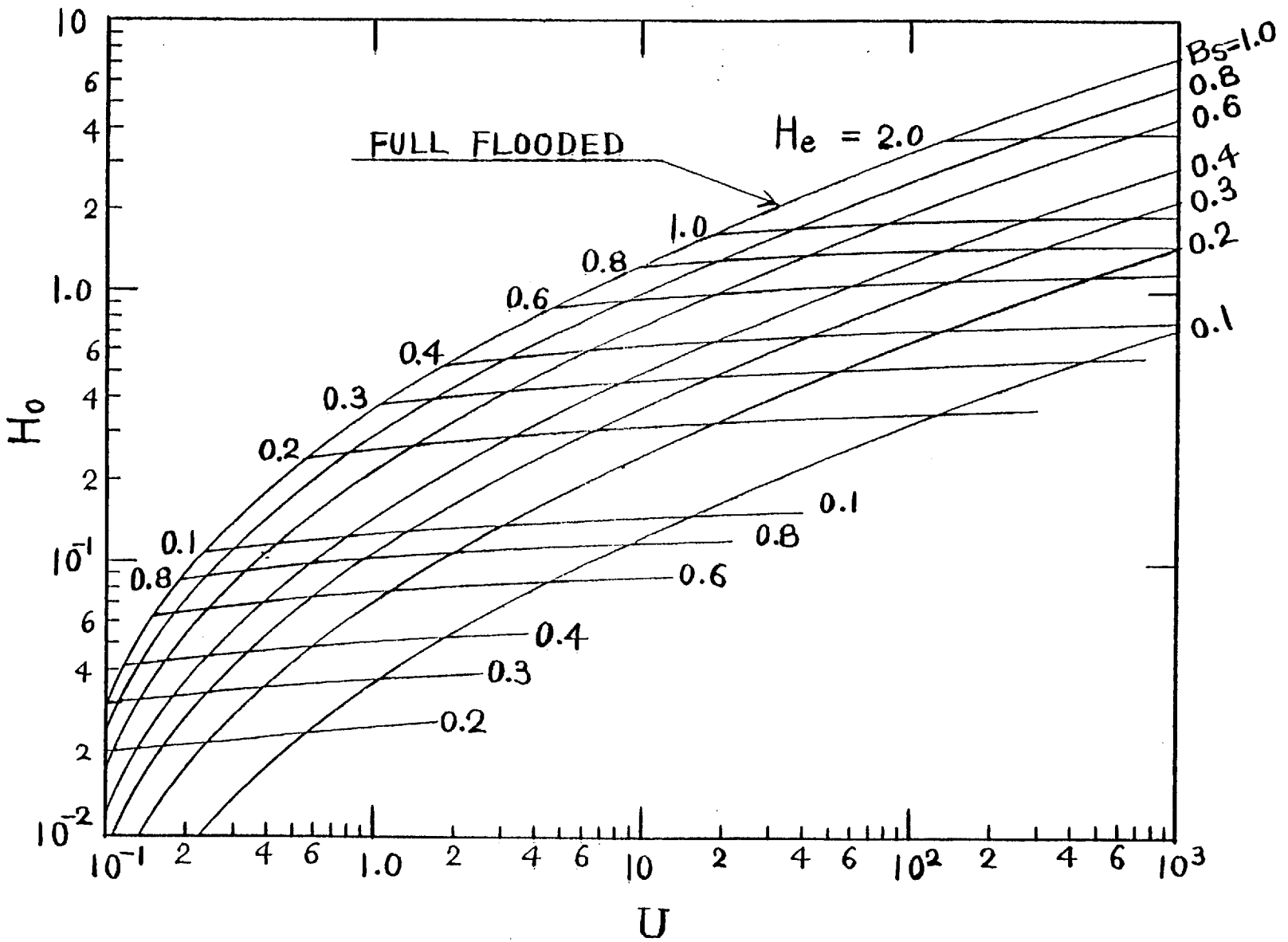


Figure 5.2 Starved Lubrication of Inclined Pad Bearing

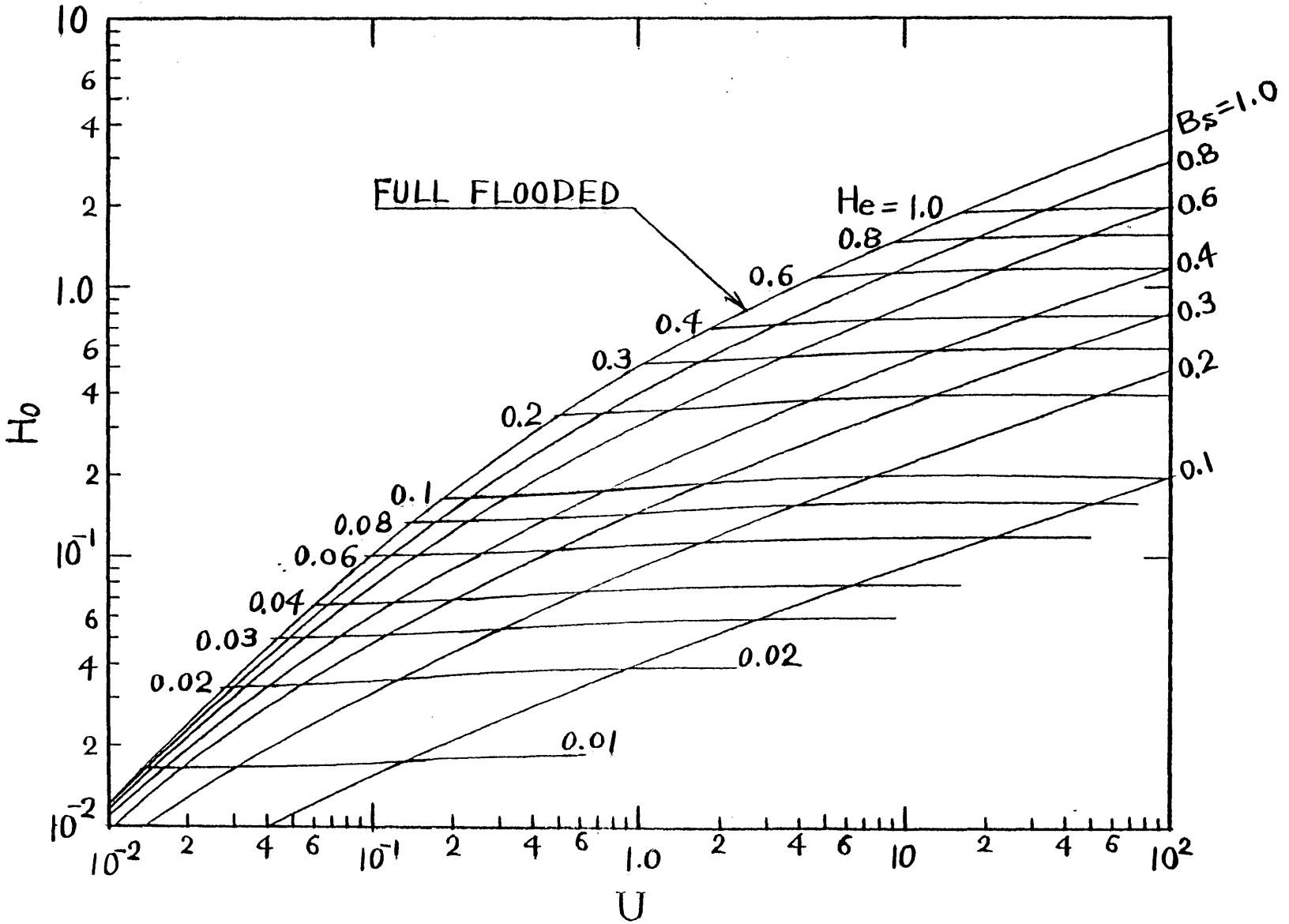


Figure 5.3 Starved Lubrication of Parabolic Face Slider Bearing

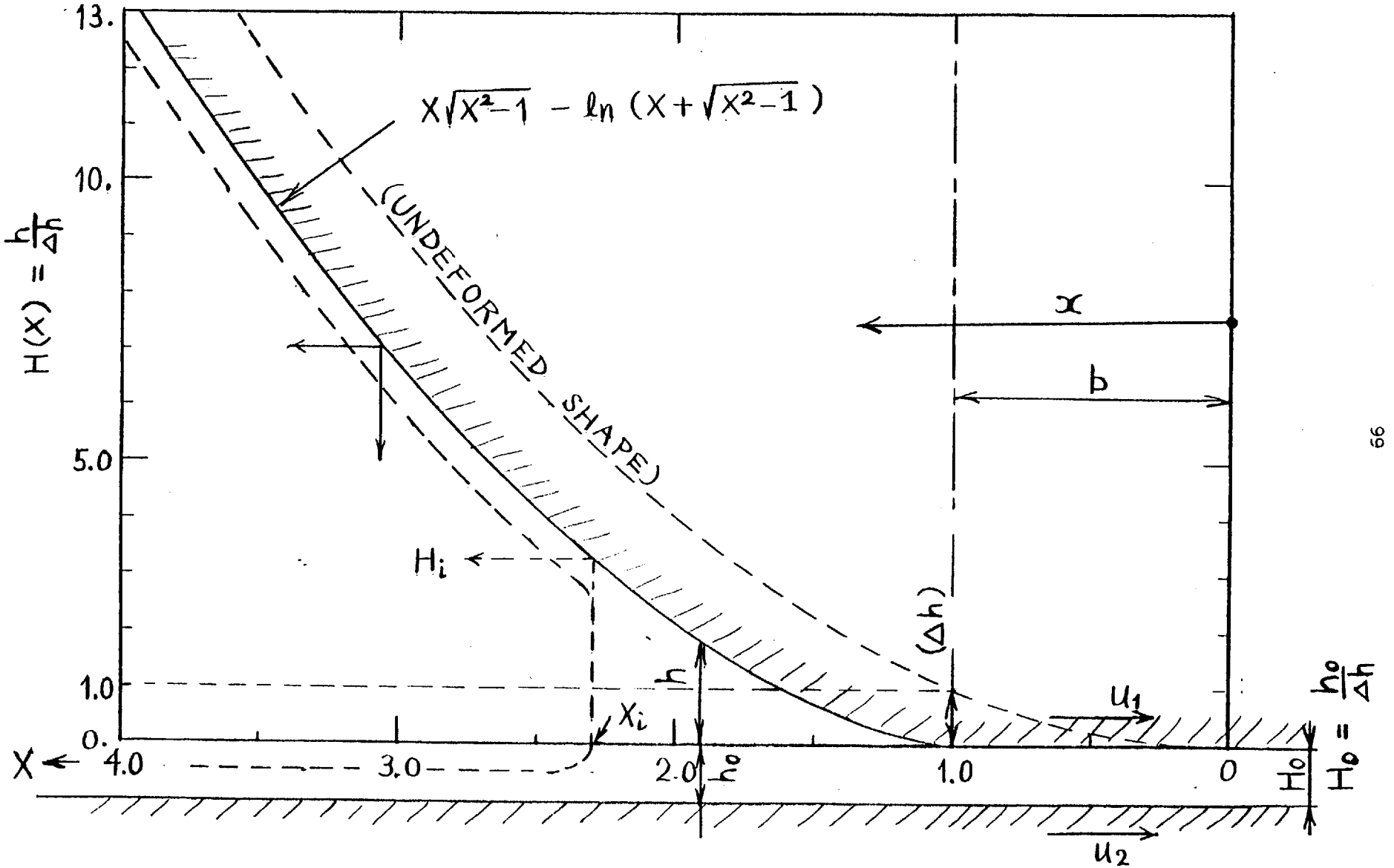


Figure 5.4 Co-ordinate System of EHL Line Contact

	H_0	0.1	0.25	0.5	0.65
$\frac{P_0}{6}$	OBTAINED	3.628	1.039	0.4000	0.2772
	BY REF.	3.601	1.018	0.3944	0.2724

H_0 : H_0 OF REF. DIVIDE BY 2

P_0 : p_0^* OF REF. MULTIPY BY 4

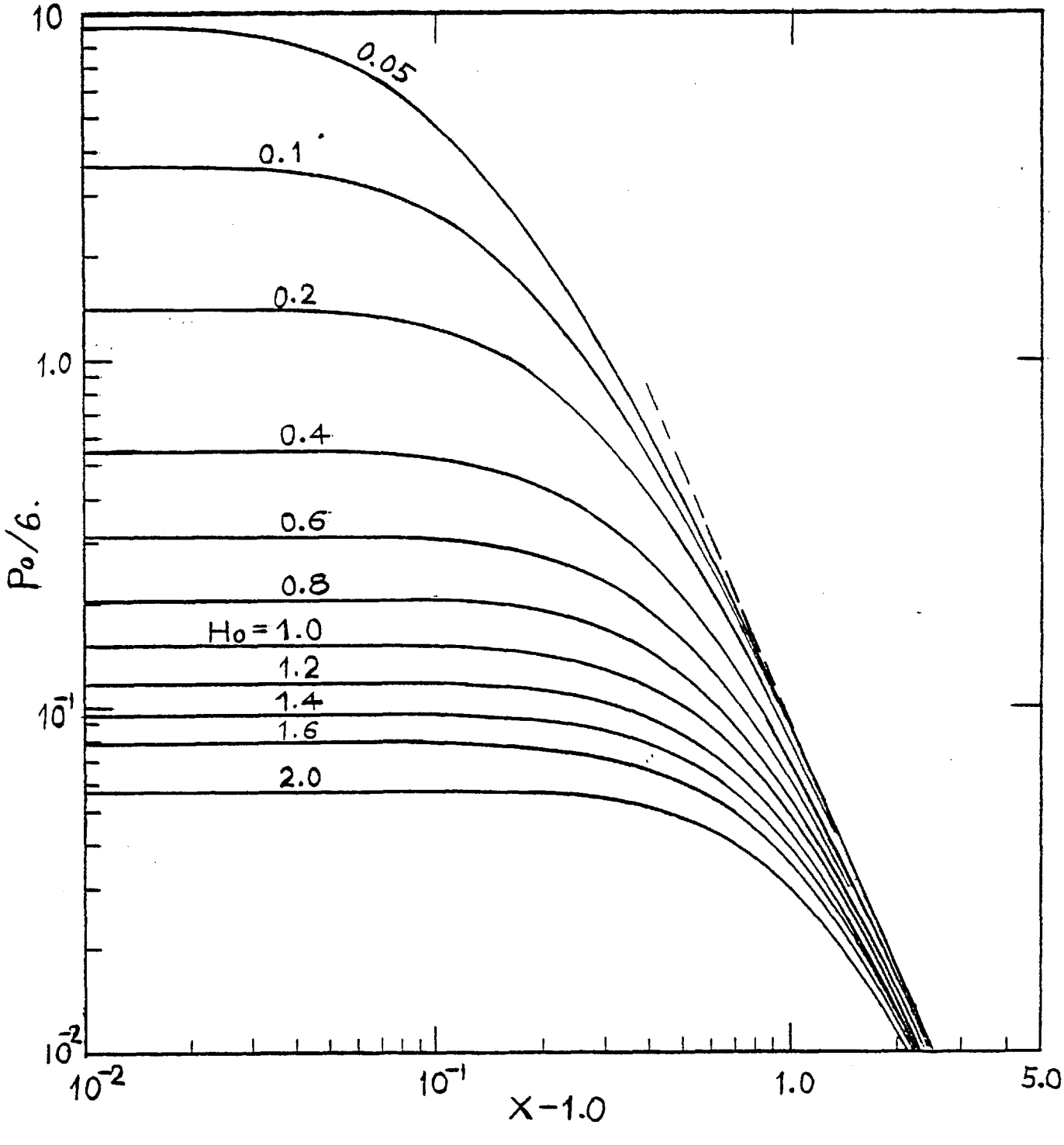


Figure 5.5 Reduced Pressure Distribution Along the Inlet Axis

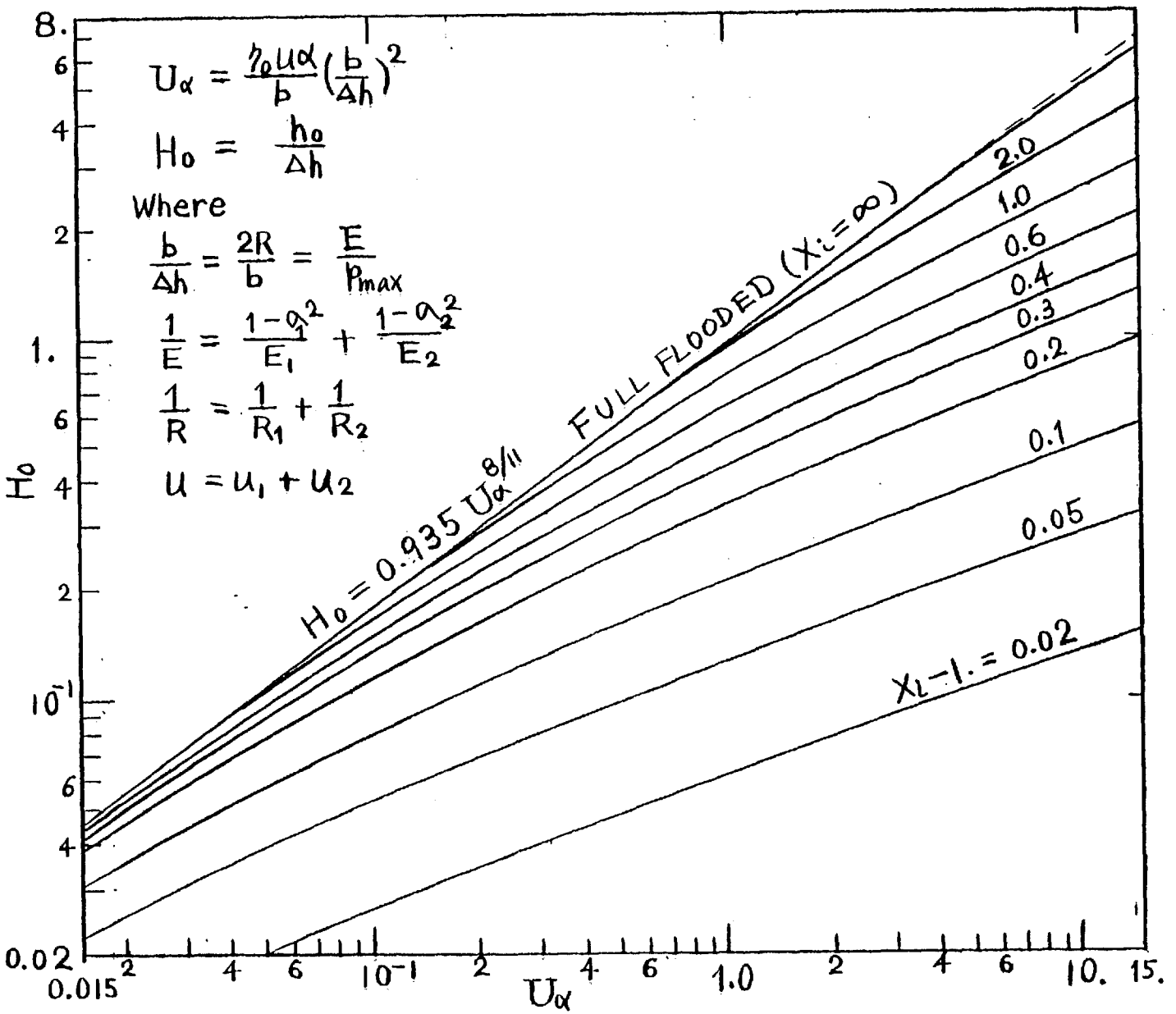
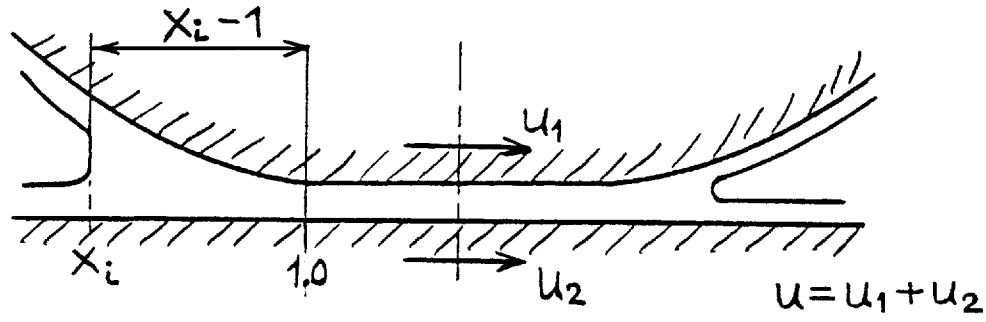


Figure 5.6 General Solution of EHL Film Thickness



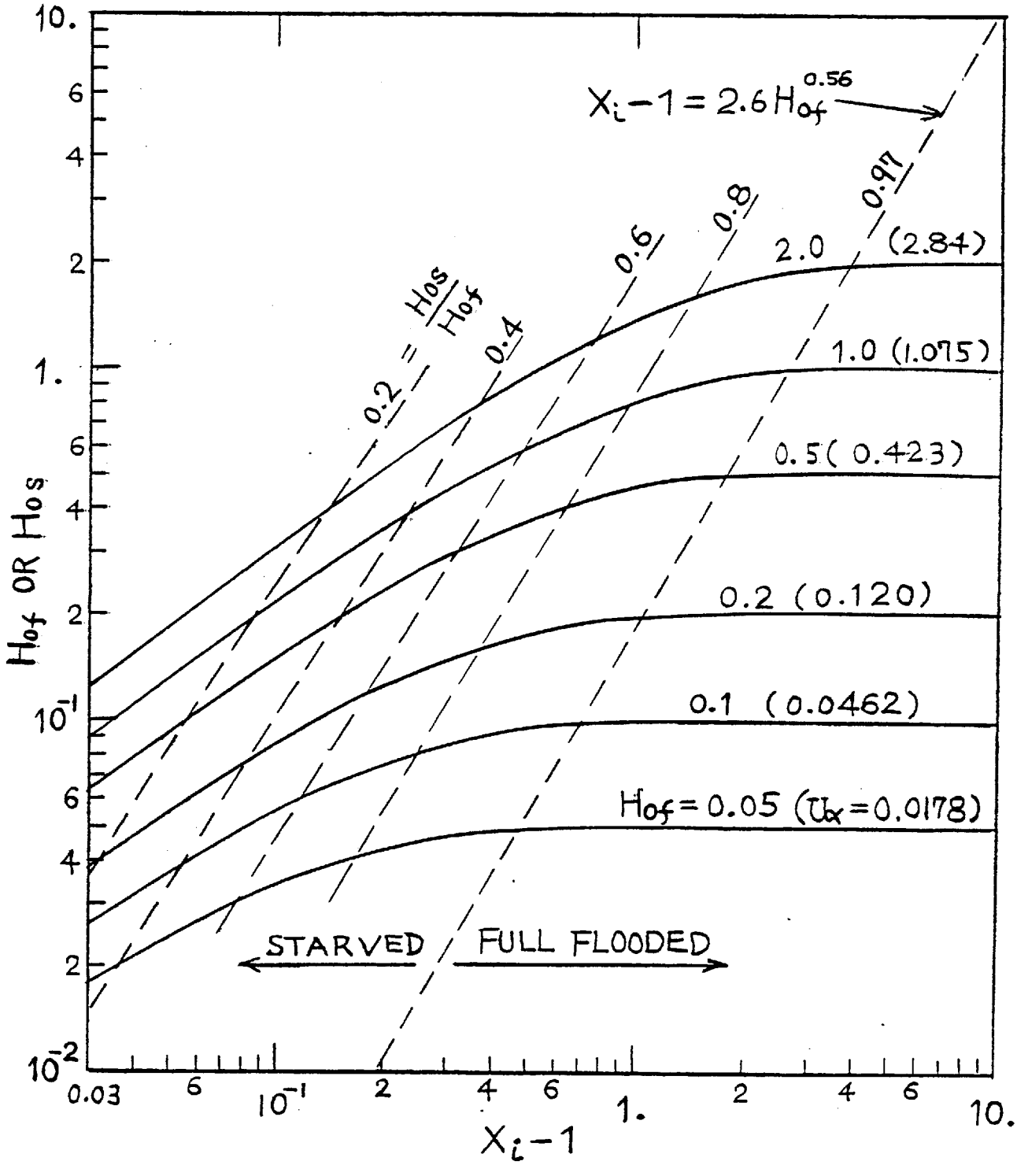


Figure 5.7 EHL Film Thickness Against Inlet Film Distance

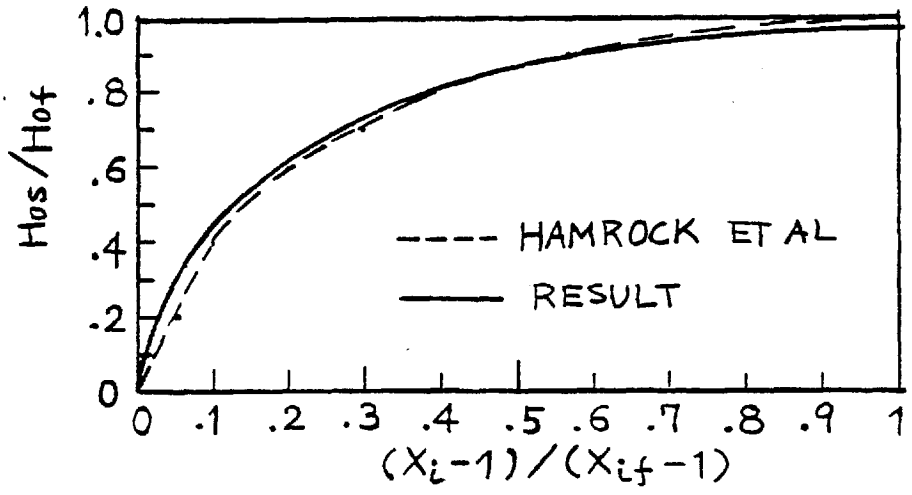


Figure 5.8 EHL Film Thickness Reduction Aginst Relative Inlet Distance

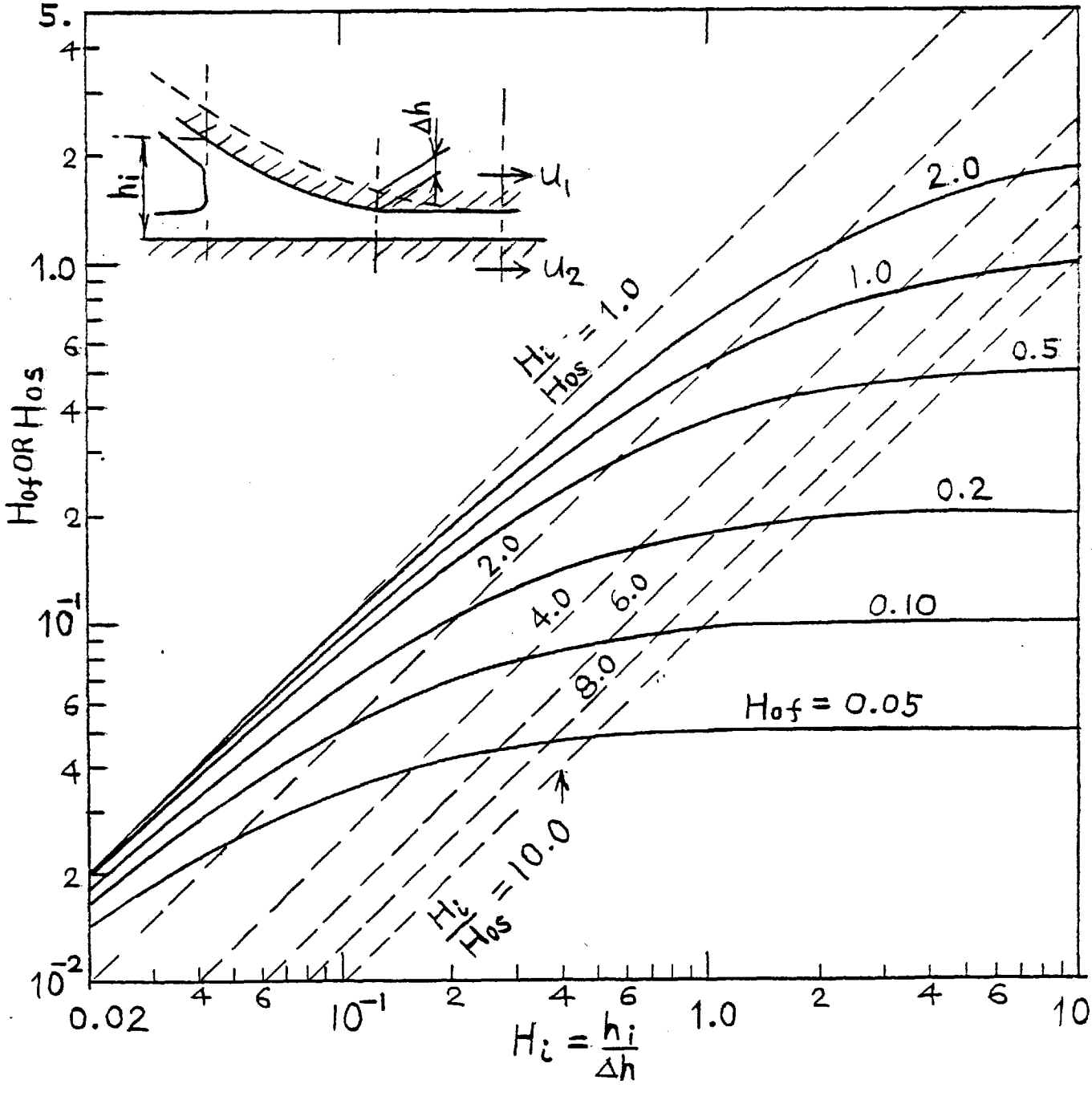


Figure 5.9 EHL Film Thickness Against Inlet Film Thickness

CHAPTER SIX

DYNAMIC BEHAVIOUR OF PARABOLIC PAD BEARINGS

6.1 Introduction

In the foregoing chapters steady state hydrodynamic lubrication under the effects of tilting and starvation has been analysed. In this chapter and in the following two chapters the theory is expanded to include the effects of squeeze velocity, thus the conditions are not steady but dynamic. In this chapter, mainly the effects of squeeze velocity on load carrying capacity of parabolic pad bearings will be analysed.

The equation (2.10) of chapter two shows that the non-dimensional load carrying capacity of the thrust bearings is a function of non-dimensional film thickness and squeeze velocity only. Thus this chapter is about its application to parabolic pad bearings.

6.2 Theoretical Formulation

Using the non-dimensional parabolic surface profile function $Hp(X) = X^2$, the general form of non-dimensional Reynolds equation (2.7) reduces to,

$$\frac{dP}{dX} = 6\left\{\frac{1}{(H_o + X^2)^2} - \frac{H_o + \bar{X}^2}{(H_o + X^2)^3}\right\} + 12\,V\left\{\frac{X}{(H_o + X^2)^3} - \frac{\bar{X}}{(H_o + X^2)^3}\right\} \qquad (6.1)$$

In the equation the first term is called the wedge term and the second term is called the squeeze term. Integration of the equation gives the pressure distribution.

$$P = \int_{X_{out}}^{X} \frac{dP}{dX}\, dX$$

$$= 6\,\{\alpha(X,X_{out}) - (H_o + \bar{X}^2)\gamma(X,X_{out})\}$$

$$+ 12\,V\,\{\beta(X,X_{out}) - \bar{X}\,\gamma(X,X_{out})\} + P_2 \qquad (6.2)$$

where

$$P_2 = \frac{P_2 b_1}{\eta u}\left(\frac{\Delta h_1}{b_1}\right)^2$$

Integral functions α and γ are already given in Chapter Three for steady state solutions. β is given as following.

$$\beta(X,X_{out}) = \int_{X_{out}}^{X} \frac{X}{(H_o + X^2)^3}\, dX$$

$$= \frac{1}{H_o^2} \int_{X'_{out}}^{X'} \frac{X'}{(1 + X'^2)^3}\, dX'$$

$$= \frac{1}{H_o^2}\,\{\beta'(X') - \beta'(X'_{out})\}$$

where

$$\beta'(X') = -\frac{1}{4(1 + X'^2)^2}$$

$$X' = \frac{X}{\sqrt{H_o}}\,, \quad X'_{out} = \frac{X_{out}}{\sqrt{H_o}}$$

In the equation X_{out} is a non-dimensional film outlet and decided by outlet boundary condition as following

$X_{out} = \bar{X} = \bar{X}_R$ for the Reynolds condition

$X_{out} = -B_r = -\frac{b_2}{b_1}$ for the full Sommerfeld condition

As will be discussed in Chapter Eight the most consistent boundary condition is to apply the Reynolds condition as long as the theoretical Reynolds outlet position is inside the bearing breadth ($\bar{X}_R > -B_r$). Otherwise the full Sommerfeld condition must be applied. In this Chapter the Reynolds condition only is applied, supposing that there is enough divergent breadth of the bearing.

Integral constant $\bar{X}$ in the equation can be obtained by applying the inlet boundary condition. If the inlet is fully flooded,

$$\Delta P = P_1 - P_2$$

$$= 6\{\alpha(1,\bar{X}_R) - (H_o + \bar{X}_R^2)\gamma(1,\bar{X}_R)\}$$

$$+ 12\, V\{\beta(1,\bar{X}_R) - \bar{X}_R\, \gamma(1,\bar{X}_R)\} \qquad (6.3)$$

where

$$P_1 = \frac{p_1 b_1}{\eta u} \left(\frac{\Delta h_1}{b_1}\right)^2$$

An analytical solution of the equation is not possible, but a numerical solution can be obtained by the Newton method (29), as a function of the boundary condition ΔP, the squeeze velocity V and the film thickness H_o.

$$\bar{X}_R = f_R\,(\Delta P, V, H_o) \qquad (6.4)$$

Now the integration of the equation (6.2) gives the non-dimensional load carrying capacity.

$$W = \int_{\bar{X}_R}^{1} P dX$$

$$= 6\{\alpha_i(1,\bar{X}_R) - (H_o + \bar{X}_R^2)\gamma_i(1,\bar{X}_R)\}$$

$$+ 12V\{\beta_i(1,\bar{X}_R) - \bar{X}_R\,\gamma_i(1,\bar{X}_R)\} + P_2(1 - \bar{X}_R) \qquad (6.5)$$

where

$$W = \frac{w}{\eta u}\left(\frac{\Delta h_1}{b_1}\right)^2$$

Functions α_i and γ_i are already given in Chapter Three. β_i is given as following.

$$\beta_i(1,\bar{X}_R) = \int_{\bar{X}_R}^{1} \beta(X,\bar{X}_R)\, dX$$

$$= \frac{1}{H_o^{1.5}} \int_{\bar{X}_R'}^{X_1'} \{\beta'(X') - \beta'(\bar{X}_R')\}\, dX'$$

$$= \frac{1}{H_o^{1.5}} \{\beta_i'(X_1') - \beta_i'(\bar{X}_R') - (X_1' - \bar{X}_R')\beta'(\bar{X}_R')\}$$

where

$$\beta_i'(X') = -\frac{X'}{8(1 \quad X'^2)} - \frac{1}{8}\tan^{-1}X'$$

$$X_1' = \frac{1}{\sqrt{H_o}} \quad , \quad \bar{X}_R' = \frac{\bar{X}_R}{\sqrt{H_o}}$$

If the pressure downstram of the Reynolds film outlet P_2 is not zero, the contribution of this pressure for load carrying capacity w_p must be added as

$$w_p = P_2(\bar{x}_R + b_2)$$

non-dimensionally

$$W_p = P_2(\bar{X}_R + B_r)$$

where

$$W_p = \frac{w_p}{\eta u}\left(\frac{\Delta h_1}{b_1}\right)^2$$

$$B_r = \frac{b_2}{b_1} \quad : \text{ offset of parabola}$$

Thus the total load carrying capacity of the bearing W_t is

$$W_t = W + W_p$$

$$= 6\{\alpha_i(1,\bar{X}_R) - (H_o + \bar{X}_R^2)\gamma_i(1,\bar{X}_R)\}$$

$$+ 12V\{\beta_i(1,\bar{X}_R) - \bar{X}_R\,\gamma_i(1,\bar{X}_R)\} + P_2(1 + B_r) \qquad (6.6)$$

The equation (6.6) can be expressed as a function

$$W_t = f_w(P_2, B_r, \bar{X}_R, V, H_o) \qquad (6.7)$$

Thus the dynamic (squeeze) behaviour of the parabolic pad bearing is expressed by two simulataneous non-dimensional equations (6.4) and (6.7). If the squeeze velocity is given first, $\bar{X}_R$ can be eliminated to give

$$W_t = f_w(P_1, P_2, B_r, V, H_o) \qquad (6.8)$$

When boundary pressure P_1 and P_2 are taken as zero, B_r disappears from the equation (6.8). Then

$$W = f_w(V, H_o) \tag{6.9}$$

This equation was the conclusion of Chapter Two.

6.3 Results of Calculation

The equations (6.4) and (6.5) were calculated under the condition $P_1 = P_2 = 0$. The results are shown in Figure 6.2(a),(b) for a different range of values. In these figures non-dimensional load carrying capacity is replaced by its reciprocal, non-dimensional sliding velocity ($U = W^{-1} = \frac{\eta u}{w} (\frac{b_1}{\Delta h_1})^2$). Also shown are the relationships between the instantaneous minimum film thickness and the squeeze velocity for various constant sliding velocities (or load carrying capacity of the film). In order to make clear the film pressure generation area broken lines are added which show this area for various constant values of film outlet $\bar{X}_R$. As shown in the figures squeeze velocity can either be positive or negative, and V is taken as positive when the film thickness decreases (film pressure increases). When V = 0 this is the solution for steady state condition and is shown in Chapter Three, Figure 3.2.

From the figures several characteristics of the dynamic film response can be observed.

They are:

1. Squeeze velocity V is approximately proportional to the difference between instantaneous and steady state film thickness under constant sliding velocity U.
2. When the film thickness is transient(unsteady) the film outlet position $\bar{X}_R$, and the hydrodynamic pressure generation area, increase or decrease depending on the sign of corresponding squeeze velocity. $\bar{X}_R$ can become even positive (in the convergent

zone of the bearing).

3. When the transient film thickness (H_{ot}) appraoches zero, the squeeze velocity approaches a finite value depending on the sliding velocity U. The corresponding film outlet position $\bar{X}_R$ also approaches a finite value.

When the transient film thickness H_{ot} goes to infinity for a given sliding velocity U, the squeeze velocity V and the film outlet $\bar{X}_R$ also go to infinity. But there is a definite relationship between V and $\bar{X}_R$.

6.4 Discussion

Each characteristic mentioned is discussed.

1. When this is expressed in an equation

$$\frac{dH_o}{dt} = -\frac{u}{b_1} K(H_o - H_{os})$$

K : constant and a function of U and H_o

H_{os} : steady state film thickness and a function of U only

Rearranging

$$\frac{dH_o}{dt} + \frac{u}{b_1} K H_o = \frac{u}{b_1} H_{os}$$

Thus for a condition whose load or velocity are unsteady, the equation is non-linear and an analytical solution is not possible. But if the non-dimensional velocity U is given as a function of time together with initial film thickness, these define K and H_{os}. The other constant in the equation is

$\frac{u}{b_1}$ only. Thus $\frac{u}{b_1}$ and $U(=\frac{\eta u}{w}(\frac{b_1}{\Delta h_1})^2)$ as a function of time decides the non-linear differential equation and the solution can be obtained numerically.

2. The fact that the outlet boundary contracts or expands depending on the squeeze velocity, indicates that if different boundary conditions other than the Reynolds condition is imposed on the theoretical formulation the results might be quite different. As stated in the introductory chapter no attempt has been made to calculate the difference, it is decided to do it in detail in the next Chapter.

3. Under the Reynolds boundary condition there are two distinct positions which decide the film flow rate. These are the positions of maximum pressure and film outlet at which the equation $\frac{dp}{dx} = 0$ is satisfied. There the film flow velocity pattern is linear and the flow rates are,

$$q_m = \frac{Uh_m}{2} \quad : \quad \text{at maximum pressure position}$$

$$q_{out} = \frac{uh_R}{2} \quad : \quad \text{film outlet position}$$

Under the condition of squeeze velocity v, the flow continuity condition is,

$$\frac{u}{2}(h_m - h_R) = -v(x_m - \bar{x}_R)$$

The equation is rearranged using the parabolic face profile function and its non-dimensional form is

$$V = -\frac{1}{2}\frac{H_m - H_R}{X_m - \bar{X}_R} = -\frac{1}{2}(X_m + \bar{X}_R) \qquad (6.10)$$

Thus once the equations are solved numerically to give V and $\bar{X}_R$, the equation (6.10) gives the position of maximum hydrodynamic pressure. Then the equation (6.2) gives the maximum hydrodynamic film pressure.

Based on the equation (6.10) several cases can be considered

a) When $V = 0$, $X_m = -\bar{X}_R$. Thus the both positions are symmetric about the centre of the parabola. This is the case for the steady state lubrication condition.

b) Maximum values of $\bar{X}_R$ and X_m are 1. (The film pressure zone must be inside the bearing breadth). Thus the maximum possible negative squeeze velocity is $-\frac{1}{2}(1 + 1) = -1$.

c) When the squeeze velocity is very large and positive the maximum pressure point approaches to the position of minimum film thickness, thus $X_m \to 0$. Then $V = -\frac{1}{2}\bar{X}_R$. This condition also occurs when the film thickness is small because the film pressure build up is confined to near the minimum film thickness position. Thus each broken line (constant $\bar{X}_R$) in the figures intersects the axis of $H_o = 0$ at the points where $V = \frac{1}{2}\bar{X}_R$.

Thus in this chapter the generality of the non-dimensional expressions of chapter two are again demonstrated. With these non-dimensional groupings it is possible to evaluate the difference between the three kinds of boundary conditions, which are commonly applied in the theoretical analysis of hydrodynamic lubrication of piston rings.

These will be compared quantitatively, subsequently in the thesis.

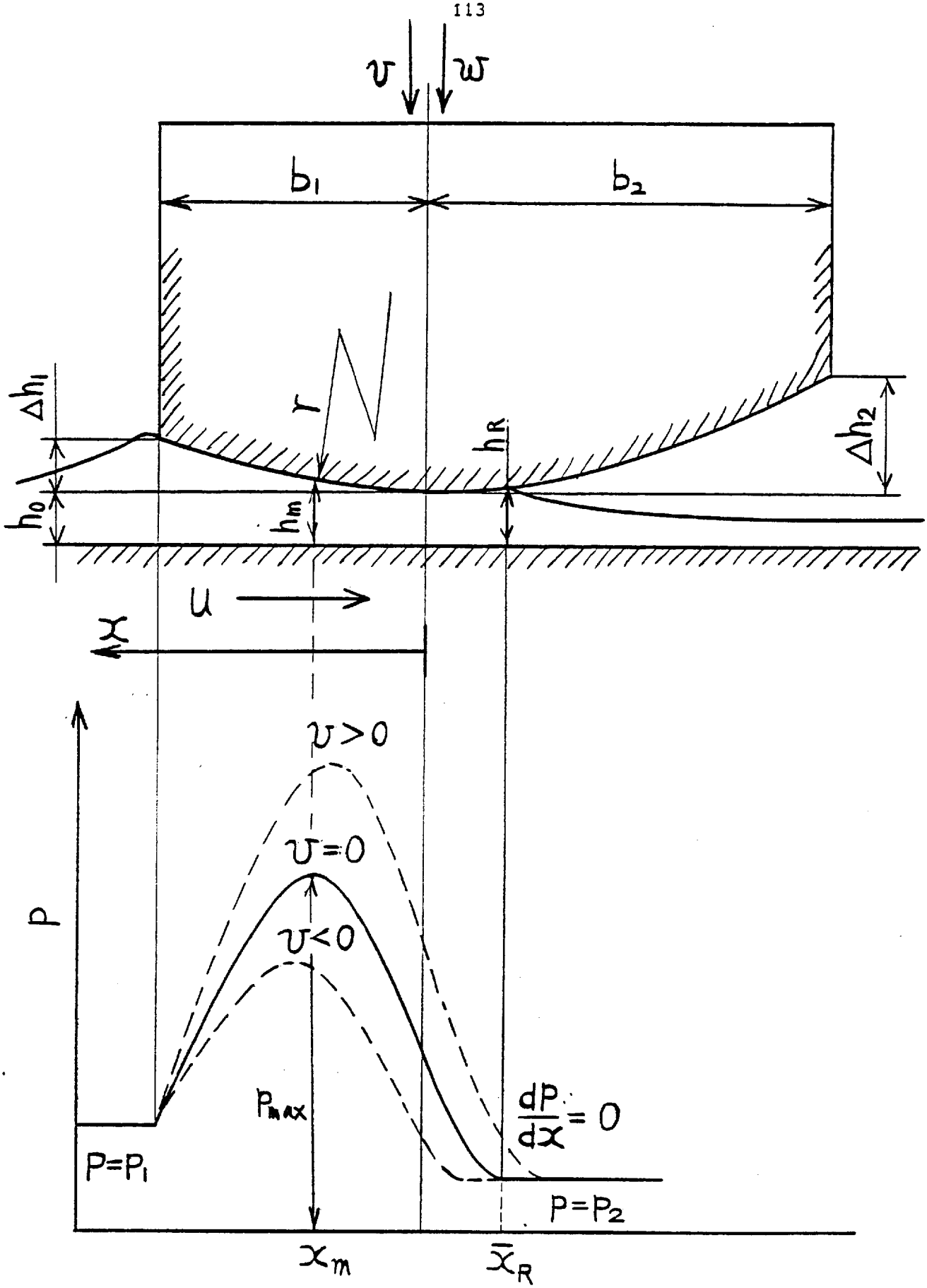


Figure 6.1 Parabolic Pad Bearing Under Squeeze Effects

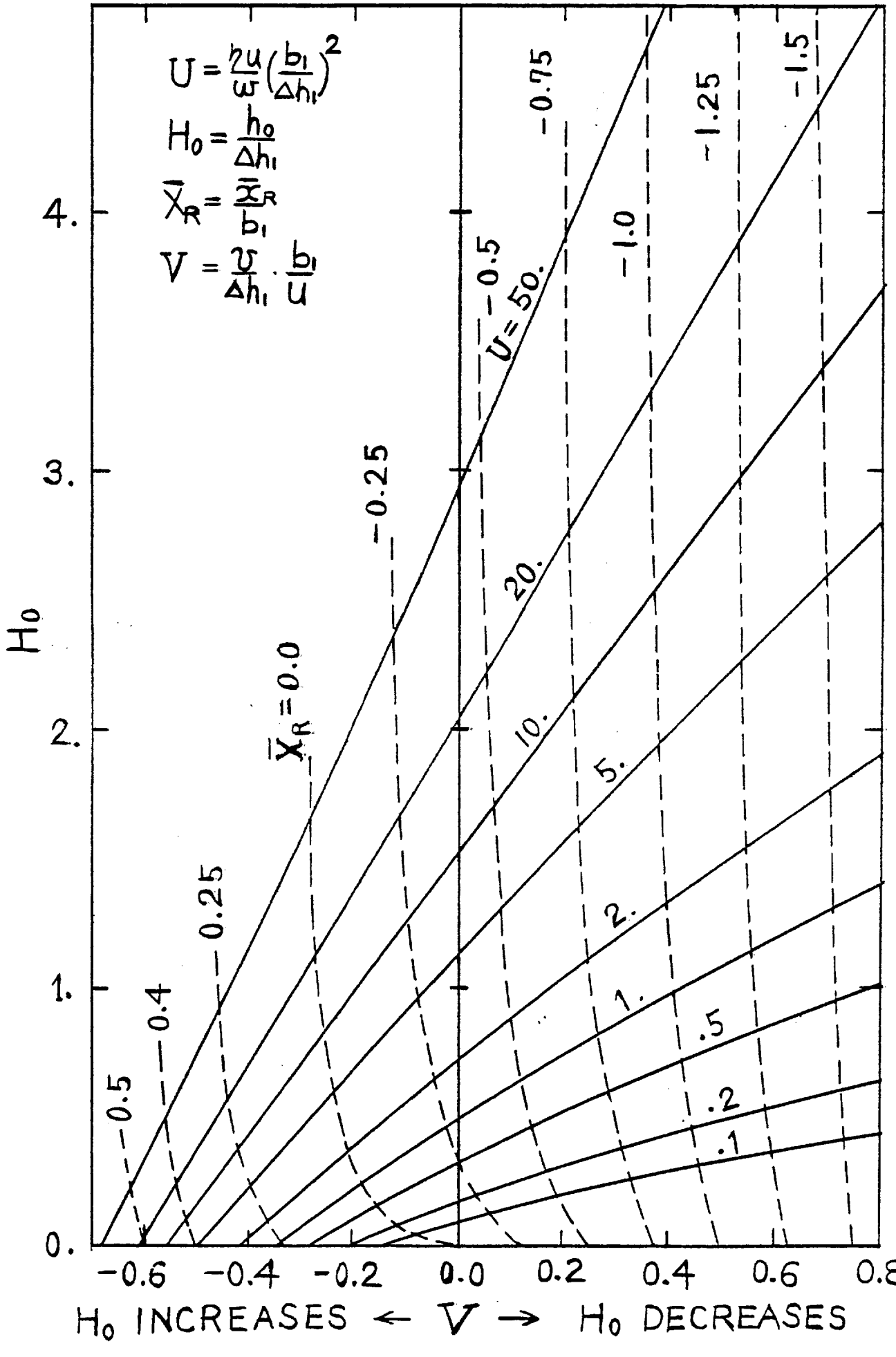


Figure 6.2(a) Load Carrying Capacity of a Parabolic Pad Bearing Under Squeeze

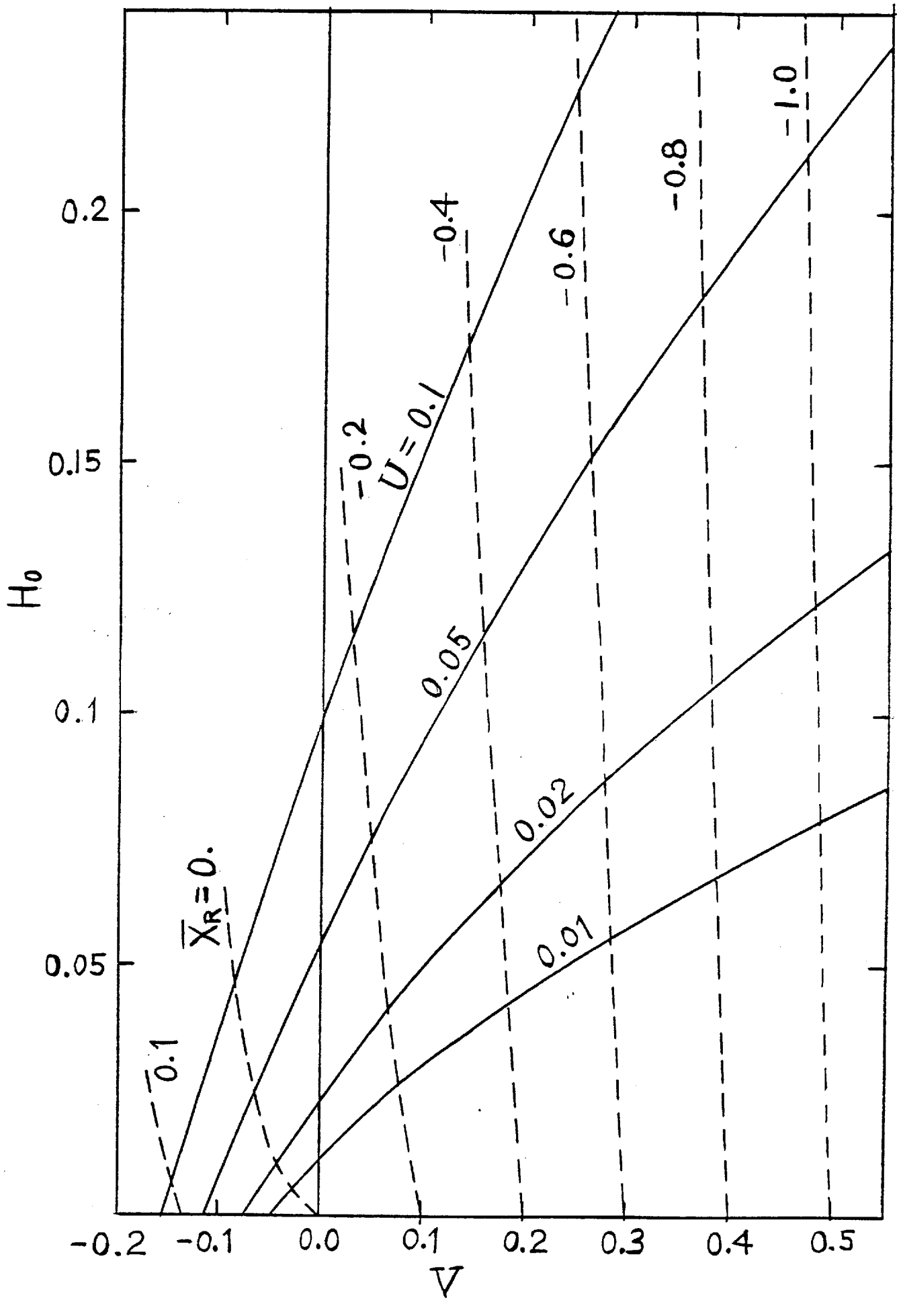


Figure 6.2(b) same as (a)

CHAPTER SEVEN

COMPARISON BETWEEN THREE DIFFERENT BOUNDARY CONDITIONS

7.1 Introduction

In the last Chapter, it was shown that squeeze effects changes the film outlet position significantly from positive to negative infinity. This indicates that the boundary conditions other than Reynolds conditions, if imposed on the theory, many produce significantly different solutions from that of Reynolds condition which are already presented in the last Chapter.

There are two different boundary conditions other than Reynolds conditions which have been applied to analytical studies on the dynamic behaviour of piston ring lubrication in the past literature. They are that $p = 0$

a) at $x = 0$ (minimum film thickness position)
   and $p = 0$ for all divergent parts

b) at $x = -b_1$ (bearings rear end) but neglect negative pressure for load carrying capacity.

These conditions have their analogy in journal bearing theory. Condition (a) is analogous to half Sommerfeld condition. Condition (b) can be considered to be "modified" full Sommerfeld condition, because the solution of the film pressure distribution is exactly analogous to full Sommerfeld condition of a journal bearing, but neglect negative pressure for load carrying capacity of the bearing.

Condition (a) does not satisfy film flow continuity at $x = 0$ and implicity neglects this physical inconsistency. Condition (b) does satisfy flow continuity for all the bearing breadth, but contains another serious physical inconsistency. Although the solution of pressure distribution can be so obtained that it satisfies flow

continuity for all the bearing breadth, negative pressure so introduced is discarded for load carrying capacity as if the negative pressure does not exist. If the negative pressure does not exist the film pressure distribution must be different because the boundary condition so imposed has no influence on the film pressure generation. This is a serious self-contradiction intrinsic to the condition (b).

Thus the correct condition, as far as can be seen at the moment, is to give the end of the pressure distribution curve at the point where $dp/dx = 0$ as long as this point is within the divergent breadth of the bearing, as shown in the foregoing Chapters.

The difference in the load carrying capacity of journal bearings between condition (a) (half Sommerfeld condition) and Reynolds condition is not excessive (4) which is the reason why condition (a) is often used in engineering practice.

Although the errors so introduced by neglecting the physical inconsistency may be small for steady state lubrication of journal bearings, they may not be small in dynamic conditions of piston rings. It must be a prerequisite to evaluate the errors quantitatively, or at least qualitatively, before interpreting the results obtained under whatever the boundary condition.

But no systematic study on this has been carried out in the past so far as is known. Thus it can be said that the boundary conditions adopted by different authors in the past entirely depended on their personal preference whatever the reason they may claim.

7.2 Theory

From the theory already described in the foregoing Chapters it

is simple to apply the boundary condition (a) and (b). For the purpose of simplicity of the comparison atmosphere pressures at both inlet and outlet of the film are taken as zero.

The procedure is to just change the integration limit in the formulation of Chapter Six for both conditions.

Film pressure distribution is

$$P = 6\{\alpha(X,X_{out}) - (H_o + \bar{X}^2)\gamma(X,X_{out})\} + 12V\{\beta(X,X_{out}) - \bar{X}\gamma(X,X_{out})\} \quad (7.1)$$

The integral constant $\bar{X}$ (position of maximum pressure) is given by

$$0 = 6\{\alpha(1,X_{out}) - (H_o + \bar{X}^2)\gamma(1,X_{out})\} + 12V\{\beta(1,X_{out}) - \bar{X}\gamma(1,X_{out})\}$$

This can be solved to give $\bar{X}$ as

$$\bar{X} = -V + \sqrt{V^2 + 2V(\beta/\gamma) + \alpha/\gamma - H_o} \quad (7.2)$$

where

$$\alpha = \alpha(1,X_{out})$$
$$\beta = \beta(1,X_{out})$$
$$\gamma = \gamma(1,X_{out}) .$$

The load carrying capacity is

$$W = 6\{\alpha_i(1,X_o) - (H_o + \bar{X}^2)\gamma_i(1,X_o)$$

$$12V\{\beta_i(1,X_o) - \bar{X}\gamma_i(1,X_o)\} \qquad (7.3)$$

In the equations (7.1),(7.2) and (7.3) integration limits must be chosen as following:

For boundary condition (a), $X_{out} = X_o = 0$

For boundary condition (b), $X_{out} = -B_r$ and X_o is a position at which p = 0, and they are given by the following equation,

$$0 = \alpha(X_o,-B_r) - (H_o + \bar{X}^2)\gamma(X_o, - B_r)$$

$$+ 2V\{\beta(X_o,- B_r) - \bar{X}\gamma(X_o - B_r)\} \qquad (7.4)$$

The equation cannot be solved analytically but can be solved numerically by the root search method.

7.3 Results and Discussions

Figures 7.1(a)(b)(c) are pressure distributions along the breadth of the bearings under three different boundary conditions. The conditions of comparison are following

$H_o = 1.0$

$B_r = 1.0$

$V = -0.5\omega + 0.5$

The B_r value is relevant only for the condition (b) (full

Sommerfeld condition). The other conditions are not influenced by the value of B_r.

In order to make the comparison clear all the figures are drawn to the same scale.

At first glance it is clear that the effects of squeeze are distinctly small for the half Sommerfeld condition, compared with other two conditions. It is easily reasoned that this is because of the film outlet pressure which is forcifully fixed as zero at the minimum film thickness position. As the pressure is artificially fixed at this position, the negative pressure appears under the negative squeeze effects. This negative pressure is automatically taken into account for the load carrying capacity and the negative load carrying capacity must be calculated under certain conditions.

In contrast to the half Sommerfeld condition, the modified full Sommerfeld condition (b) and the Reynolds condition looks similar. The squeeze effects increase or decrease the positive pressure area in a similar way for both conditions. But as the film outlet pressure is fixed at the bearing outlet, condition (b) produces zero load carrying capacity when V is about -0.4, while the Reynolds condition still shows positive pressure and positive load carrying capacity. As it has been discusssed in the last chapter Reynolds condition produces positive pressure as long as $V > -1.0$. It is apparent that the effect of squeeze velocity on film pressure distribution is more pronounced in condition (b) than with the Reynolds condition.

Thus the qualitative observation of the comparison of the pressure distribution is that,

. Condition (a) is too artificial to be a physical condition.

. Condition (b) might be tolerated as an approximation of physical

conditions, because the tendency of the effects of squeeze velocity looks similar to the Reynolds condition.

. Reynolds condition looks the most realistic physically.

In order to quantify these qualitative observations Figure 7.2(a)(b)(c) have been made. Condition (b) only requires the bearings outlet geometry so B_r is set as 1.0, thus the comparison has been made for a symmetric parabola. The abscissa is squeeze velocity V and the ordinate is load carrying capacity W. The figures give the instantaneous load carrying capacity against the instantaneous squeeze velocity for three different instantaneous film thicknesses H_o (= 0.2, 1.0, 2.5).

The solid lines marked by (R) are for the Reynolds condition. The chain lines marked by (a) and the broken line marked by (b) are for the boundary conditions (a) and (b).

From the figures the following observations can be made:

Steady state load carrying capacity (which occurs when V = 0) for the conditions (a) and (b) is the same and about 20∿30% less than the Reynolds condition in the shown range. This is because condition (a) and (b) produces the same pressure distribution, if the surface shape of the bearing is symmetric and the pressure is zero at the axis of symmetry, at which the Reynolds condition generates a postive pressure.

The dynamic response of the hydrodynamic film can be quantitatively evaluated by the gradients of the curves, which indicates how much more or less load can be supported by the film pressure instaneously, for a given squeeze velocity. The greater gradient the less squeeze velocity is caused by a given load, thus the longer time is necessary before the film converges to a steady state condition. Around the

steady state condition (V = 0) the gradient is the greatest for the condition (b), and the smallest for the condition (a). The gradient for the Reynolds condition is near the condition (b). This means that the condition (a) predicts less difference between instantaneous and steady state film thickness than the Reynolds condition or condition (b). The reason is obviously due to the pressure distribution of condition (a) shown in Figure 7.1(a). For the same reason the line of condition (a) is almost straight, as the squeeze effects merely expand or contract the pressure curves.

With reference to the discussion on the pressure distribution of the film, there are three characteristic points in Figure 7.2 (a)(b)(c) marked by dots, at which the load carrying capacities for the different boundary conditions agree with each other. This is because at these operating conditions the theoretical pressure distribution becomes the same for all.

If the approximate boundary conditions (a) and (b) are compared with the physically consistent Reynolds conditions (R), it might be concluded that (b) is more approximate than (a) because the steady state load carrying capacity of (a) and (b) is the same, (though about 20% less than (R)) and because the gradient of (b) is nearly equal to (R).

Before any conclusions can be drawn the condition (b) must be examined for the case of different offset ratio of the parabola. Only the condition (b) required the outlet geometry B_r of the bearing for the case discussed above and the comparison is given only for the case of the symmetric parabola.

Thus the calculation was carried out to examine how the outlet boundary position affects the pressure distribution of the film and load carrying capacity for the modified full Sommerfeld

condition (condition (b)). The results for the steady state condition (V = 0) are shown in Figure 7.3. The film thickness H_o is fixed as 1.0 and the offset ratio of parabola B_r is varied from 0 to 2.0. The lower figure shows the film pressure distribution for different bearing divergent breadths. It can be noticed that the positive pressure increases and then decreases when B_r is varied from 0 to 2.0. According to the variation of positive pressure distribution, the load carrying capacity of the bearing increases and reaches the maximum and then decreases as shown in the upper figure of Figure 7.3. Thus the wider bearing breadth has less load carrying capacity than the narrower bearing breadth. The reason is that the negative pressure in the divergent part of the bearing, which will be discarded for the load carrying capacity of the bearing, is "pulling down" the positive pressure in the convergent part, in order to make the pressure at the bearing outlet equal to zero.

Under dynamic (squeeze) conditions it can be simply reasoned that, although the load carrying capacity of the wider divergent breadth is less than the narrower divergent breadth bearing, the former has a greater load carrying capacity under squeeze than the latter. The wider the divergent breadth, the greater the negative pressure "submerged" as a potential load carrying capacity under squeeze. Under squeeze, this potential negative pressure emerges as positive pressure and contributes to the calculation of load carrying capacity. Thus the wider the bearing divergent breadth, the greater the dynamic load carrying capacity. This potential load carrying capacity (negative pressures) are shown as broken lines in the lower figure of Figure 7.3 and Figure 7.1(b). These unrealistic features are caused by the physical self contradiction of condition (b) described earlier.

Thus the condition (b) must be rejected at least for the case

of the parabolic pad bearing with longer divergent breadth than convergent breadth. But for the case of shorter divergent bearings this condition is the only reasonable condition. For example, case ($H_o = 1.0$) of this condition does not produce any negative pressure when $B_r \leq 0.358$, when $B_r = 0.358$, condition (b) produces the same pressure distribution as the Reynolds condition and as a result the same load carrying capacity. When $B_r > 0.358$ the condition (b) must be replaced by the Reynolds condition and the pressure distribution and the load carrying capacity should not change. This is shown in the upper figure of Figure 7.3 as a broken line.

7.4 Conclusion

The conclusions concerning approximate boundary conditions, (a) half Sommerfeld condition, (b) modified full Sommerfeld condition which were compared with the Reynolds condition for their influence on the dynamic (squeeze) performance of the parabolic pad bearing are listed as following.

1. Half Sommerfeld condition (a) should be rejected because it neglects the divergent part which should equally generate the squeeze pressure as the convergent part of the bearing. This condition predicts less than half of the increase of the load carrying capacity under squeeze than Reynolds condition.
2. Modified full Sommerfeld condition (b) should be rejected for a parabolic bearing with longer divergent breadth than convergent breadth.
3. The most reasonable boundary condition is the application of the condition (b) as long as the film pressure is positive. If negative pressure appears Reynolds condition should be applied.

This can be said in another way. Reynolds condition should be applied as long as the theoretical film outlet is within the bearing breadth, otherwise condition (b) should be applied.

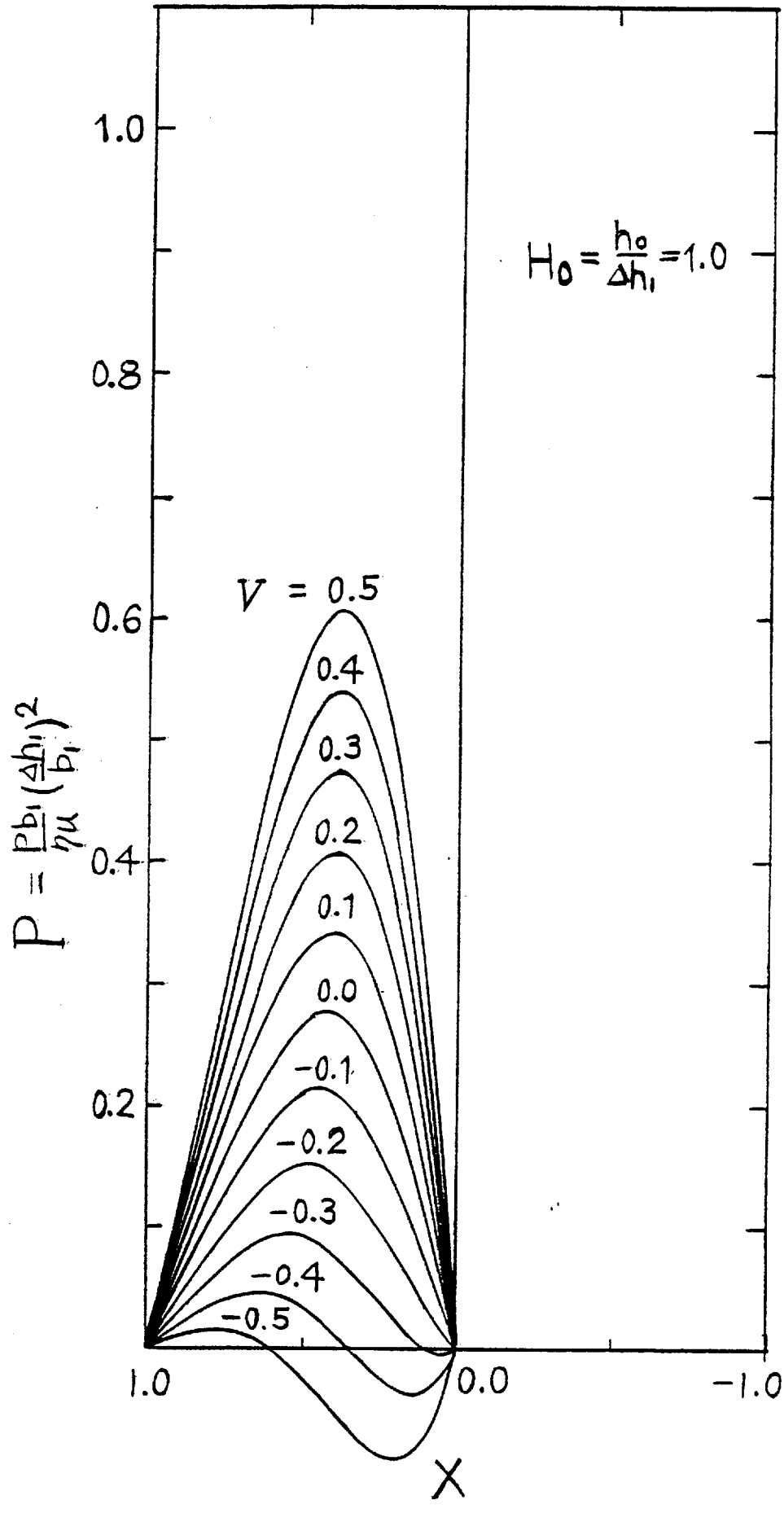


Figure 7.1(a) Film Pressure Distribution Under Half Sommerfeld Condition

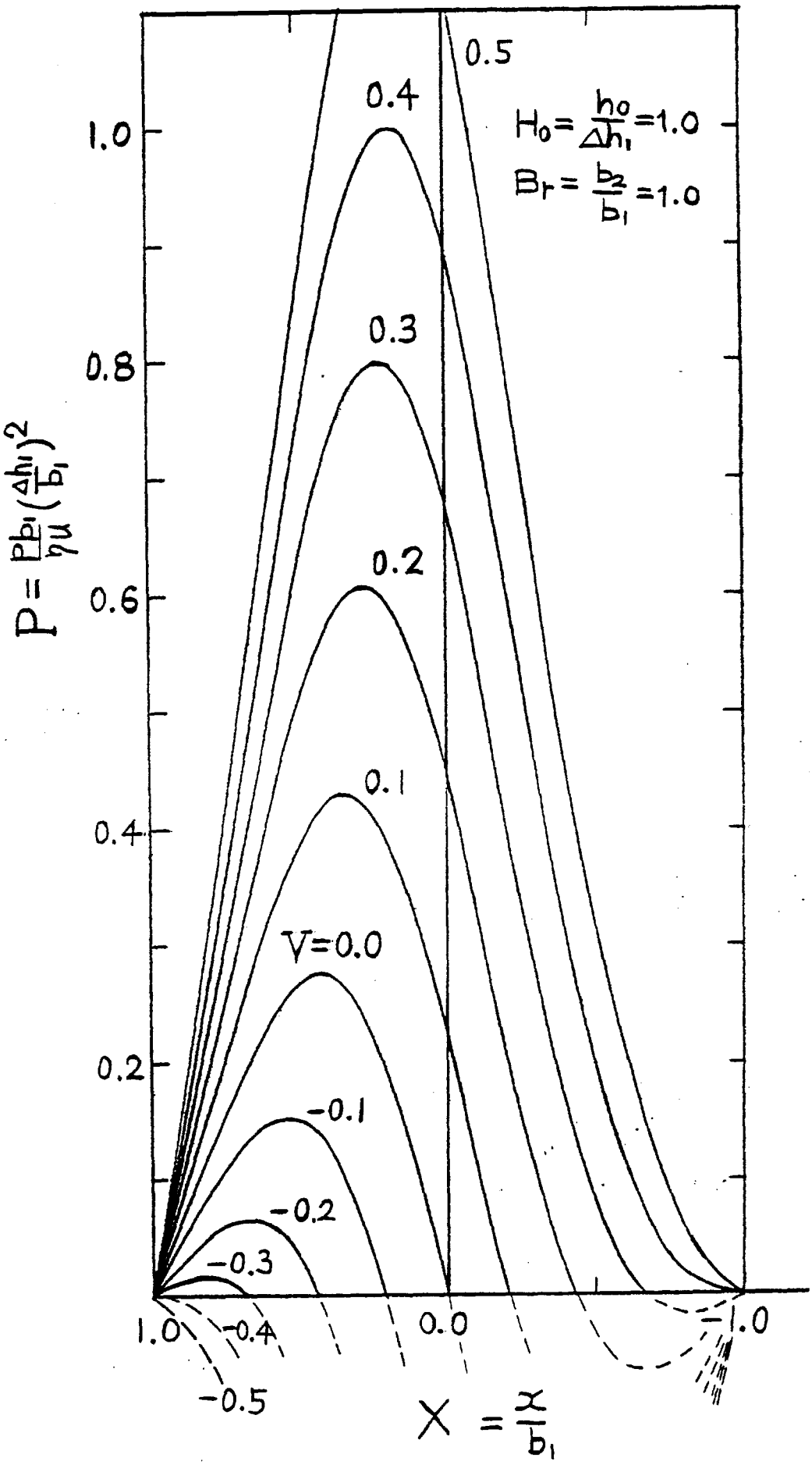


Figure 7.1(b) Film Pressure Distribution Under Full Sommerfeld Condition

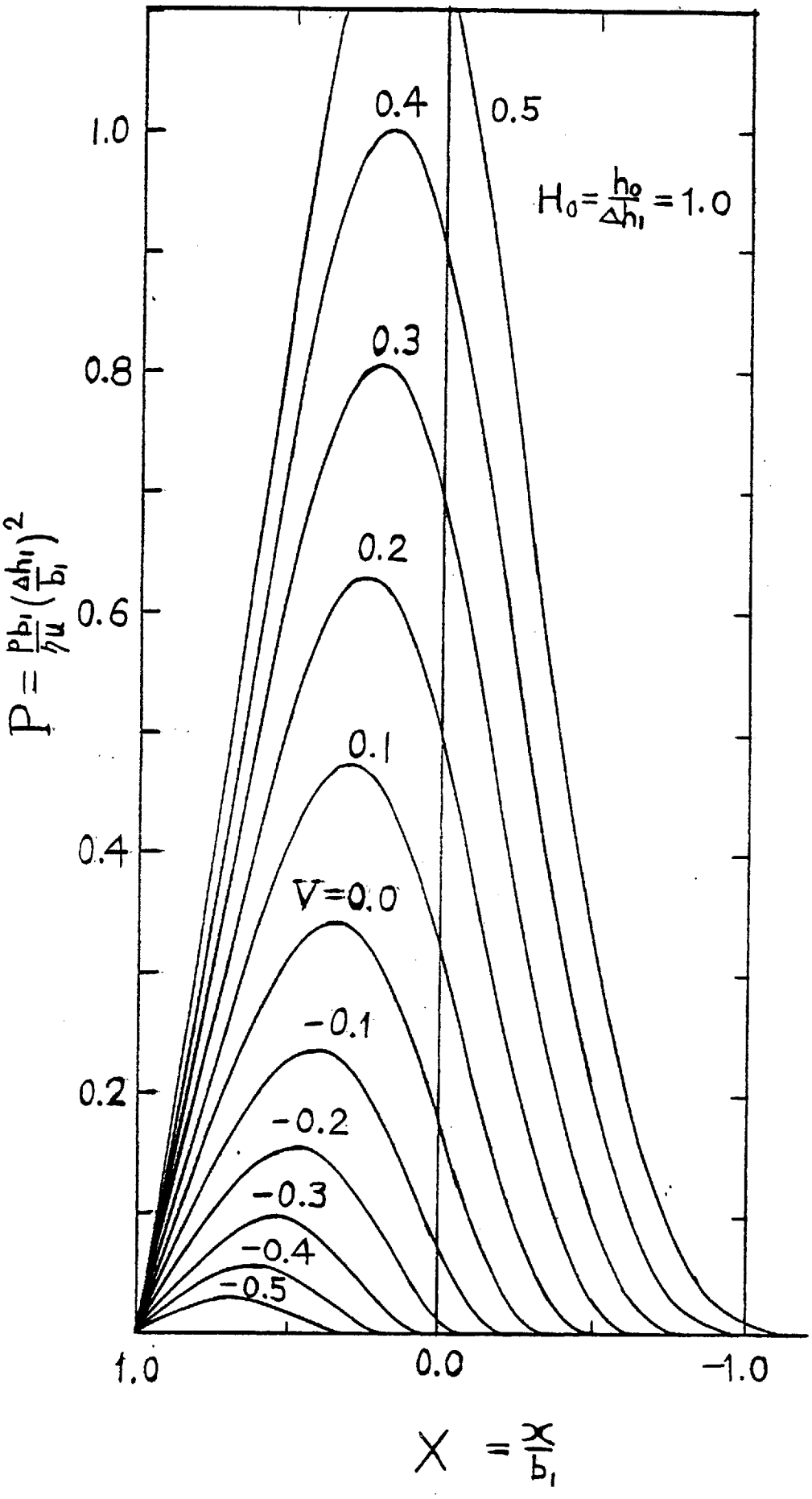


Figure 7.1(c) Film Pressure Distribution Under Reynolds Condition

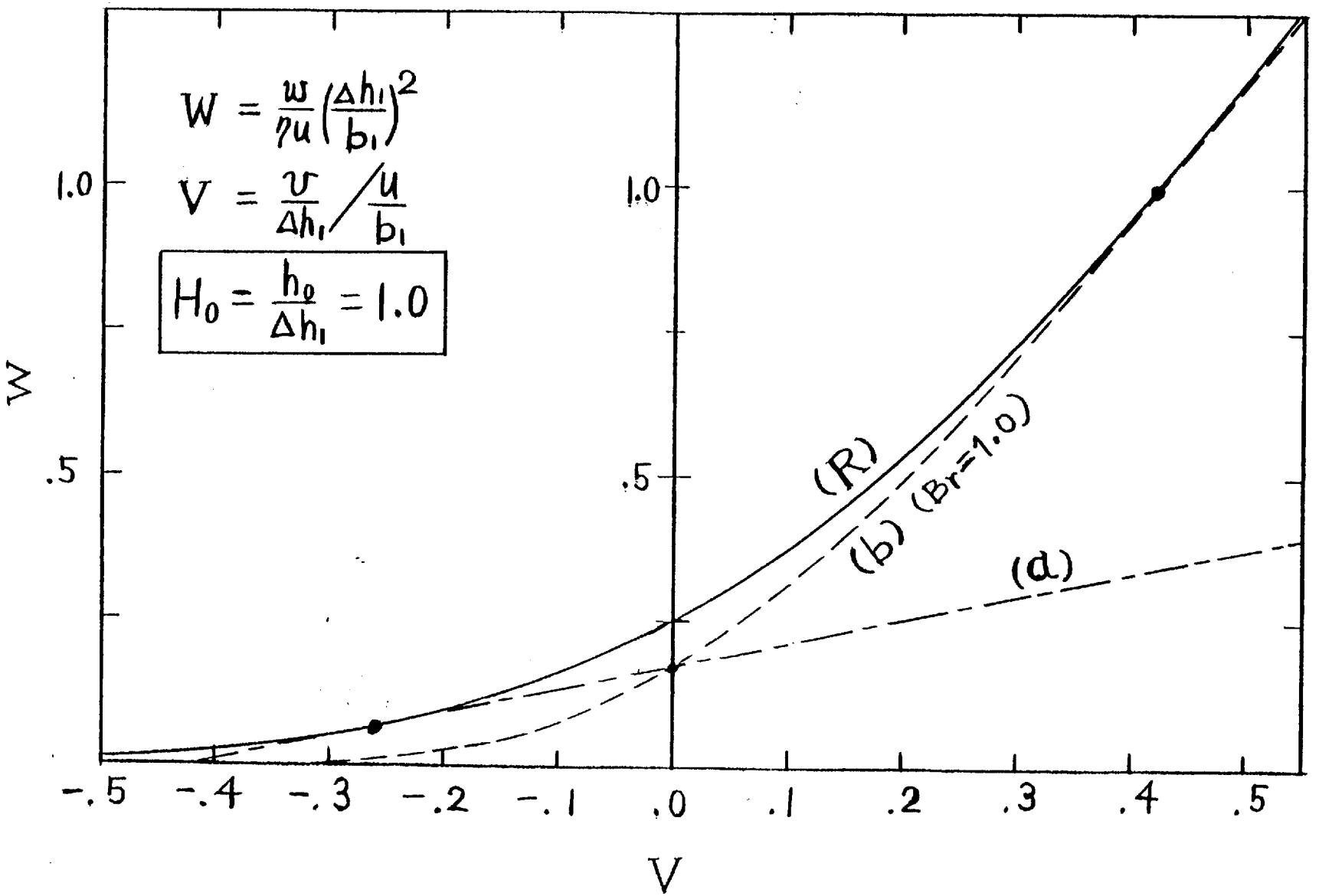


Figure 7.2(a) Load Carrying Capacity of Parabolic Pad Bearing Under Different Boundary Condition (H_o = 1.0)

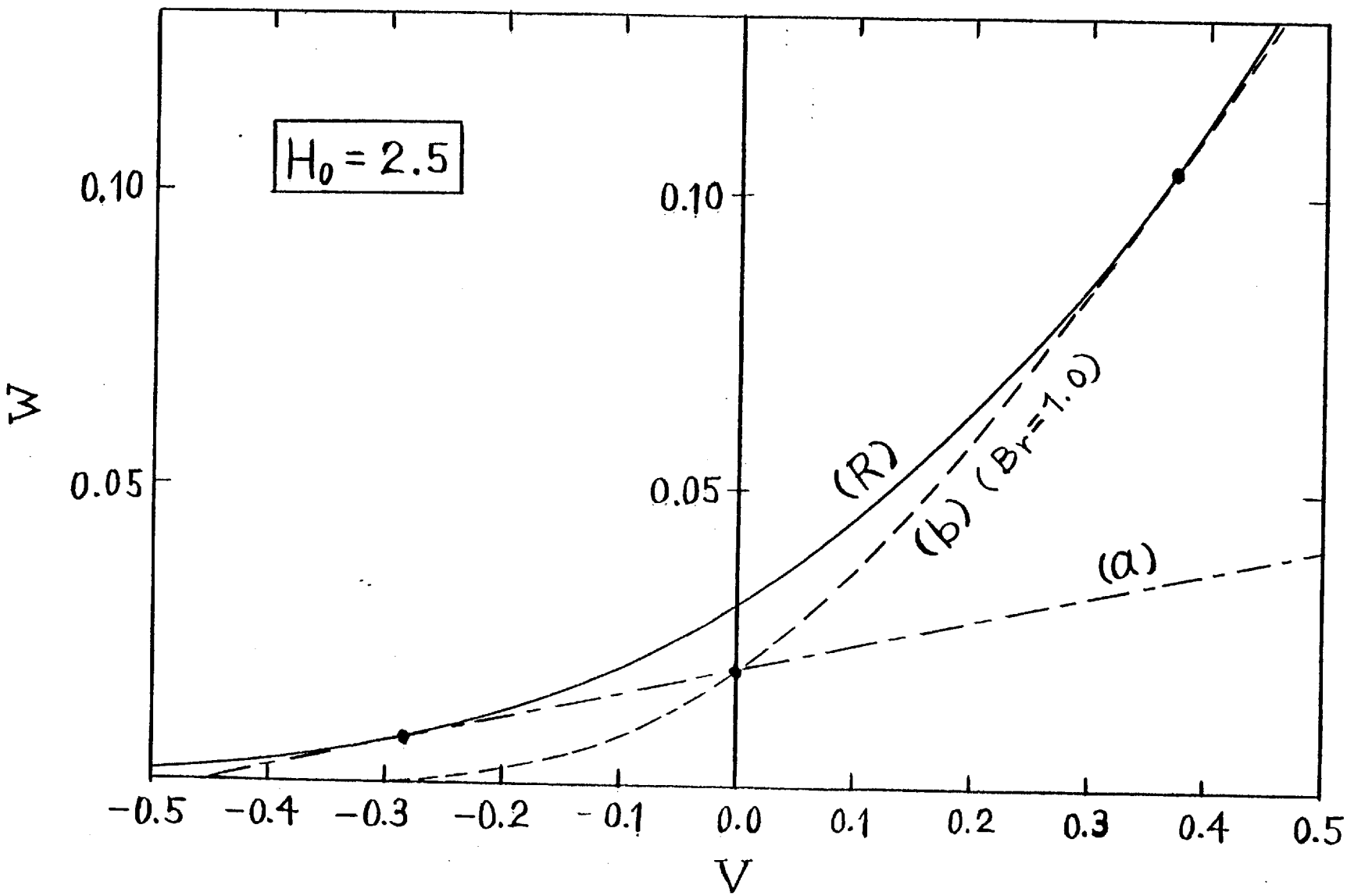


Figure 7.2(b) Load Carrying Capacity of Parabolic Pad Bearing Under Different Boundary Condition (H_o = 2.5)

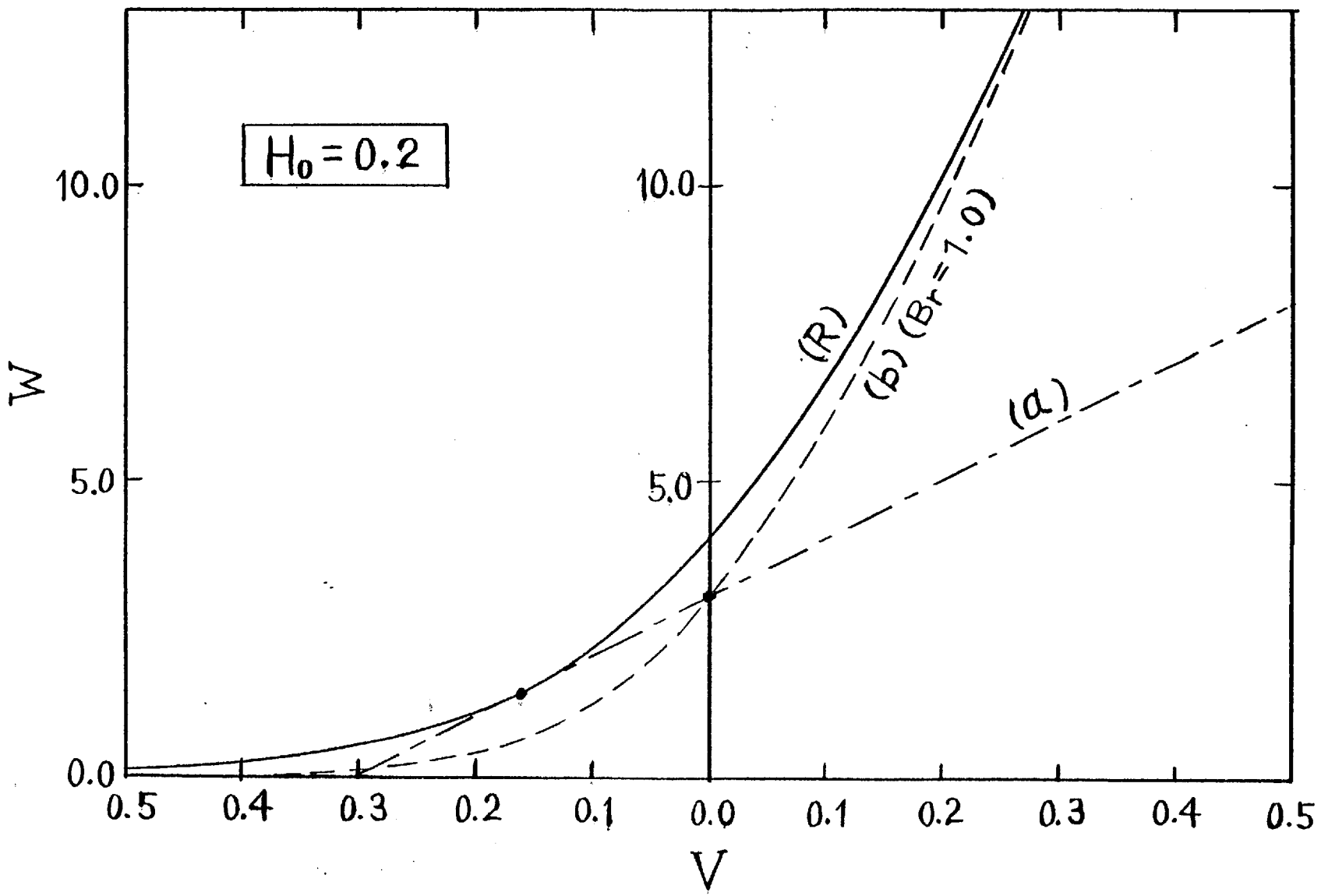


Figure 7.2(c) Load Carrying Capacity of Parabolic Pad Bearing Under Different Boundary Condition (H_o = 0.2)

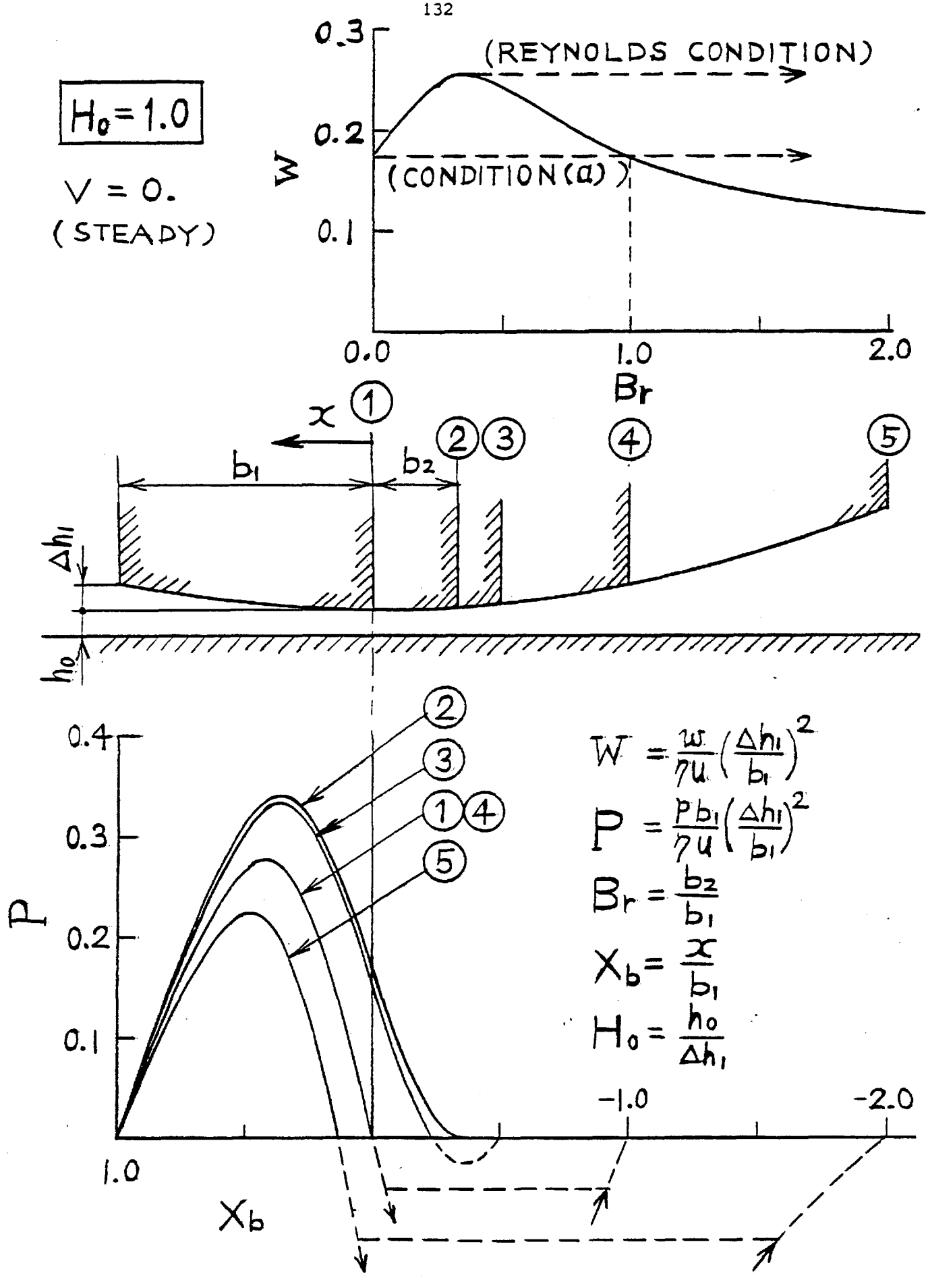


Figure 7.3 Effects of Outlet Geometry on the Solutions Under Modified Full Sommerfeld Condition

CHAPTER EIGHT

HYDRODYNAMIC LUBRICATION OF PISTON RING

8.1 Introduction

In Chapter Six the dynamic behaviour of parabolic pad bearing was analysed. In this Chapter the theory is applied on piston ring lubrication. Thus the piston ring face profile is approximated as a parabola.

A computer program which is given in Appendix I was devised and accepted the following data as input.

. Crank revolution speed.

. Ring cross sectional parabolic geometry

. Equivalent pressure due to ring elasticity.

. Gas pressure above and below the ring as a function of crank angle.

. Viscosity as a function of crank angle.

The results will be shown only for the simplest case, that is,

. Piston ring face is symmetric parabola.

. Piston ring sliding motion is purely sinusoidal.

. Load is applied as a simple constant load.

. Viscosity is constant over the stroke length.

The above rather drastic simplification can be justified on the grounds as following

. For the simplest case, the number of governing independent non-dimensional parameters reduces to two and it becomes

possible to present the results in a general graphical form. No attempt in the past has been successful to express the results in a general form. Only qualitative discussion about the interference between hdyrodynamic wedge and squeeze action was possible in the past,even for the simplest case.

It was concluded in the last chapter that the film inlet boundary condtion is the most reasonable of those considered. That is, when the theoretical film outlet under Reynolds condition exceeds the geometrical bearing rear end full Sommerfeld condition is applied. At the dead centre position the condition is a pure squeeze and the equations given before cannot be applied and the solution will be obtained separately.

8.2 Theory

Basic equations are complete in the foregoing Chapters. Necessary procedure is to express the equations against crank angle as all the varying input data are given as a function of crank angle, and to include the gas pressure load. Another additional procedure is to treat the squeeze velocity as a dependent variable in the solution of the equations, thus the procedure becomes a little more complex than the foregoing Chapters.

8.2.1 Crank Motion

Referring to Figure 8.1 crank motion is expressed as following

$$S + \ell = r(\cos\theta + 1) + \sqrt{\ell^2 - r^2 \sin\theta}$$

where S: distance from the bottom dead centre

r: crank radius

ℓ: connecting rod length

Then

$$u = \frac{dS}{dt} = \frac{d\theta}{dt}\frac{dS}{d\theta} = 2\pi n \frac{dS}{d\theta}$$

$$= 2\pi nr \left(- \sin\theta - \frac{\sin^2\theta}{2\sqrt{R^2 - \sin\theta}}\right)$$

where

$R_c = \frac{\ell}{r}$: crank ratio

u : sliding velocity

n : revolution speed

The theoretical co-ordinate system was chosen so that u is negative.

$$u = 2\pi nr\, C_r(\theta) \tag{8.1}$$

where

$$C_r(\theta) = -\left|\sin\theta + \frac{\sin^2\theta}{2\sqrt{R_c^2 - \sin^2\theta}}\right|$$

Now the squeeze velocity can be expressed against crank angle.

$$V = \frac{v}{\Delta h_1} \cdot \frac{b_1}{u} = \frac{dH_o}{dt} \cdot \frac{b_1}{2\pi rn\, C_r(\theta)}$$

Using the relationship $2\pi n\, dt = d\theta$

$$\frac{dH_o}{d\theta} = S_t . C_r(\theta) . V \tag{8.2}$$

where

$S_t = \frac{r}{b_1}$: stroke ratio

Thus the non-dimensional squeeze velocity under crank motion is a function of crank ratio which is included in $C_r(\theta)$ and stroke ratio.

8.2.2 Load

The load of the piston ring is applied by two terms, the constant pressure due to the piston ring elasticity and the gas pressure. Referring to Figure 8.2

$$w_t = (P_e + P_g)(b_1 + b_2)$$

Where $p_g = p_1$ or p_2 whichever is greater. Thus the assumption is that the ring is pressed to the lower pressure side in the groove. The force balance due to the viscous drag and inertia of the piston ring was neglected for simplicity. P_e in the equation is an equivalent nominal contact pressure due to ring elasticity and w_t is the total load applied on the piston ring. The equation can be non-dimensionalised as following,

$$W_t = (P_e + P_g)(1 + B_r) \qquad (8.3)$$

where

$$W_t = \frac{w_t}{\eta u}\left(\frac{\Delta h_1}{b_1}\right)^2$$

$$P_e = \frac{p_e b_1}{\eta u}\left(\frac{\Delta h_1}{b_1}\right)^2$$

$$P_g = \frac{p_g b_1}{\eta u}\left(\frac{\Delta h_1}{b_1}\right)^2$$

$$B_r = \frac{b_2}{b_1} \quad : \quad \text{offset of parabola}$$

Now the preparation is complete and the hydrodynamic equations of Chapter Six can be introduced.

8.2.3 Solution Under Reynolds Condition

The equation (6.3) which expresses the boundary condition is listed again,

$$\Delta P = 6\{\alpha(1,\bar{X}_R) - (H_o + \bar{X}_R^2)\gamma(1,\bar{X}_R)\}$$

$$+ 12V\{\beta(1,\bar{X}_R) - \bar{X}_R\gamma(1,\bar{X}_R) \qquad (8.4)$$

The applied load is given by the equation (8.3), thus putting this into the equation (6.6),

$$(P_e + P_g - P_2)(1 + B_r) - 6\{\alpha_i(1,\bar{X}_R) - (H_o + \bar{X}_R^2)\gamma_i(1,\bar{X}_R)\}$$

$$+ 12V\{\beta_i(1,\bar{X}_R) - \bar{X}_R\,\gamma_i(1,\bar{X}_R)\} \qquad (8.5)$$

As P_g is either P_1 or P_2, whichever is greater, the left hand side of the equation can be expressed as

$$(P_e + P_g - P_2)(1 + B_r) = (P_e + \Delta P_p)(1 + B_r)$$

where

$$\Delta P_p = \Delta P \quad \text{when} \quad \Delta P = P_1 - P_2 \geq 0$$

$$\Delta P_p = 0 \quad \text{when} \quad \Delta P < 0$$

Thus the problem is to solve the two simultaneous equations (8.4) and (8.5) with unknown variables V and $\bar{X}_R$. V can be eliminated as following,

$$V = S_q(H_o, \Delta P, \bar{X}_R) \qquad (8.6)$$

where

$$S_q(H_o,\Delta P,\bar{X}_R) = \frac{\Delta P/6 - \{\alpha(1,\bar{X}_R) - (H_o + \bar{X}_R^2)\gamma(1,\bar{X}_R)\}}{2\{\beta(1,\bar{X}_R) - \bar{X}_R\,\gamma(1,\bar{X}_R)\}}$$

Then the equation (8.6) is put into the equation (8.5),

$$(P_e + \Delta P_p)(1 + B_r)$$

$$= 6\{\alpha_i(1,\bar{X}_R) - (H_o + \bar{X}_R^2)\gamma_i(1,\bar{X}_R)\}$$

$$+ 12S_q(H_o,\Delta P,\bar{X}_R)\{\beta_i(1,\bar{X}_R) - \bar{X}_R\,\gamma_i(1,\bar{X}_R)\} \qquad (8.7)$$

The equation (8-7) can be solved numerically by the Newton method to give the Reynolds outlet position $\bar{X}_R$ for each crank angle. Then the obtained $\bar{X}_R$ is used to calculate the squeeze velocity by the equation (8.6). The film thickness change against crank angle is obtained by the equation (8.2). When the squeeze velocity V and Reynolds outlet position $\bar{X}_R$ is already known, the position of maximum film pressure $\bar{X}_m$ can be obtained by the equation (6.10), then the equation (6.2) gives the maximum film pressure P_{max}.

As long as the film outlet $\bar{X}_R$ obtained by the procedure shown above is within the bearing breadth, ($\bar{X}_R > -B_r$) the solution is valid. Otherwise the full Sommerfeld condition must be applied.

8.2.4 Solution Under Full Sommerfeld Condition

The procedure is almost the same as for Reynolds condition. The boundary condition is

$$\Delta P = 6\{\alpha(1,-B_r) - (H_o + \bar{X}^2)\gamma(1,-B_r)\}$$

$$+ 12V\{\beta(1,-B_r) - \bar{X}^2\gamma(1,-B_r)\} \qquad (8.9)$$

Load balance is,

$$(P_e + \Delta P_p)(1 + B_r) = 6\{\alpha_i(1,- B_r) - (H_o + \bar{X}^2)\gamma_i(1,- B_r)\} + 12V\{\beta_i(1,- B_r) - \bar{X}^2\gamma_i(1,- B_r)\} \tag{8.10}$$

From the equation (8.9),

$$V = S_q(H_o, \Delta P, \bar{X}) \tag{8.11}$$

where

$$S_q(H_o, \Delta P, \bar{X}_R) = \frac{\Delta P/6 - \{\alpha(1,- B_r) - (H_o + \bar{X}^2)\gamma(1,- B_r)\}}{2\{\beta(1,- B_r) - \bar{X}\gamma(1,- B_r)\}}$$

Eliminating V from the equation (8.10),

$$(P_e + \Delta P_p)(1 + B_r) = 6\{\alpha_i(1,- B_r) - (H_o + \bar{X}^2)\gamma_i(1,- B_r)\} + 12\, S_q(H_o, \Delta P, \bar{X})\{\beta_i(1,- B_r) - \bar{X}\gamma_i(1,- B_r)\}$$

Although this equation can be solved numerically by the same method as the equation (8.7), the following analytical solution is also possible,

$$\bar{X} = \frac{1}{2A}(- B \pm \sqrt{B^2 - 4AC}) \tag{8.12}$$

where

$$A = \beta_i\gamma - \beta\gamma_i$$

$$B = (\alpha\gamma_i - \alpha_i\gamma) - \gamma_i\Delta P/6 + \gamma W_t/6$$

$$C = (\beta\gamma_i - \beta_i\gamma) + H_o(\beta_i\gamma - \beta\gamma_i) + \beta_i\Delta P/6 - \beta W_t/6$$

$$W_t = (P_e + \Delta P_p)(1 + B_r)$$

(Note: Bracket of the integral functions, $(1,- B_r)$, are omiited in the above expressions)

The reason for double roots in the equation is that there are two positions in the pressure distribution, which satisfy $\frac{dp}{dx} = 0$. Under full Sommerfeld condition, one is the positive maximum pressure point and the other is the negative maximum pressure point. As long as "the most reasonable condition" is applied, the negative maximum pressure point is outside the bearing rear end and the negative pressure does not appear within the bearing breadth. Thus the positive sign of the equation (8.12) is chosen for the position of maximum pressure.

Therefore the equation (8.12) gives the maximum pressure point, then the equation (8.11) gives the squeeze velocity and then the equation (8.2) gives the film thickness charge against crank angle, When the maximum film pressure is of interest the equation (6.2) can be used.

8.2.5 Solution at Dead Centre

As the sliding velocity at the dead centre position is zero, squeeze velocity cannot be non-dimensionalised by the sliding velocity. Thus the solution must be obtained separately.

From the equation (2.5) the Reynolds equation under pure squeeze is,

$$\frac{dp}{dx} = 12 \frac{\eta v}{\Delta h_1^2} \frac{b_1}{\Delta h_1} \frac{X - \bar{X}}{\{H_o + H_p(X)\}^3}$$

$$= 12 \frac{\eta v}{\Delta h_1^2} \frac{b_1}{\Delta h_1} \left\{ \frac{X}{(H_o + X^2)^3} - \frac{\bar{X}}{(H_o + X^2)^3} \right\} \qquad (8.13)$$

In the equation either side of the bearing can be used as reference geometries. Completing the non-dimensionalisation

$$\frac{dP}{dX} = 12\{\frac{X}{(H_o + X^2)^3} - \frac{\bar{X}}{(H_o + X^2)^3}\} \tag{8.14}$$

where

$$P = \frac{p\Delta h_1}{\eta v}(\frac{\Delta h_1}{b_1})^2$$

Integrating,

$$P = 12\{\beta(X,- B_r) - \bar{X}\gamma(X,- B_r)\} + P_2 \tag{8.15}$$

where

$$P_2 = \frac{p_2\Delta h_1}{\eta v}(\frac{\Delta h_1}{b_1})^2$$

Boundary condition is,

$$\Delta P = P_1 - P_2 = 12\{\beta(1,- B_r) - \bar{X}\gamma(1,- B_r)\}$$

where

$$P_1 = \frac{p_1\Delta h_1}{\eta v}(\frac{\Delta h_1}{b_1})^2$$

Thus

$$\bar{X} = \frac{\beta(1,- B_r) - \Delta P/12}{\gamma(1,- B_r)} \tag{8.16}$$

Integrating (8.15) to find the load carrying capacity,

$$W = 12\{\beta_i(1,- B_r) - \bar{X}\gamma_i(1,- B_r)\} + P_2(1 + B_r)$$

Non-dimensional applied load W_t is given similarly as the equation (8.3)

$$W_t = (P_e + P_g)(1 + B_r)$$

where

$$P_e = \frac{p_e \Delta h_1}{\eta v} \left(\frac{\Delta h_1}{b_1}\right)^2$$

$$P_g = \frac{p_g \Delta h_1}{\eta v} \left(\frac{\Delta h_1}{b_1}\right)^2$$

Thus the equation for load balance is

$$(P_e + \Delta P_p)(1 + B_r) = 12\{\beta_i(1, - B_r) - \overline{X}\gamma_i(1, - B_r)\} \tag{8.17}$$

where

$$\Delta P_p = \Delta P \quad \text{when} \quad \Delta P \geq 0$$

$$\Delta P_p = 0 \quad \text{when} \quad \Delta P < 0$$

Eliminating $\overline{X}$ by the equation (8.16)

$$(P_e + \Delta P_p)(1 + B_r) = 12\{\beta_i(1, - B_r) - \frac{\beta(1, - B_r) - \Delta P/12}{\gamma(1, - B_r)} \gamma_i(1, - B_r)\}$$

Rearranging

$$(P_e + \Delta P_p)(1 + B_r) - \frac{\gamma_i(1, - B_r)}{\gamma(1, - B_r)} \Delta P$$

$$= 12\{\beta_i(1, - B_r) - \frac{\gamma_i(1, - B_r)}{\gamma(1, - B_r)} \beta(1, - B_r)\}$$

The term of squeeze velocity $\frac{u}{\Delta h_1}$ is included in the parameters P_e and ΔP, the film thickness change against crank angle is,

$$\frac{dH_o}{d\theta} = \frac{dH_o}{dt} \cdot \frac{dt}{d\theta} = \frac{u}{\Delta h_1} \cdot \frac{1}{2\pi n}$$

$$= \frac{1}{2\pi} \frac{pt}{\eta n} \left(\frac{\Delta h_1}{b_1}\right)^2 \frac{1}{12\{\beta_i(1, - B_r) - \frac{\gamma_i(1, - B_r)}{\gamma(1, - B_r)} \beta(1, - B_r)\}} \tag{8.18}$$

where

$$p_t = (p_e + p_b - p_2)(1 + B_r) - \Delta p \frac{\gamma_i(1, - B_r)}{\gamma(1, - B_r)}$$

Thus the mathematical formulation of the hydrodynamic lubrication of the piston ring is complete. One must ensure that all this non-dimensional expressions are refered to the dimensions of the hydrodynamic inlet side. Thus for the reciprocating motion of the piston ring, all the reference dimensions are reversed for both strokes. As for the dead centre position either side dimension can be refered to.

8.3 Non-dimensional Parameters for Piston Ring Lubrication

In order to express the numerical results in a general form, non-dimensional parameters which express the phenomena must be found. Differential equations which express the squeeze velocity against crank angle when sliding velocity is not zero are given by (8.2).

$$\frac{dH_o}{d\theta} = S_t \cdot C_r(\theta) \cdot V$$

Whichever the boundary condition, V, can be expressed as a funtion as following,

$$V = f(H_o, \Delta P, P_e + \Delta P_p, B_r)$$

Thus

$$\frac{dH_o}{d\theta} = S_t \cdot C_r(\theta) \cdot f(H_o, \Delta P, P_e + \Delta P_p, B_r)$$

As it has been mentioned before that all the parameters are refered to the hydryodynamic inlet side. Whatever the geometrical side of the piston ring that is chosen as the reference side with suffix 1, the parameters for the other stroke can be expressed by the reference side as following,

$$\frac{dH_o}{d\theta} = B_r S_t C_r(\theta) f\left(\frac{H_o}{B_r^2}, -\Delta P B_r^3, (P_e + \Delta P_{pn}) B_r^3, \frac{1}{B_r}\right) \qquad (8.20)$$

where

$$\Delta P_{pn} = P_2 - P_1 \quad \text{when} \quad P_2 > P_1$$

$$\Delta P_{pn} = 0 \quad \text{when} \quad P_2 < P_1$$

Thus the number of non-dimensional parameters does not change. The independent variables of the differential equations are given by the parameters listed below.

$B_r = \frac{b_2}{b_1}$: offset of parabola

$S_t = \frac{r}{b_1}$: stroke ratio

$C_r(\theta)$: velocity by crank motion and a function of $\frac{\ell}{r} = R_c$, crank ratio only.

$\Delta P(\theta)$: gas pressure difference above and below the ring

P_e : equivalent pressure due to ring elasticity

The term which expresses the viscosity of the lubricant does not

appear in the listing, but is included in the term ΔP and P_e. For the case of varying viscosity, ΔP and P_e takes into account the variation of viscosity over the stroke length as a function of crank angle.

Thus if the "input" independent variables listed above are constant with respect to crank angle, the "output" solution of non-dimensional film thickness against the crank angle must also be constant. Thus even in the simple case where the effects of tilting, starvation or distortion, etc. are omitted the general analysis, is very complex. If the gas load and viscosity vary, they must be expressed as a function of crank angle and the solution is differenct for each case. But the simplest case can be considered, when the ring face is a symmetric parabola, the sliding motion is purely sinusoidal and the load and viscosity are constant over the stroke. For this case, the number of parameters reduces to two as listed here.

$$S_t = \frac{r}{b_1} \quad : \text{ stroke ratio}$$

$$P_e = \frac{p_e b_1}{\eta u} \left(\frac{\Delta h_1}{b_1}\right)^2 = \frac{p_e b_1}{\eta u_{max}} \left(\frac{\Delta h_1}{b_1}\right)^2 \cdot \frac{1}{-|\sin\theta|}$$

: non-dimensional load

The other parameters disappear as they are zero or constant for every case. The term $-|\sin\theta|$ appearing in the above expression need not be taken into account as constant for the simplest case.

In the equation for the dead centre position, there is another parameter $\frac{p_e}{\eta n}\left(\frac{\Delta h_1}{b_1}\right)^2$. This can be expressed by the two parameters as follows. Using a relationship $2\pi rn = u_{max}$,

$$S_t \cdot P_e = \frac{r}{b_1} \cdot \frac{p_e b_1}{\eta u_{max}} \left(\frac{\Delta h_1}{b_1}\right)^2 = \frac{1}{2\pi} \frac{p_e}{\eta n} \left(\frac{\Delta h_1}{b_1}\right)$$

In order to relate these parameters to those of steady state lubrication the reciprocals are prefered, as will be shown later. From the presented analysis the following conclusion can be drawn:

The hydrodynamic lubrication of a symmetrically parabolic pad bearing under sinusoidal reciprocating motion, constant load and constant viscosity can be expressed by just two of the three parameters listed below.

$$S_t = \frac{r}{b_1} \quad : \quad \text{stroke ratio}$$

$$U_{max} = \frac{\eta u_{max}}{2 p_e b_1} \left(\frac{b_1}{\Delta h_1}\right)^2 \quad : \quad \text{maximum sliding velocity}$$

$$N = \frac{\eta n}{p_e} \left(\frac{b_1}{\Delta h_1}\right)^2 \quad : \quad \text{revolution speed}$$

These parameters are related as follows

$$U_{max} = \pi S_t N$$

Constant 2 in U_{max} is to make this parameter the same as it is in steady state lubrication.

$$\frac{\eta u_{max}}{2 p_e b_1} \left(\frac{b_1}{\Delta h_1}\right)^2 = \frac{\eta u_{max}}{w} \left(\frac{b_1}{\Delta h_1}\right)^2$$

8.4 Results and Discussions

8.4.1 Calculation Procedure

A computer program was devised based on the formulation given in the foregoing section which is given in Appendix I. Numerical calculation was carried out extensively for the simplest case. The numerical procedure is briefly explained as following.

Numerical calculation may start somewhere ar the midstroke assuming an approximate steady state film thickness. The calculation mesh was chosen arbitrarily as 1 degree of crank angle. At each step, the film thickness changes to that of the new crank angle. ΔH_o is calculated using the Runge Kutta method or a simpler method. The two methods are described below.

Runge Kutta method

$$\Delta H_o = \frac{1}{6}(K_1 + 2K_2 + 2K_3 + K_4)$$

where

$$K_1 = f(\theta, H_o) \cdot \Delta\theta$$

$$K_2 = f\left(\theta + \frac{\Delta\theta}{2}, H_o + \frac{K_1}{2}\right) \cdot \Delta\theta$$

$$K_3 = f\left(\theta + \frac{\Delta\theta}{2}, H_o + \frac{K_2}{2}\right) \cdot \Delta\theta$$

$$K_4 = f(\theta + \Delta\theta, H_o + K_3) \cdot \Delta\theta$$

$$f(\theta, H_o) = \frac{dH_o}{d\theta} \text{ as a function of } H_o \text{ and } \theta.$$

Simple method

$$\Delta H_o = \frac{dH_o}{d\theta} \times \Delta\theta$$

where

$\Delta\theta$ is the mesh length and equal to 1 degree.

The Ringe-Kutta method needs four times as many calculation cycles as the simple method. In order to obtain the comprehensive picture efficiently all the results shown were obtained by the simple method. Several points were calculated by the Runge-Kutta method and the comparison will be discussed later.

After one cycle (360 degrees crank angle) the film thickness is compared with the film thickness one cycle before. The iteration proceeds until the difference ratio converges 0.001. Normally, the necessary number of cycles for this convergence is less than two cycles.

8.4.2 Film Thickness Change during the Cycle

The results are shown in Figure 8.3(a)(b)(c). Upper figures of Figure 8.3 (a)(b)(c) shows the typical non-dimensional film thickness variation over the cycle. In each figure U_{max} is kept constant while N and S_t are varied by several decades. This is because U_{max} defines the steady state film thickness pattern over the stroke, shown in the figure as a broken line. Thus the broken line is a solution for an assymptotic condition of $S_t \to \infty$, $N \to 0$ keeping U_{max} constant. The other assymptota is $S_t \to 0$, $N \to \infty$ and shown in upper figures as horizontal broken lines. The lower figures of Figure 8.3(a)(b)(c) are the non-dimensional film outlet variations over the cycle. It should be noted that film outlet position determines the pressure area. This

is shown only for one stroke. As has been discussed before, when the theoretical Reynolds film outlet excees the bearing outlet, the full Sommerfeld condition is applied, thus the maximum value of $\overline{X}_R$ in each of the figures is 1.0. The broken lines are for the steady state film outlet.

From these figures several features of hydrodynamic film behaviour can be observed:

1. Film outlet position is always changing and at near dead centre position the whole breadth of the ring is utilised for pressure generation. Thus it can be deduced, that if the half Sommerfeld condition is applied, the film thickness near dead centre must be much thinner than in the Reynolds condition.
2. During the cycle there are two characteristic crank angle positions at which solely squeeze action or solely wedge action occur. The former is at the dead centre position, the latter is at maximum and minimum film thickness position. At those positions squeeze velocity is zero, thus the film thickness is the same in the steady state conditions. Thus the points of that position lie on the broken lines, which is a steady state film thickness. In the lower figures of the film outlet position it is shown that each solid line crosses the broken line, which is for the steady state condition, at the crank angle of maximum or minimum film thickness.
3. Non-dimensional maximum sliding velocity U_{max} defines the "basic film thickness pattern" or steady state film thickness variation in the cycle. When revolution speed N increases keeping U_{max} constant, the delay of film thickness "response" increases and assymptotically the film thickness becomes constant over the cycle. This constant film thickness is the same as that of the basic film

thickness pattern at 45° crank angle. These features are analogous to the response of the electric circuit system. The input is U_{max} and output is film thickness variation and the system response character is decided by N.

4. Referring to the discussion (3), the squeeze action might be expressed quantitatively by the non-dimensional parameter N. When N increases, the film thickness variation during a cycle decreases. In the same sense the wedge action might be expressed by U_{max} which defines steady state film thickness during the cycle. But this does not mean that both these actions can be treated separately. As shown in Figure 8.3 (a)(b)(c) the same value of N does not give similar film thickness variation during the cycle. They vary depending on the value of U_{max}. Thus the two dimensional expression defined by the two parameters is necessary.

8.4.3 General Presentation of the Minimum Film Thickness in the Cycle

In order to quantify the above discussions Figure 8.4 has been made. As two dimensional parameters (no more than two for the simplest case) defines the whole condition, both stroke ratio S_t and revolution speed N have been chosen as co-ordinates. Minimum film thickness H_{omin} and its crank angle position Θ_{min} are chosen as parameters of interest. The figure 8.4 shows the relationship between S_t and N for constant H_{omin} or Θ_{min}. In the figure 8.4 the lines of constant U_{max} are also included as broken lines. From this figure one can estimate the minimum film thickness and its position of crank angle in the cycle, when two of the three design parameters U_{max}, N, S_t are given. This direct estimation is unknown in the literature. This is because the "correct" interpretation of the Reynolds equation which was shown in Chapter Two has never been performed before. Thus only the qualitative

description on the effect of viscosity, load, speed, etc. was possible and the condition itself is the simplest.

As it has been mentioned earlier Figure 8.4 is based on the calculation by the simple method. The difference between the Runge-Kutta method and this simple method is summarised in Table 8.1.

S_t \ N	0.001	0.01	0.1	1.0
100	11.2	3.55	1.4	0.6
10	5.26	1.92	0.58	0.1
1	2.25	0.72	<0.1	<0.1

Table 8.1 Difference unit % ratio of H_{omin} between the Runge-Kutta method and the simple method. The former gives bigger H_{omin} than the latter in % shown in the table.

As shown in Table 8.1 the simple method gives less than a few per cent error compared with the Runge-Kutta method within most of the range of the graph. The difference in Θ_{min} is less than 1^{o} in all the shown range.

The base data for Figure 8.4 were calculated by changing the value of S_t and N as a geometrical series of the ratio $10^{1/4} = 1.778$. The curves in the figure were obtained by interpolating the calculated data.

It is shown in Figure 8.4, that any changes of the parameters U_{max}, N or S_t change H_{omin} or Θ_{min}. Among them the effects of N on

H_{omin} is the greatest. This is shown in the figure that the curves of constant H_{omin} are rather steeply inclined. This is because H_{omin} is mainly decided by the squeeze action at near dead centres and N expresses the squeeze action as discussed earlier. But the gradient of the curve is about -1 and θ_{min} approaches to 45° around the lower right corner of the figure. At this condition the film thickness becomes constant all over the cycle and the film thickness is mainly decided by U_{max}. This was explained in Figure 8.3 (a) (b) (c) for the case of $N \to \infty$, $S_t \to 0$.

8.4.4 Design Optimization

It was mentioned in the discussion of steady state lubrication that the design optimization can be achieved by maximizing the film thickness for a given bearing breadth. This can be expressed by the parameter H_{ob} of the bearing. The equivalent value of H_{ob} for piston ring lubrication can be defined in the same manner.

$$H_{obmin} = H_{omin} U_{max}^{-\frac{1}{2}} = \frac{h_{omin}}{b} \sqrt{\frac{w}{\eta u_{max}}}$$

Thus Figure 8.5 was made. In the figure S_t is kept constant and the relationships between H_{omin} and U_{max} are shown. In the figure the assymptotic case $S_t \to 0$, $N \to \infty$ and the steady state condition which is the same as Figure 3.2 are also included. H_{obmin} is shown as an inclined scale in the same manner as earlier. The figure shows how the reciprocating motion (S_t) changes the value of H_{omin} and the maximum value of H_{obmin}. The optimum points at which H_{obmin} become maximum are shown by crosses. Since the procedure includes graphical interpolation, the accuracy of each point is not very good (say 5% or so), but how the reciprocating motion (S_t) shifts, the optimum point is clear. This is

when S_t increases H_{omin} also increases, which means that the inlet wedge height Δh should decrease, or the face shape should become flatter. This is because the squeeze action must be utilised more in order to keep the minimum film thickness thicker under reciprocating motion. This also means that the wedge action must be sacrificed and the film thickness at the middle stroke reduced. This is a common known theoretical fact which has been only qualitatively discussed in the past but never quantitatively as shown in Figure 8.5.

One example of design optimisation can be made as following:

For the case of $S_t = 50$, conditions of maximum H_{obmin} can be read by the figure as $H_{obmin} = 0.22$, which is about 40% of the steady state optimum, $H_{omin} = 2.4$. Thus,

$$\frac{\Delta h_1}{b_1} = \frac{0.22}{2.4}\sqrt{\frac{\eta u_{max}}{w}} = 0.092\sqrt{\frac{\eta U_{max}}{w}}$$

For the steady state condition this is calculated based on the Table of Figure 3.2.

$$\frac{\Delta h_1}{b_1} = \frac{0.5049}{0.8308}\sqrt{\frac{\eta u}{w}} = 0.608\sqrt{\frac{\eta u}{w}}$$

Thus the surface shape should be much more flatter than for the steady state condition.

Although the minimum film thickness under reciprocating motion can be kept to about 40% of the steady state condition, if the condition is optimised, the film thickness reduction for low speed (small U_{max} or small N) is more rapid than for the steady state condition. Thus it is more difficult to keep the hydrodynamic film for a wide range of operating conditions under reciprocating motion than under steady conditions.

8.5 Conclusion

1. Hydrodynamic lubrication of symmetrically parabolic pad bearing under steady state (constant load and viscosity) sinusoidal reciprocating motion is wholly decided by the two of the three parameters listed below.

$$S_t = \frac{r}{b_1} \quad \text{stroke ratio}$$

$$U_{max} = \frac{\eta u_{max}}{w} \left(\frac{b_1}{\Delta h_1}\right)^2 \quad \text{non-dimensional maximum sliding velocity}$$

$$N = \frac{\eta u}{p_e} \left(\frac{b_1}{\Delta h_1}\right)^2 \quad \text{non-dimensional revolution speed.}$$

These parameters decide completely the hydrodynamic parameters of the pad bearing which can be derived from the Reynolds equation.

2. In order to minimise the reduction of film thickness under reciprocating motion the face of the ring should be much flatter than the optimised steady state condition. This is because the piston ring lubrication must rely on squeeze action as well as wedge action. For the case of the stroke ratio of 50 the film thickness reduction can be kept to about 60% from the steady state film thickness at its midstroke.

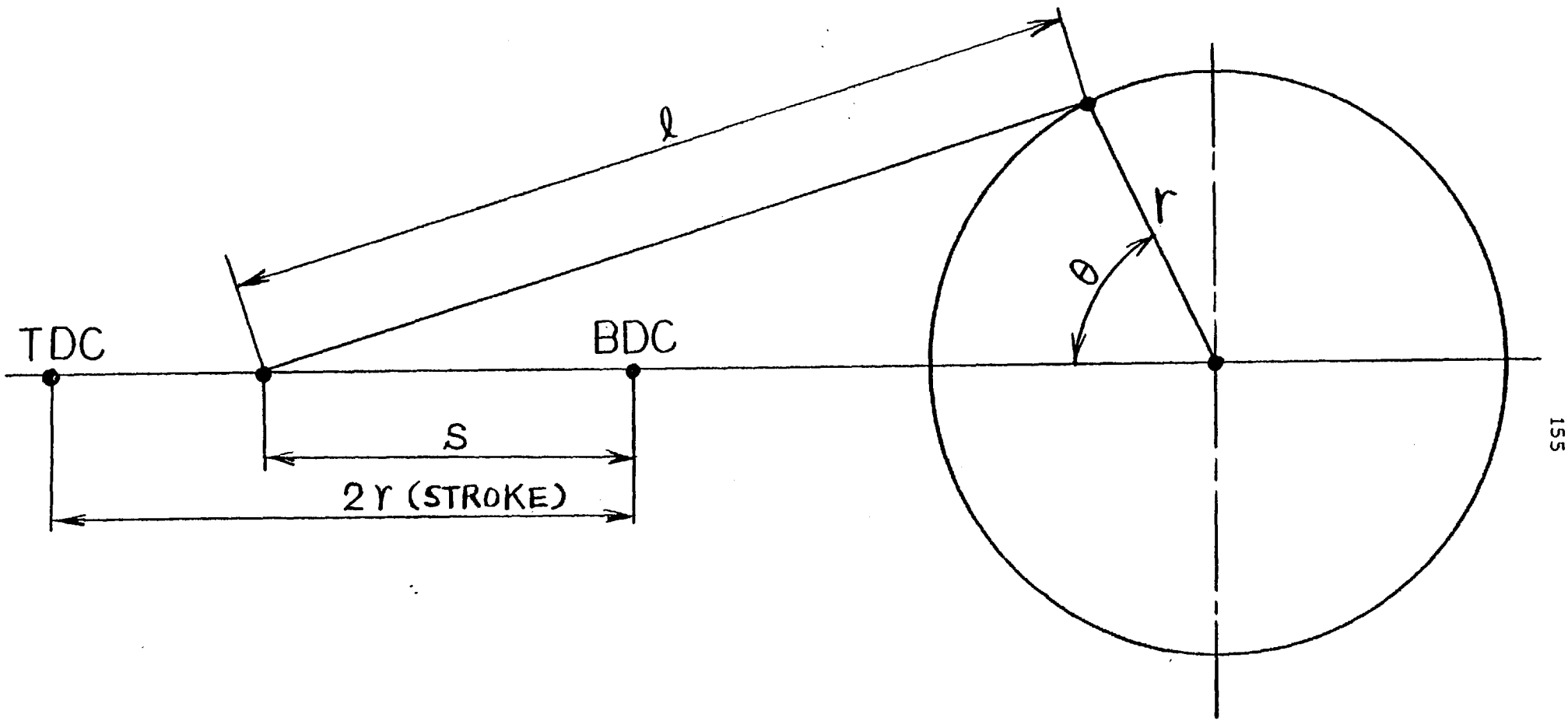


Figure 8.1 Crank Mechanism

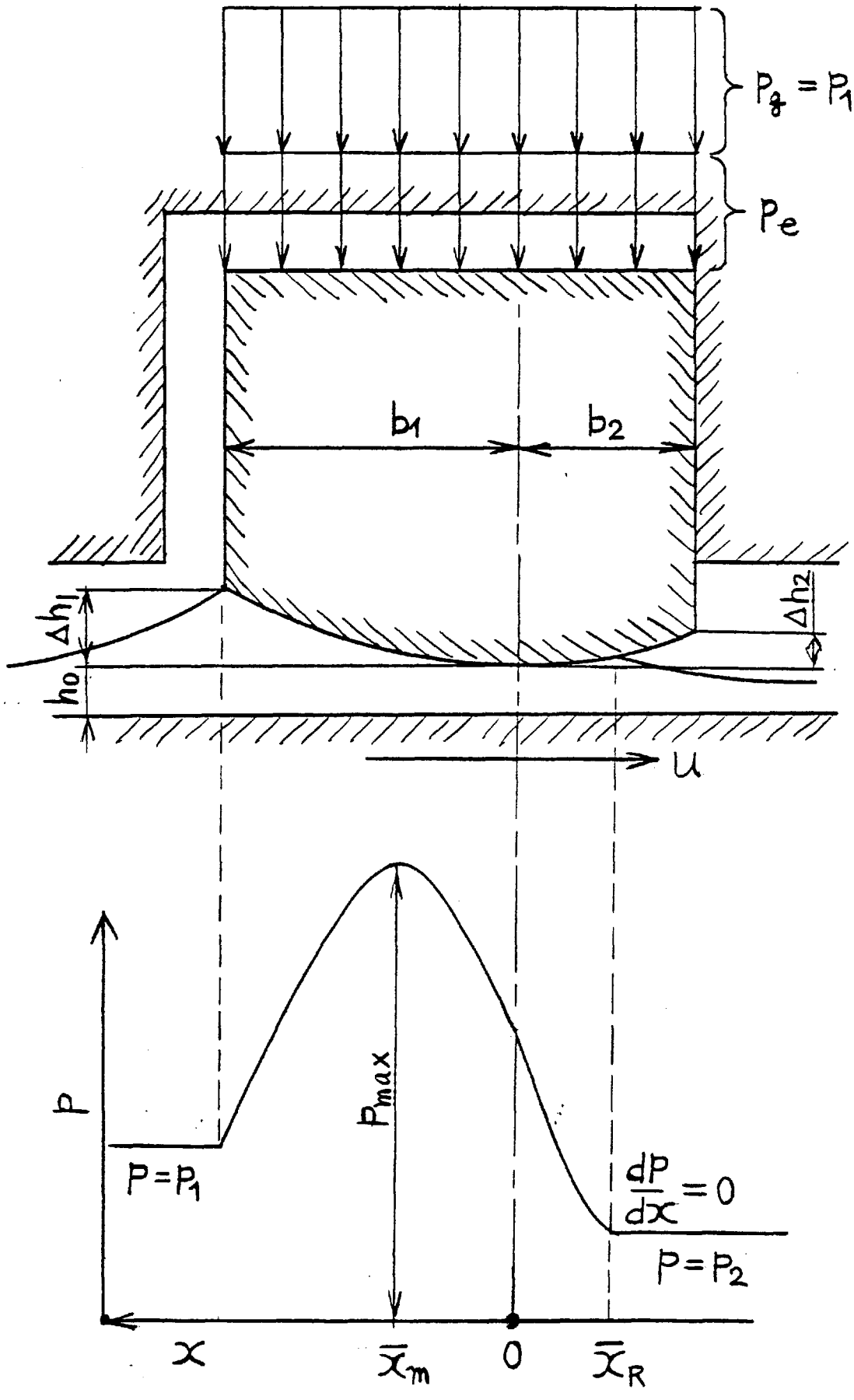


Figure 8.2 Piston Ring Geometry and Pressure Distribution

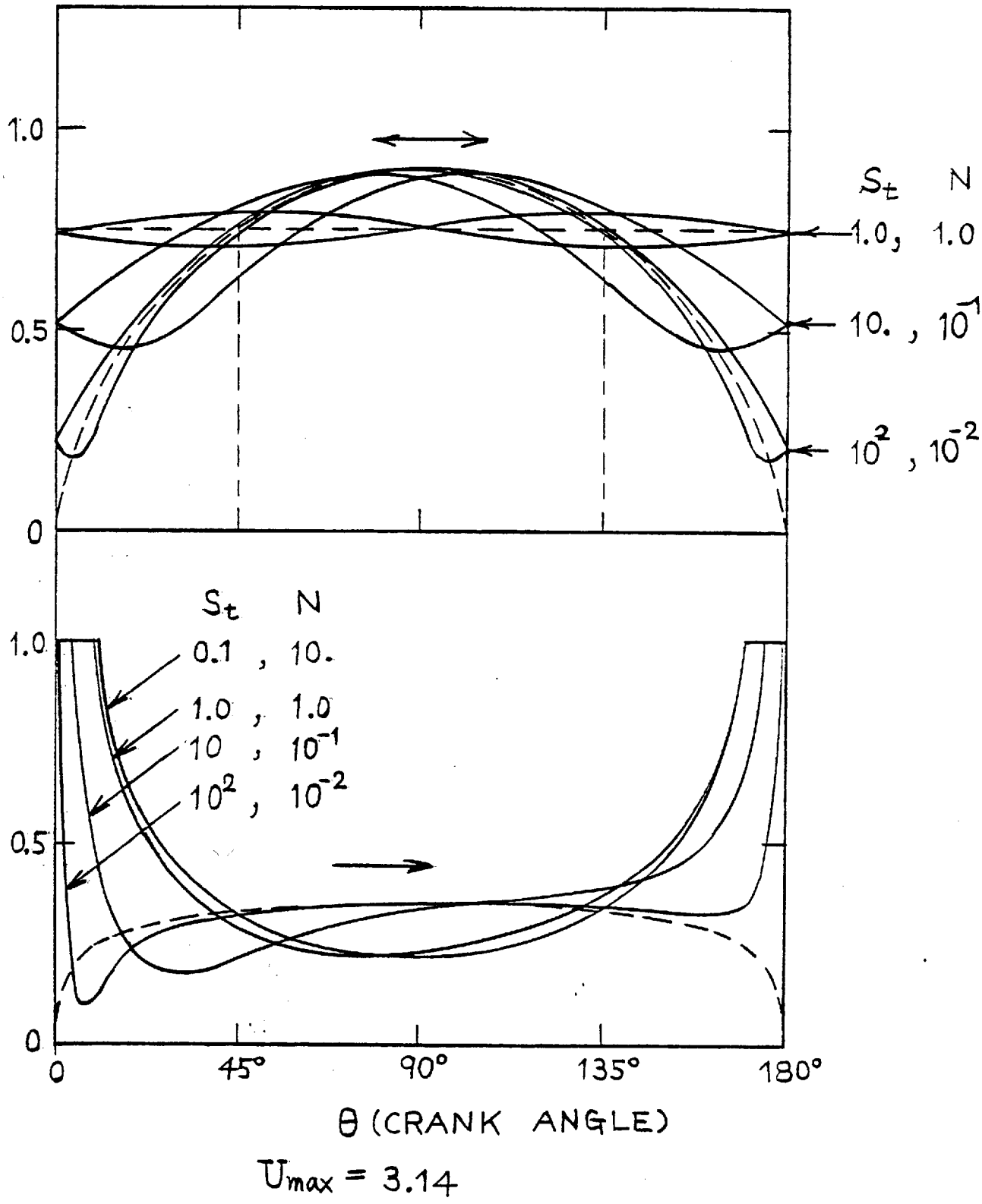


Figure 8.3(a) Film Thickness and Outlet Position Over the Stroke

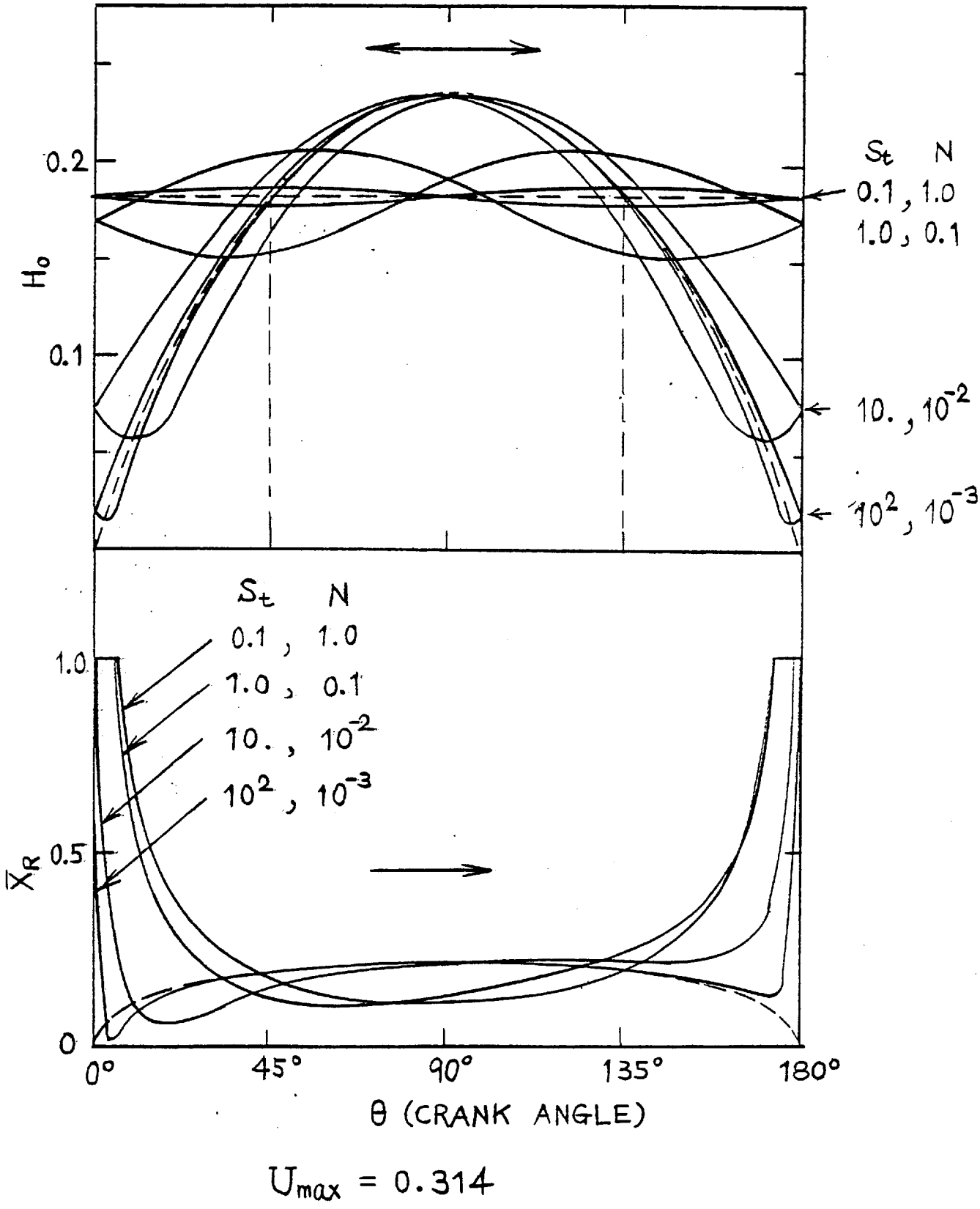


Figure 8.3(b) same as (a)

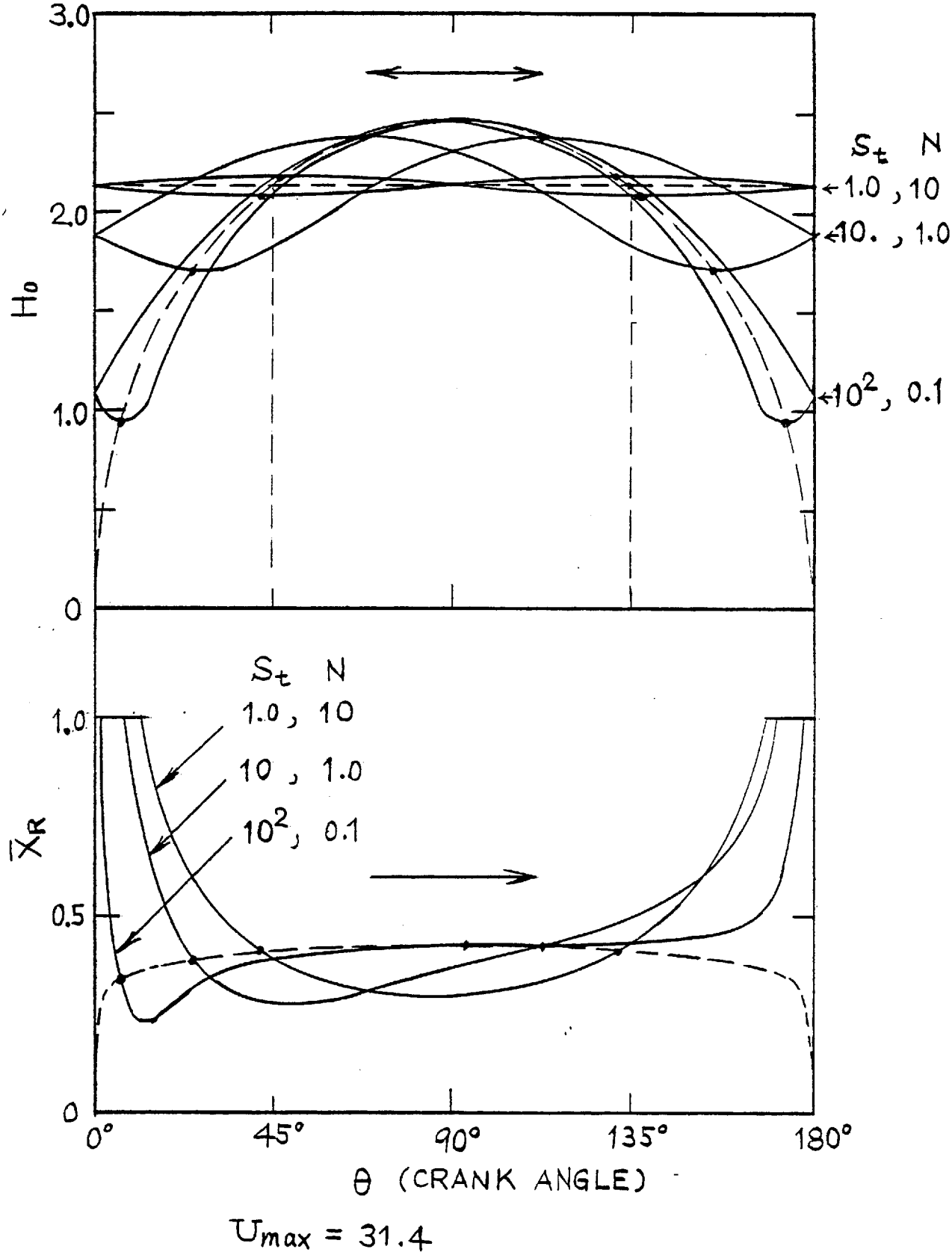


Figure 8.3(c) same as (a)

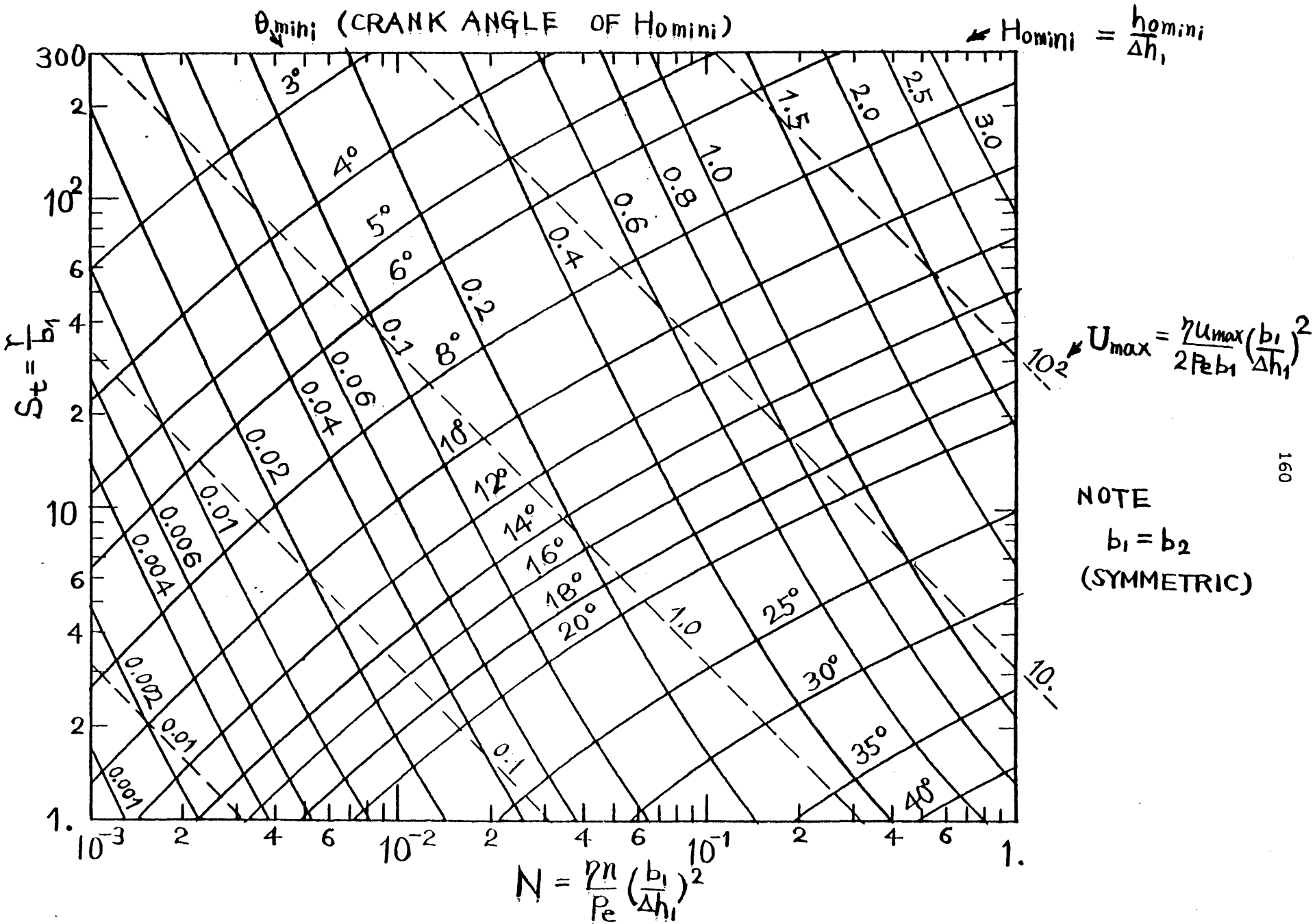


Figure 8.4 Minimum Film Thickness and its Position of Crank Angle under Reciprocating Motion

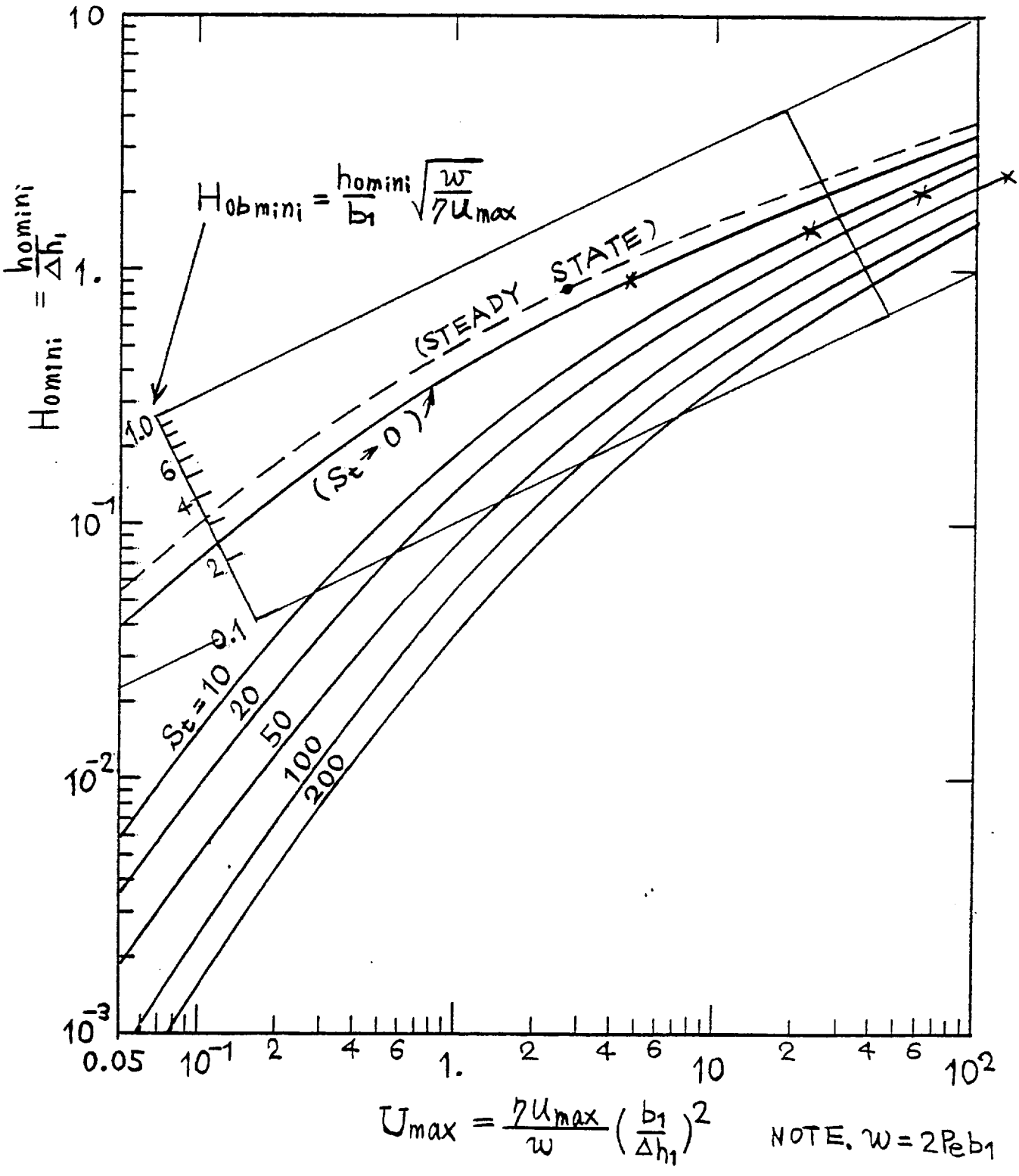


Figure 8.5 Minimum Film Thickness Against Maximum Sliding Velocity Under Reciprocating Motion

CHAPTER NINE

EXPERIMENTAL APPARATUS

9.1 Introduction

As explained in the Introduction, experimental apparatus was developed mainly for the study of piston ring scuffing at the near dead centre position. The maximum stroke is limited to 5mm to avoid the uncontrollable flash temperature effects.

The apparatus described below is also of considerable value for the study of boundary lubrication. In order that its use may later be extended to lubricity tests, the apparatus incorporates the facility to measure parameters in addition to those required for the purpose of this thesis. The parameters which can be measured are described in this Chapter.

Figure 9.1 shows an overall view of the experimental set up. Explanation of the experimental set up is put into three sections, (i) experimental apparatus itself, (ii) instrumentation, (iii) control.

9.2 Apparatus

In the back cover of the thesis the assembly drawing of the apparatus is given and Figure 9.2 is a view of the apparatus. The drawing was made for the purpose of production based on this thesis and contains a slight difference between the picture of this thesis, but essentially the same. Figure 9.3 shows a schematic diagram of the apparatus. The dynamic test piece is clamped by a holder and driven forward and backward by a vibrator. The clamp can be changed to accommodate different shaped test pieces; examples are shown in Figure 9.4. The relevant specifications of the vibrator and its power amplifier are given in Table 9.1.

The vibrator is mounted on a trunnion by two ball bearings, so it can tilt with practically negligible torsional friction.

Vibrator

Model Number	201
Manufacturer	Ling Dynamic Systems Ltd
Sine Vector Force	19.6N (Natural) 27.0N (Forced Air Cooled)
Frequency Range	dc to 13KHz
Maximum Displacement	5mm peak to peak
Maximum Velocity	1.78 m/s
Resistance	1.5Ωdc
Maximum Current	2.5A rms (Unblown) 4.5A rms (Blown)

Oscillator/Power Amplifier

Model Number	TPO 100
Manufacturer	Ling Lynamic Systems Ltd
Maximum Power Output	100W
Frequency Range	1.5 to 15KHz
Maximum Output Voltage	18V rms
Rateel Output Current at Maximum Power	1.25A

Table 9.1

The whole vibrator assembly is mounted on the base by two horizontal guide shafts, thus the position of the upper test piece can be shifted horizontally about 25mm by the adjusting nut.

The static test piece is held in an oil bath inside the heater box. The heater box is machined from an aluminium block because of its good heat conductivity and low specific weight. The 200W cartridge heaters are inserted into each upper and lower heater box, thus the total maximum heating capacity is 800W.

With this arrangement the maximum temperature used is 350°C. The heater capacity is more than enough to obtain higher temperature than this if required.

The lower heater box is "flexibly" supported by two thin (0.6mm) beams via heat insulating material (Syndanio). Calculated stiffness of the beam in the direction of sliding motion is about 120N/mm, which is considered to be flexible enough compared with the order of stiffness of 10^5N/mm of the connecting load and force gauge. By this arrangement there are no obstacles above the test pieces other than the upper heater box which can be easily taken off. Thus the replacement of the test pieces can be done with practically no inconvenience.

Under the heater box assembly a connecting block is fixed which transfers friction force from the lower test piece to the force gauge through a connecting rod. The force gauge is fixed to the steel block which is then bolted to the base of the lower test piece assembly. The lower test piece assembly is so designed that the stiffness of each component related friction force measurement is as high as possible in order to avoid undesirable resonance of the friction force measurement. Supposing the stiffness of the supporting block of the force gauge and the base is high enough compared with the stiffness of the connecting rod and force gauge itself, calculated resonance frequency of the force measuring system is about 1.8KHz.

The load is applied by a swinging yoke attached to the dynamic test piece assembly. Two thin wires connect the yoke bar of the test piece and a equaliser beam, which is pulled down by a spring balance through a lever as shown in Figure 9.5. The equaliser beam itself works as a load cell which measures the applied load by its fixed strain gauges.

9.3 Instrumentation

Instrumentation of the experiment is explained individually as (i) Friction force, (ii) Applied load, (iii) Electric contact resistance, (iv) Displacement. Temperature measurement will be explained in the section on control.

9.3.1 Friction Force

Friction force is measured by a piezo electric crystal impedance head which converts the applied force to an electric charge. The specifications relevant to the experiment are taken from the catalogue and shown in Table 9.2.

Force Gauge Specification

Type	Impedance Head Type 8001
Manufacturer	Bruel & Kjaer
Force Gauge Voltage Sensitivity	394 mV/N*
Force Gauge Charge Sensitivity	389 pc/N*
Stiffness	25 x 10^5 N/mm
Force Gauge Capacitance	987 PF

* Calibrated by the manufacturer

Table 9.2

The impedance head is an integrated piezo electric accelerometer and force gauge which is commonly used to measure mechanical impedance of a structure. In the original design of the apparatus the impedance head was mounted on

the dynamic test piece and measured the friction force and acceleration simultaneously as given in the Appendix of reference (6). Inertia force of the dynamic test piece assembly picked up by the force gauge was electrically subtracted by the accelerometer output, the gain of which was so adjusted that the subtracted output has negligible inertia force component. As the force gauge was mounted on the dynamic test piece unacceptable noise was picked up. This configuration was abandoned, and no use was made of the accelerometer in this thesis.The output of the force gauge is fed into the charge amplifier which converts the electric charge to voltage. The circuit diagram is shown in Figure 9.6. As the amplifier was built for the original configuration of the apparatus it has two channels. One channel has a double integration circuit which is redundant in the final design of the apparatus.

The output of the charge amplifier is rectified by the precise rectification circuit as shown in Figure 9.7. The diode bridge is positioned in a feed back loop of the operational amplifier and the output differential amplifier gives the accurately rectified output. This design can practically eliminate the undesirable potential drop (about 0.6V) of a silicon diode of a simple rectifying bridge. The rectified output is smoothed by a combination of capacitance and resistance with calculated time constant of 1.6 seconds. The smoothed output is then fed into a chart recorder to record the average friction force.

When the friction co-efficient is the main interest the friction force output is electrically divided by the strain gauge output of the applied load which will be explained later. This electrical division is achieved by use of an integrated circuit of an analogue divider as shown in Figure 9.8.

9.3.2 Applied Load

Applied load is measured by a strain gauge bridge fixed on the equaliser bar as shown in Figure 9.5. The change of the unbalanced resistance of the strain gauges is amplified by a strain gauge amplifier and the output is measured by a conventional voltmeter. The output is also fed into the analogue divider which is described earlier to obtain the friction coefficient. The strain gauge amplifier is manufactured by Creative Instrumentation Limited, and the type No is SGA700.

9.3.3 Electric Contact Resistance

In order to measure the electric contact resistance of the test pieces the dynamic specimen is electrically insulated from the apparatus base which is earthed to the common ground of the measuring system. The diagram is shown in Figure 9.9. One operational amplifier is used as a constant voltage source which can keep the output voltage constant up to about 20mA. As the applied voltage to measure the contact resistance is normally less than 20mV its capacity of output current is enough for the measurement of resistance in a range of a fraction of one ohm. The output of the constant voltage source can be varied by the potentiometer up to 1V. The ouput of the constant voltage source is connected to the dynamic test piece through one of the reference resistances ranging from 10Ω to 10kΩ. The potential drop between the contact of test pieces is amplified and smoothed and the smoothed output is fed into a chart recorder to give a qualitative measure of the existence of lubricant film.

In order to obtain an X-Y display trace of the contact reistance as shown in Figure 9.10, on a CRT, the contact resistance trace must be separated for both strokes. For this purpose a shift

circuit is incorporated which is the lower circuit line in the diagram. This is a Schmit trigger circuit which generates a square wave triggered by the friction force output. As the friction force changes its direction the polarity of the square wave changes. This square wave is summed with the output of the contact resistance amplifier, thus the output of the summing amplifier is a contact resistance output plus constant bias voltage the polarity of which reverses for both strokes. This output is fed into one of the Y input of two channel CRT. X input is a stroke displacement which is described in the next section. By this arrangement it is possible to monitor the existence of lubricant film and friction force against stroke position simultaneously as shown in Figure 9.10.

9.3.4 Stroke Length

The stroke is measured by two independent methods, one is direct reading, the other is electrical reading method.

Absolute value of the stroke length was measured by the direct reading method: A scale slip as shown in Figure 9.11 which is produced by

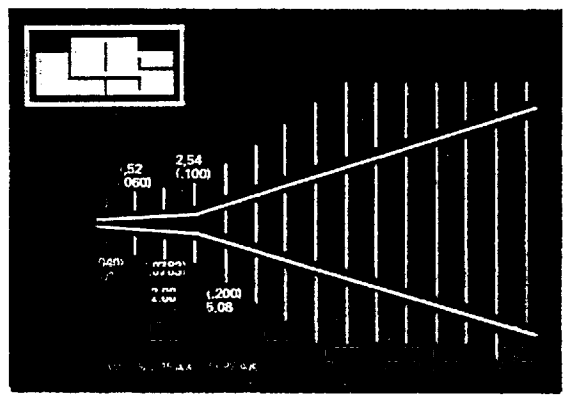


Figure 9.11 Stroke Measurement Slip

Ling Dynamic Systems Inc. is fixed to the dynamic test piece support rod as shown in Figure 9.12(a). When the rod is vibrating the two inclined lines of the slip look wider because of an afterimage effect of eye sight as shown in Figure 9.12(b). The crossing point of the apparently widened two lines is read to give an absolute value of the peak to peak displacement.

In order to obtain the X-Y display as explained earlier the eletric signal of displacement of the dynamic test piece is necessary. This signal is obtained by a strain gauge bridge attached to the auxiliary suspension spider of the vibrator. The same strain gauge amplifier as for the applied load measurement is used and the output gain is so adjusted that the horizontal deflection of the CRT display agrees with the direct reading. An example of the X-Y display is already explained for Figure 9.10.

9.4 Control

Controlled quantities are stroke length and temperature of the test pieces.

9.4.1 Stroke Length Control

It is desirable to keep the stroke length constant especially for the experiment on scuffing. Without control the vibrator amplitude changes depending on the change of the friction force and the power input of the vibrator should be controlled manually in order to keep the stroke length constant.

In order to avoid this inconvenience a feed back control circuit which controls the vibrator's power amplifier output voltage was built.

The diagram is shown in Figure 9.13(a)(b)(c) and it is essentially

an automatic gain control circuit. The sine wave output voltage amplitude is proportional to the control signal.

Figure 9.13(a) is the wave form generator. Three types of output are available, a sine wave is used as an input signal of the power amplifier of the vibrator. Output of the wave form generator is fed into the X input of the analogue multiplier which is shown in Figure 9.13(c), thus the output sine wave amplitude of the multiplier is proportional to the control signal of the Y input. The analogue multiplier is the same as that used for friction coefficient measurement but the connection is changed. The control signal is generated by the circuit shown in Figure 9.13(b). Vibration stroke output is rectified and smoothed by the same circuit mentioned before but the time constant can be adjusted in the range of 0.26 seconds to 4.7 seconds by the variable resistance. Thus the response time of the feed back control can be adjusted for that range. The smoothed signal is then subtracted by the negative reference voltage and the polarity is reversed by the output stage. Thus the control signal is proportional to the difference between the signal of the stroke length and the reference signal but the polarity is reversed. The whole system makes up a negative proportional feed back control system. Constant of the proportionality is adjusted by changing the feed back resistance of the output stage. The diode in the output stage is to prevent a possible negative control signal in which case the system becomes a positive feed back control and is unstable.

9.4.2 Temperature Control

For the study of boundary lubrication of scuffing, the temperature is one of the most important factors (47)(48). How the tempera-

ture should be controlled is an essential factor of the experimental work. The amount of oxidation or chemical reaction of lubricant is in general dependent on the reaction time available. Thus it is desirable to be able to adjust the ratio of temperature rise arbitrarily as well as being able to keep the temperature constant.

Thus the temperature controller of the same concept of stroke length controller circuit was built.

The diagram of the controller is shown in Figure 9.12(a)(b). Figure 9.14(a) is the control signal circuit. Chrome Alumel thermocouple is used as a temperature sensor which is positioned near the contact of the test pieces. Thermocouple emf is amplified by a milivoltometer (Comark Type 1221) and the reading is converted to temperature by a standard table. As the millivoltmeter has a voltage output of 1V per full scale this amplified voltage is used as a control signal source. This signal is fed into the input differential amplifier and at the second stage the gain is so adjusted that the output voltage marked by (1) is approximately 1V per 100^{o}C. At the next stage the voltage is subtracted from the reference voltage and the polarity is reversed. The control sensitivity is so adjusted by the final stage that the temperature of the test pieces follow the reference temperature with minimum oscillation.

Reference voltage (temperature) is generated by a constant current source and large capacitance (10,000μF). Thus the voltage rise is decided by the current though the variable (100kΩ) and constant 100Ω resistance divided by the capacitance. As the voltage difference of the resistances is kept nearly constant by the feed back loop, the current is nearly constant and almost linear voltage rise is achieved. The voltage rise is mainly adjusted by the negative input voltage.

To the reference boltage line a standby current sink is connected. This works only when the reference voltage (2) exceeds the preset voltage (3). Thus the reference voltage cannot exceed the preset voltage (3).

The controller is used to set the rate of temperature rise and the maximum temperatures. Heater power input is controlled by a triac which operates with a zero voltage switch (provided in an integrated circuit, IC) as shown in figure 9.14(b). The use of zero voltage switch eliminates radio frequency interference by ensuring that power is only switched on or off as the AC sine wave passes through zero. Control signal is fed to the terminal 5 through 47K resistor. Inside the IC a ramp wave form is generated and compared by a comaparator (shown as COMP in the figure) with the control signal and the power triac switched on only when the control signal is above the ramp wave form as shown in the figure. Thus the switch on time is nearly proportional to the control signal level. The interval of ramp wave cycle is decided by a capacitor of terminal 1 of zero voltage switch. 47μF gives about 4 seconds interval of the cycle.



Figure 9.1 Overall View of the Experimental Set Up

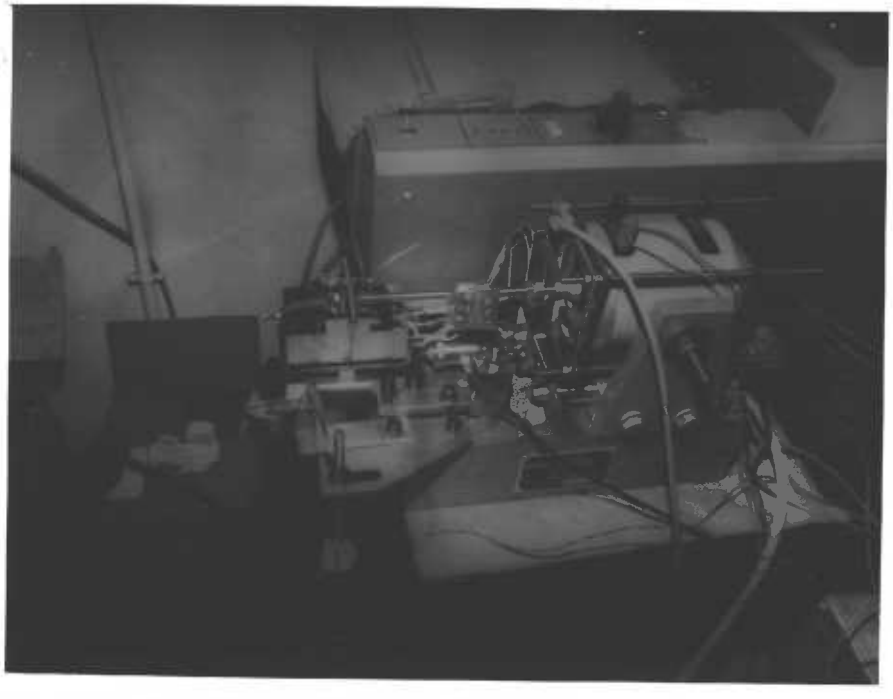
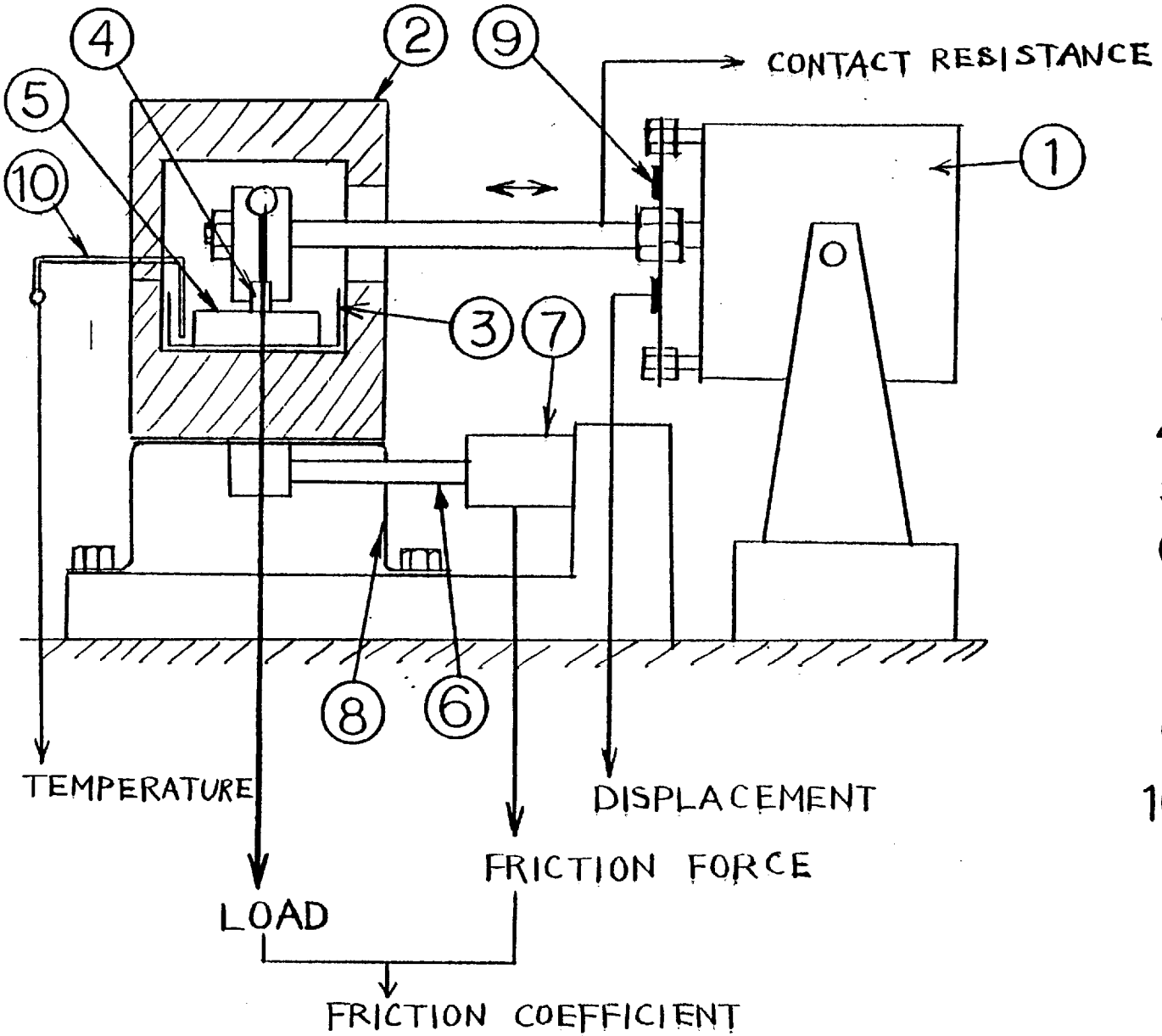


Figure 9.2 A View of the Apparatus



1. VIBRATOR
2. HEATER BOX
3. OIL BATH
4. DYNAMIC TEST PIECE
5. STATIC TEST PIECE
6. CONNECTING ROD
7. FORCE GAUGE
8. FLEXUAL SUPPORT
9. STRAIN GAUGE
10. THERMOCOUPLE

Figure 9.3 Schematic Diagram of the Apparatus

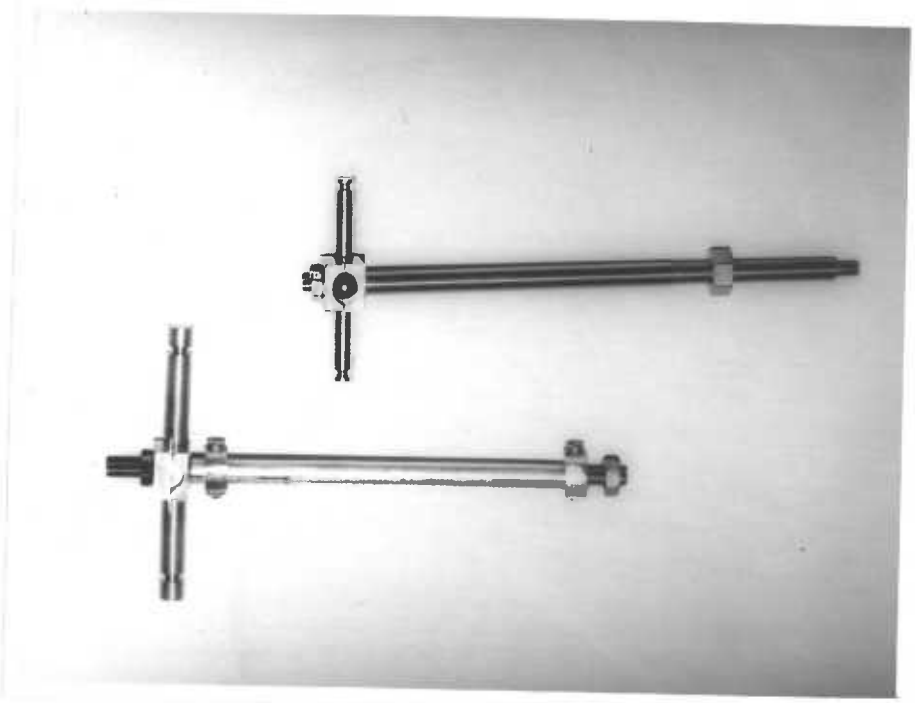


Figure 9.4 Dynamic Test Piece

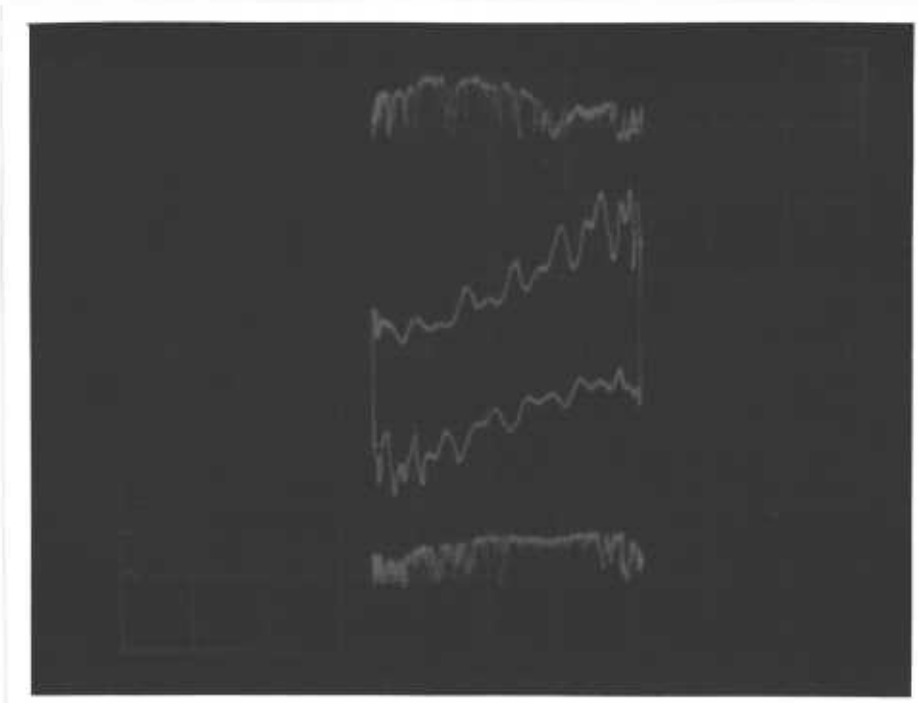


Figure 9.10 Typical X-Y Display of Contact Resistance and Friction Force

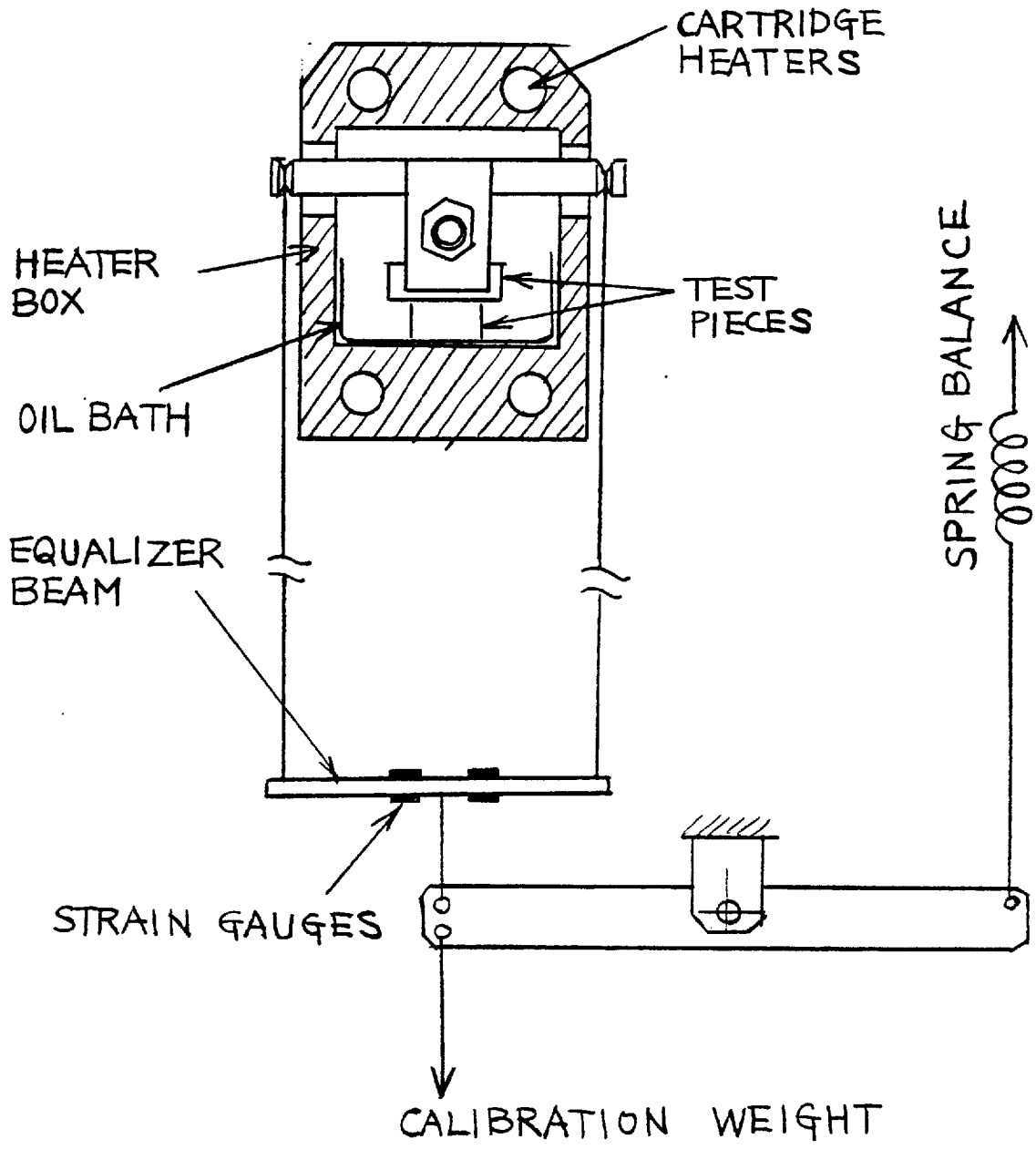
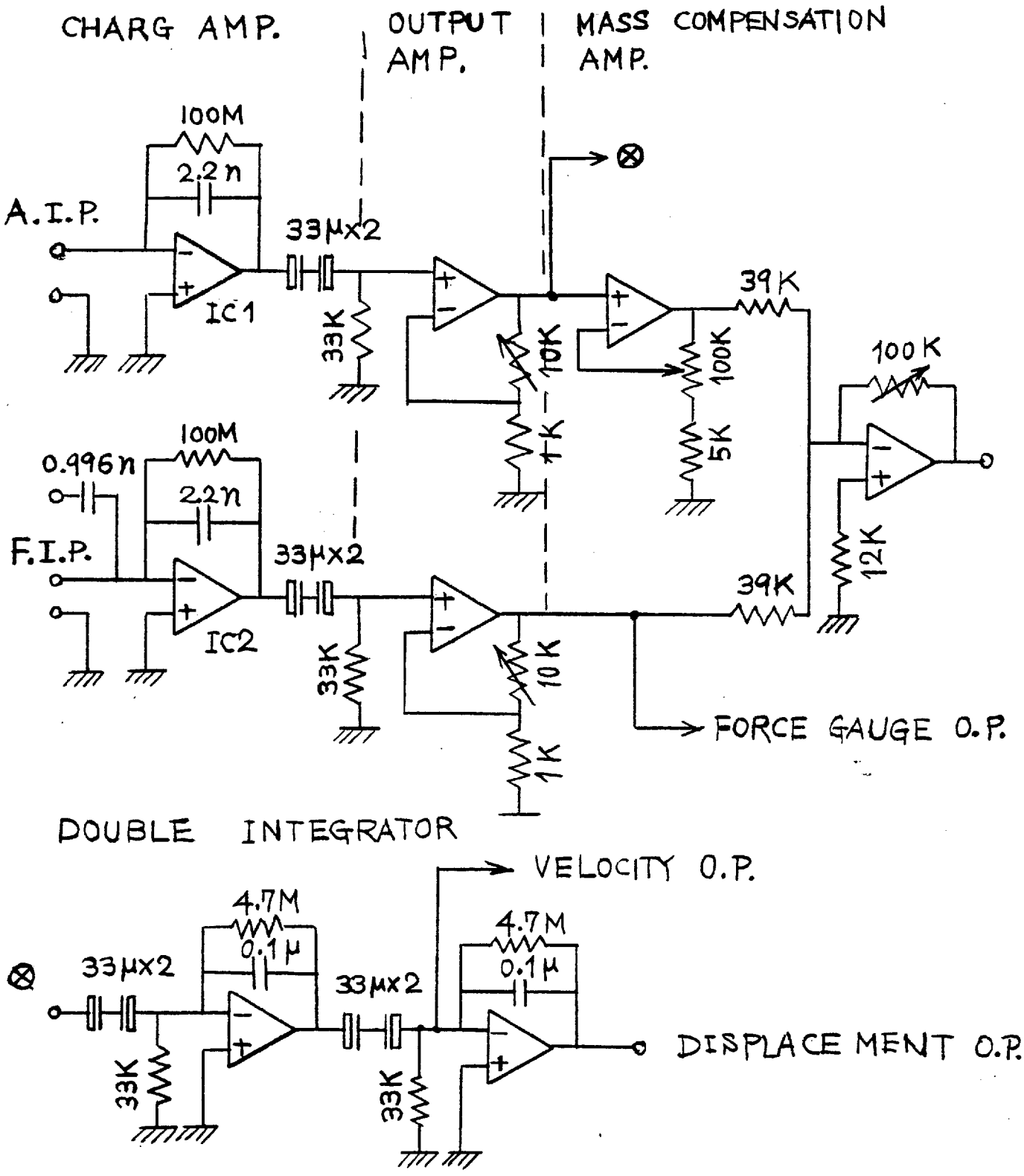
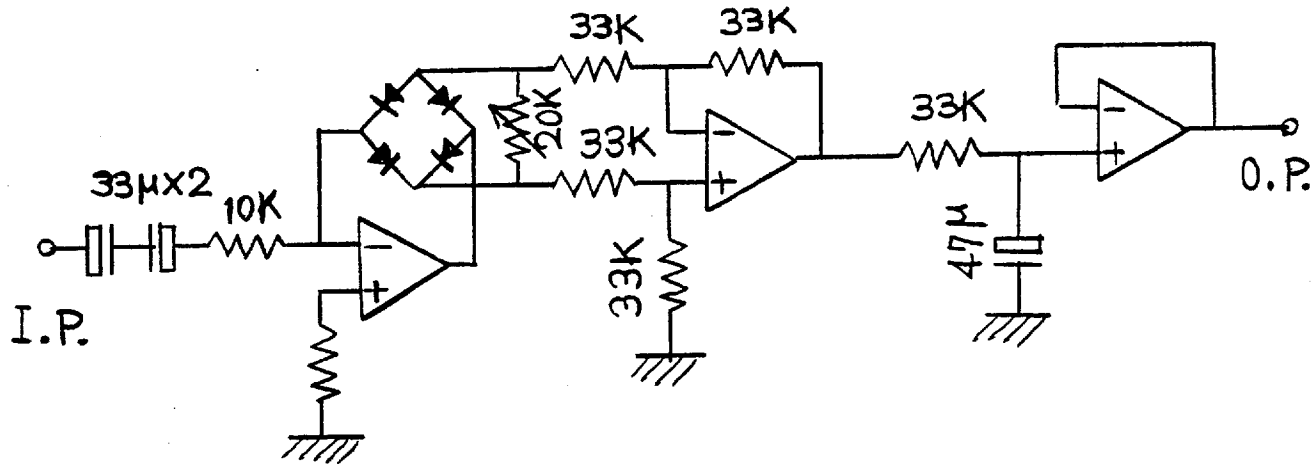


Figure 9.5 Front Section of the Heater Box and Loading Schematic



IC1, IC2, FET Operational Amplifier
(RS Component No. 305-939)
The Others, 741

Figure 9.6 Circuit Diagram of Charge Amplifier



All Operational Amplifiers are 741

Figure 9.7 Precise Rectifier and Smoothing Circuit

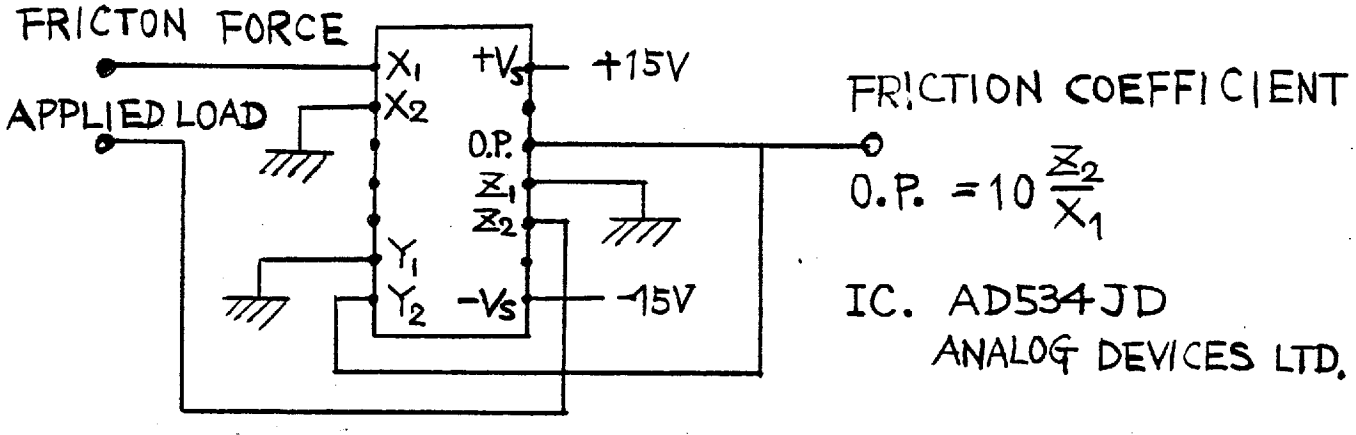
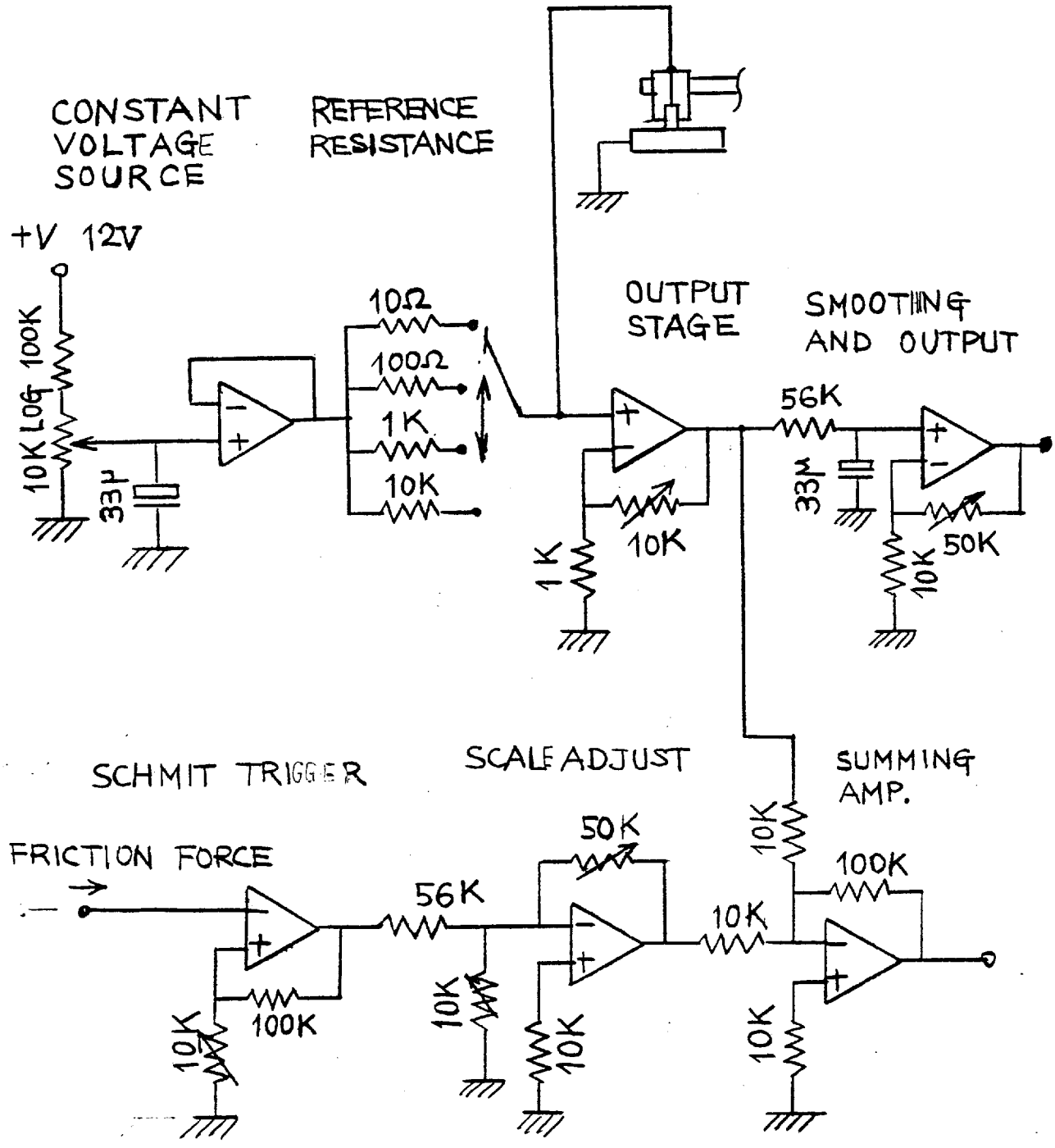


Figure 9.8 Analogue Divider Circuit



Formula of Contact Resistance

$$R_c = R_r \frac{1 - V_r}{V_r}$$

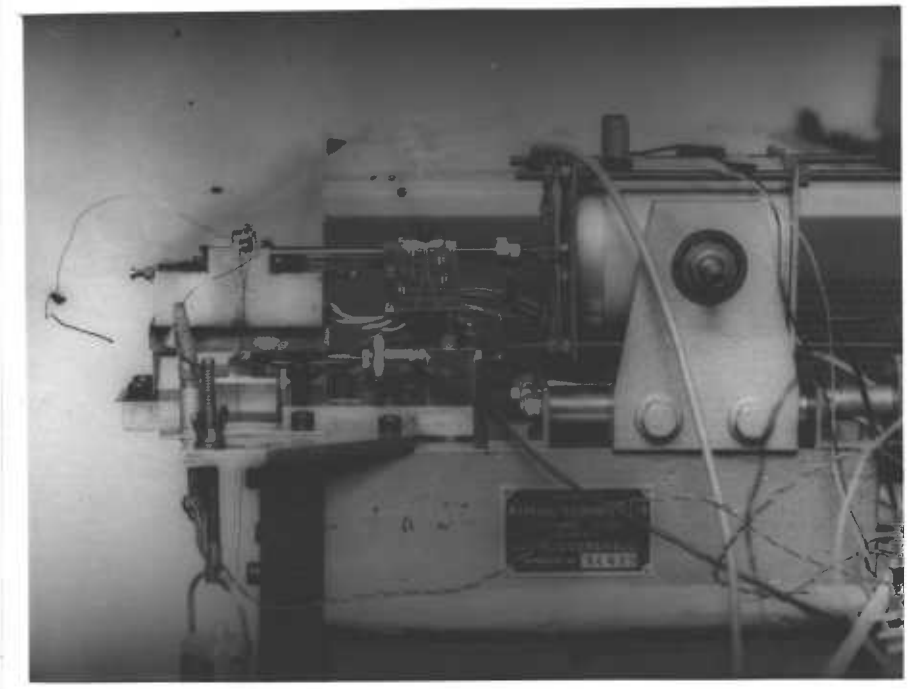
V_r : Ratio of input and output voltage

R_r : Reference Resistance

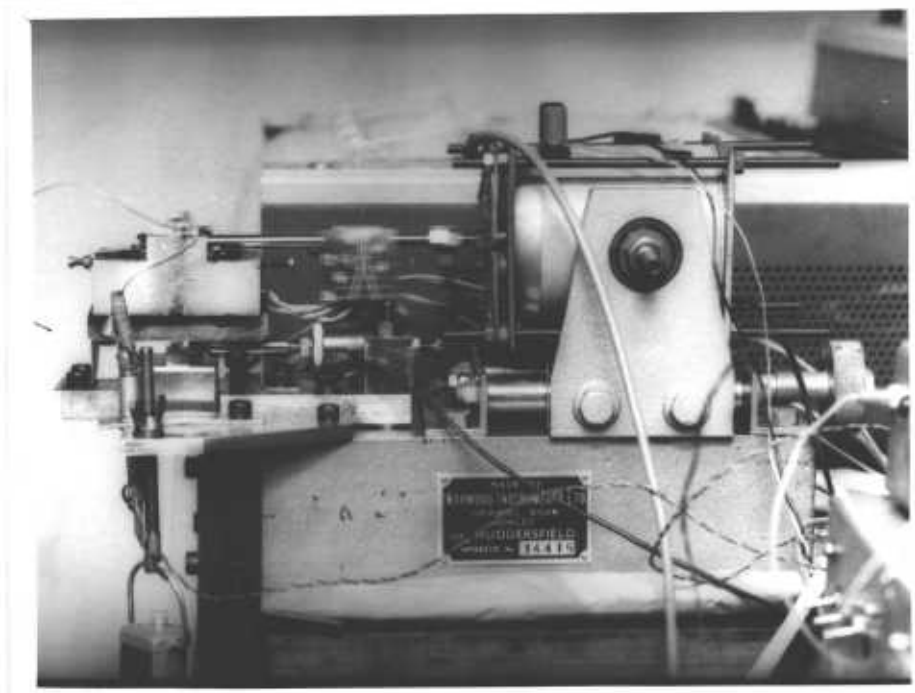
R_c : Contact Resistance

All operational amplifiers are 741

Figure 9.9 Circuit Diagram of Contact Resistance Measurement

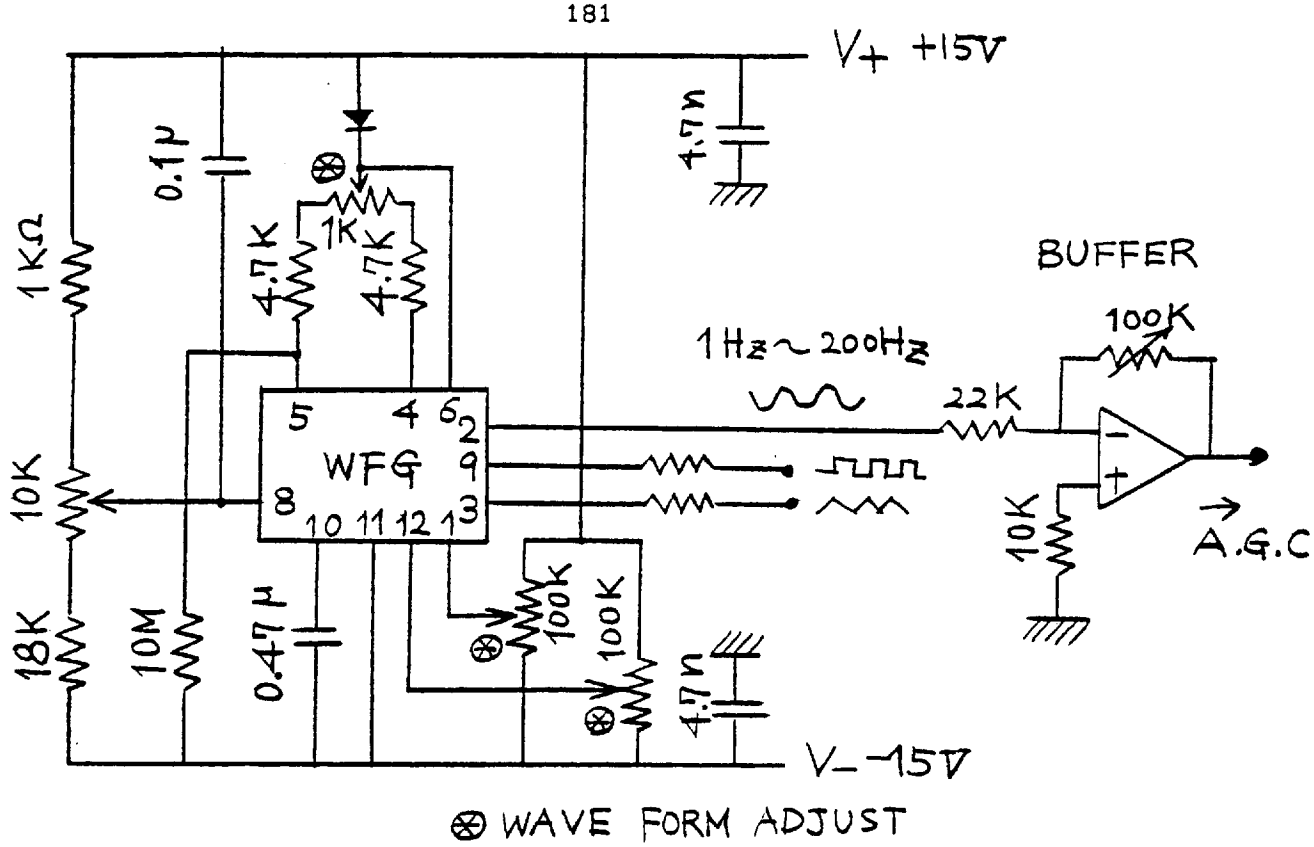


(a) Stationary



(b) Moving

Figure 9.12 Direct Reading Method of Stroke Length



W.F.G. Wave Form Generator (RS Components Ltd. 305 844)

Figure 9.13(a) Diagram of the Stroke Control Circuit (Wave Form Generator)

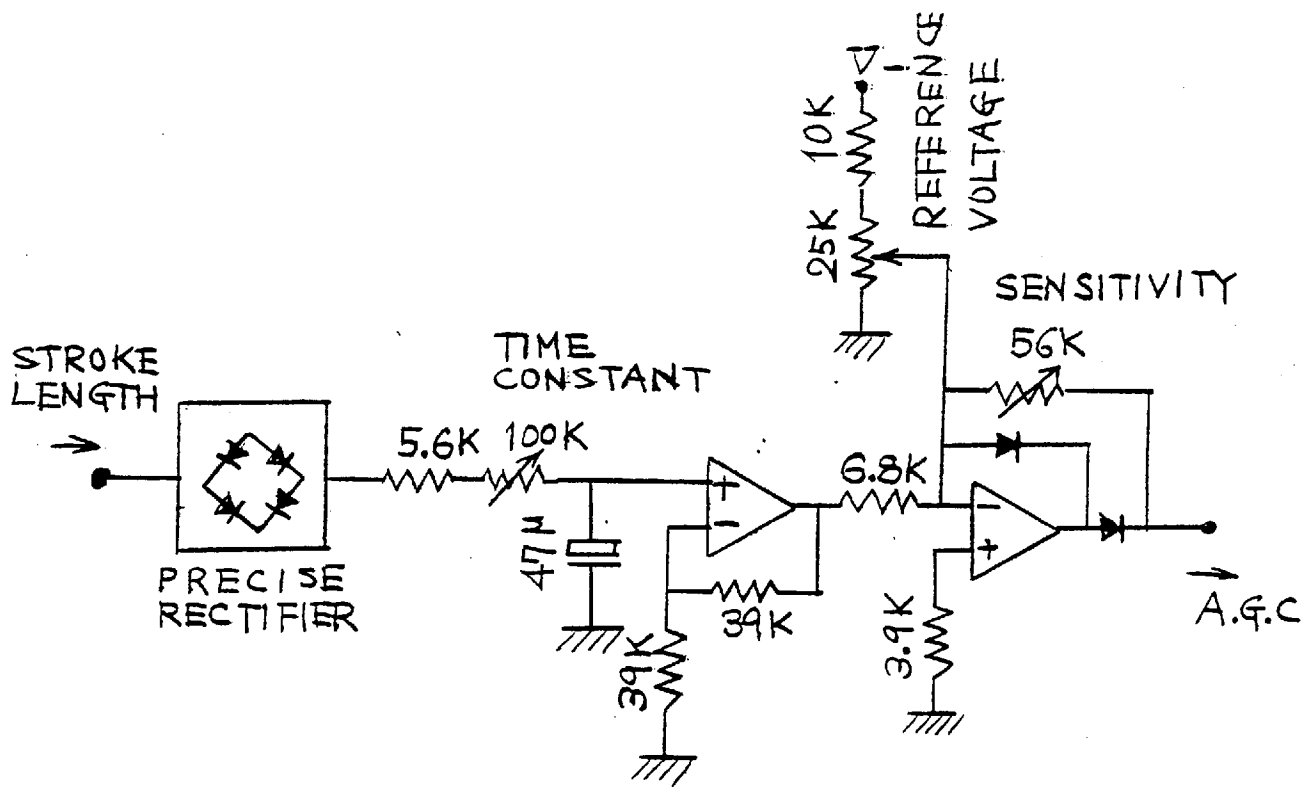


Figure 9.13(b) Diagram of the Stroke Control Circuit (Control Signal Circuit)

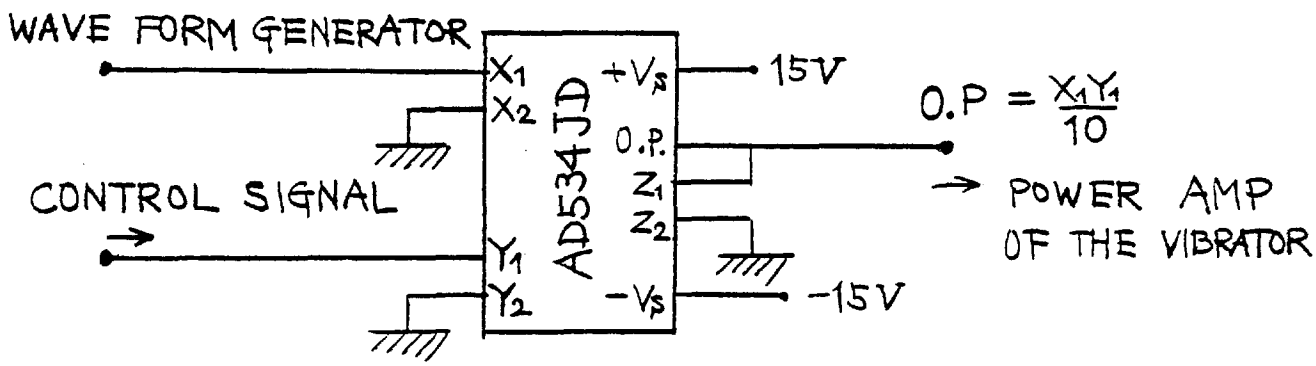


Figure 9.13(c) Diagram of the Stroke Control Circuit (Automatic Gain Control (A.G.C.))

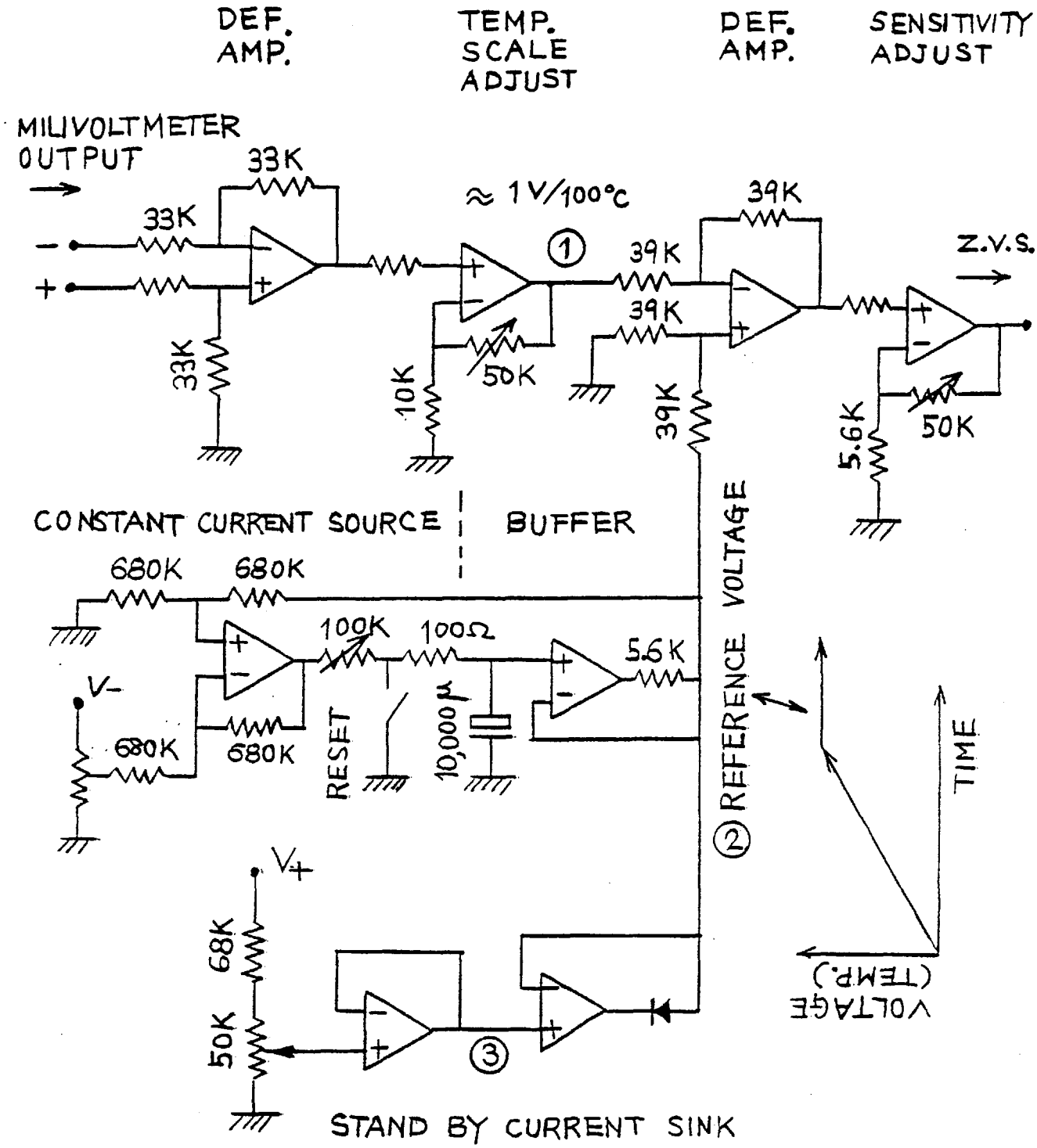
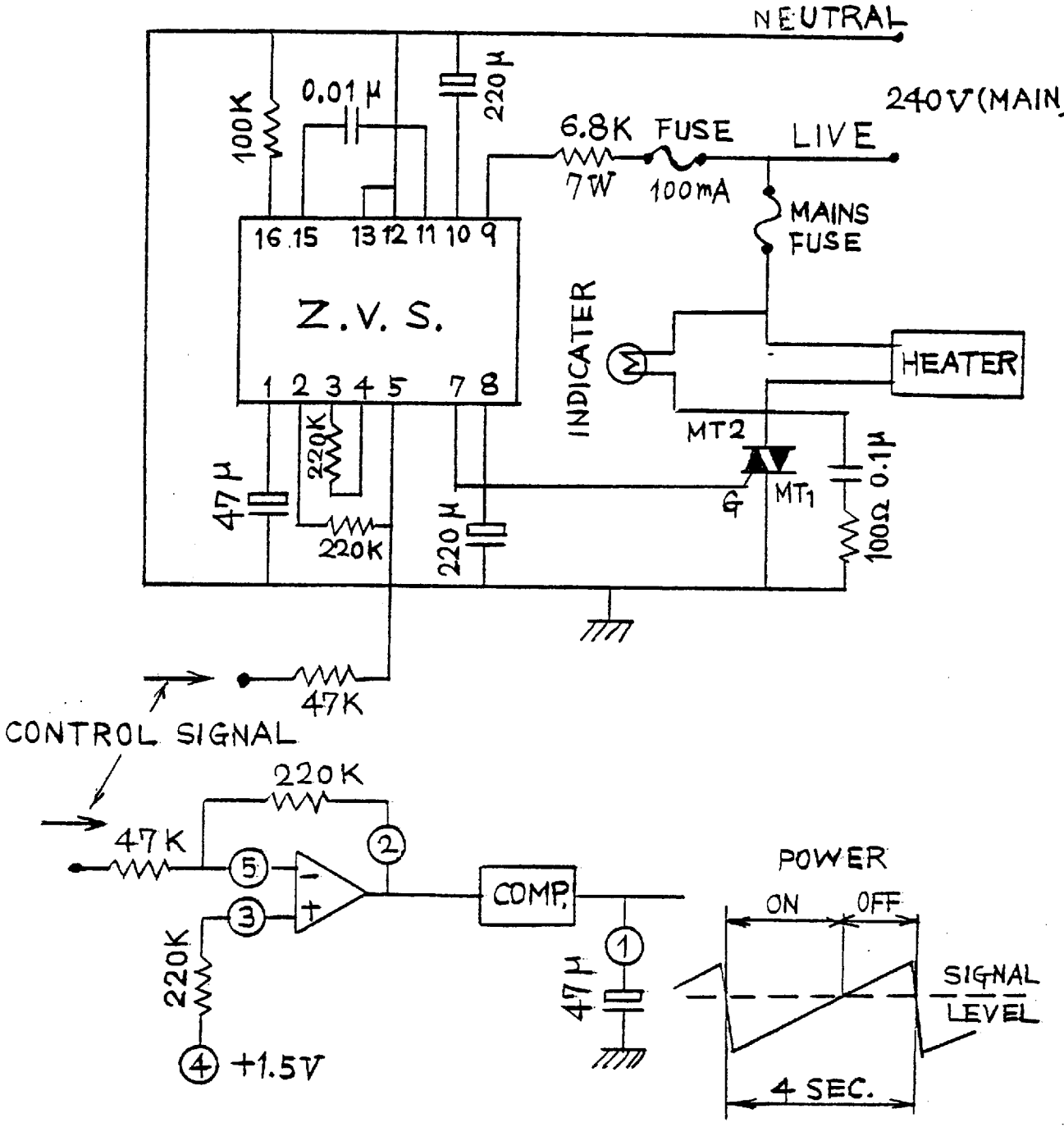


Figure 9.14(a) Circuit Diagram of the Temperature Controller (Control Signal Circuit)



Z.V.S. Zero Voltage Switch
(RS Components Lts. 305 800)

Figure 9.14(b) Circuit Diagram of the Temperature Controller (Power Switch Controller)

CHAPTER TEN

EXPERIMENTAL STUDY ON THREE REGIME OF LUBRICATION MODE UNDER RECIPROCATING MOTION

10.1 Introduction

Based on the theoretical results of Chapter Eight brief experimental study was carried out to examine the boundary of three lubrication regimesunder reciprocating motion. They are

(i) full hydrodynamic regime, where sliding surfaces are separated by hydrodynamic film all over the stroke

(ii) partial hydrodynamic regime where hydrodynamic film exists for a fraction of a stroke

(iii) boundary regime where hydrodynamic film cannot exist for all over the stroke.

The experimental results were compared with the theoretical results and the agreement was reasonable.

10.2 Experimental Method

10.2.1 Contact Resistance and General Procedure

The three lubrication regimes were distinguished experimentally by electric contact resistance. The reference resistance was arbitrarily chosen as 10Ω and 20mV was applied on the contact by the contact voltage source as explained in the last Chapter. The contact resistance was measured by a potential drop between the contacts and monitored by a CRT. Typical outputs of CRT are shown in Figure 10.1. As shown in the figures the contact resistance does not change from zero to infinity abruptly but there is a certain transition range. The boundary between whether hydrodynamic film exists

or not was set when the potential drop of the contact is about half of the applied voltage. Thus the equivalent contact resistance of the hydrodynamic film was taken as 10Ω.

At the start of the experiment the reciprocating frequency is set constant and the amplitude of the stroke is increased gradually until the contact resistance of the middle stroke increases more than 10Ω. This condition is considered to be the boundary between boundary and partial hydrodynamic regime. Actually this boundary has its width as there exists a certain amount of hysteresis. So the boundary has a certain width. When this boundary is identified the stroke amplitude is increased again until all of the strokes show the contact resistance more than 10Ω. This condition is considered to be a boundary between full and partial hydrodynamic regime. This boundary has also its hysteresis. During the above procedure shown above, the contact resistance is not completely stable. There exists an intermittent fluctuation because of wear debris etc.. This fluctuation was neglected because this does not continue more than a fraction of a second, though it is intermittent. When both boundaries were identified then the frequency was changed and the same procedure was repeated.

As the contact is nominally flat, caution was taken to arrange the test pieces that there was no edge contact. By examining the wear scar after the test the contact was considered to be satisfactory.

10.2.2 Reciprocating Frequency

The reciprocating frequency was first measured by the CRT calibrated time scale. Then it was compared with the dial reading of the oscillator amplifier. The difference was found that the dial reading was about 6% less than the frequency given by the CRT

time base. Then this difference was taken into account for the latter experiments and the frequency was set by the dial reading of the oscillator amplifier.

10.2.3 Stroke Amplitude

Stroke amplitude was at first measured by the label as explained before. Then the gain of the strain gauge amplifier was adjusted so that the horizontal deflection of the CRT display gave two divisions per 1mm stroke amplitude. Then the stroke amplitude of the boundary between the three lubrication regimeswas measured by the horizontal deflection of the CRT. By this method the accuracy of the measurement is considered to be about 5% when the stroke is more than 1mm and about 10% when it is less than 1mm.

10.2.4 Load

Load was applied simply by measured weight to avoid calibration procedures.

10.3 Test Specimen

10.3.1 Sliding Test Specimen

The test specimens are shown in Figure 10.2. The dynamic upper test specimen is a mild steel block of nominal dimension of 2 x 4 x 15mm. One face is ground by hand with #800 emery paper to give a slight roundness. As the procedure had to rely on hand grinding several tries were necessary to obtain the final sliding surface shape as shown in the figure. The dimension shown as Δh was measured by a microscope with a precision moving bed. The surface was finally polished with diamond paste and the measured surface

roughness is less than about 0.05μm peak to peak.

The static test piece is also a mild steel block of 20 x 10 x 5mm dimensions. The sliding surface was ground and polished by the same procedure as the dynamic test piece.

Both specimens are immersed in the oil bath so that the contact of the specimens is about 1mm below the oil surface.

10.3.2 Lubricant

The lubricant used is heavy neutral distillate oil of viscosity category about SAE30. This was used in earlier work and designated as B_2 (p.181 of reference (6)), or labelled as 2 in part 4 of reference (7). The viscosity was measured at room temperature before and after the experiment and the results are shown in Table 10.1 together with manufacturer's specification.

Measured Viscosity	
Before Experiment	2.173* Poise (at 18.5°C)
After Experiment	2.152* Poise (at 18.5°C)
Average	2.16 Poise
Manufacturer's Specification	
Density at 15°C	0.884
Viscosity	46 Cst at 50°C
	82.34 Cst at 100°F
	9.50 Cst at 210°F
Viscosity Index	101

Instrument Feranti viscometer Model VL

* Averaged value under three different shear rates (114.3, 144.2, 172.9 sec^{-1}). Cylinder used, VM-C.

Table 10.1 Viscosity of the Lubricant

10.4 Results

The results are shown in Figure 10.3 and Figure 10.4. Figure 10.3 shows the boundary between full and partial hydrodynamic regime and Figure 10.4 shows that of partial hydrodynamic and boundary regime. The abscissa is stroke frequency and the ordinate is stroke length for both figures. During the experiment it was found that the repeatability of the boundary of lubrication regime was not very good. The reason of this was found that the surface roughness of the test pieces was changing because of wear. So the data which are shown in the figures are taken when the wear condition was considered to be stable. This condition was that starting the experiment from the polished surface (less than 0.05μm surface roughness) and operating the apparatus partial hydrodynamic and boundary lubrication regime under the constant load (5.9N) for about 30 minutes. The surface roughness was measured after the experiment, and the Talysurf traces are shown in Figure 10.5. As shown in the figure the surface of the dynamic test specimen is more rough than the static specimen. The waviness of the surface, estimated from the Talysurf trace, is about 0.25μm/3mm for both test specimens. There was a round off of length about 0.3mm near the corner of the static test specimen, but this was neglected.

Neglecting the sporadic deep valley of dynamic test specimen the total hydrodynamic surface roughness is in the range of 0.5 to 1.5μm.

From figure 10.3 and figure 10.4 it is seen that when the applied load is increased the stroke length or frequency should be increased in order to keep the hydrodynamic condition. It is also observed that there are transitions at which stroke length cannot become smaller than certain length to keep the hydrodynamic regime. The

transitional stroke lengths are about 0.7mm for the full hydrodynamic regime and 0.3mm for partial hydrodynamic regime.

In order to compare the experimental results with the theory the experimental results are non-dimensionalised and shown in Figure 10.6 and Figure 10.7, the forms of which are the same as Figure 8.4.

In Figure 10.6 the theoretical non-dimensional minimum film thickness given by Figure 8.4 are included as broken lines for comparison. Actual theoretical film thicknesses based on the measured dimension $\Delta h = 52\mu m$ are shown in brackets. Theoretically all the experimental lines should come together in a non-dimensional figure. As the estimated total surface roughess is about 0.5 to 1.5μm agreement between theory and experiment is fairly good except the transition at about St = 0.3.

Figure 10.7 shows the non-dimensionalised boundary between partial hydrodynamic and boundary regime. In this figure theoretical steady state film thicknesses at the midstroke are included.

In this case all the experimental results are practically on the same lines and the film thickness of the boundary of the two lubrication regimes is about 0.5 to 1μm. This film thickness roughly agrees with the estimated surface roughness of 0.5 to 1.5μm.

10.5 Discussions

It was experimentally found that there is a transition stroke amplitude. When the stroke amplitude is less than that hydrodynamic film cannot exist. This transition from hydrodynamic lubrication to possibly a fretting wear situation is of practical importance. If fretting wear occurs, then wear begins at either end of the stroke length. It is shown in figure 10.6 and 10.7 that the transitions of both

boundaries of lubrication regime are different. Quantitative discussion on this is not possible from this brief experimental result The physical use of this transition can be considered as following. Theoretically a hydrodynamic film can be attained only when the hydrodynamical inlet side of the surface is filled with the lubricant. Under reciprocating movement of high frequency the lubricant can not fill the inlet side of the surface in a short time interval of frequency. Thus the moving surface is always scraping the lubricant in both directions of movement. The hydrodynamically flooded condition can not be realised because of the scraping action of the sliding surface itself, though the contact is apparently full flooded (immersed in lubricant). It was observed in the experiment that the electric contact resistance just before the full hydrodynamic regime is always low at both dead ends of the stroke as shown in the lower figure of Figure 10.1. Theoretically the position of minimum film thickness is about 20 to 25^{o} crank angle later than the dead end, which corresponds about 5% of stroke length from both dead ends of the stroke.

This "self starved" condition could happen in piston ring lubrication and it was experimentally reported by Hamilton et al (37)(38)(39) that an artificial oil supply arrangement was needed to obtain the full flooded condition of piston ring lubrication in their experimental apparatus. This was also reported by Wakurai et al (14) that the different oil supply method on their experimental rig gave different oil film thickness pattern during a cycle from their theory. For the case of piston ring lubrication the lubrication condition is still hydrodynamically normal, though the "self starved" condition occurs.

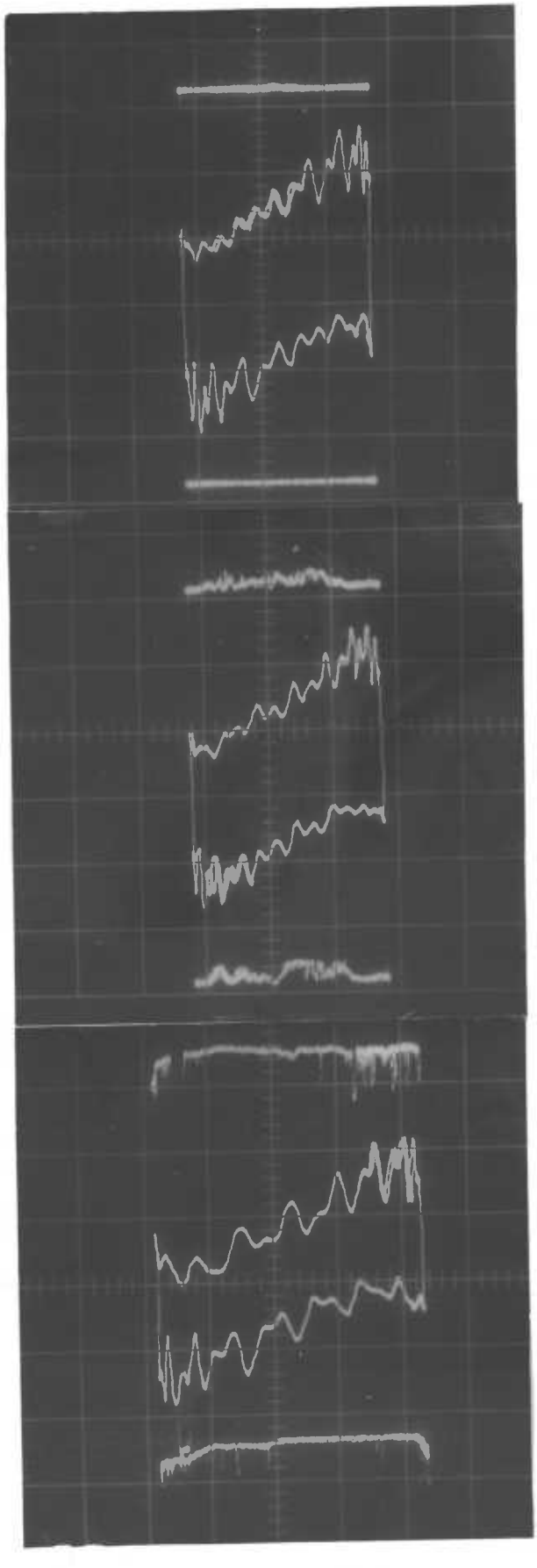
10.6 Conclusion

Although the experiment is brief several conclusions can be drawn as follows

(i) Hydrodynamic film can still exist when the stroke length is less than the breadth of the sliding surface.

(ii) There is a transitional stroke length under which hydrodynamic film cannot exist whatever the stroke frequency is.

(iii) Comparison between theoretical prediction and experimental results of the boundary of the three lubrication regimes, i.e. full hydrodynamic regime, partial hydrodynamic regime and boundary lubrication regime, is fairly good.



(a) Boundary Lubrication

(b) Partial Hydrodynamic

(c) Near Full Hydrodynamic Regime

Figure 10.1 Three Regimes of Lubrication

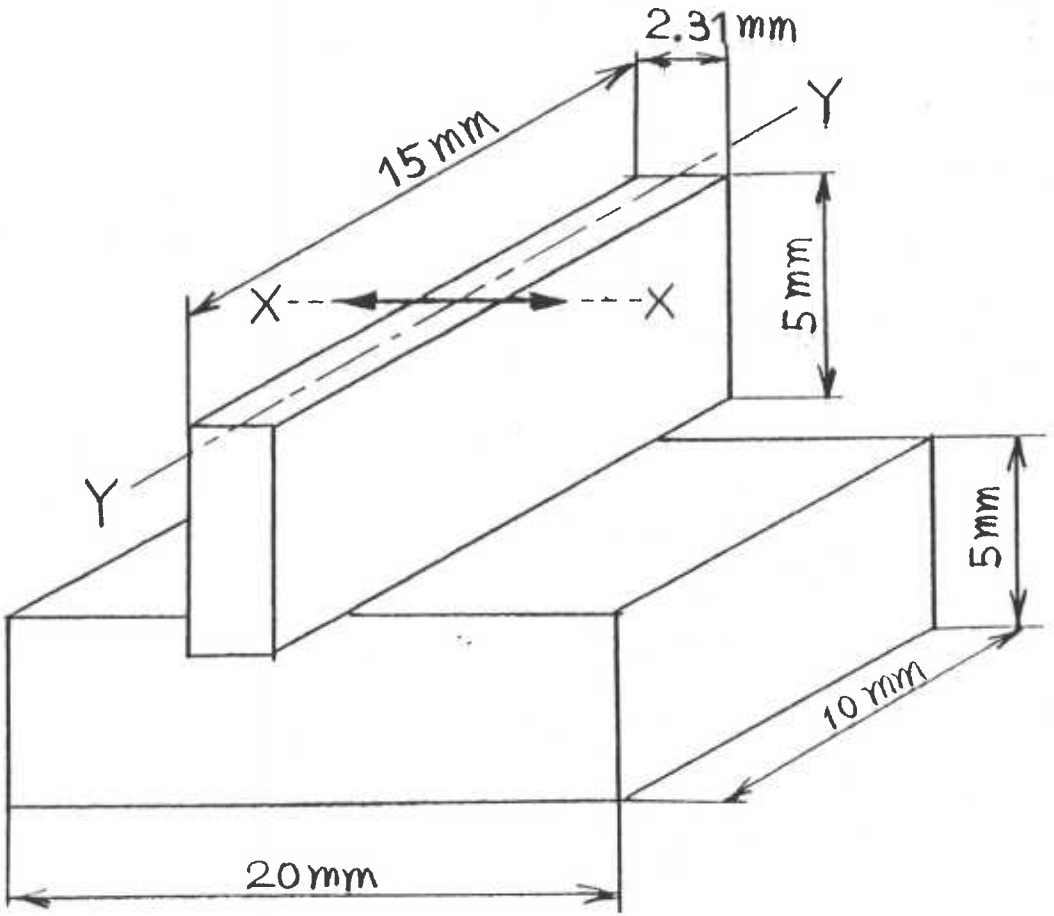
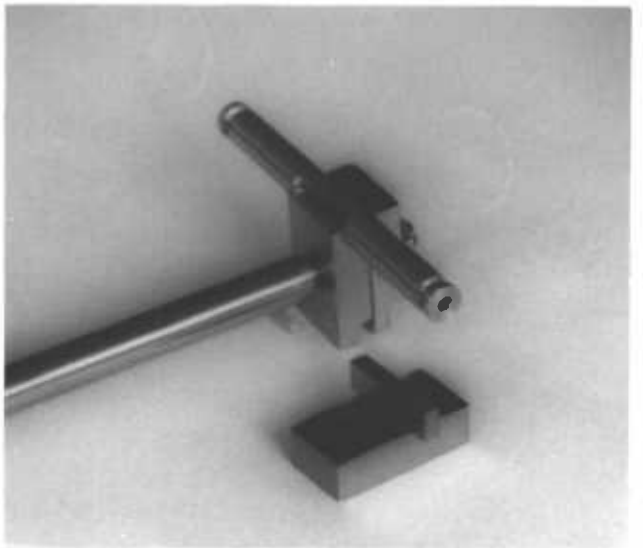
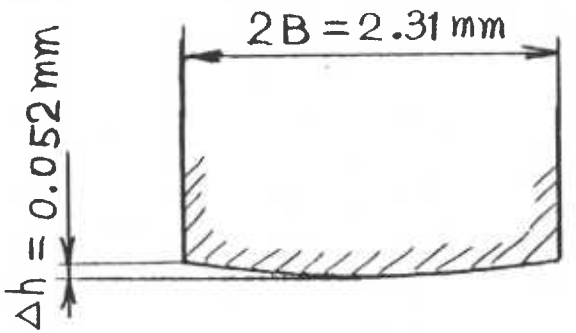


Figure 10.2 Test Specimens





Sliding Surface Shape (measured)

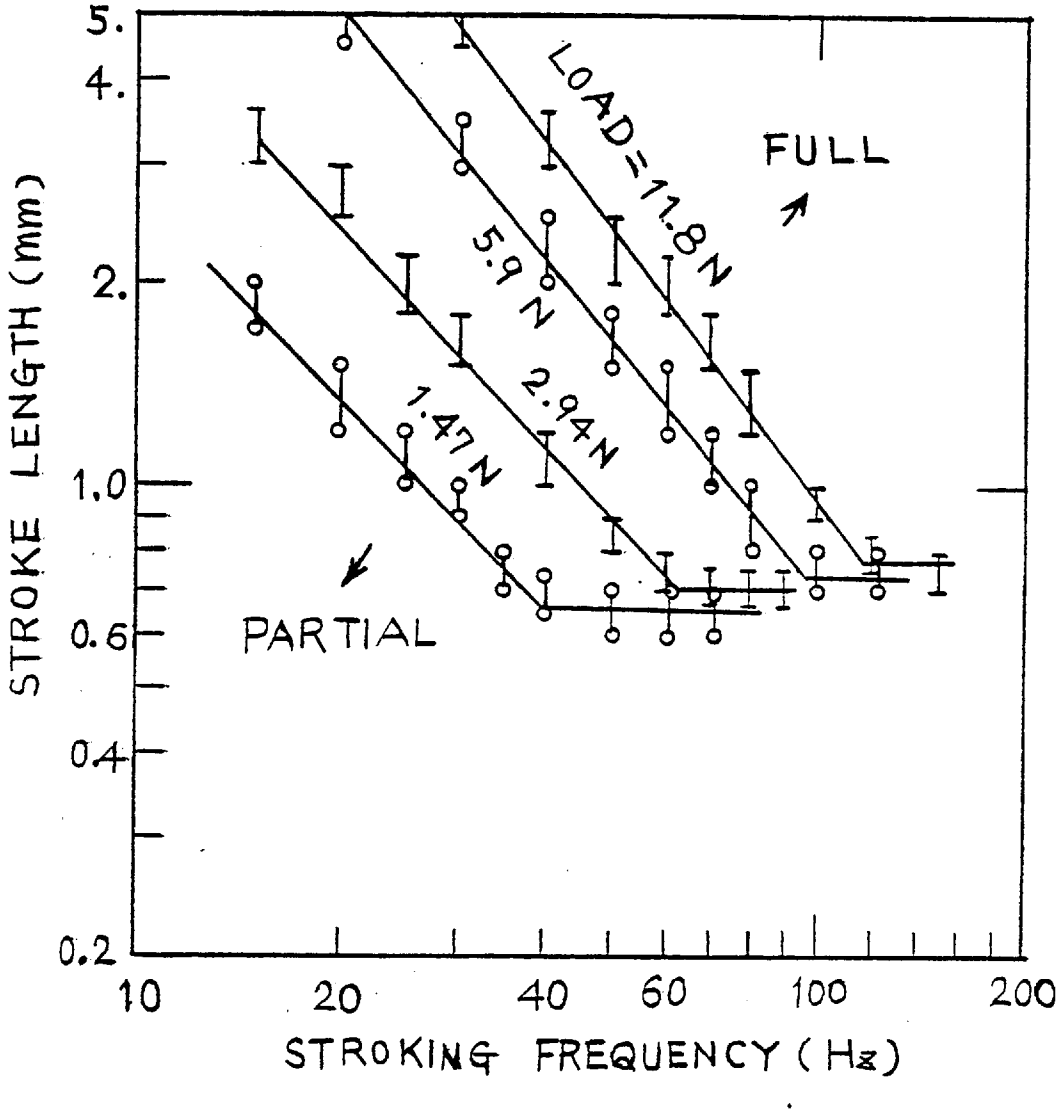


Figure 10.3 Boundary Between Full and Partial Hydrodynamic Regime

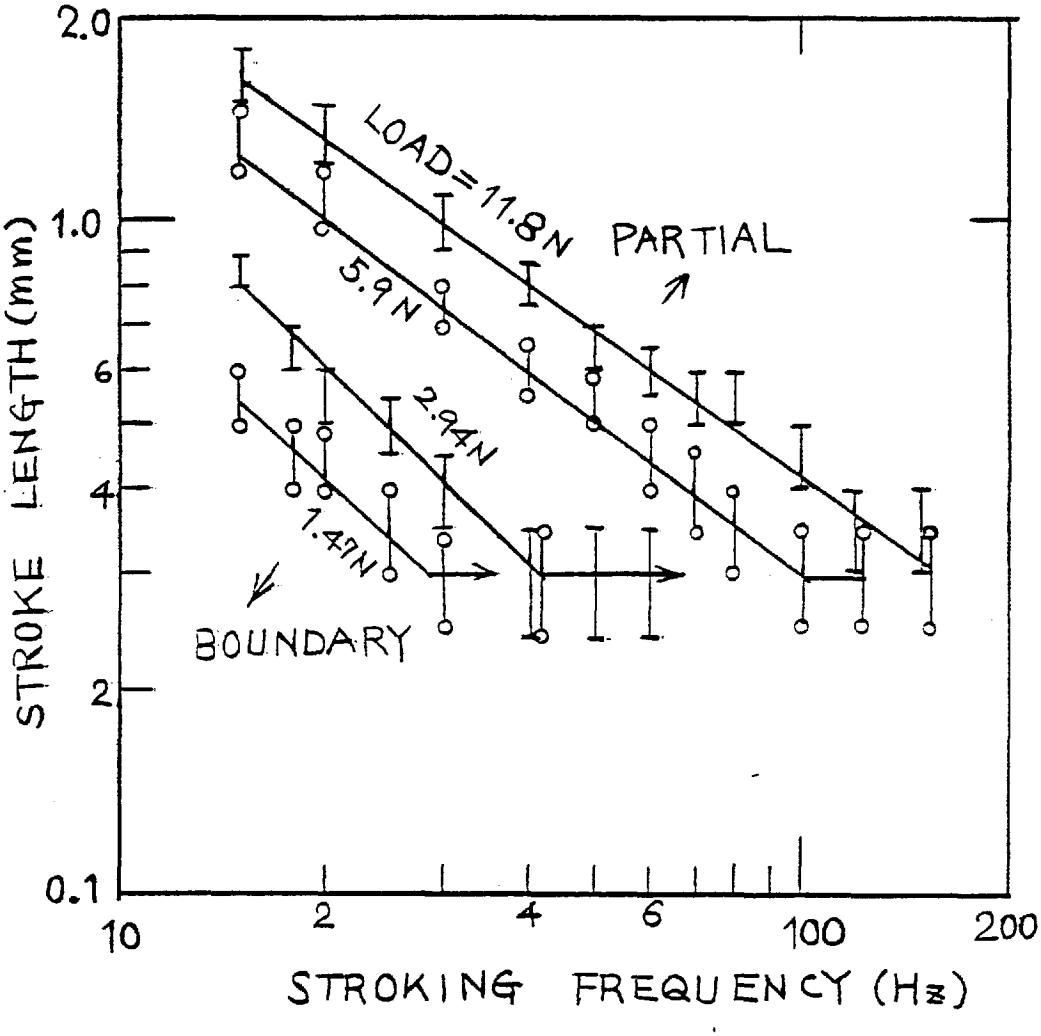
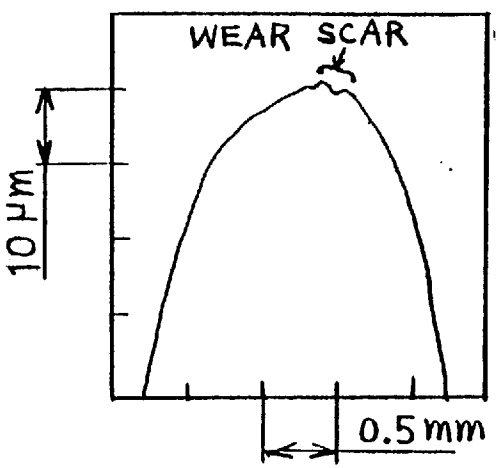
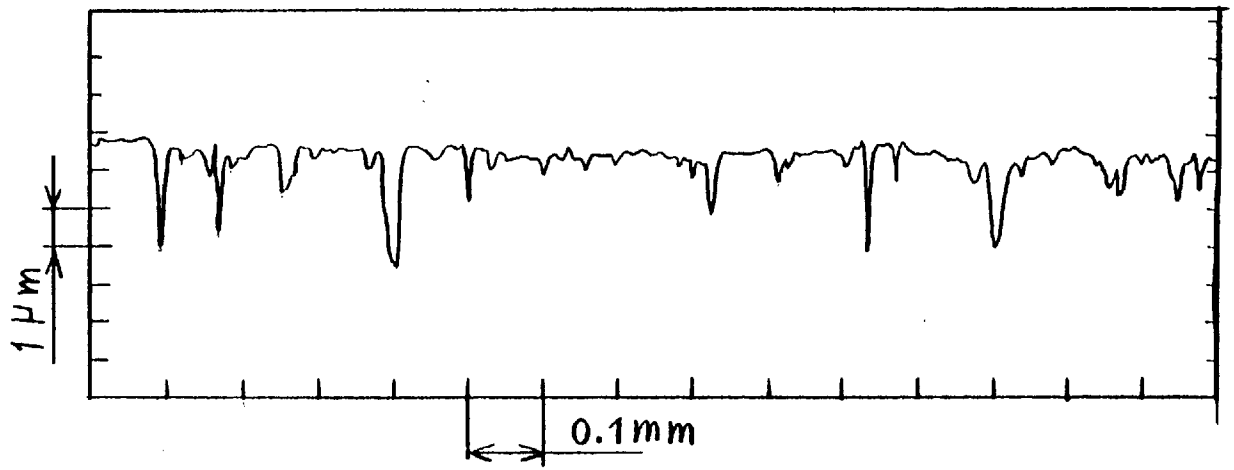


Figure 10.4 Boundary Between Partial Hydrodynamic and Boundary Lubrication Regime



c) Dynamic Test Specimen (in the direction of X-X)

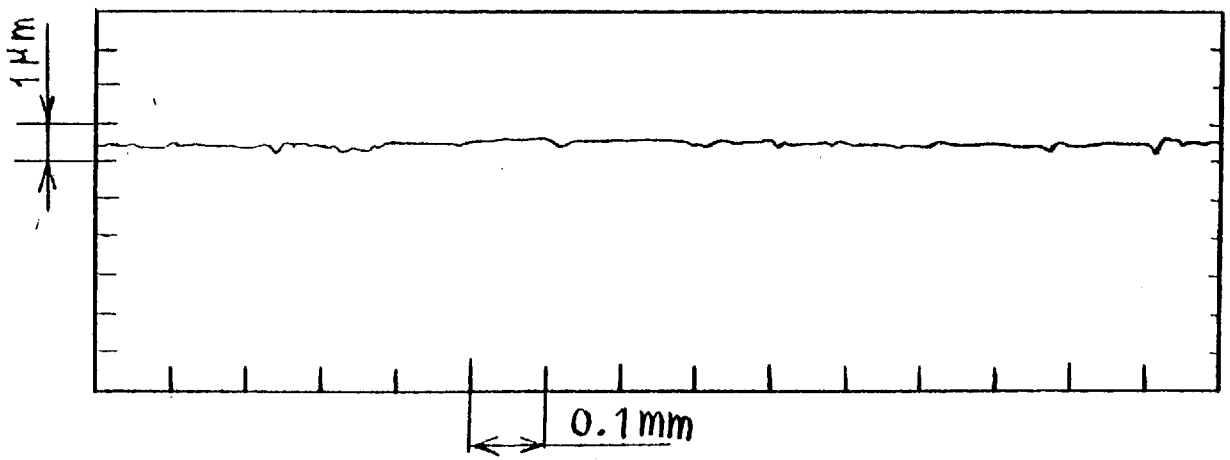


b) Dynamic Test Specimen (in the direction of Y-Y)

Refer to Figure 10.1 for X-X and Y-Y

Instrument
Tarysurf Model 3

Recorder
Rectilinear Recorder ME795
(Taylor Hobson Limited)



a) Static Test Specimen (across the middle of the wear scar, Y-Y direction)

Figure 10.5 Tarisurface Traces of the Test Specimens

H_{omini} : same as Figure 8.4

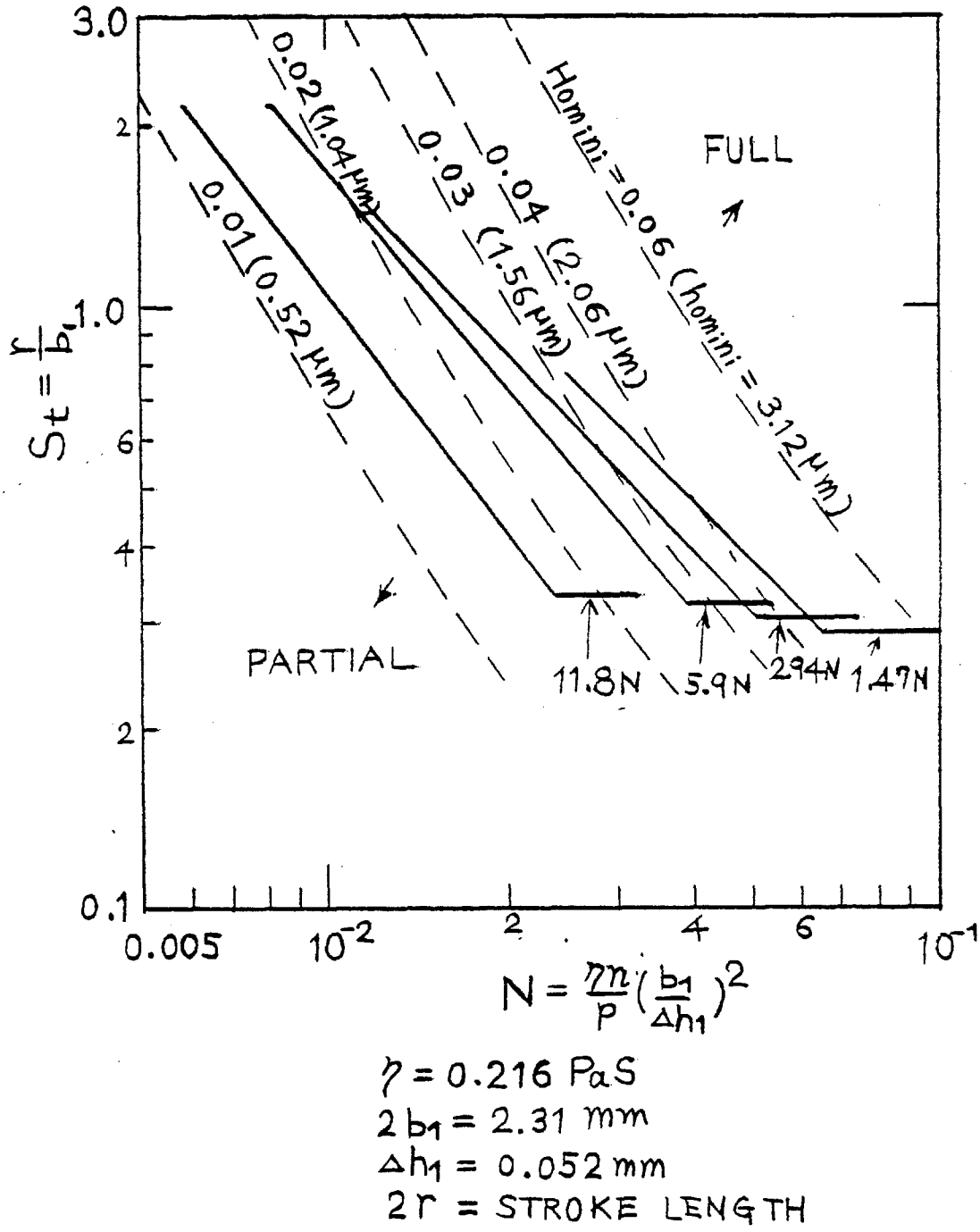


Figure 10.6 Non-dimensionalised Experimental Results (1) (Boundary between full and partial hydrodynamic regime)

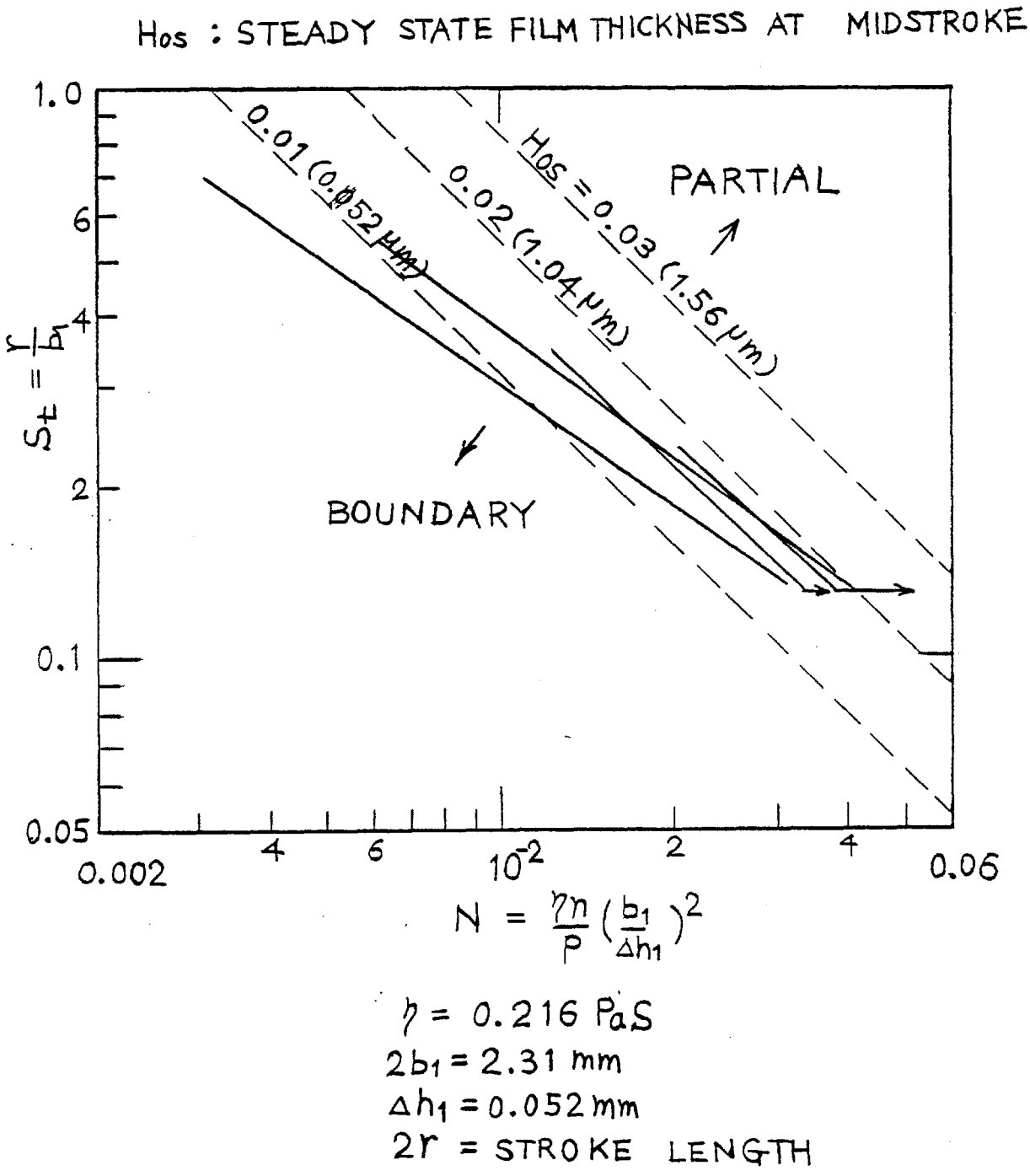


Figure 10.7 Non-dimensionalised experimental results (2) (Boundary between partial hydrodynamic and boundary lubrication regime)

CHAPTER ELEVEN

GENERAL DISCUSSION, CONCLUSIONS AND SUGGESTIONS FOR FURTHER WORK

11.1 Introduction

As mentioned in the introduction, the project of this thesis started as a development of the new friction test device based on the predecessor and the study on piston ring scuffing. But the final form of this thesis does not mention anything about scuffing or boundary lubrication in its main text. The new non-dimensional expression is so general that almost all basic theory of hydrodynamic lubrication of thrust bearings was simplified, though actual mathematical formulation may be complex depending on the surface shape. This simplification is achieved in a consistent and natural expansion of the basic expression. Additional parameters to the basic equation enabled the comprehensive analysis of the hydrodynamic lubrication of thrust bearings under tilted condition, starved condition, dynamic condition (squeeze) and reciprocating motion. This comprehensive analysis has never been achieved before, because the convetional non-dimensional expression was not "correct". "Correct" intepretation of the Reynolds equation also simplified the analysis of EHL lubrication.

In this final chapter the meaning of Δh which is consistently used in the main text of this thesis will be examined. Then brief qualitative discussions on the lubrication on piston ring in general will be given based on the theoretical results given in the main text. Finally the conculsions from the theory and suggestions for further work will be given.

11.2 The Meaning of Δh

The correct intepretation of the Reynolds equation lies in the importance of Δh which represents the difference between inlet and outlet film flow, not the ratio of inlet and outlet film thickness. This is because hydrodynamic film pressure is generated as a result of two opposing flows. One is Couette flow and the other is Poiseuille flow. The former is caused by the drag force of the moving surface and has no direct relationship to film pressure. The latter is caused by the pressure gradient along the narrow flow passage. Referring to Figure 11.1, if the inlet film thickness h_1 is larger than the outlet h_2 the inlet flow and outlet flow caused by Couette flow is different and the difference is

$$(q_{in} - q_{out})_{Couette} = \frac{u}{2}(h_1 - h_2) = \frac{u\Delta h}{2}$$

In order to keep the physical continuity (flow continuity) this difference must be compensated by Poiseuille flow. The formula of Poiseuille flow between a narrow plain passage is

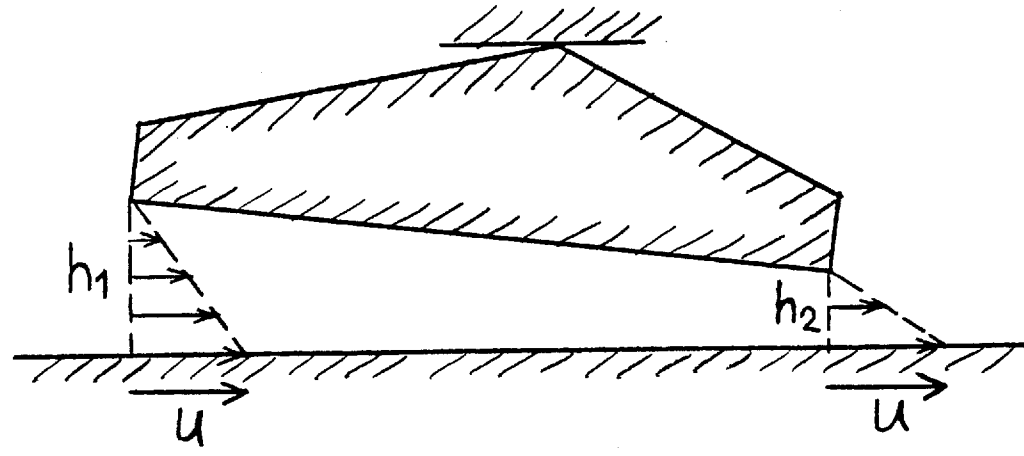
$$q_{Poiseuille} = \frac{1}{12} \frac{h^3}{\eta} \frac{dp}{dx}$$

Thus both flows must be equal, equating then produces

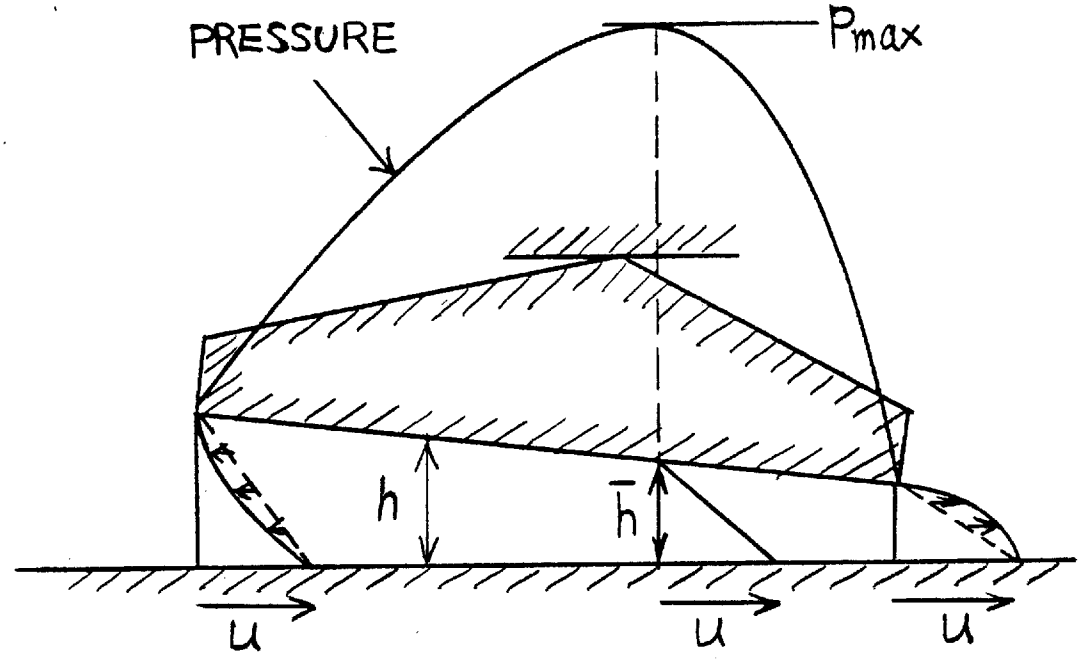
$$\frac{1}{12} \frac{h^3}{\eta} \frac{dp}{dx} = \frac{u\Delta h}{2}$$

Rearranging

$$\frac{dp}{dx} = 6\eta u \frac{\Delta h}{h^3}$$



(a) Couett flow



(b) (a) + Poiseuille flow

Figure 11.1 Flow Balance in a Narrow Passage

In the beginning of this discussion the "flow difference" caused by Couette flow is hypothetically taken as that of inlet and outlet. But Couette flow is actually defined somewhere within the bearing breadth. This position is at the point where dp/dx = 0 and the film thickness h = $\bar{h}$ as is shown in the figure (11.1). Thus the actual "flow difference" caused by Couette flow, between an arbitrary point at which the film thickness is h and the position of dp/dx = 0, is $\frac{u(h - \bar{h})}{2}$. Then the equation is

$$\frac{dp}{dx} = 6 \eta u \frac{h - \bar{h}}{h^3}$$

This is the one dimensional Reynolds equation. A simple procedure that takes into account two opposing flows can derive the Reynolds equation in one dimension. Thus the physical meaning of the Reynolds equation is clear, it expresses the equilibrium between two opposing flows. Δh or $h-\bar{h}$, represents the difference between the Couette flow and the Poiseuille flow. The Poiseuille flow is caused by the film pressure field, thus the load can be supported.

11.3 Discussion on Piston Ring Lubrication

In Chapter Eight it was shown that the reduction of the minimum film thickness under reciprocating motion from the steady state condition can be kept to a minimum when the condition is optimised, and the reduction is not so large, e.g. 60% when the stroke ratio is 50. Thus the condition of piston ring lubrication is mainly hydrodynamic which agrees with experimental results. The decline in film thickness from the steady state condition is more marked when U_{max} decreases. Thus the

piston ring is more difficult to lubricate hydrodynamically and consideration of the boundary lubrication becomes more important than the steady state lubrication.

In an actual reciprccating engine piston rings are usually used as a ring pack. It was concluded in chapter five that once starvation occurs the film thickness is entirely defined by incoming oil flow deposited on the sliding surface. The natural consequence of this analysis is, that the film thickness of each piston ring in a ring pack is entirely difined by one critical ring which gives the smallest film thickness. Obviously the critical ring must be an oil control ring. Thus if the oil control ring dictates the oil supply, the upper rings must always operate under starved conditions and the film thickness of them is almost equal to that of the oil control ring. Each ring adjusts its film pressure area (B_s in Figure 5.3) depending on its own operating conditions. Thus the most important fact in piston ring pack lubrication is the important role of the oil control ring.

The other important feature in actual piston ring lubrication is the effect of ring face tilting. The tilting might be caused by piston tilt, or thermal and elastical distortion of the related components. This tilt may be negative or positive hydrodynamically. If it is negative, the film thickness reduction is significant as shown in figure 4.3. If the ring face is purely parabolic there might be a tilting condition in which no inlet convergent zone exists. Thus there is no film thickness. But an actual piston ring has normally a round corner whatever the cause though the main part of the face is nearly parabolic. This round corner might be helping to reduce the wear by supporting part of the hydrodynamically applied load as it has been discussed in Chapter Two.

The complexity of piston ring lubrication constrains its discussion

to a purely qualitative level. The full cognition of the problem remains for future workers.

11.4 Conclusion

11.4.1 Theory

As was shown in the section refering to the meaning of Δh, the conclusion of the theoretical part of this thesis can be concisely summarised as following.

The decisive physical quantity in the hydrodynamic lubrication which can be expressed by the Reynolds equation, is the discrepancy between the inlet and outlet lubricant film flow caused by the moving surface. This quantity is most correctly represented by the difference between the inlet and minimum film thickness.

The conclusions of each application of this concept are already given in several chapters. The general conculsions of this concept are following:

1. Hydrodynamic lubrication of thrust bearings can be expressed in a general non-dimensional expression as following.
   The simplest form for steady state condition is,
   $X = f(H_o)$
   where H_o is non-dimensional film thickness and X can be any non-dimensional quantity which is related to the Reynolds equation, e.g. load carrying capacity, film pressure distribution, centre of load or film flow. The expression can be expanded to include several operating parameters as following,

$X = f(H_o, Y)$

Y can be squeeze velocity, starvation parameter, tiling parameter or stroke ratio for reciprocating motion.

2. If the operating condition expressed by Y does not change the non-dimensional surface profile function $H_p(X)$, defined in Chapter Two, the same function for the original condition can be applied to other conditions expressed by Y. The parabola is the most convenient surface shape because $H_p(X)$ does not change under tilt or starvation.

11.4.2 Experiment

1. Comparison between theory and experiment was done on the boundaries between three lubrication regimes. The agreement was fairly good within the operating range of the apparatus, when the stroke length was more than a certian transitional stroke length.
2. It was experimentally shown that there exists a transitional stroke length under which no hydrodynamic film can be generated.

11.5 Suggestions for Further Work

11.5.1 Theory

The corollary of this thesis is to complete the performance diagrams for thrust bearings as following.

1. Analyse viscous friction of thrust bearings in the same non-dimensional form as used in this thesis.
2. Analyse the side leakage effects of finite length thrust bearings. This may involve a numerical computation mehtod, but since comprehensive diagrams for infinitely long bearings are given in this thesis the side leakage effects can be analysed more

efficiently than before. This is especially the case for curved face tilting pad bearings.

3. Analyse the piston ring lubrication for more complex conditions than the simplest case given in Chapter Eight. This is to include the following influencing parameters,

   (i) Crank motion.

   (ii) Assymmetric ring profile.

   (iii) Effects of gas pressure.

   (iv) Effects of varying viscosity along the stroke length.

   The above analysis can be achieved using the non-dimensionsal parameters given in Chapter Eight.

11.5.2 Experiment

The purpose of the development of the new apparatus was to study boundary lubrication (scuffing, lubricity performance of additives). But it has not been used for that purpose in this thesis. So there are several possible lines of investigation as following.

(i) Compare the anti-scuffing performance of lubricant or surface treatment between the results of the newly developed apparatus and the field experience. If some correlation can be obtained the apparatus can be used as a standard test rig for screening lubricants or surface finishes. This will greatly economise the cost of industrial performance tests.

If clear correlations can not be obtained it gives another possible line of investigation. The study of why there is no correlation might find the deciding factors on piston ring scuffing performance in an actual engine.

(ii) Although they are brief the experimental results in Chapter Ten show that there exists a transitional stroke length under

which no hydrodynamic film can be generated. This suggests a transition to fretting wear. Thus more quantitative and more comprehensive experimental study on this transitional stroke length might possibly clear the fretting wear mechanisms. Theoretical study on this must include the effects of surface tension and wettability of the lubricant. The theory also must include the effects of inertia of the lubricant under vibration. All these effects are neglected in this thesis, so the theory predicts that there is an equilibrium between squeeze and wedge action of the film under infinitely small stroke length. To adapt the theory to small stroke lengths would be a useful further advance.

(iii) The newly developed apparatus can monitor the existence of film and friction force simultaneously in a form of X-Y display of CRT. So that it would be possible to study the lubricant performance more precisely than before. It is a worthwhile line of investigation to study thick chemical film formation as reported by Cameron et al (7) by fully utilising the above mentioned advantage of the apparatus.

REFERENCES

1. Bowden, F.P. and Tabor, D.
"The Friction and Lubrication of Solids, I",
Oxford. The Claredon Press (1950)

2. Bowden, F.P. and Tabor, D.
"The Friction and Lubrication of Solids, II",
Oxford. The Claredon Press (1964)

3. Rabinowicz, E.
"Friction and Wear of Materials",
Wiley-Interscience, New York (1965)

4. Cameron, A.
"Principles of Lubrication",
Longmans (1966)

5. Cameron, A.
"Basic Lubrication Theory",
Ellis Horwood (1976)

6. Mills, T.N.
"Boundary Lubricated Contacts at High Repetition Rate",
PhD Thesis, University of London, 1979

7. Mills, T.N. and Cameron, A.
"A New Lubricant Test Device",
ASLE to be published

8. Castleman, R.A.
"A Hydrodynamic Theroy of Piston Lubrication",
Physical Review V.49, p.410 and p.886 (1937)

9. Eilon, S. and Saunders, O.A.
"A Study of Piston Ring Lubrication",
Proc. I.M.E. Vol. 171, p.427 (1957)

10. Lloyd, T.
"The Hydrodynamic Lubrication of Piston Ring",
Paper No.5, I.M.E., Tribology Convention 1961

11. Furuham, S.
"A Dynamic Theory of Piston Ring Lubrication",
(i) First Report - Calculation
Bull. JSME. Vol. 2, p.423 (1959)
(ii) Second Report - Experiment
Bull. JSME. Vol. 3, p.291 (1960)
(iii) Third Report - Measurement of Oil Film Thickness
Bull. JSME. Vol. 4, p.747 (1961)

12. Ting, L.L. and Mayer, Jr., J.E.
"Piston Ring Lubrication and Cylinder Bore Wear Analysis",
Part 1 - Theory
J. of Lub. Tech. ASME p.305 (1974)
Part II - Theory Verification
J. of Lub. Tech. ASME p.258 (1974)

13. Allen, D.G., Dudley, B.R., Middleton, V. and Parker, D.A.
"Prediction of Piston Ring-Cylinder Bore Oil Film Thickness in Two Particular Engines and Correlation with Experimental Evidence",
I.M.E. Piston Ring Scuffing Conference C73/75 p.107 (1975)

14. Wakuri, Y., Ono, S., Soejima, M. and Tankguchi, T.
"Oil Film Behaviour of a Circular Faced Slider in the Reciprocating Motion",
JSLE, ASLE Conference, Tokyo, p.63 (1975)

15. Baker, A.J.S., Dowson, D. and Economu, P.
"Dynamic Factors Related to Piston Ring Scuffing",
I.M.E. Convention Piston Ring Scuffing C66/75 p.25 (1975)

16. Neal, N.J.

"Piston Ring Scuffing - A Broad Survey of Problems and Practice",

Proc. I.M.E., Vol. 185, 2/17 p.21 (1971)

17. Dyson, Y.

"Scuffing - A Review",

Tribology International, April 1975, p.77

18. Institution of Mechanical Engineers

Memorandum of Definitions, Symbols and Units.

Inst. Mech. E., London

19. Willen, J.E. and Brett, P.S.

"An Investigation into Piston Ring Scuffing during Running In",

Inst. Mech. E. Piston Ring Scuffing C70/75 p.71 (1975)

20. Willen, J.E. and Brett, P.S.

"Piston Ring Scuffing during Running In - The Influence of Lubricant and Materials",

Proc. I.M.E. vol. 191, 22/77 p.241 (1977)

21. Block, H.

"The Flash Temperature Concept",

Wear, Vol. 6, p.483 (1963)

22. Block, H.

"Theoretical Study of Temperature Rise at Surfaces of Actual Contact Under Boundary Lubrication Conditions",

Proc. Inst. Mech. E., Vol.2 p.222 (1937)

23. Block, H.

"The Posturate about the Consistency of Scoring Temperature",

NASA Sp-237 (Interdisciplinary approach to the lubrication of concentrated contacts) p.153 (1969)

24. Wakuri, U.,
"A Study on the Oil Loss Past a Series of Piston Rings",
JSME 13-55, p.150 (1970)

25. Dykes, P.
"An Investigation into the Mechanism of Oil Loss past Piston Rings",
Proc. I. Mech. E. Vol.171, p.413 (1957)

26. Dowson, D. and Higginson, G.R.
"Elastohydrodynamic Lubrication",
Pergamon Press (1976)

27. Halling, J.
"Principles of Tribology",
The MacMillan Press (1975)

28. Lord Rayleigh
"Notes on the Theory of Lubrication",
Phil. Mag. (1918) Vol.35, p.1-12

29. Fenner, R.T.
"Computing for Engineers",
MacMillan Press 1974

30. Martin, H.M.
"Lubrication of Gear Teeth",
Engineering, London, Vol.102 p.199

31. Purday, H.F.P.
"Stream Line Flow",
Constable, London (1949)

32. Raimondi, A.A.,
"Influence on Longitudinal and Transverse Profile on the Load Capacity of Pivoted Pad Bearings",
Trans. ASME Vol.3, p.265 (1960)

33. Pemberton, J.C. and Cameron, A.
"An Optical Study of the Lubrication of a 65mm Cylinder Roller Bearing",
ASME/ASLE Minneapolis, No.78-Lub-17 (1978)

34. Wymer, D. and Cameron, A.
"Optical Analysis of Roller Bearings",
Proc. I. Mech. E., 1974, p.221

35. Wedeven, L.D., Evans, D. and Cameron, A.
"Optical Analysis of Ball Bearing Starvation",
ASME/ASLE Cincinnati, No.70-Lub-19, 1971

36. Hamilton, G.M. and Moore, S.L.
"Measurement of the Oil Film Thickness Between the Piston Rings and Liner of a Small Diesel Engine",
Proc. I. Mech. E., Vol. 188, 20/74, p.253, 1974

37. Hamilton, G.M. and Moore, S.L.
"Comparison Between Measured and Calculated Thickness of the Oil Film Lubricating Piston Rings",
Proc. I. Mech. E. vol. 188, 20/74, p.262, 1974

38. Moore, S.L. and Hamilton, G.M.
"The Starved Lubrication of Piston Rings in a Diesel Engine"
Journal of Mech. Eng. Sci. I. Mech. Vol.20, p.345, 1978

39. Brown, S.R. and Hamilton, G.M.
"Partially Lubricated Piston Ring",
J. Mech. Eng. Sci. 1977, Vol.19, p.81, 1977

40. Hargreaves, R.A. and Higginson, G.R.
"Some Effects of Lubricant Starvation in Cylindrical Roller Bearings",
ASME J. Lub. Tech. p.66, 1976

41. Wolveridge, P.E., Baglin, K.P. and Archard, J.F.
"The Starved Lubrication of Cylinders on Line Contact",
Proc. I. Mech. E. Vol. 185, p.1159, 1971

42. Anderson, J.W.
The discussion of reference (41)

43. Dowson, D. and Higginson, G.R.
"Elastohydrodynamic Lubrication",
Pergamon Press, 1966

44. Hamrock, B.J. and Dowson, D.
"Isothermal Elastohydrodynamic Lubrication of Point Contacts",
Part I - Theoretical Formulation
ASME J. Lub. Tech. p.223, 1976
Part II - Ellipticity Parameter Results
ASME J. Lub. Tech. p.375, 1976
Part III - Fully Flooded Results
ASME J. Lub. Tech. p.264, 1977
Part IV - Starvation Results
ASME J. Lub. Tech. p.15, 1977

45. Wedeven, L.D.
"Transition from Macro to Micro EHL",
Limits of Lubrication, 1979

46. Constantinescu, V.N.
"On Some Starvation Phenomena in Fluid Films",
ASME J. Lub. Tech. p.441, 1977

47. Bailey, M.W. and Cameron, A.
"The Influence of Temperature and Metal Parts on the Scuffing of a Commercial Oil",
Proc. I. Mech. E. Vol.67, p.757, 1973

48. Spikes, H.A. and Cameron, A.

"Scuffing as a Desorption Process - An Explanation of the Borsoff Effect",

ASLE Preprint Chicago, Illinois, 1973

APPENDIX 1

```
      PROGRAM  HDLPR(INPUT,OUTPUT,TAPE5=INPUT,TAPE6=OUTPUT)
C
C  -------HYDRODYNAMIC LUBRICATION OF PISTON RING ----------
C
      DIMENSION  HH0(1000),BBOUT(1000),BBPMAX(1000),SSQVNU(1000)
      DIMENSION  HMAX(4),HMAXP(4),HMIN(4),HMINP(4)
      DIMENSION  DEGA(100),DELPA(100),ETAA(100)
      DIMENSION  DEGT(10)
      COMMON/FINL/HH0,BBOUT,BBPMAX,SSQVNU
      COMMON/DTSORT/HMAX,HMAXP,HMIN,HMINP
      COMMON/DTFIX1/DELH1,DELH2,G1,G2
      COMMON/DTFIX2/PE,RPS,RCON,CRNKR,PAI
      COMMON/HDDIME/DELH,BR,BR,H0N
      COMMON/VRBL1/H0,BPMAX,BOUT,BOUTR,SQVNU,N
      COMMON/VRBL2/DELP,ETA
      COMMON/DTVRIA/DEGA,DELPA,ETAA,NDATA,IPRES,IVIS,NCW
      PAI=3.1415926576
C  -------INPUT CYCLE SIMULATION CONDITION -------
      READ(5,1200)  IRUNG,MAXCYC,ISTRT,MESH,INTSMP,CONVER
 1200 FORMAT(2I1,I8,2I10,F10.6)
      DANG=3.1415926576/FLOAT(MESH/2)
      STANG=FLOAT(ISTRT)*DANG
      IMAX=MESH
      ANGMAX=2.*PAI
C  --------INPUT /DTFIX1/ AND /DTFIX2/ AND PRINT  ----------
      CALL RDCNST
C  -------INPUT VARIABL DATA IF SO ----------
      READ(5,1010)  IPRES,IVIS,VISCON
 1010 FORMAT(2I1,8X,F10.4)
      IF(IVIS.EQ.0)  WRITE(6,2300) VISCON
      ETA=VISCON*0.001
 2300 FORMAT(1H0,20HCONSTANT VISCOSITY  ,F10.4, 6H CPOIS )
      IF(IPRES.EQ.0) GO TO 1
      CALL RDVARI (IMAX,ANGMAX)
      IF(NDATA-999) 3,999,3
    1 CONTINUE
C  ------- NO VARIABL INPUT  ----------
      DELP=0.0
C  --------PRINT NONDIMENSIONAL PARAMETERS  ----------
      CALL PARANO (ETA)
    3 CONTINUE
C  ------- CLEAR HH0(I)  ---------
      DO 5  I=1,IMAX
    5 HH0(I)=0.0
C  ------- INITIAL FILM THICKNESS  ----------
      I=ISTRT
      ANG=STANG
      CALL SLIVEL(USLION,USLIDE,   ANG)
      IF(IPRES.NE.0) NOW=1
      IF(IPRES.NE.0) CALL DTINTP(ANG)
      H0=0.0
      CALL DIRECT(H0,USLION)
      CALL  PARAME(DELPN,WTOTLN,   USLIDE)
      H0NX=FTHICK(WTOTLN)*DELH
      H0START=H0NX
      BOUTR=0.0
      L=0
      N=0
C  ------- CYCLE INLET  ----------
   10 CONTINUE
      HH0(I)=H0NX
      H0=H0NX
      CALL  RUNGK(DELTH0,BBOUT(I),BBPMAX(I),SSQVNU(I),   ANG,DANG,IRUNG)
      H0NX=H0NX+DELTH0
C
      L=L+1
      I=I+1
      ANG=FLOAT(I)*DANG
C  ------- CYCLE END CHECK  ----------
      IF(ANG.LE.ANGMAX)  GO TO 11
      I=1
      ANG=DANG
   11 CONTINUE
```

```
      IF(L.LE.IMAX)  GO TO 10
C     ------- CONVERGENT CHECK  ----------
      CONVH0=(H0NX-HH0(I))/H0NX
      IF(ABS(CONVH0).LT.CONVEP)  GO TO 20
      IF(L.LT.IMAX*MAXCYC)  GO TO 10
C     ------- NO CONVERGENCE ----------
      WRITE(6,9200)  MAXCYC,CONVH0
 9200 FORMAT(1H0,30HCYCLE IS NOT CONVERGENT AFTER ,I2,2X,5HCYCLE   /
     1       1H ,10HERROR IS  ,E12.4)
   20 CONTINUE
C     ------- CYCLE FINISH   -----------
      AVITE=FLOAT(N)/FLOAT(L)
      WRITE(6,2700) AVITE,L

 2700 FORMAT(1H0,35HAVERAGE ITERATION BY NEWTON METHOD  ,F10.4,
     1       8H   FOR  ,1I4,26H  TIMES RUNGE KUTTA METHOD  )
      WRITE(6,2710)  MESH,MAXCYC,CONVER
 2710 FORMAT(1H0,10X,5HMESH=,I5,10X,7HMAXCYC=,I3,10X,8HCONVER= ,F10.6)
      DDEG=DANG*180./PAI
      STTDEG=FLOAT(ISTRT)*DDEG
      STPDEG=FLOAT(I-1)*DDEG
      H0STRT=H0STRT*1000.
      WRITE(6,4000) STTDEG,H0STRT,STPDEG,CONVH0
 4000 FORMAT(1H0,12HCYCLE START ,F6.2,10H  DEG WITH  ,F10.6,
     1       8H MICRON , 6H  STOP, F8.2,4H DEG,10H ERROR IS ,E12.4)
      CALL  SORT(MESH,IMAX,   DDEG)
      WRITE (6,3000)
 3000 FORMAT(1H0,40HFILMTHICKNESS(MICRON) AND ANGLE(DEG)      /
     1       1H0,23X, 7HMINIMUM,  33X,  7HMAXIMUM   )
      DO 50 I=1,4
   50 WRITE(6,3010)  HMIN(I),HMINP(I),HMAX(I),HMAXP(I)
 3010 FORMAT(1H0,2(10X,F10.5,10X,F10.2))
      WRITE(6,3050)
 3050 FORMAT(1H0,11HSAMPLE DATA )
      INT=INTSMP
      KF=INT
   51 CONTINUE
      KE=KF+9*INT
      IF(KE.GE.IMAX) KE=IMAX
      IT=1
      DO 52  I=KF,KE,INT
      DEGT(IT)=FLOAT(I)*DDEG
      IT=IT+1
   52 CONTINUE
      WRITE(6,3060)  (DEGT(I),I=1,10)
 3060 FORMAT(1H0, 7X,3HDEG,10(1X,F10.2))
      WRITE(6,3070) (HH0(I),I=KF,KE,INT)
      WRITE(6,3080) (BBOUT(I),I=KF,KE,INT)
      WRITE(6,3090) (BBPMAX(I),I=KF,KE,INT)
      WRITE(6,3100) (SSQVNU(I),I=KF,KE,INT)
 3070 FORMAT(1H  ,10HHH0(MICRO),10(1X,F10.6))
 3080 FORMAT(1H ,10HBBOUT(NON),10(1X,F10.7))
 3090 FORMAT(1H ,10HBBPMAX(NON),10(1X,F10.7))
 3100 FORMAT(1H ,10H     SQVNU,10(1X,F10.7))
      KF=KF+10*INT
      IF(KF.LT.IMAX) GO TO 51
  999 CONTINUE
      STOP
      END
```

```
      SUBROUTINE  RDCNST
C     ------- INPUT ROUTINE 1  ----------
C
      COMMON/DTFIX1/DELH1,DELH2,B1,B2
      COMMON/DTFIX2/PE,RPS,RCON,CRNKR,PAI
C
      READ(5,1000)  DELH1,DELH2,B12
      READ(5,1100)  PE,RPM,RCON,CRNKR
      B1=B12*SQRT(DELH1)/(SQRT(DELH1)+SQRT(DELH2))
      B2=B12-B1
      WRITE(6,2000)  DELH1,DELH2,B1,B2
      WRITE(6,2010)  PE,RPM,RCON,CRNKR
C     ------- MAKE IT  SI UNIT  ----------
      DELH1=DELH1*0.0000001
      DELH2=DELH2*0.0000001
      B1    =B1    *0.001
      B2    =B2    *0.001
      PE    =PE    *10000.
      RPS   =RPM   /60.
      CRNKR=CRNKR*0.001
      RETURN
 1000 FORMAT(3F10.4)
 1100 FORMAT(4F10.4)
 2000 FORMAT (1H1,30HPING GEOMETRY (MICRON OR MM)    /1H0,
     1         6HDELH1=,F10.4,5X,6HDELH2=,F10.4,5X,  3HB1=,F10.4,5X,
     2         3HB2=,F10.4)
 2010 FORMAT (1H0,20HOPERATING CONDITION  /1H0,
     1         3HPE=,F10.4,5HN/CM2,5X,F10.4,3HRPM,5X,5HRCON=,F10.4,
     2         5X,6HCRNKR=,F10.4,3H MM)
      END

      SUBROUTINE  RDVARI(IMAX,ANGMAX)
      COMMON/DTVRIA/DEGA,DELPA,ETAA,NDATA,IPRES,IVIS,NCW
      DIMENSION  DEGA(100),DELPA(100),ETAA(100)
C
      DO  1  I=1,100
      READ(5,1100)  DEGA(I),DELPA(I),ETAA(I)
      IF(IVIS.EQ.0)  ETAA(I)=0.0
      IF((DEGA(I).EQ.360.).OR.(DEGA(I).EQ.720.))  GO TO 2
 1100 FORMAT(3F10.4)
    1 CONTINUE
      GO TO 999

    2 CONTINUE
      NDATA=I
      WRITE(6,2010)
 2010 FORMAT(1H0,30HINPUT DATA DEG,N/CM2,CPOIS       )
      IS=1
      IE=10
    4 CONTINUE
      IF (IE.GE.NDATA) IE=NDATA
      WRITE(6,2020) (DEGA(J),J=IS,IE)
      WRITE(6,2030) (DELPA(J),J=IS,IE)
      WRITE(6,2030) (ETAA(J),J=IS,IE)
      IS=IS+10
      IE=IE+10
      IF (IS.LE.NDATA) GO TO 4
 2020 FORMAT(1H0,10(1X,F10.5))
 2030 FORMAT(1H ,10(1X,F10.5))
C     ------- UNIT ADJUST RADIAN ,PASCAL, PASCALSECOND  --------
      IF (DEGA(1).NE.0.0)  GO TO 999
      PAI180=3.1415926576/180.
      DO 5 I=1,NDATA
      DEGA(I) =DEGA(I)*PAI180
      DELPA(I)=DELPA(I)*10000.
      ETAA(I) = ETAA(I)*0.001
    5 CONTINUE

      IF(DEGA(NDATA).GT.8.0)  IMAX=IMAX*2
      ANGMAX=DEGA(NDATA)
      RETURN
  999 CONTINUE
      NDATA=999
      WRITE(6,9000)
 9000 FORMAT(1H1,16HINPUT DATA ERROR   )
      RETURN
      END
```

```
      SUBROUTINE  PARANO(VISCON)
C     -------- NONDIMENSIONAL PARAMETERS FOR CONSTANT LOAD AND VISCOSITY
      COMMON/DTFIX1/DELH1,DELH2,B1,B2
      COMMON/DTFIX2/PE,RPS,RCON,CRNKR,PAI
      UMAX=RPS*2.*PAI*CRNKR
      DUTY1=(UMAX*VISCON)/(PE*(B1+B2))
      DUTY2=(RPS*VISCON)/PE
      FGEO1=(B1/DELH1)**2
      FGEO2=(B2/DELH2)**2
      UMAX1=DUTY1*FGEO1
      UMAX2=DUTY1*FGEO2
      REVN1=DUTY2*FGEO1
      REVN2=DUTY2*FGEO2
      RSTRK1=CRNKR/B1
      RSTRK2=CRNKR/B2
      WRITE(6,1500)
      WRITE(6,1510) UMAX1,REVN1,RSTRK1
      WRITE(6,1520) UMAX2,REVN2,RSTRK2
      RETURN
 1500 FORMAT(1H0,25HNONDIMENSIONAL PARAMETERS      /1H0,
     1        16X,4HUMAX,16X,4HREVN,15X,5HRSTRK    )
 1510 FORMAT(1H0,3(10X,F10.6),10X,20HPREFERED TO SUFIX 1      )
 1520 FORMAT(1H0,3(10X,F10.6),10X,20HPREFERED TO SUFIX 2      )
      END

      FUNCTION    FTHICK(WTOTLN)
C     -------- APPROXIMATE FILM THICKNESS (NONDIMENSIONAL)  ----------
      UN=1./WTOTLN
      IF  (UN.LE.0.01)                          H0=0.122*UN
      IF((UN.GT.0.01).AND.(UN.LE.0.1))   H0=0.85*UN**0.929
      IF((UN.GT.0.10).AND.(UN.LE.1.0))   H0=0.43*UN**0.681
      IF((UN.GT.1.00).AND.(UN.LE.10.0))  H0=0.43*UN**0.466
      IF((UN.GT.10.0).AND.(UN.LE.100.)) H0=0.592*UN**0.414
      IF((UN.GT.100.).AND.(UN.LE.1000.))H0=1.677*UN**0.373
      IF  (UN.GT.1000.)                         H0=0.946*UN**0.3333
      FTHICK=ABS(H0)
      RETURN
      END

      SUBROUTINE  RUNGK(DELTH0,BOUT1,BPMAX1,SQVNU1,  ANG,DANG,IRUNG)
      COMMON/HODIME/DELH,B3,B5,H0N
      COMMON/VARL1/H0,BPMAX,BOUT,BOUTP,SQVNU,N
C
      H0NOW=H0
      ANG0=ANG
      CALL  DH0DTH(DH0DAN,    ANG0)
      RK1=DH0DAN*DANG
      BOUT1=BOUT*B5
      BPMAX1=BPMAX*B3
      SQVNU1=SQVNU
      IF(IRUNG.EQ.0)  GO TO 1
      ANG0=ANG+0.5*DANG
      H0=H0NOW+0.5*RK1
      IF(H0.LE.0.0)  GO TO 2

      CALL  DH0DTH(DH0DAN,    ANG0)
      RK2=DH0DAN*DANG
      H0=H0NOW+0.5*RK2
      IF(H0.LE.0.0)  GO TO 2
      CALL  DH0DTH(DH0DAN,    ANG0)
      RK3=DH0DAN*DANG
      H0=H0NOW+RK3
      IF(H0.LE.0.0)  GO TO 2
      ANG0=ANG+DANG
      CALL  DH0DTH(DH0DAN,    ANG0)
      RK4=DH0DAN*DANG
      DELTH0=(RK1+2.*RK2+2.*RK3+RK4)/6.
      RETURN
    1 CONTINUE
      DELTH0=RK1
      RETURN
    2 CONTINUE
      IRUNG=9
      RETURN
      END
```

```
      SUBROUTINE  CHOOTH(DHODAN,    ANG)
      COMMON/DTFIX1/DELH1,DELH2,B1,B2
      COMMON/DTFIX2/PE,RPS,RCON,CRNKR,PAI
      COMMON/HODIME/DELH,BB,BR,HON
      COMMON/VRBL1/H0,BMAX,BOUT,BOUTP,SQVNU,N
      COMMON/DTVRIA/DEGA,DELPA,ETAA,NDATA,IPRES,IVIS,NCW
      COMMON/VRBL2/DELP,ETA
      DIMENSION  DEGA(100),DELPA(100),ETAA(100)
      CALL   SLIVEL  (USLION,USLIDE,    ANG)
      IF(IPRES.NE.0)   CALL DTINTP(ANG)
      CALL   DIRECT(H0,USLION)
      IF(ABS(USLION).LT.0.001)   GO TO 1
      CALL  PARAME(DELPN,WTOTLN,    USLIDE)
      CALL   DHODUB(DELPN,WTOTLN)
      DHODAN=SQVNU*(-ABS(USLION))*CRNKR*DELH/BB
      RETURN
    1 CONTINUE
      CALL  DSDEND(SQVDT)
      DHODAN=SQVDT*DELH/(2.*PAI*RPS)
      RETURN
      END
      SUBROUTINE  SLIVEL(USLION,USLIDE,    ANG)
      COMMON/DTFIX2/PE,RPS,RCON,CRNKR,PAI
      USLION=-SIN(ANG)
      IF(RCON.EQ.0.0)  GO TO 1
      USLION=USLION-SIN(2.*ANG)/(2.*SQRT(RCON**2-SIN(ANG)**2))
    1 CONTINUE
      USLIDE=-ABS(USLION)*2.*PAI*CRNKR*RPS
      RETURN
      END

      SUBROUTINE  DTINTP(ANG)
C     ------- LINEAR DATA INTERPORATION  ----------
      COMMON/DTVRIA/DEGA,DELPA,ETAA,NDATA,IPRES,IVIS,NCW
      COMMON/VRBL2/DELP,ETA
      DIMENSION  DEGA(100),DELPA(100),ETAA(100)
C
      NDATA1=NDATA-1
      K=1
    3 CONTINUE
      DO 1  J=NCW,NDATA1
      IF((ANG.GE.DEGA(J)).AND.(ANG.LE.DEGA(J+1)))  GO TO 2
    1 CONTINUE
      NCW=1
      K=K+1
      IF(K.LE.2)   GO TO 3
      J=NDATA1
    2 CONTINUE
      NCW=J
      ANGR=(ANG-DEGA(J))/(DEGA(J+1)-DEGA(J))
      IF(IVIS.NE.0)   ETA=(ETAA(J+1)-ETAA(J))*ANGR+ETAA(J)
      DELP=(DELPA(J+1)-DELPA(J))*ANGR+DELPA(J)
      RETURN
      END
      SUBROUTINE  DIRECT (H0,USLION)
      COMMON/HODIME/DELH,BB,BR,HON
      COMMON/DTFIX1/DELH1,DELH2,B1,B2
      COMMON/VRBL2/DELP,ETA
      IF(USLION.LT.0.0)  GO TO 1
      BB=B1
      DELH=DELH1
      BR=B2/B1
      GO TO 2
    1 CONTINUE
      DELP=-DELP
      BB=B2
      DELH=DELH2

      BR=B1/B2
    2 CONTINUE
      HON=H0/DELH
      RETURN
      END
```

```
      SUBROUTINE  PARAME(DELPN,WTOTLN,    USLIDE)
      COMMON/HDDIME/DELH,BE,BR,HON
      COMMON/DTFIX2/PE,RPS,RCON,CRNKR,PAI
      COMMON/VRBL2/DELP,ETA
C
      X=DELH**2/(ETA*USLIDE*BR)
      DELPN=DELP*X
      POSIP=DELPN
      IF(POSIP.GT.0.0)  POSIP=0.0
      WTOTLN=(PE*X+POSIP)*(1.+BR)
      RETURN
      END

      SUBROUTINE  DHODUB(DELPN,WTOTLN)
      COMMON/VRBL1/H0,BPMAX,BOLT,BOUTR,SQVNU,N
      COMMON/HDDIME/DELH,BE,BR,HON
      CALL  REYNOL(SQVNU,BPMAX,BOUTR,N,    HON,DELPN,WTOTLN)
      BOUT=BOUTR
      IF(BOUTR.GE.-BR)   GO TO 1
      CALL FULSOM(SQVNU,BPMAX,BPMINI,    BR,HON,DELPN,WTOTLN)
      BOUT=-BR
    1 CONTINUE
      RETURN
      END

      SUBROUTINE  DEDEND(SQVOT)
      COMMON/DTFIX2/PE,RPS,RCON,CRNKR,PAI
      COMMON/VRBL1/H0,BPMAX,BOUT,BOUTR,SQVNU,N
      COMMON/VRBL2/DELP,ETA
      COMMON/HDDIME/DELH,BE,BR,HON
C
      RTH0=SQRT(HON)
      X1=1./RTH0
      X2=-X1*BR
      CALL  AHTOGA(AH,BH,GH,A,B,G,    X1,X2)
      BOSIP=DELP
      IF(POSIP.LT.0.0)  POSIP=0.0
      PTOTL=(PE+POSIP)*(1.+BR)
      PR=DELP/PTOTL
      BPMAX=RTH0*(G-PR*RTH0*BH)/(G-PR*RTH0*GH)
      SQVOT=PTOTL*(DELH/BB)**2/ETA
      SQVOT=SQVOT*HON*HON/(12.*(RTH0*BH-BPMAX*GH))
      BOUT=-BR
      RETURN
      END
```

```
      SUBROUTINE  SORT(MESH,IMAX,    DDEG)
      COMMON/FINL/  HH0,BBOUT,BBPMAX,SSQVNU
      COMMON/DTFIX1/DELH1,DELH2,B1,B2
      COMMON/DTSORT/HMAX,HMAXP,HMIN,HMINP
      DIMENSION  HH0(1000),BBOUT(1000),BBPMAX(1000),SSQVNU(1000)
      DIMENSION  HMAX(4),HMAXP(4),HMIN(4),HMINP(4)
      BBIG=AMAX1(B1,B2)
      BBIGR=1./BBIG
      MESHS=MESH/2
      DO 1   I=1,4
      HMAX(I)=0.0
      HMIN(I)=1000.0
    1 CONTINUE
      K=1
    2 CONTINUE
      KF=MESHS*(K-1)+1
      KE=KF+MESHS-1
      IF(KF.GT.IMAX)  GO TO 10
      IF(KE.GT.IMAX)  KE=IMAX
      DO 5 I=KF,KE
      BBOUT(I)=BBOUT(I)*BBIGR
      BBPMAX(I)=BBPMAX(I)*BBIGR
      HH0(I)=HH0(I)*1000000.
      IF(HH0(I).LT.HMAX(K))  GO TO 3
      HMAX(K)=HH0(I)
      HMAXP(K)=FLOAT(I)*DDEG
    3 CONTINUE
      IF(HH0(I).GT.HMIN(K))  GO TO 5
      HMIN(K)=HH0(I)
      HMINP(K)=FLOAT(I)*DDEG
    5 CONTINUE
      K=K+1
      GO TO 2
   10 CONTINUE
      RETURN
      END

      SUBROUTINE  REYNOL(SQVN,BBA1,BBAR,N,      H0,DELPN,PWN)
C     -----  FILM THICKNESS AND LOAD GIVE SQUEEZE VELOCITY  -----

C     -----  AND OUTLET BOUNDARY , PMAX POSITION  -----
      RTH0=SQRT(H0)
      X1=1./RTH0
      XBA = BBAR*X1
    1 CONTINUE
      N=N+1
      X2  = XBA
      CALL  AHTOGA (AH,BH,GH,A,B,G,    X1,X2)
      CALL  SQVELO (SQVN,DSQDX,    A,B,G,XBA,H0,DELPN)
      WHYDN = 6.*(AH-(1.+XBA**2)*GH)/H0
      WHYDN = WHYDN + 12.*SQVN*(BH-XBA*GH)/(H0*RTH0)
      FDWDX = -12.*XBA*GH/H0 - 12.*SQVN*GH/(H0*RTH0)
     1          + 12.*DSQDX*(BH-XBA*GH)/(H0*RTH0)
      DELX  = (WHYDN-PWN)/FDWDX
      IF (ABS(DELX/X1).LT.0.000001)  GO TO 2
      XBA  = XBA - DELX
      GO TO 1
    2 CONTINUE
      BBAR = XBA/X1
      BBA1 = -2.*SQVN - BBAR
      RETURN
      END
```

```
      SUBROUTINE   FULSOM(SQVN,SBAS1,BBAS2,    BR,HJ,DELPN,PWN)
      RTHO=SQRT(HO)
      X1=1./RTHO
      X2   = -X1*BB
      CALL    QUADS(C1,C2,C3,A,B,G,    X1,X2,DELPN,PWN,HO)
      ROOTR=  -C2/(2.*C1)
      ROOTI=  SQRT(C2*C2-4.*C1*C3)/(2.*C1)
      XBA1=ROOTR  - SIGN(ROOTI,C1)
      XBA2=ROOTR  + SIGN(ROOTI,C1)
      BBAS1=  XBA1/X1
      BBAS2=XBA2*RTHO
      XBA  =  XBA1
      CALL   SQVELO  (SQVN,DSQDX,    A,B,G,XBA,HO,DELPN)
      RETURN
      END


      SUBROUTINE   QUADS(C1,C2,C3,A,B,G,    X1,X2,DELPN,PWN,HO)
      RTHO=SQRT(HO)
      CALL    AHTOGA  (AH,BH,GH,A,B,G,    X1,X2)
      C1    =  GH*G  -  B*GH
      C2    =  GH*A  -  G*AH  -  DELPN*HO*RTHO*GH/6.0
      C2    =  C2  +  PWN*HO*G/6.0
          C3    =  B*(AH-GH)  -BH*(A-G)  +  DELPN*HO*RTHO*BH/6.0
      C3    =  C3  -  PWN*HO*B/6.0
      RETURN
      END


      SUBROUTINE   SQVELO  (SQVN,DSQDX,    A,B,G,XBA,HO,DELPN)
      SQNOMI  =  DELPN*HO*HO  -  6.0*SQRT(HO)*(A-(1.+XBA**2)*G)
      SQDENO  =    12.*(B-XBA*G)
      SQVN    =    SQNOMI  /  SQDENO
      DSQDX   =  12.*SQRT(HO)*XBA*G  +  SQDENO  +  12.0*G*SQNOMI
       DSQDX   =  DSQDX  /  SQDENO**2
      RETURN
      END


      SUBROUTINE   AHTOGA   (AH,BH,GH,  A,B,G,    H,X)
      ATANH  =  ATAN(H)
      ATANX  =  ATAN(X)
      HX     =  H-X
      F1X    =  1./(1.+X*X)
      F1H    =  1./(1.+H*H)
      F2X    =  F1X*F1X
      F2H    =  F1H*F1H
      A      =  (H*F1H  +  ATANH  -  X*F1X  -  ATANX)/2.
      B      =  (F2X  -  F2H)/4.
      G      =  (2.*H*F2H  +  3.*H*F1H  +  3.*ATANH)/8.
      G    =   G-(2.*X*F2X  +  3.*X*F1X  +  3.*ATANX)/8.
      AH     =  (H*(ATANH-ATANX)  -  X*HX*F1X)/2.
      BH     =  (2.*HX*F2X  +  X*F1X  +  ATANX  -H*F1H  -  ATANH)/8.
      GH     =  (F1X-F1H  -  3.*X*ATANX+3.*H*ATANH)/8.
      GH     =  GH  -  HX*(2.*X*F2X+3.*X*F1X+3.*ATANX)/8.
      RETURN
      END
```

APPENDIX 2

```
      PROGRAM  ATILPA(INPUT,OUTPUT,TAPE5=INPUT,TAPE6=OUTPUT)
C     ------- PERFORMANCE OF PARABOLIC THRUST BEARING -------
C     ------- FOR TILTING BEARING INPUT   IFIX=0   (NOT 1 )
C     ------- FOR FIXED BEARING INPUT     IFIX=1
      READ(5,1000)  IFIX, IMAX,HOSTRT,POINT,BTIN
 1000 FORMAT(I1,I9  ,3F10.6)
      READ(5,1100) NUM,BRS,BRINC
 1100 FORMAT(I2,8X,2F10.6)
      RETIO=10.0**(1.0/POINT)
      SQVN=0.0
      DELPN=0.0
      BBAR=-1.0
      BTCON=0.000001
      DO 4   K=1,NUM
      BR=BRS+BRINC*FLOAT(K-1)
      BTOTL=1.0+BR
      IF(IFIX.EQ.1)   WRITE(6,2200)   BR
 2200 FORMAT(1H1,25HFIXED PARABOLA   BR=       ,F10.5)
      IF(IFIX.NE.1)   WRITE(6,2100)   BR
 2100 FORMAT(1H1,20HTILTING PAD PARABOLA,10X,3HBR=,F10.5)
      WRITE(6,2000)
 2000 FORMAT(1H0,11X,2HHO, 9X,4HUNOT, 9X,4HWRET, 9X,4HPMAT, 9X,4HBBAT,
     1       11X,2HBT,10X,3HXTL, 9X,4HHOBT, 7X,6HHOBTBP,11X,2HH0/ )
      BT=1.01305
      IF(BTIN.NE.0.0)    BT=BTIN
      DO 1   I=1,IMAX
      HO  =HOSTRT*RETIO**(I-1)
      IF(IFIX.EQ.1)   BT=BTIN
      ITERA=100
      DO 3    MM=1,ITERA
      BT2=BT*BT
      BRT=BTOTL/BT-1.0
      HOT=HO/BT2
      IF(BT.LE.BTOTL)   GO TO  7
      HOT=HOT-(BT-BTOTL)**2/BT2
      IF(HOT.LE.0.0)  GO TO 2
      GO TO 6
    7 CONTINUE
      CALL WREYNC(WREY,BEA1,BBAR,PMAX,   HOT,SQVN,DELPN)
      BOUT=BBAR
      BBA=BBAR
      IF(BBAR.GT.-BRT)   GO TO 5
    6 CONTINUE
      CALL   WLOYD(WREY,BEA ,BBA2,XBO,PMAX,   SQVN,HOT,BRT)
      BOUT=-BRT
    5 CONTINUE
      CALL   XMOMNT(WL6,   HOT,BBA,BOUT)
      XL=WL6*6.0/WREY
      IF(IFIX.EQ.1)   GO TO 2
      BTR=1.0/(1.0-XL)
      IF(ABS(BT-BTR).LT.BTCON)   GO TO 2
      BT=BTR
    3 CONTINUE
    2 CONTINUE
      BBAT=-BR
      IF(BBAR.GT.-BRT)   BBAT=1.0-BT+BT*BBAR
      XLT=1.0-BT+BT*XL
      WRET=WREY/BT2
      UNOT=1.0/WRET
      PMAT=PMAX/BT2
      HOBT=HO*SQRT(ABS(WRET))
      HOBTBR=HOBT/(1.0+BR)
      IF(HOT.LT.0.0)    HO=-HO
      IF(MM.GE.ITERA)    HOBT=-HOBT
      BT=BBA
      WRITE(6,3000) HO,UNOT,WRET,PMAT,BBAT,BT,XLT,HOBT,HOBTBP,HO
 3000 FORMAT(1H ,10(1X,E12.6))
    1 CONTINUE
    4 CONTINUE
      STOP
      END
```

```
      SUBROUTINE  WLOYD  (W,BBA1,BBA2,XB0,PMAX,   SQV, H0,BR)
C     -----  LOAD  OF  LLOYDS  BOUNDARY CONDITION  -----
      SQRTH0 = SQRT(H0)
      H=1./SQRTH0
      X= -H*BR
      CALL  AHTOGA (AH,BH,GH, A,B,G,   H,X)
      D=(SQV*G)**2 - SQRTH0*G*(SQRTH0*(G-A)-2.*3*SQV)
      XBA1=-SQV*G+SQRT(D)
      XBA1=XBA1/(SQRTH0*G)
      XBA2=-SQV*G-SQRT(D)
      XBA2=XBA2/(SQRTH0*G)
      BBA1=XBA1*SQRTH0
      BBA2=XBA2*SQRTH0
      XB   =BBA1
      BOUT=-BR


      CALL PDIST(PMAX,PW,PS,   SQV ,H0,BBA1,BOUT,   BBA1)
      GO TO 2
      IF (BBA2.LE.-BR)  GO TO 2
      IF (BR.EQ.0.0)    GO TO 2
      IF(BBA1.GE.1.0)   GO TO 2
      DXB =0.1
      P1=PMAX
   30 CONTINUE
      XB =XB-DXB
      P2=P1
      CALL PDIST(P1  ,PW,PS,   SQV ,H0,BBA1,BOUT,   XB)
      IF (ABS(P1/PMAX).LT.0.00001)   GO TO 20
      IF(P1*P2)   10,20,30
   10 CONTINUE
      DXB=-0.5*DXB
      GO TO 30
   20 CONTINUE
      XB0=XB
      X=XB*H
    2 CONTINUE
      CALL AHTOGA(AH,BH,GH, A,B,G,   H,X)
      W    =  6.*(AH-(1.+XBA1**2)*GH)/H0
     1     +12.*SQV*(BH-XBA1*GH) / SQRTH0**3
      RETURN
      END

      SUBROUTINE  XMOMNT(WL6,   H0,BBA,BOUT)
C     ------ FILM THICKNESS AND BOUNDARY CONDITION GIVE
C     ------- MOMENT OF PRESSURE   WL/6
C     ------  REYNOLDS CONDITION  BBA=BOUT,
C     ------- SOMMERFELDS CONDITION  BBA=BPMAX,  BOUT=-BR
C
      RTH0=SQRT(H0)
      X1=1./RTH0
      XOUT=BOUT*X1
      XBA=BBA*X1
      XBA1=1.+XBA*XBA
      CALL  AMTOGD(AM,GM,AD,GD,   X1,XOUT)
      WL6=(AM-XBA1*GM)/RTH0
      WL6=WL6-(AD-XBA1*GD)*(X1*X1-XOUT**2)/(2.*RTH0)
      RETURN
      END

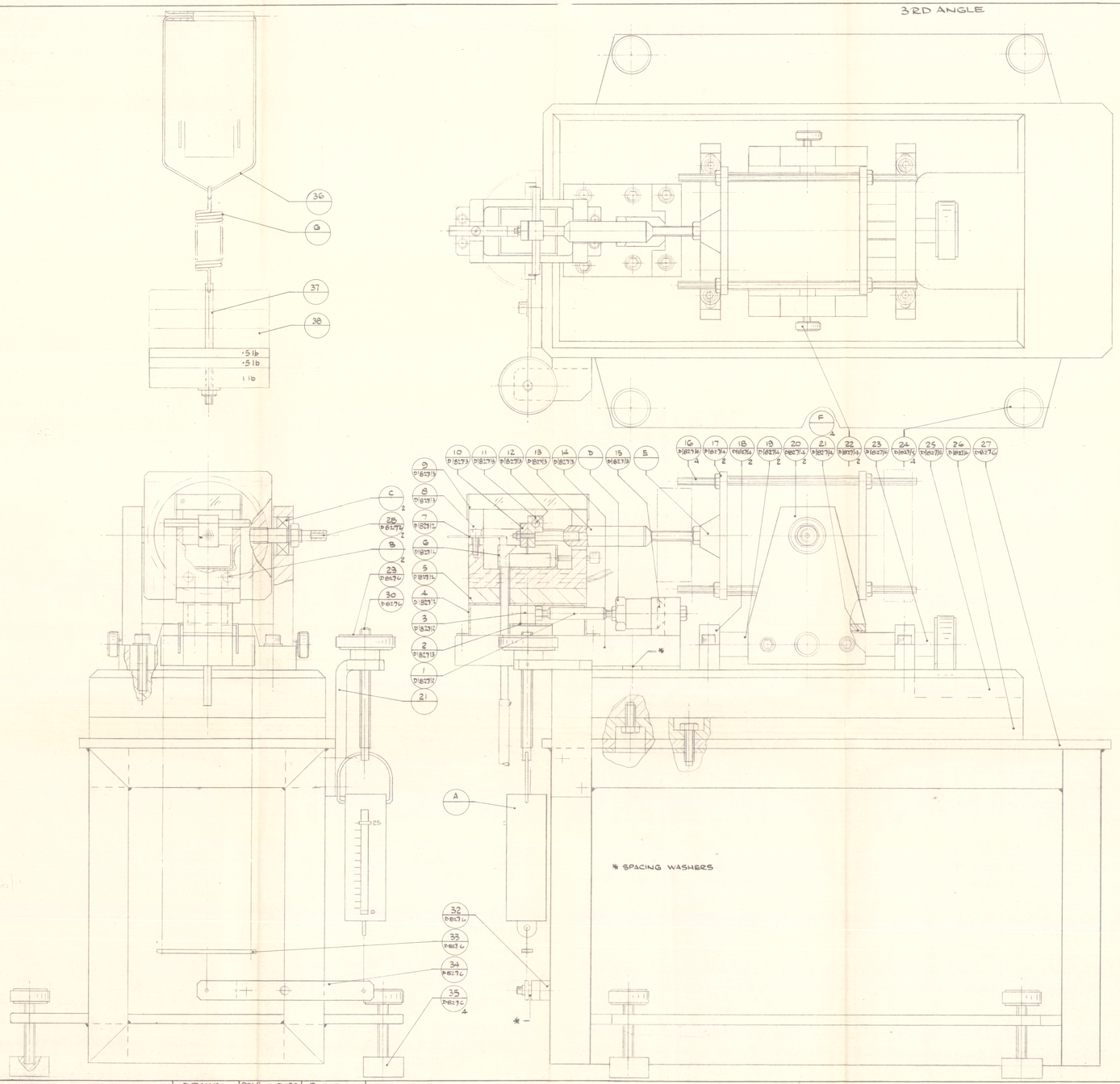
      SUBROUTINE  AMTOGD(AM,GM,AD,GD,   H,X)
C     ------  INTEGRAL FUNCTIONS OF MOMENT OF PRESSURE  -----
      ATANX=ATAN(X)
      ATANH=ATAN(H)
      F1X=X/(1.+X*X)
      F1H=H/(1.+H*H)
      AM =     H-ATANH+H*H*ATANH
      AM =AM-(X-ATANX+X*X*ATANX)
      AM =AM/4.0
      GM =     3.*H - 2.*F1H - ATANH + 3.*H*H*ATANH
      GM =GM-(3.*X - 2.*F1X - ATANX + 3.*X*X*ATANX)
      GM= GM/16.0
      AD = (F1X + ATANX)*0.5
      GD = (2.*F1X/(1.+X*X) + 3.*F1X + 3.*ATANX)/8.0
      RETURN
      END
```

```
      SUBROUTINE  WREYNO(WREY,BBA1,BBAR, PMAX,    H0,SQVN,DELPN)
C     -----   FILM THICKNESS AND SQUEEZE VELOCITY GIVE OUTLET BOUNDARY
C     -----   AND PMAX POSITION.  AND LOAD CAPACITY   -----
      XCONV=0.000000001
      SQRTH0=SQRT(H0)
      XBA   =BBAR/SQRTH0
      X1    =1.0/SQRTH0
    1 CONTINUE
      X2    =XBA
      CALL   AHTOGA(AH,BH,GH, A,B,G,    X1,X2)
      DELP = 6.*(A-(1.+XBA**2)*G)/SQRTH0**3
     1      +12.*SQVN*(B-XBA*G) / H0**2
      FDPDX= 6.*(-2.*XBA*G)/SQRTH0**3
     1      +12.*SQVN*(-G) / H0**2
      IF(FDPDX.EQ.0.0) GO TO 3
      DELX = (DELP-DELPN)/FDPDX
      IF(ABS(DELX).LT.XCONV)  GO TO 2
      XBA   = XBA-DELX
      GO TO 1
    2 CONTINUE
      BBAR = XBA*SQRTH0
      BBA1 = -2.*SQVN - BBAR
      CALL   PDIST(PMAX,PW,PS,    SQVN,H0,BBAR,BBAR,    BBA1)
      WREY   =  6.*(AH - (1.+XBA**2)*GH) / H0
     1      +12.*SQVN*(BH-XBA*GH) / SQRTH0**3
      RETURN
    3 CONTINUE
      XBA=XBA-1.0
      GO TO 1

      END
      SUBROUTINE  PDIST (P,PWEDG,PSQ,    SQVN,H0 ,BBA,BOUT,      XB)
C     -----   PRESSURE DISTRIBUTION   -----
C     -----   REFERENCE DIMENSIONS ARE INLET DIMENSIONS   -----
      SQRTH0=SQRT(H0)
      X     =XB/SQRTH0
      XBA   =BBA/SQRTH0
      X2    =BOUT/SQRTH0
      CALL   AHTOGA  (AH,BH,GH,A,B,G,      X,X2)
      PWEDG =  6.*(A-(1.+XBA**2)*G)/H0**1.5
      PSQ   =  12.*SQVN*(B-XBA*G) / H0**2
      P     =  PWEDG + PSQ
      RETURN
      END

      SUBROUTINE  AHTOGA  (AH,BH,GH, A,B,G,    H,X)
      ATANH = ATAN(H)
      ATANX = ATAN(X)
      HX    = H-X
      F1X   = 1./(1.+X*X)
      F1H   = 1./(1.+H*H)
      F2X   = F1X*F1X
      F2H   = F1H*F1H
      A     = (H*F1H + ATANH - X*F1X - ATANX)/2.
      B     = (F2X - F2H)/4.
      G     = (2.*H*F2H + 3.*H*F1H + 3.*ATANH)/8.
      G   = G-(2.*X*F2X + 3.*X*F1X + 3.*ATANX)/8.
      AH    = (H*(ATANH-ATANX) - X*HX*F1X)/2.
      BH    = (2.*HX*F2X + X*F1X + ATANX -H*F1H - ATANH)/8.
      GH    = (F1X-F1H - 3.*X*ATANX+3.*H*ATANH)/8.
      GH    = GH - HX*(2.*X*F2X+3.*X*F1X+3.*ATANX)/8.
      RETURN
      END
```

3RD ANGLE



ITEM NO	NO OFF	DESCRIPTION	MATERIAL
G	1	SPRING TERRY T32140	OD·606" d·083" L2·5"
F	4	BEARING, 'GLACIER' DU	
E	1	VIBRATOR (LDS 201)	
D	1	TRANSDUCER (BRUEL&KJAER 8001)	
C	2	BEARING (FAG, EE3)	
B	2	HEATER (GRIMWOOD 283960)	
A	1	SPRING BALANCE 0-25 lb	

ITEM NO	NO OFF	DESCRIPTION	MATERIAL
38	G	WEIGHT	STEEL
37	1	ROD	"
36	1	HANGER	"
35	4	FOOT	'TICO'
34	1	LEVER	STEEL
33	1	MEASURING BEAM	"
32	1	BRACKET	"
31	1	BRACKET	"
30	1	SCREW	"
29	1	KNOB	"
28	2	SHAFT	"
27	1	FRAME	"
26	1	INSULATION PAD	'TICO'
25	1	BASE (W.D.S.920-085-6"+12"x1¼")	CAST IRON
24	1	SCREW	STEEL
23	1	SCREW	"
22	2	LOCK SCR	"
21	2	SLIDE	"
20	2	SIDE PLATE	"
19	2	GUIDE RAIL	SILVER STEEL
18	2	BRACKET	STEEL
17	2	SUPPORT PLATE	"
16	4	TIE ROD	"
15	1	BLOCK	"
14	1	MOUNTING BLOCK	"
13	1	PUSH ROD	STAINLESS STEEL
12	1	BAR	"
11	1	SUPPORT	"
10	1	CLAMP	"
9	1	COVER	"
8	1	HEATER BLOCK	ALUMINIUM ALLOY
7	1	CLAMP	STAINLESS STEEL
6	1	OIL BATH	"
5	1	INSULATION	SYNDANIO
4	1	BRIDGE	STAINLESS STEEL
3	1	BLOCK	"
2	1	FIN	ALUMINIUM ALLOY
1	1	CONNECTING ROD	SILVER STEEL

MECHANICAL ENGINEERING DEPT	DRAWN	P.M.SAUNDERS	SCALE
IMPERIAL COLLEGE	APPROVED		1:1
LONDON SW7 2BX			DATE
			10-10-79

HIGH FREQUENCY FRICTION MACHINE

FOR ITEMS SEE ME/D828/2 TO 7

DRAWING NUMBER

ME/E828/1